# The Role of Metabolite Transport across Organellar Membranes in Plants and Algae

Inaugural-Dissertation

zur Erlangung des Doktorgrades
der Mathematisch-Naturwissenschaftlichen Fakultät
der Heinrich-Heine-Universität Düsseldorf

vorgelegt von

**Anastasija Plett**
aus Barnaul

Düsseldorf, September 2025

aus dem
Institut für Biochemie der Pflanzen
der Heinrich-Heine-Universität Düsseldorf

Gedruckt mit der Genehmigung der
Mathematisch-Naturwissenschaftlichen Fakultät der
Heinrich-Heine-Universität Düsseldorf

Referent: Prof. Dr. Andreas P.M. Weber
Korreferent: Prof. Dr. Stanislav Kopriva

Tag der mündlichen Prüfung: 26.02.2026

**Eidesstattliche Erklärung**

Ich versichere an Eides Statt, dass die Dissertation von mir selbständig und ohne unzulässige fremde Hilfe unter Beachtung der „Grundsätze zur Sicherung guter wissenschaftlicher Praxis an der Heinrich-Heine-Universität Düsseldorf“ erstellt worden ist.

Die Dissertation habe ich in der vorgelegten oder in ähnlicher Form noch bei keiner anderen Institution eingereicht.

Ich habe bisher keine erfolglosen Promotionsversuche unternommen.

Düsseldorf, den

_____

Anastasija Plett

**Statement of authorship**

I hereby certify that this dissertation is the result of my own work. No other person’s work has been used without due acknowledgement. This dissertation has not been submitted in the same or similar form to other institutions. I have not previously failed a doctoral examination procedure.

Table of contents

## Summary

Compartmentalization is a key feature of eukaryotic cells, creating distinct areas for various metabolic processes and enabling the formation of chemical gradients and optimal environments for enzymes. To enable exchange of metabolites and connect biochemical pathways across several organellar membranes, transporters, channels, and pores are essential.

Peroxisomes are comparatively small but essential organelles in all eukaryotic organisms. They are involved in several processes such as beta-oxidation, photorespiration and biosynthesis of secondary and defense molecules. Since many of those pathways are shared between organelles, peroxisomes are closely interconnected to those organelles and the cellular metabolism. The peroxisomal membrane contains several active and passive transporters as well as channels (reviewed in Manuscript I).

One of the most abundant peroxisomal membrane proteins is PEROXISOMAL MEMBRANE PROTEIN 22 (PMP22) which belongs to the MPV17/PMP22 family. Based on studies of mammalian orthologues, it is proposed to function as a non-selective pore-forming channel. In Manuscript II we analyzed the role of PMP22 in context of beta-oxidation and amino acid metabolism under certain environmental conditions.

Transporters are not only important in higher plants but also in microalgae. The green algae *Chlamydomonas reinhardtii* is a model organism to study photosynthesis. The origin of plastids can be traced back several billion years ago through endosymbiosis. One prime example of plastid evolution from the perspective of transport proteins is the plastidial phosphate translocator (pPT) family. This family is conserved in *Archaeplastida* and encodes for transporters catalyzing a strict counter exchange carbons in exchange for inorganic phosphate. We analyzed the biochemical and physiological role of two TRIOSE PHOSPHATE TRANSLOCATORS in *Chlamydomonas reinhardtii* (CreTPT) (Manuscript III).

Finally, we provide a detailed protocol for metabolite extraction and analysis for plants exposed to transient environmental conditions (Manuscript IV).

# Zusammenfassung

Die Kompartimentierung ist ein wesentliches Merkmal eukaryotischer Zellen und schafft getrennte Bereiche für verschiedene Stoffwechselprozesse, ermöglicht die Bildung chemischer Gradienten und somit optimale Bedingungen für Enzyme. Der Austausch von Metaboliten und Ionen erfolgt über Transporter, Kanäle und Poren in der Membran.

Peroxisomen sind vergleichsweise kleine, aber essentielle Organellen aller eukaryontischen Organismen. Sie erfüllen eine Vielzahl unterschiedlicher Funktionen darunter die beta-Oxidation, Photorespiration und Biosynthese von Sekundär- und Abwehrmolekülen. Da viele dieser Stoffwechselwege auf mehrere Organellen verteilt stattfinden, sind Peroxisomen eng mit Organellen und dem zellulären Stoffwechsel verknüpft. Um den Austausch zu garantieren, enthält die peroxisomale Membran mehrere aktive und passive Transporter sowie Kanäle (Manuskript I).

Eines der am stärksten vertretenen peroxisomalen Membranproteine ist PEROXISOMAL MEMBRANE PROTEIN 22 (PMP22), das zur MPV17/PMP22-Familie gehört. Auf Grundlage von Untersuchungen an Orthologen von Säugetieren wird angenommen, dass PMP22 als nicht-selektiver porenbildender Kanal agiert. In Manuskript II haben wir die Funktion von PMP22 im Kontext der beta-Oxidation und des Aminosäurestoffwechsels unter bestimmten Umwelteinflüssen untersucht.

Transporter sind auch bei Mikroalgen wie *Chlamydomonas reinhardtii*, einem Modellorganismus zur Untersuchung der Photosynthese, von großer Bedeutung. Plastidäre Phosphattranslokatoren (pPT), die in *Archaeplastida* konserviert sind, erleichtern den Austausch von Kohlenstoffverbindungen und anorganischem Phosphat. Wir haben die biochemische und physiologische Rolle von zwei Triosephosphat-Translokatoren (TPT) analysiert (Manuskript III).

Schließlich beschreiben wir in einem detaillierten Protokoll die Extraktion und Analyse von Metaboliten bei Pflanzen, die transienten Umwelteinflüssen ausgesetzt sind (Manuskript IV).

# Introduction

Global warming accompanied with increasing world population is one of the greatest challenges of our time. Since the industrial revolution, the average global surface temperature has risen by about 1.1 °C (Tollefson, 2021). Consequences are extreme weather events such as floods and heatwaves followed by drought periods (Hoegh-Guldberg, 2018). Rapidly changing climate conditions are a major threat to agriculture and food security. Moreover, it is estimated that the world's population will reach 9.7 billion people by 2050 (UnitedNations, 2022). Growing demand for food and unpredictable climate conditions require sustainable solutions for agriculture. These solutions can target the plant's metabolism itself or environmental threats surrounding it such as pathogens or insects. Approaches in synthetic biology include improvement of $CO_2$ fixing reactions, bypassing photorespiration or enhancing carbon concentrating mechanism (Bar-Even et al., 2010; Weber and Bar-Even, 2019; Roell and Zurbriggen, 2020; Roell et al., 2021; Zeng et al., 2022). Genome engineering made impressive progress in the last decade, resulting in a precise method for gene modification (Wada et al., 2020). Research on herbicides and pesticides is becoming increasingly important for plant protection or weed control (Ndikuryayo and Yang, 2023). All in all, ideas and possible solutions for a sustainable agriculture do exist. However, both applied and synthetic approaches are limited by possible targets. To enable resistance against certain diseases, target genes need to be identified. In addition, fundamental research is needed to understand the complexity behind metabolic pathways in order to alter or bypass them. Eukaryotic metabolism is complex due to compartmentalization. Each plant cell is divided into different compartments which are surrounded by at least one lipid bilayer. This allows a spatiotemporal control of multiple biochemical reactions in response to cellular metabolism (Barbier-Brygoo et al., 1997). One advantage of compartmentalization is the creation of different local environments that can provide an optimal pH environment for certain enzymes, thereby accelerating their activity (Fick, 1995). Along with compartmentalization, enzymes and proteins must be targeted to a specific organelle, and more importantly, intracellular transporters and channels are needed to connect metabolic pathways and make substrates available in specific compartments (Heinig et al., 2013). Transporters and channels are integral membrane proteins which are essential for the uptake and

translocation of ions, solutes and cofactors (Haferkamp and Linka, 2012). Depending on their properties, dynamics and substrates may vary. In general, channels differ from transport protein in their ability to form a hydrophilic pore across a membrane (Alberts B, 2002). They do not need to interact with their substrate, which allows them to be less selective (Drew and Boudker, 2016). In order to control ion fluxes, gating properties of channels can be caused by several stimuli. Changes in voltage (voltage-gated channels), mechanical stress (mechanically gated channels) or upon binding of a ligand (ligand-gated channels) can lead to open the channel and allowing flux of ions (Alberts B, 2002). In general, channels conduct a passive transport mode, downhill the concentration gradient (Alberts B, 2002). In contrast, transporters do interact with their substrate directly by binding, leading to a conformational change, allowing the substrate to cross the membrane (Drew and Boudker, 2016). Transporters or carriers can be categorized into active, secondary active and passive transporters. The latter exhibit the same transport mode, downhill the concentration gradient as channels (Drew and Boudker, 2016). Active transporters are able to move solutes against a concentration gradient by consuming energy e.g., ATP in case of ABC transporters (Linka and Theodoulou, 2013; Charton et al., 2019; Plett et al., 2020). Secondary active transporters do use an electrochemical gradient, to transporter two solutes in opposite direction (antiport) or two solutes in the same direction (symport) (Drew and Boudker, 2016).

## Plastidial Membrane Transport Proteins

Chloroplasts are hallmarks of all photosynthetic eukaryotes; their origin can be traced back several billion years ago. According to the endosymbiosis theory, a eukaryotic host cell captured a cyanobacterium-like ancestor. A complex host-endosymbiont relationship was established leading to the subgroup *Archaeplastida* (Yoon et al., 2004; Gould et al., 2008). This subgroup is divided into three major lineages: *Glaucophyta*, *Rhodophyta* and *Chlorophyta* (Yoon et al., 2004; Gould et al., 2008; Facchinelli and Weber, 2011). Plastids which derived from primary endosymbiosis contain two membranes: the outer and the inner envelope membrane. Secondary and tertiary endosymbiosis gave rise to new species with plastids containing three or four membranes (Cavalier-Smith, 2000). Comparative (plastidial) genome analyses contribute to a better understanding of plastid evolution. The green lineage (*Chlorophyta*) can be traced back from unicellular and multi-cellular green algae to

mosses to monocotyledon and dicotyledons, such as the model plant *Arabidopsis thaliana* (Arabidopsis) (Initiative, 2000; Cove, 2005; Merchant et al., 2007). The evolution of Rhodophytes is addressed by comparing sequences form various micro- and macro-algae with secondary and tertiary plastids (Matsuzaki et al., 2004). The newly sequenced and assembled genome of *Cyanophora paradoxa* represents the third subclass: the Glaucophytes (Price et al., 2012; Price et al., 2019).

Chloroplasts have a unique function in plants, they perform photosynthesis. In order to distribute fixed carbon throughout the cell plastidial metabolism needs to be connected to the metabolism of the cytosol and other cellular compartments. Transport across the chloroplast envelope involves two membranes: the outer and the inner envelope membrane. In addition, transport can occur across the thylakoid membrane, connecting the metabolism of the thylakoid lumen with that of the chloroplast stroma. One of the first discovered envelope membrane protein family is the plastidic phosphate translocator family (pPT) (Flügge, 1999). Although several other plastidial transporters exist, the pPT family is one of the best characterized and is found in all *Archaeplastida* (Weber and Linka, 2011). Members of this family catalyze an antiport of phosphorylated C3, C5 or C6 carbon compounds against inorganic phosphate ($P_i$). This antiport transport mode guarantees a phosphate balance between the chloroplast stroma and the cytosol (Weber et al., 2005). Phylogenetic analysis revealed the evolutionary origin of pPTs within *Archaeplastida* from nucleotide sugar transporters in the host endomembrane system (Colleoni et al., 2010). Metabolic connection between the host and the cyanobiont was a crucial step during endosymbiosis. The ancestral nucleotide sugar transporters existed before the capture of cyanobacteria. Subsequently, they were recruited to the envelope membrane resulting in today's pPTs. The phylogenetic tree demonstrates a division of the pPT family into three sub groups, each named according to their substrate specificity: (1) triose phosphate translocators (TPT), (2) glucose 6-phosphate/xylose 5-phosphate translocators (GTP/XPT), and (3) phosphoenolpyruvate translocators (PPT) (Weber and Linka, 2011).

Both the GPT and XPT are involved in supplying the oxidative pentose phosphate pathway (OPPP) and are found in non-green plastids (Eicks et al., 2002; Niewiadomski et al., 2005). GPT exhibits a rather broad substrate specificity, accepting glucose-6-phoshate (Glc-6-P), triose phosphate (TP) and 3-phosphoglycerate (3-PGA) in exchange for $P_i$ (Kammerer et al., 1998). Further it is

also important in starch biosynthesis, as Glc-6-P can be converted to the starch biosynthetic precursor ADP-glucose. As a consequence, plants with repressed expression of GPT show a reduced starch content (Rolletschek et al., 2007). In Arabidopsis, loss-of-function mutants have less storage lipids during pollen development (Niewiadomski et al., 2005). In Arabidopsis, GPT1 is dual-targeted to plastids and peroxisomes, supporting OPPP activity in peroxisomes, which is crucial for fertilization (Baune et al., 2020). The XPT catalyzes the antiport of xylulose 5-phosphate TP, ribulose 5-phosphate and erythrose 4-phosphate against $P_i$ (Eicks et al., 2002). Based on its substrate spectrum, it is proposed that XPT transports pentose phosphates for plastidial OPPP pathway and the Calvin-Benson-Bassham (CBB) cycle (Eicks et al., 2002).

The PPT imports cytosolic phosphoenolpyruvate (PEP) in exchange for plastidial $P_i$ (Fischer et al., 1997). PEP is essential as a precursor for aromatic amino acid biosynthesis and secondary metabolites (Herrmann, 1995; Tzin and Galili, 2010). In Arabidopsis, loss-of-function mutants show a reticulated leaf phenotype with altered chloroplast morphology (Streatfield et al., 1999).

As the first identified member of the pPT family, TPT is responsible for the export of TP produced during the CBB cycle (Weber and Linka, 2011). Similar to other members of the protein family, TPT functions as an antiporter by exchanging TP for $P_i$. The main function of TPT is to allocate fixed carbon which is subsequently used for sucrose and cell wall biosynthesis (Flügge and Heldt, 1984; Flügge, 1999). Mutant plants with a repressed expression or a loss-of-function mutation can compensate for loss of TP export by investing into transitory starch biosynthesis (Riesmeier et al., 1993; Schneider et al., 2002). Only mutants deficient in both TP export and transitory starch biosynthesis are severely impaired in plant growth (Hattenbach et al., 1997; Schneider et al., 2002). These mutant plants show reduced photosynthetic activity, impaired growth, hyperstacking of thylakoid membranes, and increased plastoglobules (Häusler et al., 2009). Another proposed function of TPT is its role as a redox regulator, since it is not only capable of exporting TP, but also reducing power by exchanging TP for 3-PGA. TP is exported from the chloroplast, oxidized by glyceraldehyde phosphate dehydrogenase to 3-PGA which is returned to the chloroplast (Bräutigam and Weber, 2011). TPT plays a crucial role not only in vascular plants but is also present in microalgae. In the red algae *Galdieria sulphuraria,* TPT exclusively accepts TP as substrate in exchange for $P_i$ (Linka et al., 2008). The existence and characterization of

a TPT in Glaucophytes remains unexplored to date. In the green algae *Chlamydomonas reinhardtii*, two out of four putative pPTs (CreTPTs) exhibit TPT activity *in vitro*, as shown with liposome transport assays (Huang et al., 2023). Despite phylogenetic analyses and predictions suggesting differences, both CreTPTs demonstrated overlapping substrates specificities. This finding leads to the conclusion that both CreTPTs are differently regulated on transcriptional, temporal, and environmental levels. Chlamydomonas is a unicellular organism that integrates photosynthesis, carbon storage and other cellular pathways within a single cell, providing a direct readout pf plastidial transport function on cellular metabolism (Gutman and Niyogi, 2004; Chang et al., 2011). Comparative analysis of algal and plant pPTs is therefore exciting, as is allows to identify conserved core functions as well as lineage-specific adaptations.

## Role of peroxisomes in cellular metabolism

Besides plastids, plant peroxisomes have unique functions for the plant metabolism compared to other eukaryotes. Peroxisomes were first discovered in 1954 by Rhodin in cells of mouse kidneys and further characterized by De Duve as small eukaryotic organelles (Rhodin, 1954; De Duve, 1969, 2007). In contrast to chloroplasts and mitochondria, peroxisomes do not contain their own genome and cannot replicate independently. They derive from the endoplasmic reticulum (ER) and are involved in various metabolic pathways (Narendra et al., 2008). In humans, mutations affecting peroxisomal function or biogenesis led to severe, lethal and inheritable diseases (Singh et al., 2009; Crane, 2014). Plant peroxisomes have unique functions contrary to mammalian peroxisomes: (1) beta-oxidation exclusively takes place in plant peroxisomes, (2) plant peroxisomes have a crucial role in the photorespiratory pathway and detoxification of the toxic byproduct 2-phosphoglycolate, (3) plant peroxisomes are indispensable for the biosynthesis of phytohormones and the defense against pathogens (Reumann and Bartel, 2016). The function of peroxisomes depends on the tissue and the life stage of the plant (Deb and Nagotu, 2017). In seed-oil storing plants such as Arabidopsis, peroxisomes are responsible for the breakdown of fatty acid during germination. When plants proceed to photoautotrophic growth, peroxisomes adapt their metabolism toward photorespiration. During senescence peroxisomal metabolism shifts toward fatty acid breakdown (Hayashi and Nishimura, 2006; Graham, 2008; Hu et al., 2012; Goto-Yamada et al., 2015).

**Peroxisomal membrane transport proteins**

Ultimately, many substrates and ions have to cross the peroxisomal membrane to connect the peroxisomal metabolism to the cellular level (reviewed in Plett et al., 2020). Up to date only three peroxisomal transport proteins were described and characterized in Arabidopsis. The peroxisomal ATP-binding cassette transporter belongs to the subfamily 'D' of the ABC transporter family (Theodoulou, 1999; Morita and Imanaka, 2012). Independently identified by four distinct research groups, it goes by various names, which are Peroxisomal ABC transporter 1 (PXA1; (Zolman et al., 2001)), COMATOSE (CTS; (Footitt et al., 2002)), Peroxisome defective 3 (PED3; (Hayashi et al., 2002)), and Acetate non-utilizing 2 (ACN2; (Hooks et al., 2004)). Mutant plants, compromised in PXA1 transport function, show distinct phenotypes related to beta-oxidation. Beyond its role in fatty acid degradation, beta-oxidation plays a vital role in various metabolic and signaling pathways in plants. These pathways include the biosynthesis of crucial signaling and secondary metabolites such as 12-oxo-phytodienoic acid, the precursor of jasmonic acid (Theodoulou et al., 2005), as well as the auxin precursors 2,4-dichlorophenoxybutyric acid (Hayashi et al., 2002) and indole butyric acid (Zolman et al., 2001).

The other two identified transporters belong to the Mitochondrial Carrier family (MCF) which is one of the largest groups of eukaryotic transport proteins. The genome of Arabidopsis encodes for 58 genes of the MCF family (Haferkamp, 2007; Palmieri et al., 2011). The predominant transport mechanism involves a strict 1:1 counter exchange of solutes (antiport). However, uniport activity or proton-coupled symport have also been observed. The MCF carriers accept a considerable number of substrates ranging from nucleotides to di-and tricarboxylates, amino acids and their derivatives (Palmieri et al., 2011; Haferkamp and Schmitz-Esser, 2012; Palmieri, 2014). Despite their name, some MCF carriers have been localized to different subcellular compartments beyond mitochondria, such as the ER, plastids and peroxisomes (Palmieri et al., 2001; Linka et al., 2008; Agrimi et al., 2012; Bernhardt et al., 2012; van Roermund et al., 2016; Kim et al., 2020).

The peroxisomal ATP carrier was first discovered *in Saccharomyces cerevisiae* (*S. cerevisiae*) (Palmieri et al., 2001; van Roermund et al., 2001). In Arabidopsis, two ATP carriers, Peroxisomal Nucleotide Carrier (PNC), PNC1 and PNC2, were identified based on their sequence similarity to the yeast orthologue (Linka et al., 2008). Both, yeast and plant carriers, exhibit an affinity for adenine nucleotides such as ATP, AMP

and ADP as substrates. They act as antiporters, shuttling ATP into the peroxisomes in exchange for either AMP or ADP. ATP is essential for beta-oxidation, as the activation of fatty acid requires ATP (Palmieri et al., 2001; van Roermund et al., 2001; Linka et al., 2008).

In 2012, the Peroxisomal NAD carrier (PXN) was identified in Arabidopsis (Agrimi et al., 2012; Bernhardt et al., 2012). NAD is essential as a cofactor in peroxisomal pathways, such as beta-oxidation, photorespiration, and reactive oxygen species detoxification. *In vitro* transport data showed that PXN catalyzes the transport of NAD, NADH, AMP, ADP and coenzyme A (CoA). Concentration-dependent CoA uptake experiments revealed only a low affinity for CoA, suggesting a less prominent role for PXN to supply peroxisomes with CoA. This also hints to another carrier responsible for the CoA import (Charton et al., 2019). *In vivo* studies, by using various yeast mutants, indicated that PXN facilitates the influx of NAD in exchange for AMP, confirming the role of PXN in beta-oxidation (van Roermund et al., 2016). Interestingly, plants with loss-of-function mutations in the *PXN* gene, exhibit only mild phenotypic alterations in terms of beta-oxidation, suggesting the existence of alternative NAD uptake systems. One possibility might be an additional carrier importing NAD into the peroxisome. Alternatively, NAD might be present during biogenesis from the ER and PXN only replenish the already existing pool. Further, NAD can be regenerated by the peroxisomal malate/oxaloacetate shuttle, which is dependent on a malate dehydrogenase (Pracharoenwattana et al., 2007). Next to its role in beta oxidation, PXN is also involved in photorespiration. During fluctuating light conditions mutant plants show a reduced photosynthesis rate, which can be restored und elevated $CO_2$ concentrations (Li et al., 2018). Due to the higher demand during high-light conditions, PXN supports NADH-generating reactions by importing additional NAD. Eventually, it cannot be excluded that under those conditions PXN could import NADH, which is an accepted substrate in *in vitro* transport studies (Agrimi et al., 2012; Bernhardt et al., 2012; Li et al., 2018)

Besides the specific solute transporters described above, it is widely accepted that the peroxisomal membrane harbors non-selective pore-forming channels (Antonenkov and Hiltunen, 2012). Channels facilitate the transport of ions and small molecules with an electrochemical gradient and are therefore comparable to porins found in the outer membrane of mitochondria and plastids (Linka and Theodoulou, 2013; Charton et al., 2019). The advantages of having both types of transport

mechanisms are (1) high substrate specificity due to the carriers, and (2) fast transport rates of small molecules through pore-forming channels (Antonenkov and Hiltunen, 2012). Studies on isolated leaf peroxisomes confirmed the channel activity for the peroxisomal membrane. The postulated channel showed a single channel conductance of 0.3 nS in 1 M KCl (Reumann et al., 1995; Reumann et al., 1997; Reumann et al., 1998). To date, no protein has been characterized to perform this function in plant peroxisomes.

In 2009 Rokka and colleagues characterized the peroxisomal membrane protein 2 (Pxmp2) from *Mus musculus* (Rokka et al., 2009). *In vitro* electrophysiological measurements demonstrated that Pxmp2 functions as a porin-like channel which allows the transport of small molecules (up to 600 Da) such as glycolate, allantoin and 2-oxoglutarate. Loss-of-function mutants display a rather mild phenotype: *Pxmp2*-deficient mice show partial restriction of uric acid in the liver leading to elevated levels of uric acid in the blood stream. Additionally, the excretion of allantoin, a byproduct of uric acid breakdown, is decreased (Rokka et al., 2009). Pxmp2 belongs to the eukaryotic MPV17/PMP22 family (Dalla Rosa et al., 2014). Members of this family are integral membrane proteins consisting of four alpha-helices (Antonenkov et al., 2015). Studies showed that these proteins can be found in the membrane of mitochondria in addition to peroxisomes (Trott and Morano, 2004; Spinazzola et al., 2006; Rokka et al., 2009; Dallabona et al., 2010; Dalla Rosa et al., 2014; Kodani et al., 2022). In plants, members of this family might even be localized in the chloroplast (Lunn et al., 2022). Based on phylogenetic analysis mammals contain four homologs of the *Mus musculus Pxmp2*: *Pxmp2/PMP22*, *Mpv17* and two *Mpv17-like* genes with a C-terminal Mpv17/PMP22 domain (Dalla Rosa et al., 2014). Mutations in the human *Mpv17* gene lead to the Mitochondrial DNA Depletion Syndrome. Human MPV17 localizes to the inner mitochondrial membrane and was characterized as a non-selective channel. *In vitro* investigations showed that MPV17 has a weak cation selectivity, and gating properties are dependent on redox potential and pH (Antonenkov et al., 2015). Based on the high negative membrane potential of the inner mitochondrial membrane, these results propose a function of MPV17 in the modulation of the mitochondrial membrane potential by opening and closing under distinct external stimuli (Antonenkov et al., 2015).

The baker's yeast *S. cerevisiae* contains two genes encoding for the MPV17/PMP22 family: *Stress-inducible yeast Mpv17* (*SYM1*; *YLR251W*) and

*YOR292cp*, which encodes for a peroxisomal localized protein (Trott and Morano, 2004; Antonenkov and Hiltunen, 2012). SYM1 localizes to the inner mitochondrial membrane and has been studied as a model for human MPV17. SYM1 is essential for the maintenance of mitochondrial respiration under elevated temperatures on non-fermentable carbon sources such as ethanol (Trott and Morano, 2004). Electrophysiological measurements confirmed channel activity for SYM1. Recombinant expressed SYM1 forms a channel in lipid membranes and showed a voltage-dependent closure of the channel (Reinhold et al., 2012).

In Arabidopsis, *PMP22* has the highest sequence similarity to *Pxmp2* (Dalla Rosa et al., 2014). It was first identified by subcellular fractionation (Tugal et al., 1999) which was later confirmed by peroxisomal proteomic studies (Reumann et al., 2007; Reumann et al., 2009). Similar to its orthologues, Arabidopsis PMP22 may function as a non-selective pore-forming channel. The functional and physiological role remains unknown.

Peroxisomal function is crucial for plant performance, as they are involved a several metabolic and biochemical pathways. For instance, most of the transport proteins remain unknown. In contrast to mitochondria and chloroplasts, targeting of peroxisomal membrane proteins is poorly understood (Küchler and Soll, 2001; Reumann et al., 2007; Møller et al., 2020). Soluble, matrix targeted proteins contain either a C- or N-terminal PTS1 or PTS2 motif, the mechanism or peroxisomal membrane targeting remains unsolved (Reumann et al., 2007). Therefore, the identification of highly needed transport proteins is challenging.

## References

**Agrimi G, Russo A, Pierri CL, Palmieri F** (2012) The peroxisomal NAD+ carrier of Arabidopsis thaliana transports coenzyme A and its derivatives. J Bioenerg Biomembr **44:** 333-340

**Agrimi G, Russo A, Scarcia P, Palmieri F** (2012) The human gene SLC25A17 encodes a peroxisomal transporter of coenzyme A, FAD and NAD+. Biochem J **443:** 241-247

**Alberts B JA, Lewis J, et al.** (2002) Molecular Biology of the Cell. 4th edition. Garland Science, New York

**Antonenkov VD, Hiltunen JK** (2012) Transfer of metabolites across the peroxisomal membrane. Biochim Biophys Acta **1822:** 1374-1386

**Antonenkov VD, Isomursu A, Mennerich D, Vapola MH, Weiher H, Kietzmann T, Hiltunen JK** (2015) The Human Mitochondrial DNA Depletion Syndrome Gene MPV17 Encodes a Non-selective Channel That Modulates Membrane Potential. J Biol Chem **290:** 13840-13861

**Bar-Even A, Noor E, Lewis NE, Milo R** (2010) Design and analysis of synthetic carbon fixation pathways. Proc Natl Acad Sci U S A **107:** 8889-8894

**Barbier-Brygoo H, Joyard JP, Alain and , Ranjeva R** (1997) Intracellular compartmentation and plant cell signalling. Trends Plant Sci **2**

**Baune M-C, Lansing H, Fischer K, Meyer T, Charton L, Linka N, von Schaewen A** (2020) The Arabidopsis Plastidial Glucose-6-Phosphate Transporter GPT1 is Dually Targeted to Peroxisomes via the Endoplasmic Reticulum. The Plant Cell **32:** 1703-1726

**Bernhardt K, Wilkinson S, Weber AP, Linka N** (2012) A peroxisomal carrier delivers NAD(+) and contributes to optimal fatty acid degradation during storage oil mobilization. Plant J **69:** 1-13

**Bräutigam A, Weber AP** (2011) Do metabolite transport processes limit photosynthesis? Plant Physiol **155:** 43-48

**Cavalier-Smith T** (2000) Membrane heredity and early chloroplast evolution. Trends Plant Sci **5**

**Chang RL, Ghamsari L, Manichaikul A, Hom EFY, Balaji S, Fu W, Shen Y, Hao T, Palsson BØ, Salehi-Ashtiani K, Papin JA** (2011) Metabolic network reconstruction of Chlamydomonas offers insight into light‐driven algal metabolism. Molecular Systems Biology **7:** 518

**Charton L, Plett A, Linka N** (2019) Plant peroxisomal solute transporter proteins. J Integr Plant Biol **61:** 817-835

**Colleoni C, Linka M, Deschamps P, Handford MG, Dupree P, Weber AP, Ball SG** (2010) Phylogenetic and biochemical evidence supports the recruitment of an ADP-glucose translocator for the export of photosynthate during plastid endosymbiosis. Mol Biol Evol **27:** 2691-2701

**Cove D** (2005) The moss Physcomitrella patens. Annu Rev Genet **39:** 339-358

**Crane DI** (2014) Revisiting the neuropathogenesis of Zellweger syndrome. Neurochemistry International **69:** 1-8

**Dalla Rosa I, Durigon R, Pearce SF, Rorbach J, Hirst EM, Vidoni S, Reyes A, Brea-Calvo G, Minczuk M, Woellhaf MW, Herrmann JM, Huynen MA, Holt IJ, Spinazzola A** (2014) MPV17L2 is required for ribosome assembly in mitochondria. Nucleic Acids Res **42:** 8500-8515

**Dallabona C, Marsano RM, Arzuffi P, Ghezzi D, Mancini P, Zeviani M, Ferrero I, Donnini C** (2010) Sym1, the yeast ortholog of the MPV17 human disease protein, is a stress-

induced bioenergetic and morphogenetic mitochondrial modulator. Hum Mol Genet **19:** 1098-1107

**De Duve C** (1969) Evolution of the peroxisome. Ann N Y Acad Sci **168:** 369-381

**De Duve C** (2007) The origin of eukaryotes: a reappraisal. Nature Reviews Genetics **8**

**Deb R, Nagotu S** (2017) Versatility of peroxisomes: An evolving concept. Tissue Cell **49:** 209-226

**Drew D, Boudker O** (2016) Shared Molecular Mechanisms of Membrane Transporters. Annual Review of Biochemistry **85:** 543-572

**Eicks M, Maurino V, Knappe S, Flugge UI, Fischer K** (2002) The plastidic pentose phosphate translocator represents a link between the cytosolic and the plastidic pentose phosphate pathways in plants. Plant Physiol **128:** 512-522

**Facchinelli F, Weber AP** (2011) The metabolite transporters of the plastid envelope: an update. Front Plant Sci **2:** 50

**Fick A** (1995) On liquid diffusion. Journal of Membrane Science **100:** 33-38

**Fischer K, Kammerer B, Arbinger B, Weber A, Häusler RE, Flügge U-I** (1997) A New Class of Plastidic PhosphateTranslocators: A Putative Link between Primary and Secondary Metabolism by the Phosphoenolpyruvate/Phosphate Antiporter. The Plant Cell **9:** 453-462

**Flügge U-I** (1999) PHOSPHATE TRANSLOCATORS IN PLASTIDS. Annu. Rev. Plant Physiol. Plant Mol. **50:** 27-45

**Flügge UI, Heldt HW** (1984) The phosphate—triose phosphate—phosphoglycerate translocator of the chloroplast. TIBS

**Footitt S, Slocombe SP, Larner V, Smita Kurup , Wu Y, Larson T, Graham I, Baker A, Holdsworth M** (2002) Control of germination and lipid mobilization by COMATOSE, the Arabidopsis homologue of human ALDP. The EMBO Journal **21:** 2912-2922

**Goto-Yamada S, Mano S, Yamada K, Oikawa K, Hosokawa Y, Hara-Nishimura I, Nishimura M** (2015) Dynamics of the Light-Dependent Transition of Plant Peroxisomes. Plant Cell Physiol **56:** 1264-1271

**Gould SB, Waller RF, McFadden GI** (2008) Plastid evolution. Annu Rev Plant Biol **59:** 491-517

**Graham IA** (2008) Seed storage oil mobilization. Annu Rev Plant Biol **59:** 115-142

**Gutman BL, Niyogi KK** (2004) Chlamydomonas and Arabidopsis. A dynamic duo. Plant Physiol **135:** 607-610

**Haferkamp I** (2007) The diverse members of the mitochondrial carrier family in plants. FEBS Lett **581:** 2375-2379

**Haferkamp I, Linka N** (2012) Functional expression and characterisation of membrane transport proteins. Plant Biology **14:** 675-690

**Haferkamp I, Schmitz-Esser S** (2012) The plant mitochondrial carrier family: functional and evolutionary aspects. Front Plant Sci **3:** 2

**Hattenbach A, Müller-Rober B, Nast C, Heineke D** (1997) Antisense Repression of Both ADP-Glucose Pyrophosphorylase and Triose Phosphate Translocator Modifies Carbohydrate Partitioning in Potato leaves. Plant Physiology **115:** 471-475

**Häusler RE, Geimer S, Kunz HH, Schmitz J, Dormann P, Bell K, Hetfeld S, Guballa A, Flügge UI** (2009) Chlororespiration and grana hyperstacking: how an Arabidopsis double mutant can survive despite defects in starch biosynthesis and daily carbon export from chloroplasts. Plant Physiol **149:** 515-533

**Hayashi M, Nishimura M** (2006) Arabidopsis thaliana--a model organism to study plant peroxisomes. Biochim Biophys Acta **1763:** 1382-1391

**Hayashi M, Nito K, Takei-Hoshi R, Yagi M, Kondo M, Suenaga A, Yamaya T, Nishimura M** (2002) Ped3p is a Peroxisomal ATP-Binding Cassette Transporter that might Supply Substrates for Fatty Acid β-Oxidation. Plant Cell Physiol **43:** 1-11

**Heinig U, Gutensohn M, Dudareva N, Aharoni A** (2013) The challenges of cellular compartmentalization in plant metabolic engineering. Curr Opin Biotechnol **24:** 239-246

**Herrmann KM** (1995) The Shikimate Pathway: Early Steps in the Biosynthesis of Aromatic Compounds. The Plant Cell **7:** 907-919

**Hoegh-Guldberg O, and Coauthors,** (2018) Impacts of 1.5°C global warming on natural and human systems.Global Warming of 1.5°C: An IPCC Special Report. IPCC**:** 175–311

**Hooks MA, Turner JE, Murphy EC, Graham IA** (2004) Acetate non-utilizing mutants of Arabidopsis: evidence that organic acids influence carbohydrate perception in germinating seedlings. Mol Genet Genomics **271:** 249-256

**Hu J, Baker A, Bartel B, Linka N, Mullen RT, Reumann S, Zolman BK** (2012) Plant peroxisomes: biogenesis and function. Plant Cell **24:** 2279-2303

**Huang W, Krishnan A, Plett A, Meagher M, Linka N, Wang Y, Ren B, Findinier J, Redekop P, Fakhimi N, Kim RG, Karns DA, Boyle N, Posewitz MC, Grossman AR** (2023) Chlamydomonas mutants lacking chloroplast TRIOSE PHOSPHATE TRANSPORTER3 are metabolically compromised and light sensitive. Plant Cell **35:** 2592-2614

**Initiative TAG** (2000) Analysis of the genome sequence of the flowering plant *Arabidopsis thaliana*. Nature **408:** 796-815

**Kammerer B, Fischer K, Hilpert B, Schubert S, Gutensohn M, Weber A, Flügge U-I** (1998) Molecular Characterization of a Carbon Transporter in Plastids from Heterotrophic Tissues: The Glucose 6-Phosphate/ Phosphate Antiporter. The Plant Cell **10:** 105–117

**Kim YI, Nam IK, Lee DK, Bhandari S, Charton L, Kwak S, Lim JY, Hong K, Kim SJ, Lee JN, Kwon SW, So HS, Linka N, Park R, Choe SK** (2020) Slc25a17 acts as a peroxisomal coenzyme A transporter and regulates multiorgan development in zebrafish. J Cell Physiol **235:** 151-165

**Kodani A, Yamaguchi M, Itoh R, Huynh MA, Yoshida H** (2022) A Drosophila model of the neurological symptoms in Mpv17-related diseases. Sci Rep **12:** 22632

**Küchler M, Soll J** (2001) From nuclear genes to chloroplast localized proteins. Plant Science **161:** 379-389

**Li J, Tietz S, Cruz JA, Strand DD, Xu Y, Chen J, Kramer DM, Hu J** (2018) Photometric screens identified Arabidopsis peroxisome proteins that impact photosynthesis under dynamic light conditions. The Plant Journal **97:** 460-474

**Linka M, Jamai A, Weber AP** (2008) Functional characterization of the plastidic phosphate translocator gene family from the thermo-acidophilic red alga Galdieria sulphuraria reveals specific adaptations of primary carbon partitioning in green plants and red algae. Plant Physiol **148:** 1487-1496

**Linka N, Theodoulou FL** (2013) Metabolite transporters of the plant peroxisomal membrane - known and unknown. Subcell Biochem **69:** 169-194

**Linka N, Theodoulou FL, Haslam RP, Linka M, Napier JA, Neuhaus HE, Weber AP** (2008) Peroxisomal ATP import is essential for seedling development in Arabidopsis thaliana. Plant Cell **20:** 3241-3257

**Lunn D, Smith GA, Wallis JG, Browse J** (2022) Overexpression mutants reveal a role for a chloroplast MPD protein in regulation of reactive oxygen species during chilling in Arabidopsis. J Exp Bot **73:** 2666-2681

**Matsuzaki M, Misumi O, Shin-i T, Maruyama S, Takahara M, Miyagishima S-y, Mori T, Nishida K, Yagisawa F, Nishida K, Yoshida Y, Nishimura Y, *et al*.** (2004) Genome sequence of the ultrasmall unicellular red alga *Cyanidioschyzon merolae* 10D. Nature **428**

**Merchant SS, Prochnik SE, Vallon O, Harris EH, Karpowitz SJ, Witman GB, Terry A, Salamov A, Fritz-Laylin LK, Marechal-Drouard L, Marshall WF, Qu LH, *et al*.** (2007) The *Chlamydomonas* Genome Reveals the Evolution of Key Animal and Plant Functions. Science **318:** 245-250

**Møller I, Rao R, Jiang Y, Thelen J, Xu D** (2020) Proteomic and Bioinformatic Profiling of Transporters in Higher Plant Mitochondria. Biomolecules **10**

**Morita M, Imanaka T** (2012) Peroxisomal ABC transporters: structure, function and role in disease. Biochim Biophys Acta **1822:** 1387-1396

**Narendra D, Satoshi S, Kazuo H, Daisuke M, Tokumasa H, Takao S** (2008) A Study on the Origin of Peroxisomes: Possibility of Actinobacteria Symbiosis. Nature Precedings

**Ndikuryayo F, Yang W-C** (2023) New Insights into the Interactions between Herbicides: Trends from Recent Studies. Journal of Agricultural and Food Chemistry **71:** 10970-10981

**Niewiadomski P, Knappe S, Geimer S, Fischer K, Schulz B, Unte US, Rosso MG, Ache P, Flugge UI, Schneider A** (2005) The Arabidopsis plastidic glucose 6-phosphate/phosphate translocator GPT1 is essential for pollen maturation and embryo sac development. Plant Cell **17:** 760-775

**Palmieri F** (2014) Mitochondrial transporters of the SLC25 family and associated diseases: a review. J Inherit Metab Dis **37:** 565-575

**Palmieri F, Pierri CL, De Grassi A, Nunes-Nesi A, Fernie AR** (2011) Evolution, structure and function of mitochondrial carriers: a review with new insights. Plant J **66:** 161-181

**Palmieri L, Rottensteiner H, Girzalsky W, Scarcia P, Palmieri F, Erdmann R** (2001) Identification and functional reconstitution of the yeast peroxisomal adenine nucleotide transporter. The EMBO Journal **20:** 5049-5059

**Plett A, Charton L, Linka N** (2020) Peroxisomal Cofactor Transport. Biomolecules **10**

**Pracharoenwattana I, Cornah JE, Smith SM** (2007) Arabidopsis peroxisomal malate dehydrogenase functions in β-oxidation but not in the glyoxylate cycle. The Plant Journal **50:** 381-390

**Price DC, Chan CX, Yoon HS, Yang EC, Qiu H, Weber APM, Schwacke R, Gross J, Blouin NA** (2012) *Cyanophora paradoxa* Genome Elucidates Origin of Photosynthesis in Algae and Plants. Science **335:** 843-847

**Price DC, Goodenough UW, Roth R, Lee JH, Kariyawasam T, Mutwil M, Ferrari C, Facchinelli F, Ball SG, Cenci U, Chan CX, Wagner NE, Yoon HS, Weber APM, Bhattacharya D** (2019) Analysis of an improved Cyanophora paradoxa genome assembly. DNA Res **26:** 287-299

**Reinhold R, Kruger V, Meinecke M, Schulz C, Schmidt B, Grunau SD, Guiard B, Wiedemann N, van der Laan M, Wagner R, Rehling P, Dudek J** (2012) The channel-forming Sym1 protein is transported by the TIM23 complex in a presequence-independent manner. Mol Cell Biol **32:** 5009-5021

**Reumann S, Babujee L, Ma C, Wienkoop S, Siemsen T, Antonicelli GE, Rasche N, Luder F, Weckwerth W, Jahn O** (2007) Proteome analysis of Arabidopsis leaf peroxisomes reveals novel targeting peptides, metabolic pathways, and defense mechanisms. Plant Cell **19:** 3170-3193

**Reumann S, Bartel B** (2016) Plant peroxisomes: recent discoveries in functional complexity, organelle homeostasis, and morphological dynamics. Curr Opin Plant Biol **34:** 17-26

**Reumann S, Bettermann M, Benz R, Heldt HW** (1997) Evidence for the Presence of a Porin in the Membrane of Glyoxysomes of Castor Bean. Plant Physiol **115:** 891-899

**Reumann S, Maier E, Benz R, Heldt HW** (1995) The membrane of leaf peroxisomes contains a porin-like channel. J Biol Chem **270:** 17559-17565

**Reumann S, Maier E, Heldt HW, Benz R** (1998) Permeability properties of the porin of spinach leaf peroxisomes. Eur J Biochem **251:** 359-366

**Reumann S, Quan S, Aung K, Yang P, Manandhar-Shrestha K, Holbrook D, Linka N, Switzenberg R, Wilkerson CG, Weber AP, Olsen LJ, Hu J** (2009) In-depth proteome analysis of Arabidopsis leaf peroxisomes combined with in vivo subcellular targeting verification indicates novel metabolic and regulatory functions of peroxisomes. Plant Physiol **150:** 125-143

**Rhodin J** (1954) Correlation of ultrastructural organization and function in normal and experimentally changed proximal convoluted tubule cells of the mouse kidney. Thesis Kalolinska Instutet

**Riesmeier JW, Flügge U-I, Schulz B, Heineke D, Heldt H-W, Willmitzer L, Frommer WB** (1993) Antisense repression of the chloroplast triose phosphate translocator affects carbon partitioning in transgenic potato plants. Proc Natl Acad Sci USA **90:** 6160-6164

**Roell MS, Schada von Borzykowski L, Westhoff P, Plett A, Paczia N, Claus P, Urte S, Erb TJ, Weber APM** (2021) A synthetic C4 shuttle via the beta-hydroxyaspartate cycle in C3 plants. Proc Natl Acad Sci U S A **118**

**Roell MS, Zurbriggen MD** (2020) The impact of synthetic biology for future agriculture and nutrition. Curr Opin Biotechnol **61:** 102-109

**Rokka A, Antonenkov VD, Soininen R, Immonen HL, Pirila PL, Bergmann U, Sormunen RT, Weckstrom M, Benz R, Hiltunen JK** (2009) Pxmp2 is a channel-forming protein in Mammalian peroxisomal membrane. PLoS One **4:** e5090

**Rolletschek H, Nguyen TH, Hausler RE, Rutten T, Gobel C, Feussner I, Radchuk R, Tewes A, Claus B, Klukas C, Linemann U, Weber H, Wobus U, Borisjuk L** (2007) Antisense inhibition of the plastidial glucose-6-phosphate/phosphate translocator in Vicia seeds shifts cellular differentiation and promotes protein storage. Plant J **51:** 468-484

**Schneider A, Häusler RE, Kolukisaoglu Ü, Kunze R, Graaff Evd, Schwacke R, Catoni E, Desimone M, Flügge U-I** (2002) An Arabidopsis thaliana knock-out mutant of the chloroplast triose phosphate/phosphate translocator is severely compromised only when starch synthesis, but not starch mobilisation is abolished. The Plant Journal **32:** 685–699

**Singh I, Singh AK, Contreras MA** (2009) Peroxisomal Dysfunction in Inflammatory Childhood White Matter Disorders: An Unexpected Contributor to Neuropathology. Journal of Child Neurology **24:** 1147-1157

**Spinazzola A, Viscomi C, Fernandez-Vizarra E, Carrara F, D'Adamo P, Calvo S, Marsano RM, Donnini C, Weiher H, Strisciuglio P, Parini R, Sarzi E, Chan A, DiMauro S, Rotig A, Gasparini P, Ferrero I, Mootha VK, Tiranti V, Zeviani M** (2006) MPV17 encodes an inner mitochondrial membrane protein and is mutated in infantile hepatic mitochondrial DNA depletion. Nat Genet **38:** 570-575

**Streatfield SJ, Weber A, Kinsman EA, Häusler RE, Li J, Post-Beittenmiller D, Kaiser WM, Pyke KA, Flügge U-I, Chorya J** (1999) The Phosphoenolpyruvate/Phosphate Translocator Is Required for Phenolic Metabolism, Palisade Cell Development, and Plastid-Dependent Nuclear Gene Expression. The Plant Cell **11:** 1609–1621

**Theodoulou FL** (1999) Plant ABC transporters. Biochimica et Biophys Acta **1465:** 79-103

**Theodoulou FL, Job K, Slocombe SP, Footitt S, Holdsworth M, Baker A, Larson TR, Graham IA** (2005) Jasmonic acid levels are reduced in COMATOSE ATP-binding cassette transporter mutants. Implications for transport of jasmonate precursors into peroxisomes. Plant Physiol **137:** 835-840

**Tollefson J** (2021) Top Climate Scientists Are Sceptical That Nations Can Rein In Global Warming. Nature

**Trott A, Morano KA** (2004) SYM1 is the stress-induced Saccharomyces cerevisiae ortholog of the mammalian kidney disease gene Mpv17 and is required for ethanol metabolism and tolerance during heat shock. Eukaryot Cell **3:** 620-631

**Tugal HB, Pool M, Baker A** (1999) Arabidopsis 22-Kilodalton Peroxisomal Membrane Protein. Nucleotide Sequence Analysis and Biochemical Characterization. Plant Physiology **120:** 309–320

**Tzin V, Galili G** (2010) The Biosynthetic Pathways for Shikimate and Aromatic Amino Acids in Arabidopsis thaliana. *In* The Arabidopsis Book,

**UnitedNations** (2022) World Population Prospects 2022: Summary of Results.

**van Roermund CW, Drissen R, van Den Berg M, Ijlst L, Hettema EH, Tabak HF, Waterham HR, Wanders RJ** (2001) Identification of a peroxisomal ATP carrier required for medium-chain fatty acid beta-oxidation and normal peroxisome proliferation in Saccharomyces cerevisiae. Mol Cell Biol **21:** 4321-4329

**van Roermund CW, Schroers MG, Wiese J, Facchinelli F, Kurz S, Wilkinson S, Charton L, Wanders RJ, Waterham HR, Weber AP, Link N** (2016) The Peroxisomal NAD Carrier from Arabidopsis Imports NAD in Exchange with AMP. Plant Physiol **171:** 2127-2139

**Wada N, Ueta R, Osakabe Y, Osakabe K** (2020) Precision genome editing in plants: state-of-the-art in CRISPR/Cas9-based genome engineering. BMC Plant Biology **20**

**Weber AP, Linka N** (2011) Connecting the plastid: transporters of the plastid envelope and their role in linking plastidial with cytosolic metabolism. Annu Rev Plant Biol **62:** 53-77

**Weber AP, Schwacke R, Flugge UI** (2005) Solute transporters of the plastid envelope membrane. Annu Rev Plant Biol **56:** 133-164

**Weber APM, Bar-Even A** (2019) Update: Improving the Efficiency of Photosynthetic Carbon Reactions. Plant Physiol **179:** 803-812

**Yoon HS, Hackett JD, Ciniglia C, Pinto G, Bhattacharya D** (2004) A molecular timeline for the origin of photosynthetic eukaryotes. Mol Biol Evol **21:** 809-818

**Zeng R, Lv C, Zang J, Zhang T, Zhao G** (2022) Designing Stacked Assembly of Type III Rubisco for CO2 Fixation with Higher Efficiency. Journal of Agricultural and Food Chemistry **70:** 7049-7057

**Zolman BK, Silva ID, Bartel B** (2001) The Arabidopsis pxa1 Mutant Is Defective in an ATP-Binding Cassette Transporter-Like Protein Required for Peroxisomal Fatty Acid β-Oxidation. Plant Physiology **127:** 1266-1278

# Manuscript I

## Peroxisomal Cofactor Transport

**Status**: published

**Author contributions**: Conceptualization, N.L.; writing and editing, **A.P**., L.C., and N.L.

biomolecules

MDPI

*Review*

# Peroxisomal Cofactor Transport

**Anastasija Plett, Lennart Charton and Nicole Linka ***

Institute of Plant Biochemistry and Cluster of Excellence on Plant Sciences (CEPLAS), Heinrich Heine University, Universitätsstrasse 1, 40,225 Düsseldorf, Germany; Anastasija.Plett@hhu.de (A.P.); Lennart.Charton@hhu.de (L.C.)
* Correspondence: Nicole.Linka@hhu.de; Tel.: +49-(0)211-81-10412; Fax: +49-(0)211-81-13706

Academic Editor: Ferdinando Palmieri
Received: 2 July 2020; Accepted: 7 August 2020; Published: 12 August 2020

check for updates

**Abstract:** Peroxisomes are eukaryotic organelles that are essential for growth and development. They are highly metabolically active and house many biochemical reactions, including lipid metabolism and synthesis of signaling molecules. Most of these metabolic pathways are shared with other compartments, such as Endoplasmic reticulum (ER), mitochondria, and plastids. Peroxisomes, in common with all other cellular organelles are dependent on a wide range of cofactors, such as adenosine 5'-triphosphate (ATP), Coenzyme A (CoA), and nicotinamide adenine dinucleotide (NAD). The availability of the peroxisomal cofactor pool controls peroxisome function. The levels of these cofactors available for peroxisomal metabolism is determined by the balance between synthesis, import, export, binding, and degradation. Since the final steps of cofactor synthesis are thought to be located in the cytosol, cofactors must be imported into peroxisomes. This review gives an overview about our current knowledge of the permeability of the peroxisomal membrane with the focus on ATP, CoA, and NAD. Several members of the mitochondrial carrier family are located in peroxisomes, catalyzing the transfer of these organic cofactors across the peroxisomal membrane. Most of the functions of these peroxisomal cofactor transporters are known from studies in yeast, humans, and plants. Parallels and differences between the transporters in the different organisms are discussed here.

**Keywords:** peroxisomes; metabolism; carrier; cofactor

## 1. Introduction

Peroxisomes are eukaryotic organelles that are surrounded by a single lipid bilayer membrane [1,2]. They fulfil a range of metabolic functions, which are essential for development and cellular signaling. Depending on the organism, cell type, growth, and environmental conditions, peroxisomes participate in the detoxification of reactive oxygen/nitrogen species, β-oxidation of fatty acids, synthesis of plasminogen, isoprenoids, penicillin, phylloquinone, glycine betaine, biotin and hormonal signal molecules, catabolism of purines, polyamines, amino acids, and methanol, as well as in the glyoxylate cycle, pentose phosphate pathway, and photorespiration [1,2]. Currently, the list of peroxisomal tasks appears to be far from exhaustive.

The multiple roles of peroxisomes depend on the functional interplay with other organelles. A large number of chemically diverse metabolites consumed and released by the peroxisomes have to be exchanged between subcellular compartments [3–6]. The transfer of metabolites across the peroxisomal membrane has been a controversial scientific debate for several decades. Initial studies on isolated peroxisomes suggested that the peroxisomes are freely permeable. However, this in vitro permeability was later withdrawn and explained by disruptions of protein/membrane structures during peroxisome isolation procedure. The current consensus is that transport proteins are responsible for the transfer of solutes into and out of peroxisomes [3–6]. Electrophysiological experiments using purified peroxisomal

membranes revealed the existence of nonspecific porin-like channels that allow the free diffusion of low-molecular weight compounds (<300 Da) with a broad substrate specificity [7,8]. In addition, genetic mutant analyses discovered genes encoding for specific carrier proteins that catalyze the flux of larger hydrophilic solutes, like cofactor molecules, such as ATP, Coenzyme A (CoA), and NAD [9–13].

The transport of these cofactors has a crucial impact on peroxisome function. For example, ATP, CoA, and NAD are required for peroxisomal fatty-acid activation and oxidation via β-oxidation, which is a conserved metabolic pathway in yeast, mammals, humans, and plants [3,14,15]. These cofactor molecules are synthesized outside peroxisomes. Due to their size and charge, they cannot pass the lipid bilayer by free diffusion. Thus, peroxisomal transport proteins are mandatory to replenish the cofactor demand of the peroxisomal enzymes [3,14,15]. Notably, peroxisomes offer an alternative route for cofactor transport. In contrast to mitochondria and chloroplasts, peroxisomes lack a protein synthesis machinery and have the capacity to import folded and even oligomeric proteins [16–18]. It was assumed that the import of tightly bound cofactors, such as flavin adenine dinucleotide (FAD) and thiamine pyrophosphate (TPP), could be coupled to protein transport, as is the case for the Tat system of bacteria and chloroplasts, which export folded proteins to the periplasm or the thylakoid lumen, respectively [19]. For instance, the FAD-dependent alcohol oxidase and acyl-CoA oxidase bind their cofactor FAD in the cytosol and are then imported as fully folded holo-enzymes into yeast peroxisomes [20,21]. Such a cofactor-coupled protein import mechanism was also reported for the mammalian 2-hydroxyacyl-CoA lyase, a TPP-dependent enzyme [22]. However, specific cofactor carrier proteins for ATP, CoA, and NAD are essential to generate and maintain a physiologically relevant peroxisomal pool of free cofactor molecules, which are essential for an efficient and functional metabolism.

Members of the mitochondrial carrier family (MCF) that mediate the transport of a wide range of organic cofactors into peroxisomes have been discovered in diverse eukaryotes [23–27]. This eukaryotic group of membrane transport proteins corresponds to the 2.A.29 family according to the Transporter Classification Database (TCDB) and is named in mammals solute carrier family 25 (SLC25) [28]. MCF is a large family of proteins with about 30 members in yeast and more than 50 in humans and plants. Although the name of this family suggests that they are exclusively located to mitochondria, several members are present in other organelles, such as peroxisomes, endoplasmic reticulum, chloroplasts, and plasma membrane [23,24,26,27,29]. Despite their conserved basic structure composed of three repetitive modules, MCF proteins are highly diverse in terms of substrate specificity and transport mode. They mediate the transport of a large variety of solutes that differ in size and nature, such as protons, inorganic ions, inorganic form of "phosphate", carboxylic acids, amino acids, and nucleotides. In most cases, MCF members mediate a strict counter-exchange but also operate as a uniporter or symporter [26,27,29,30]. These features suggest that this protein family was most likely exploited as a valuable basis for a fast establishment of a subset of carriers with a broad range of different transport functions in the cell during eukaryotic evolution.

This review deals with MCF proteins that are known to be peroxisomal cofactor carriers in budding yeast *Saccharomyces cerevisiae*, humans, and the model plant *Arabidopsis thaliana* and highlights the recent progress on their biochemical and physiological function for the peroxisomal metabolism.

## 2. Cofactor Transport for Yeast Peroxisomes

The main metabolic function of peroxisomes in *S. cerevisiae* is the degradation of fatty acids via β-oxidation to use these compounds as carbon and energy source [31]. The pathway depends on the availability of ATP, CoA, and NAD in the peroxisomal matrix (Figure 1). The uptake of fatty acids into peroxisomes occurs via two routes depending on the fatty-acid chain length [32]. Small- and medium-chain fatty acids (C4–12) are transported as free fatty acids through passive diffusion, while long-chain fatty acids (C14–20) are delivered as acyl-CoA esters by a peroxisomal ATP-binding cassette (ABC) transporter Pxa1p-Pxa2p [33,34]. However, during this transport process the CoA moiety is cleaved off. Thus, both entry pathways for fatty acids lead to the delivery of nonesterified fatty acids [35]. However, prior to peroxisomal β-oxidation, these free fatty acids must

be activated to acyl-CoA esters. This intraperoxisomal esterification is catalyzed by a peroxisomal acyl-CoA synthetase Faa2p and/or a bifunctional fatty-acid transporter Fat1p at the peroxisomal membrane and requires ATP and CoA [35]. Once the acyl-CoA esters are fed into the peroxisomal β-oxidation cycle, their oxidative degradation requires NAD as an electron acceptor [31].

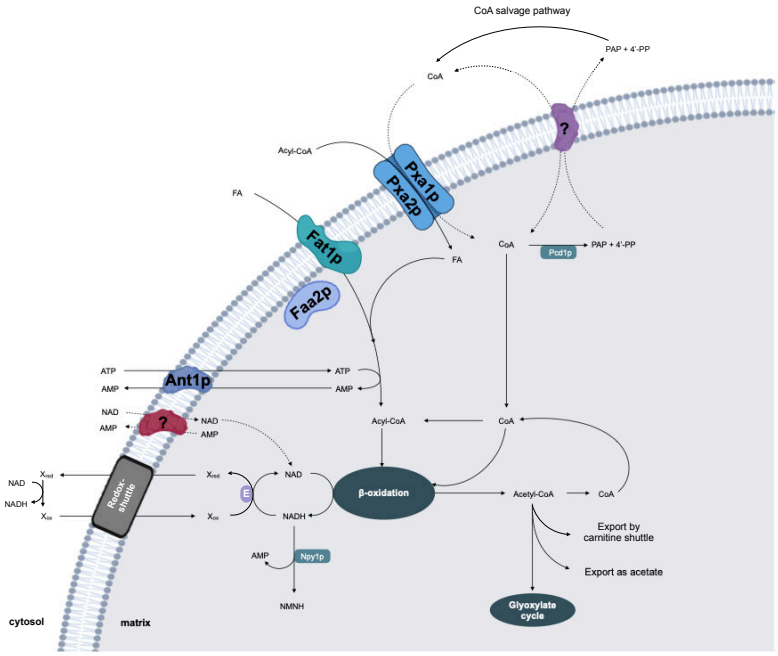


**Figure 1.** Model for the peroxisomal cofactor transport in yeast. Ant1p: peroxisomal ATP carrier 1; FA, fatty acid; Faa2p: peroxisomal acyl-CoA synthetase 2 (associated at the matrix side of the peroxisomal membrane); Fat1p: peroxisomal acyl-CoA synthetase, also known as peroxisomal fatty-acid transporter 1 (integral membrane protein); NMN(H): nicotinamide mononucleotide (reduced); Npy1p: peroxisomal NAD(H) diphosphatase 1, catalyzing the hydrolysis of NADH to AMP and NMN(H); PAP: adenosine 3′,5′-diphosphate; 4′-PP: 4′-phospho-pantetheine; Pcd1p: peroxisomal CoA diphosphatase 1, catalyzing the hydrolysis of CoA to PAP and 4′-PP; Pxa1p/Pxa2p: peroxisomal ATP-binding cassette (ABC) transporter, mediating the import of fatty acids as acyl-CoA esters; (?): proposed cofactor carrier proteins.

In 2001, two groups independently identified one MCF member from *S. cerevisiae* as a peroxisomal ATP carrier, which was named Ant1p for Adenine nucleotide transporter 1 [9,10]. Disruption of Ant1p results in yeast cells that exhibit an impaired growth in the presence of medium-chain fatty acids, such as lauric acid, as the sole carbon source. In vivo activity of the ATP-consuming firefly luciferase, targeted to *ant1*Δ peroxisomes, was strongly reduced, implying a depleted peroxisomal ATP content in the intact mutant cells [36]. Gene expression analysis revealed the presence of oleate response elements in the promoters of ANT1 and other β-oxidation genes, which are responsible for an induced gene expression via the Pip2p-Oaf1p transcription factor when grown in the presence of the long-chain fatty acid, oleic acid [36]. These observations led to the hypothesis that Ant1p is necessary for metabolizing fatty acids via peroxisomal β-oxidation as a carbon and energy source [9,10].

Direct transport studies with purified Ant1p protein provided conclusive evidence for the role of Ant1p as an ATP transporter [9]. *Escherichia coli* has been a suitable system for expression, purification,

and subsequent functional reconstitution into liposomes. In vitro uptake studies using diverse nucleotides as substrates demonstrated that Ant1p specifically catalyzes the transport of ATP, ADP, and AMP [9]. However, the protein does not accept other ATP-related molecules, such as CoA or NAD, as transport substrates [37]. Another unique characteristic of Ant1p is that it exhibits two transport modes. It mediates not only the exchange but also catalyzes the uniport of adenine nucleotides [9].

Based on its transport features, two physiological functions for Ant1p can be concluded: (1) It facilitates the uptake of cytosolic ATP in a unidirectional mode for loading peroxisomes with ATP early in their genesis. (2) During high rates of β-oxidation, ATP is directly consumed by the ATP-dependent fatty-acid activation, releasing high amounts of AMP. Ant1p ensures the counter-exchange of ATP into peroxisomes against AMP to avoid accumulation of the latter molecule in the peroxisome, which would, on the other hand, deplete the nucleotide pool in the cytosol [9,10]. However, the loss of the Ant1p in *S. cerevisiae* did not fully abolish fatty-acid oxidation activity [10]. The *ant1*Δ mutant was still able to degrade lauric acid and oleic acid. Moreover, 20% of the peroxisomal luciferase activity was still detectable, indicating the presence of low ATP levels in *ant1*Δ peroxisomes [10]. In contrast, a complete block of β-oxidation rates for medium- and long-chain fatty acids was observed in yeast cells lacking the two ATP-dependent acyl-CoA synthetases Faa2p and Fat1p [35]. Since no other ATP-generating systems have been discovered so far, future research will address how an alternative bypass route provides peroxisomes with ATP particularly for fatty-acid metabolism.

Very little is known about the uptake of CoA and NAD by yeast peroxisomes. In yeast, cytosolic CoA probably enters the peroxisomal matrix via the Pxa1p–Pxa2p transporter, which cleaves off the CoA moiety from the imported acyl-CoA ester. Alternatively, a specific transport protein might facilitate the CoA uptake. Inside peroxisomes CoA is not only essential for the fatty-acid activation but also for the thiolytic cleavage within the β-oxidation cycle via the action of acyl-CoA thiolases [31]. The CoA bound to the acyl chain is released when acetyl-CoA, the product of β-oxidation, is exported via the carnitine shuttle or enters the glyoxylate cycle. In order to regulate the CoA homeostasis, the peroxisomal CoA diphosphatase Pcd1p hydrolyzes CoA to adenosine 3′,5′-diphosphate and 4′-phospho-pantetheine [38]. The resulting products need to exit the peroxisomes to enter the cytosolic CoA salvage pathway. Both CoA derivatives might function as potential counter-exchange substrates for the peroxisomal CoA importer. However, it is currently unclear whether yeast peroxisomes harbor such a CoA transport protein.

An additional cofactor uptake system must exist in yeast for loading the peroxisomal lumen with NAD. During the β-oxidation cycle, NAD is reduced to NADH, which is directly re-oxidized by the peroxisomal malate dehydrogenase Mdh3p, an important component of the malate–oxaloacetate shuttle [39]. By action of this shuttle, peroxisomal NADH is indirectly transported to mitochondria, where it is re-oxidized to NAD, and then returned back to peroxisomes. Genetic in vivo studies with *mdh3*Δ mutants, which were unable to metabolize fatty acids, demonstrated that the peroxisomal membrane of *S. cerevisiae* is impermeable to NAD(H) [39]. This indicated that a direct exchange of NAD against NADH across the peroxisomal membrane does not occur in yeast, and thus the transfer of reducing equivalents is mediated by NAD-linked redox shuttles [40]. In addition, yeast possess additional redox shuttles to maintain the intraperoxisomal redox balance, such as the glycerol-3-phosphate/dihydroxyacetone phosphate NAD-linked shuttle and the 2-oxoglutarate/isocitrate NADP-linked shuttle [40,41]. A prerequisite for redox metabolism is a constant concentration of NAD(H) inside peroxisomal lumen. The NAD(H) homeostasis is achieved by the peroxisomal NADH diphosphatase Npy1p [42], converting NAD(H) to AMP and nicotinamide mononucleotide. In order to recycle these products of NAD hydrolysis in the cytosol, they have to be exported by a specific carrier, which might be coupled to the import of NAD. However, the mechanism to initially generate an NAD pool inside peroxisomes is still unknown.

Members of the MCF have been identified to mediate an efficient subcellular distribution of ATP, CoA, and NAD within the eukaryotic cell. *S. cerevisiae* contains 35 MCF-type proteins, including the mitochondrial CoA carrier Leu5p [43] and the mitochondrial NAD carriers Ndt1p and Ndt2p [44].

Two scenarios are possible: (1) One of the so far uncharacterized MCF or even non-MCF proteins in yeast might catalyze the peroxisomal cofactor uptake. (2) The mitochondrial CoA and/or NAD transporter might be dually localized to mitochondria and peroxisomes to adapt to the cellular needs. Future analyses will discover whether and which carrier-type protein might mediate the peroxisomal cofactor transport.

**3. Cofactor Transport for Human Peroxisomes**

In humans, peroxisomes are present in all cell types, except in erythrocytes [1,45,46]. The pivotal role of these organelles is emphasized by a variety of severe genetic diseases linked to peroxisome dysfunction. Most of these disorders are caused by mutations in genes coding for peroxisomal enzymes involved in metabolic pathways [45]. In humans, the key metabolic function of human peroxisomes is β-oxidation. While mitochondrial β-oxidation handles the bulk of dietary fatty acids, such as palmitic acid and oleic acid, the peroxisomal β-oxidation plays a crucial role in the degradation of a more diverse spectrum of carboxylic acids, including long-chain fatty acids (LCFAs), very long-chain fatty acids (VLCFAs, >C22), branched-chain fatty acids (e.g., pristanic and phytanic acids), and long-chain dicarboxylic acids. In addition to its catabolic functions, peroxisomal β-oxidation is involved in the biosynthesis of the bile acid intermediates di- and tri-hydroxycholestanoic acid and the essential omega-3-fatty acid docosahexaenoic acid (C22:6 n-3), a primary structural component of the human brain, cerebral cortex, skin, and retina [1,45,46].

To import the diverse carboxylic acids into peroxisomes, three half-size ABC transporters of the subfamily D (ABCD) reside in the peroxisomal membrane [47–49]. They function mainly as homodimers with partially overlapping substrate specificities. ABCD1 (ALDP) has a higher affinity for saturated VLCFAs, whereas ABCD2 (ALDR) transports shorter and (poly)unsaturated VLCFAs [50,51]. In contrast, ABCD3 (PMP70) imports branched-chain fatty acids, long-chain dicarboxylic acids, and bile acid intermediates into human peroxisomes [52,53]. The peroxisomal ABCD proteins transport their substrates as CoA esters, whereas the peroxisomal membrane-bound acyl-CoA binding protein ACBD5 functions as a cytosolic receptor for VLCFA-CoAs and passes them on to the VLCFA transporter ABCD1 [54]. Furthermore, ABCD1–3 share the same transport mode with the yeast fatty-acid transporter described in the previous chapter [55,56]. An intrinsic acyl-CoA thioesterase activity couples the translocation step to the hydrolysis of the CoA ester, leaving a free acid in the peroxisomes that must be re-activated with CoA for β-oxidation [57]. The human genome encodes several different acyl-CoA synthetases, catalyzing the ATP-dependent activation of fatty acids and related compounds to acyl-CoA in the presence of ATP [58,59]. Few isoforms have been reported to be linked to the peroxisomal membrane, but whether these membrane-associated proteins are active inside or outside the peroxisome has been the subject of recent debates [58,59]. Still, the active site of one human acyl-CoA synthetase has been located to the peroxisomal matrix. It is assumed that the enzyme specifically activates peroxisomal pristanic acid produced by α-oxidation of phytanic acid [60]. Reports on the human ABCD1 suggest that the import of VLCFA-CoA esters into peroxisomes is not dependent on peroxisome internal activation [61]. Still, the complementation of the yeast *pxa1/pxa2*Δ double mutant with the human ABCD1 requires the presence of the peroxisomal acyl-CoA synthetase Faa2p for the activation of the β-oxidation substrates [35]. Future research will resolve these partly contradictory hypotheses.

In the case that β-oxidation substrates enter peroxisomes as free fatty acids, a pool of ATP and CoA is needed for the peroxisomal re-esterification (Figure 2). Consequently, human peroxisomes have to be supplied with both cofactor molecules, if CoA is released in the cytosol by ABCD proteins [55,56]. The resulting acyl-CoA esters are then fed into β-oxidation, which depends on peroxisomal NAD as an electron acceptor. The last step of this pathway, catalyzed by the acyl-CoA thiolase, uses free CoA to cleave off one acetyl-CoA molecule from the acyl-chain [46]. The shortened acyl-CoA ester undergoes additional cycles but will not be completely degraded. Thus, the peroxisomal β-oxidation generates several different medium-chain acyl-CoAs, besides propionyl-CoA and acetyl-CoA. These

products are then exported via the peroxisomal carnitine shuttle from peroxisomes to mitochondria for further metabolism [46]. This export mechanism releases CoA in the peroxisomal lumen, which can be

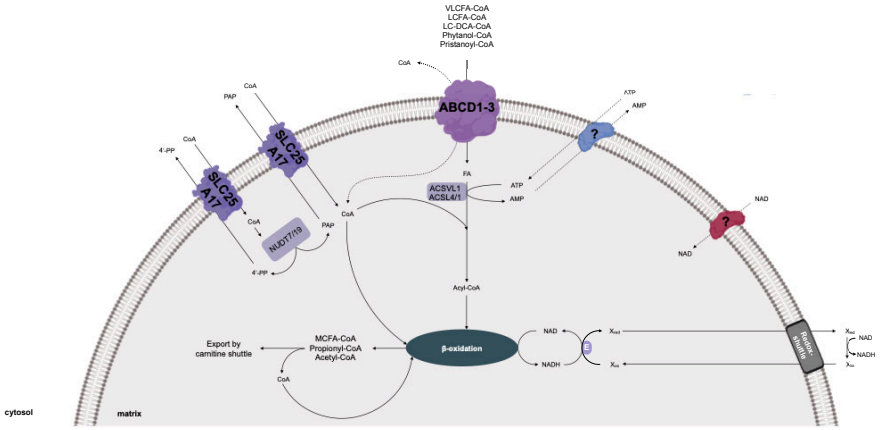


**Figure 2.** Model for the peroxisomal cofactor transport in human. ABCD1–3: ABC transporters of the subfamily D (ABCD) member 1–3, mediating the import of fatty acids and other β-oxidation-related substrates as CoA esters; ACSVL1: very-long-chain acyl-CoA synthetase 1 (associated at the matrix site of the peroxisomal membrane); ACSL1/4: long-chain acyl-CoA synthetase1 and 4 (associated at the cytosolic site of the peroxisomal membrane); FA, fatty acid; NUDT7/19: peroxisomal Nudix hydrolase 7 and 19, catalyzing the hydrolysis of CoA to PAP and 4′-PP.; LCFA-CoA: long-chain acyl-CoAs; LC-DCA-CoA: long-chain dicarboxyl-CoA; PAP: adenosine 3′,5′-diphosphate; 4′-PP: 4′-phospho-pantetheine; VLCFA-CoA: very long-chain acyl-CoAs; SLC25A17: solute carrier family 25 member 17, putative peroxisomal CoA carrier; (?): proposed cofactor carrier proteins.

In humans, one member the MCF has been discovered as peroxisomal membrane protein of 34 kDa (PMP34) [63]. This human MCF protein is classified as member 17 of the solute carrier family 25 (SLC25A17). Due to its high homology to the yeast peroxisomal ATP carrier, it was hypothesized that human SLC25A17 is a functional ortholog of Ant1p [63,64]. To address this, human SLC25A17 was expressed in the *ant1*Δ yeast mutant [64]. While peroxisomal β-oxidation activity in *ant1*Δ cells were only 20% of wild type cells, the fatty-acid degradation was restored to approximately 60% of wild type in *ant1*Δ, expressing the human SLC25A17. This partial rescue of the *ant1*Δ phenotype with human SLC25A17 suggested a role in providing peroxisomes with ATP for fatty-acid oxidation [64]. Functional reconstitution of yeast expressed and purified SLC25A17 protein in lipid vesicles revealed detectable ATP import activity across the liposomal membrane [64]. Both observations led to the conclusion that the human SLC25A17 functions as an adenine nucleotide transporter, catalyzing an exchange of adenine nucleotides across the peroxisomal membrane [64]. The group of Ferdinando Palmieri repeated the uptake assays with the human SLC25A17 recombinantly expressed in *E.coli* and purified by affinity chromatography [65]. Surprisingly, it exhibited extremely low uptake rates of ATP, which might explain the partial complementation of the *ant1*Δ mutant with the human SLC25A17 [64]. In contrast, high transport activities of recombinant SLC25A17 were discovered for AMP exchange against CoA, dephospho-CoA, and FAD. It also catalyzes the AMP import against internal FMN, ADP, adenosine 3′,5′-diphosphate (PAP), and to a lesser extent, NAD [65]. Considering lower $K_M$ and $K_i$ values suggested a higher affinity of SLC25A17 for CoA, AMP, FAD, and FMN as substrates than for

NAD, ADP, and ATP [65]. The physiological role of such a cofactor carrier with a versatile transport functions remains unclear for human peroxisomes.

The in vivo function of SLC25A17 has been further investigated in genetic mutants of orthologs in the model organisms zebrafish (*Danio rerio*) and mice (*Mus musculus*) [66,67]. The zebrafish genome contains two Slc25a17 proteins, which have been both simultaneously down-regulated by a morpholino-based antisense approach [66]. During the first four days of development, zebrafish embryos rely entirely on its nutrient-rich yolk sac to sustain growth and survival. In this phase, peroxisomal β-oxidation supports the utilization of very long-chain fatty acids, as well as the synthesis of plasmalogens, providing energy and structural cellular components [68]. Silencing of the two *slc25a17* genes at 3–4 days post-fertilization led to an accumulation of very long-chain fatty acids and a reduction of ether-phospholipids in the zebrafish embryos [66]. This altered cellular lipid composition caused a severe failure in the development of multiple organs, including the swim bladder. To test if the loss of peroxisomal CoA or NAD impairs β-oxidation function, these cofactors were co-injected together with the *slc25a17*-specific antisense oligomers into zebrafish embryos. Exogenously supplied CoA efficiently rescued the defective swim bladder, whereas NAD co-injection failed to restore the developmental defects associated with *slc25a17* knockdown [66]. In vitro uptake experiments demonstrated that both Slc25a17 proteins function redundantly with a preference towards CoA, instead of NAD and ATP, similar to the human carrier [66]. These findings suggest that Slc25a17 and Slc25a17-like functions additively as CoA transporters, which are involved in peroxisomal lipid metabolism and are thus essential for normal embryonic growth in zebrafish [66].

Mice lacking the SLC25A17 carrier by insertional mutagenesis did not show any obvious phenotype [67]. In particular, the diverse functions of the peroxisomal β-oxidation were not compromised in the SLC25A17-deficient mice. Only the degradation of phytol-derived branched-chain fatty acids was considerably impaired. Phytol, a constituent of chlorophyll, is converted to phytanic acid [69–71]. This methyl-branched fatty acid first activated by the long-chain acyl-CoA synthetases ACSL1/4 in the cytosol and then imported as acyl-CoA ester via ABCD3 transporter into peroxisomes [58,59], where it enters the peroxisomal α-oxidation. This pathway produces pristanic acid inside peroxisomes. This fatty acid is activated to pristanoyl-CoA catalyzed by the peroxisomal very-long-chain acyl-CoA synthetase ACSVL1 [60] for further conversion by multiple rounds of peroxisomal β-oxidation. The resulting medium-chain fatty acids are then completely oxidized by the mitochondrial β-oxidation [69–71]. Notably, pristanic acid is also present in human diets, and for its degradation via the peroxisomal β-oxidation, it is activated in the cytosol and imported as acyl-CoA ester via the ABCD3 transporter into peroxisomes [69–71].

Upon phytol feeding, the SLC25A17 knockout mice accumulated phytanic and pristanic acid as well as their CoA-esters in the liver, resulting in an enlarged organ and hepatic inflammation [67]. These abnormalities of the phytol-fed knockout mice suggested that the phytol degradation process depends on the peroxisomal cofactor supplied by SLC25A17. Unfortunately, the transport function of mice SLC25A17 has not yet been characterized, and thus we can only hypothesize about its preference for ATP, CoA, or NAD as a substrate [67]. Assuming that mouse SLC25A17 functions as a peroxisomal CoA carrier, as postulated for the zebrafish ortholog, the specific phenotype of the slc25a17-deficient mice might be caused by a shortage of peroxisomal CoA. Since the peroxisomal activation of pristanic acid as well as the thiolytic cleavage during β-oxidation of the resulting medium-chain fatty acids demand free CoA in the peroxisomal matrix, the levels of both phytol-derived fatty acids and acyl-CoA esters were elevated in the liver of the KO mice after phytol feeding [67].

In general, the activity of the acyl-CoA thioesterases prevent CoA deficiencies in peroxisomes from humans and mice [62]. These peroxisomal enzymes hydrolyze CoA esters, resulting in CoA formation, and thus can regulate the peroxisomal CoA pool [62]. In order to ensure a net CoA influx, the mice SLC25A17 carrier might catalyze the import of two CoA molecules against one molecule of adenosine 3′,5′-diphosphate (PAP) and 4′-phosphopantetheine (4′-PP). Both counter-exchange substrates are products of the hydrolysis of one CoA molecule, provided by peroxisomal Nudix hydrolases [72–74].

For the human SLC25A17, it was shown that it transports PAP, however 4'-PP as a potential substrate has not been tested in this work [65].

Another open question is why the CoA-dependent activation of other β-oxidation substrates is not impaired in the SLC25A17-deficient mice. The mild phenotype of the loss-of-function mutant, which can only be unmasked upon phytol treatments, might point to an alternative way to provide peroxisomes with CoA. For instance, another CoA carrier protein may exist in the peroxisomal membrane or an alternative splicing variant could lead to dual targeting of the human mitochondrial CoA carrier [75,76]. In addition, it cannot be excluded that peroxisomal CoA-dependent enzymes are imported together with their cofactor, as it was described for FAD-dependent enzymes previously [20,21]. Nevertheless, this study may be applicable to the human system, indicating that SLC25A17 deficiency in humans is unlikely to be lethal but could cause an impaired metabolization of branched-chain fatty acids in older adults [67].

Up to now, the SLC25A17 proteins are the only MCF-type cofactor carrier known to be present in peroxisomes of humans, mice, and zebrafish. Orthologs of the peroxisomal ATP carrier Ant1p from yeast or the peroxisomal NAD carrier from Arabidopsis are required to provide metabolic pathways with ATP and NAD. Beside β-oxidation, ATP and NAD are also involved in different peroxisome-associated processes in humans and mice. For instance, intraperoxisomal ATP can be used for the post-translational phosphorylation of peroxisomal enzymes by protein kinases [77], proper folding of peroxisomal matrix proteins [78], removal of oxidatively damaged, and misfolded proteins via ATP-stimulated proteases [79,80]. NAD, in particular the phosphorylated, reduced form NADPH, is also needed for the oxidation of unsaturated fatty acids [46,70], as well as for the antioxidants defense systems, such as the ascorbate–glutathione cycle, to detoxify reactive oxygen species, such as the glutathione cycle [81]. Diverse peroxisomal NAD(P)-redox shuttle mechanisms, such as malate/oxaloacetate, lactate/pyruvate, and 2-oxoglutarate/isocitrate-based shuttle systems, regenerate NAD or NADPH and thus participate in regulating the redox homeostasis in human peroxisomes [4]. However, it remains to be investigated whether specific transport proteins are involved in the provision of ATP and NAD for peroxisomes in humans and animals.

## 4. Cofactor Transport for Plant Peroxisomes

In contrast to humans and animals, peroxisomes are the sole site of β-oxidation in plants. This essential metabolic pathway is involved in diverse developmental and signaling processes, participating in fatty-acid catabolism and the biosynthesis of several major phytohormones, including jasmonic acid, indole-3-acetic acid (auxin), and salicylic acid [2,82,83].

Another important function of β-oxidation is the mobilization of storage oil in oil-seed species, such as the model plant *Arabidopsis thaliana* [84,85]. These plants store energy in form of triacylglycerol in the seeds in order to secure survival of the next generation. During germination the embryos utilize the storage oil to enable the seedling growth and development, until it becomes photoautotrophic. In Arabidopsis, the long-chain fatty acids that are hydrolyzed from reserve lipids are imported into peroxisomes for further degradation by β-oxidation [84,85]. The import of fatty acids as CoA esters is mediated by the peroxisomal ABC transporter, which was named COMATOSE (CTS) after its dormancy phenotype in Arabidopsis [86–89]. The CTS transport mechanism is the same as described for the peroxisomal ABC transport proteins from yeast and human. The CoA-moiety is cleaved off during the import, which necessitates the re-esterification of fatty acids to CoA prior to entering β-oxidation [90]. This activation reaction is catalyzed by two peroxisomal long-chain acyl-CoA synthetases LACS6 and LCAS7 in an ATP-consuming reaction [91]. In the absence of both enzymes in peroxisomes, Arabidopsis seedlings were compromised in storage-oil mobilization, leading to an arrested seedling growth shortly after germination [91]. This phenotype implies that the activation of the fatty acid inside plant peroxisomes is essential for their breakdown. The resulting acyl-CoAs are then degraded by the NAD-dependent β-oxidation cycle [84,85]. The last step of this pathway uses free CoA for the thiolytic cleavage of the acyl-CoA, generating acetyl-CoA and a shortened acyl-CoA. The latter can

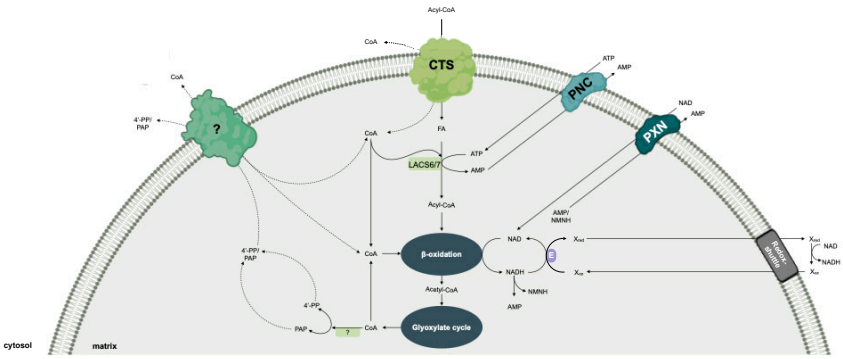


**Figure 3.** Model for the peroxisomal cofactor transport in plants. CTS: peroxisomal ABC transporter, mediating the import of fatty acids as acyl-CoA esters; FA: fatty acid; LACS6/7: long-chain acyl-CoA synthetase 6 and 7 (associated at the matrix site of the peroxisomal membrane); NMN(H): nicotinamide mononucleotide (reduced); PAP: adenosine 3′,5′-diphosphate; 4′-PP: 4′-phospho-pantetheine; PNC, peroxisomal ATP carrier; PXN, peroxisomal NAD carrier; (?): proposed cofactor carrier proteins.

On the basis of amino-acid-sequence similarity to the peroxisomal ATP carrier Ant1p from *S. cerevisiae*, two Arabidopsis MCF members have been identified to be localized to the peroxisomal membrane [12,13]. These plant carriers were independently able to suppress the β-oxidation phenotype of the ant1Δ yeast mutant [13], indicating that both proteins import ATP into yeast peroxisomes. A biochemical characterization using recombinant PNC proteins revealed that the ATP import was mediated in a strict counter exchange transport mode with ADP or AMP, similar to the yeast ortholog [12,13]. Whereas substrate specificity was similar to the yeast ortholog, none of the PNC proteins showed uniport transport activity. Due to their restricted substrate spectrum, the Arabidopsis MCF members were annotated as peroxisomal adenine nucleotide carriers PNC1 and PNC2. Arabidopsis mutants were generated in which PNC1 and PNC2 were simultaneously silenced using RNA interference to analyze their in vivo role [12,13]. Since the import of cytosolic ATP into peroxisomes is essential for β-oxidation, the seedlings of the RNAi lines were compromised in seedling establishment [12,13]. The arrested seedling phenotype was caused by a block in storage-oil mobilization, resulting in an accumulation of storage-oil-derived fatty acids and acyl-CoA esters. This result suggests that peroxisomal ATP uptake mediated by PNC1/2 is critical for utilizing fatty acids through β-oxidation to fuel seedling growth [12,13]. It is hypothesized that PNC-mediated ATP import occurs in exchange with peroxisomal AMP, which is released during the fatty-acid activation step by LACS6/7 [91]. In addition, other metabolic pathways that are linked to peroxisomal β-oxidation were also affected in these *pnc1/2* RNAi lines, such as biosynthesis of phytohormones, the catabolism of membrane lipids during dark-induced senescence, and the degradation of branched-chain amino acids (unpublished work). Together, these findings emphasize that the peroxisomal ATP carriers are the primary source of peroxisomal ATP, meaning no other major ATP-generating systems, such as substrate-level phosphorylation, exist in Arabidopsis peroxisomes.

Our knowledge about other ATP-consuming reactions in plant peroxisomes beside β-oxidation is limited. Recently, it was demonstrated that the ATP-dependent enzymes that catalyze the last steps of the cytosolic mevalonate pathway for the synthesis of isopentenyl diphosphate are located inside plant

peroxisomes [93,94]. Peroxisomal ATP might also be crucial for the regulation of protein function. Phospho-proteomic studies revealed that many enzymes involved in photorespiration are regulated via post-translational phosphorylation [95–97]. Accordingly, several protein kinases have also been identified in plant peroxisomes, but their target proteins still need to be discovered [98,99]. A role of the PNC proteins as ATP/ADP carrier remains to be tested.

In order to support NAD-dependent fatty-acid oxidation during early seedling growth, the import of NAD into Arabidopsis peroxisomes is mediated by the peroxisomal NAD carrier, called PXN [100,101]. PXN belongs to the MCF and represents, regardless of the species, the first, and so far, only discovered peroxisomal carrier for NAD. In vitro uptake experiments of reconstituted recombinant protein discovered that PXN can transport many organic cofactors and related molecules, including NAD, NADH, ADP, AMP, and CoA, in an antiport mode [100,101]. The outcome of the biochemical (in vitro) assays suggest versatile transport functions for PXN, catalyzing the import of NAD or CoA against AMP or the exchange of NAD/NADH. However, complementation studies using different yeast mutants restricted the in vivo function of PXN to provide peroxisomes with cytosolic NAD in exchange with intraperoxisomal AMP [37]. Since the peroxisomal malate/oxaloacetate shuttle is involved in the export of NADH from peroxisomes and the import of re-oxidized NAD [102,103], PXN as an NAD/AMP exchanger might function to build up and/or replenish the peroxisomal NAD pool [14,37,101]. For instance, a net NAD import is facilitated, if the exported AMP is strictly accompanied by a unidirectional AMP import to balance the loss of peroxisomal AMP. Such an adenylate uniporter has only been described for chloroplasts so far [104,105]. In another scenario, PXN might transport two NAD molecules. One NAD is used for the peroxisomal metabolism, the other is hydrolyzed to AMP and reduced nicotinamide mononucleotide by the peroxisomal Nudix hydrolase in Arabidopsis [106,107]. Both hydrolysis products might counter-exchange during the uptake of two NAD molecules [14,101].

The role of PXN in providing the peroxisomal β-oxidation with NAD implies that a deletion of this gene would affect storage-oil mobilization, which is essential for seedling establishment. Surprisingly, Arabidopsis *pxn* knockout mutants did not display any obvious seedling phenotype, as described for the *PNC1/2* RNAi lines [100,101]. The fatty-acid composition in these mutant seedlings revealed that fatty-acid breakdown was delayed during storage-oil turnover, indicating that peroxisomal NAD import mediated by PXN contributes to an optimal operation of storage-oil degradation [100,101]. Recently, PXN was identified to be involved in photorespiration under fluctuating and high-light conditions [108]. The decreased activity of the photosystems in the *pxn* plants could be rescued by elevated $CO_2$ concentrations, which represses the flux through the photorespiratory pathway. The authors proposed that PXN can supply plant peroxisomes with the increased demand of NADH during photorespiration [108]. Both defined phenotypes point to an alternative mechanism to fuel plant peroxisomes with NAD; most likely by a redundant uptake system, that is either mediated by a specific carrier, protein-coupled NAD import, or by fusion of NAD-preloaded pre-peroxisomes derived from the ER [14].

Plant peroxisomes have to control their peroxisomal CoA pool, since this cofactor is crucial for the proper functioning of β-oxidation. The peroxisomal CoA is again released, for instance, once the acetyl-CoA is fed into the glyoxylate cycle, resulting in CoA recycling. Like in humans and yeast, plant peroxisomes possess several acyl-CoA thioesterases to ensure optimal flux through β-oxidation. They have been proposed to regulate the availability of free CoA in the peroxisomal matrix, by releasing CoA from acyl-CoA esters [109]. In addition, a role in maintaining the peroxisomal CoA has also been reported for the putative Nudix hydrolases of plant peroxisomes [110]. Since the CoA biosynthesis and salvage pathway takes place outside peroxisomes [111], plant peroxisomes depend on the uptake of CoA, which might be mediated by a specific CoA transport protein. A mitochondrial carrier for the distribution of CoA has been identified and characterized in humans, yeast, and plants [43,75], but the knowledge about a peroxisomal CoA carrier is restricted to non-plant organisms. An ortholog of the peroxisomal CoA carrier SLC25A17 in humans and animals is still unknown in Arabidopsis. The peroxisomal NAD carrier PXN, however, showed transport activities for CoA in vitro [100].

However, due to its low affinity to CoA, it is unlikely that PXN is able to transport CoA under physiological conditions [37]. Biochemical and genetic analyses will demonstrate the existence of a peroxisomal CoA carrier in plants in the future.

## 5. Conclusions

The mitochondrial carrier family (MCF) is a large family of proteins present in all eukaryotic lineages, which are present in several other cellular compartments, including peroxisomes. The peroxisomal MCF-type proteins described so far in yeast, humans, and plants, cluster as a functional branch in phylogenetic analyses [18,110]. These carriers ensure a stable exchange of structurally related cofactor molecules, such as ATP, CoA, and NAD, which are required for the maintenance of peroxisomal reactions, in particular β-oxidation. A detailed characterization of the transport function is indispensable to understand their physiological role in peroxisomes. However, the exciting findings of the knockout mutant displayed that alternative routes with a so far unknown mechanism exist for the cofactor exchange across the peroxisomal membrane.

Beyond cofactors, the diverse anabolic and catabolic reactions in peroxisomes produce a large number of small hydrophilic metabolites, which have to be shuttled across the peroxisomal membrane. Peroxisomes appear to be permeable to small hydrophilic solutes. Experimental evidences suggest a nonselective channel responsible for this exchange, but the proposed protein could not yet be conclusively assigned to the observed channel activity [3,6,8]. This raises the question if other transport proteins might be involved in peroxisomal metabolite transfer. For instance, MCF represents a carrier family with a broad substrate spectrum, catalyzing the transport of small hydrophilic solutes, like amino acids, mono, di- and tricarboxylates, and an inorganic form of phosphate. It could be hypothesized that—beyond the cofactor uptake—MCF-type proteins might play a role in these transport processes. Until now, such an MCF protein has not yet been located in peroxisomes in any eukaryotic organisms.

**Author Contributions:** Conceptualization, N.L.; writing and editing, A.P., L.C., and N.L. All authors have read and agreed to the published version of the manuscript.

**Funding:** This research was supported by German Research Foundations (DFG Grant LI1781/2-2).

**Acknowledgments:** We would like to thank members of the laboratories for stimulating discussions and critical comments on the manuscript. We apologize to those whose scientific work has not been cited. The figures were created with BioRender.com.

**Conflicts of Interest:** The authors declare no conflicts of interest.

## References

1. Islinger, M.; Voelkl, A.; Fahimi, H.D.; Schrader, M. The peroxisome: An update on mysteries 2.0. *Histochem. Cell Biol.* **2018**, *150*, 443–471. [CrossRef]
2. Pan, R.; Liu, J.; Wang, S.; Hu, J. Peroxisomes: Versatile organelles with diverse roles in plants. *New Phytol.* **2020**, *225*, 1410–1427. [CrossRef] [PubMed]
3. Charton, L.; Plett, A.; Linka, N. Plant peroxisomal solute transporter proteins. *J. Integr. Plant Biol.* **2019**, *169*, 1469–1835. [CrossRef]
4. Wanders, R.J.A.; Waterham, H.R.; Ferdinandusse, S. Metabolic interplay between peroxisomes and other subcellular organelles including mitochondria and the endoplasmic reticulum. *Front. Cell Dev. Biol.* **2015**, *3*, 83. [CrossRef] [PubMed]
5. Rottensteiner, H.; Theodoulou, F.L. The ins and outs of peroxisomes: Co-ordination of membrane transport and peroxisomal metabolism. *Biochim. Biophys. Acta* **2006**, *1763*, 1527–1540. [CrossRef] [PubMed]
6. Antonenkov, V.D.; Hiltunen, J.K. Peroxisomal membrane permeability and solute transfer. *Biochim. Biophys. Acta* **2006**, *1763*, 1697–1706. [CrossRef] [PubMed]
7. Van Veldhoven, P.P.; Just, W.W.; Mannaerts, G.P. Permeability of the peroxisomal membrane to cofactors of beta-oxidation. Evidence for the presence of a pore-forming protein. *J. Biol. Chem.* **1987**, *262*, 4310–4318.
8. Antonenkov, V.D.; Hiltunen, J.K. Transfer of metabolites across the peroxisomal membrane. *Biochim. Biophys. Acta* **2011**, *1822*, 1374–1386. [CrossRef]

9. Palmieri, L.; Rottensteiner, H.; Girzalsky, W.; Scarcia, P.; Palmieri, F.; Erdmann, R. Identification and functional reconstitution of the yeast peroxisomal adenine nucleotide transporter. *EMBO J.* **2001**, *20*, 5049–5059. [CrossRef]
10. Van Roermund, C.W.T.; Drissen, R.; van den Berg, M.; Ijlst, L.; Hettema, E.H.; Tabak, H.F.; Waterham, H.R.; Wanders, R.J.A. Identification of a peroxisomal ATP carrier required for medium-chain fatty acid beta-oxidation and normal peroxisome proliferation in *Saccharomyces cerevisiae*. *Mol. Cell. Biol.* **2001**, *21*, 4321–4329. [CrossRef]
11. Bernhardt, K.; Wilkinson, S.; Weber, A.P.M.; Linka, N. A peroxisomal carrier delivers NAD and contributes to optimal fatty acid degradation during storage oil mobilization. *Plant J.* **2012**, *69*, 1–13. [CrossRef] [PubMed]
12. Arai, Y.; Hayashi, M.; Nishimura, M.; Nishimura, M. Proteomic identification and characterization of a novel peroxisomal adenine nucleotide transporter supplying ATP for fatty acid beta-oxidation in soybean and Arabidopsis. *Plant Cell* **2008**, *20*, 3227–3240. [CrossRef] [PubMed]
13. Linka, N.; Theodoulou, F.L.; Haslam, R.P.; Linka, M.; Napier, J.A.; Neuhaus, H.E.; Weber, A.P.M. Peroxisomal ATP import is essential for seedling development in *Arabidopsis thaliana*. *Plant Cell* **2008**, *20*, 3241–3257. [CrossRef]
14. Linka, N.; Esser, C. Transport proteins regulate the flux of metabolites and cofactors across the membrane of plant peroxisomes. *Front. Plant Sci.* **2012**, *3*, 3. [CrossRef] [PubMed]
15. Linka, N.; Theodoulou, F.L. Metabolite transporters of the plant peroxisomal membrane: Known and unknown. *Subcell. Biochem.* **2013**, *69*, 169–194. [PubMed]
16. Meinecke, M.; Cizmowski, C.; Schliebs, W.; Kruger, V.; Beck, S.; Wagner, R.; Erdmann, R. The peroxisomal importomer constitutes a large and highly dynamic pore. *Nat. Cell Biol.* **2010**, *12*, 273–277. [CrossRef]
17. Walter, T.; Erdmann, R. Current Advances in Protein Import into Peroxisomes. *Protein J.* **2019**, *38*, 351–362. [CrossRef]
18. Kim, P.K.; Hettema, E.H. Multiple pathways for protein transport to peroxisomes. *J. Mol. Biol.* **2015**, *427*, 1176–1190. [CrossRef]
19. Palmieri, T.; Berks, B.C. The twin-arginine translocation (Tat) protein export pathway. *Nat. Rev. Microbiol.* **2012**, *10*, 483–496. [CrossRef]
20. Titorenko, V.I.; Nicaud, J.M.; Wang, H.; Chan, H.; Rachubinski, R.A. Acyl-CoA oxidase is imported as a heteropentameric, cofactor-containing complex into peroxisomes of *Yarrowia lipolytica*. *J. Cell Biol.* **2002**, *156*, 481–494. [CrossRef]
21. Gunkel, K.; van Dijk, R.; Veenhuis, M.; van der Klei, I.J. Routing of Hansenula polymorpha alcohol oxidase: An alternative peroxisomal protein-sorting machinery. *Mol. Biol. Cell* **2004**, *15*, 1347–1355. [CrossRef] [PubMed]
22. Fraccascia, P.; Casteels, M.; De Schryver, E.; Van Veldhoven, P.P. Role of thiamine pyrophosphate in oligomerisation, functioning and import of peroxisomal 2-hydroxyacyl-CoA lyase. *Biochim. Biophys. Acta* **2011**, *1814*, 1226–1233. [CrossRef] [PubMed]
23. Palmieri, F.; Pierri, C.L.; De Grassi, A.; Nunes-Nesi, A.; Fernie, A.R. Evolution, structure and function of mitochondrial carriers: A review with new insights. *Plant J.* **2011**, *66*, 161–181. [CrossRef] [PubMed]
24. Haferkamp, I. The diverse members of the mitochondrial carrier family in plants. *FEBS Lett.* **2007**, *581*, 2375–2379. [CrossRef]
25. Palmieri, F. Mitochondrial transporters of the SLC25 family and associated diseases: A review. *J Inherit. Metab. Dis.* **2014**, *37*, 565–575. [CrossRef]
26. Toleco, M.; Naake, T.; Zhang, Y.; Heazlewood, J.; Fernie, A.R. Plant mitochondrial carriers: Molecular gatekeepers that help to regulate plant central carbon metabolism. *Plants* **2020**, *9*, 117. [CrossRef]
27. Palmieri, F.; Monné, M. Discoveries, metabolic roles and diseases of mitochondrial carriers: A review. *BBA Mol. Cell Res.* **2016**, *1863*, 2362–2378. [CrossRef]
28. Saier, M.H.; Tran, C.V.; Barabote, R.D. TCDB: The Transporter Classification Database for membrane transport protein analyses and information. *Nucleic Acids Res.* **2006**, *34*, D181–D186. [CrossRef]
29. Palmieri, F. The mitochondrial transporter family SLC25: Identification, properties and physiopathology. *Mol. Asp. Med.* **2013**, *34*, 465–484. [CrossRef]
30. Palmieri, F.; Monnè, M. Antiporters of the mitochondrial carrier family. In *Current Topics in Membranes*; Bevenses, M.O., Ed.; Elsevier Inc.: Cambridge, MA, USA, 2014; Volume 73, pp. 289–320.

31. Hiltunen, J.K.; Mursula, A.M.; Rottensteiner, H.; Wierenga, R.K.; Kastaniotis, A.J.; Gurvitz, A. The biochemistry of peroxisomal beta-oxidation in the yeast *Saccharomyces cerevisiae*. *FEMS Microbiol. Rev.* **2003**, *27*, 35–64. [CrossRef]
32. Hettema, E.H.; van Roermund, C.W.T.; Distel, B.; van den Berg, M.; Vilela, C.; Rodrigues-Pousada, C.; Wanders, R.J.A.; Tabak, H.F. The ABC transporter proteins Pat1 and Pat2 are required for import of long-chain fatty acids into peroxisomes of *Saccharomyces cerevisiae*. *EMBO J.* **1996**, *15*, 3813–3822. [CrossRef] [PubMed]
33. Shani, N.; Valle, D.A. *Saccharomyces cerevisiae* homolog of the human adrenoleukodystrophy transporter is a heterodimer of two half ATP-binding cassette transporters. *Proc. Natl. Acad. Sci. USA* **1996**, *93*, 11901–11906. [CrossRef] [PubMed]
34. Swartzman, E.E.; Viswanathan, M.N.; Thorner, J. The PAL1 gene product is a peroxisomal ATP-binding cassette transporter in the yeast *Saccharomyces cerevisiae*. *J. Cell Biol.* **1996**, *132*, 549–563. [CrossRef] [PubMed]
35. Van Roermund, C.W.T.; Ijlst, L.; Majczak, W.; Waterham, H.R.; Folkerts, H.; Wanders, R.J.A.; Hellingwerf, K.J. Peroxisomal fatty acid uptake mechanism in *Saccharomyces cerevisiae*. *J. Biol. Chem.* **2012**, *287*, 20144–20153. [CrossRef] [PubMed]
36. Rottensteiner, H.; Palmieri, L.; Hartig, A.; Hamilton, B.; Ruis, H.; Erdmann, R.; Gurvitz, A. The peroxisomal transporter gene ANT1 is regulated by a deviant oleate response element (ORE): Characterization of the signal for fatty acid induction. *Biochem. J.* **2002**, *365*, 109–117. [CrossRef]
37. Van Roermund, C.W.T.; Schroers, M.G.; Wiese, J.; Facchinelli, F.; Kurz, S.; Wilkinson, S.; Charton, L.; Wanders, R.J.A.; Waterham, H.R.; Weber, A.P.M.; et al. The peroxisomal NAD carrier from Arabidopsis imports NAD in exchange with AMP. *Plant Physiol.* **2016**, *171*, 2127–2139. [CrossRef]
38. Cartwright, J.L.; Gasmi, L.; Spiller, D.G.; McLennan, A.G. The *Saccharomyces cerevisiae* PCD1 gene encodes a peroxisomal nudix hydrolase active toward coenzyme A and its derivatives. *J. Biol. Chem.* **2000**, *275*, 32925–32930. [CrossRef]
39. Van Roermund, C.W.T.; Elgersma, Y.; Singh, N.; Wanders, R.J.A.; Tabak, H.F. The membrane of peroxisomes in *Saccharomyces cerevisiae* is impermeable to NAD(H) and acetyl-CoA under in vivo conditions. *EMBO J.* **1995**, *14*, 3480–3486. [CrossRef]
40. Al-Saryi, N.A.; Al-Hejjaj, M.Y.; van Roermund, C.W.T.; Hulmes, G.E.; Ekal, L.; Payton, C.; Wanders, R.J.A.; Hettema, E.H. Two NAD-linked redox shuttles maintain the peroxisomal redox balance in *Saccharomyces cerevisiae*. *Sci. Rep.* **2017**, *7*, 11868–11869. [CrossRef]
41. Van Roermund, C.W.T.; Hettema, E.H.; Kal, A.J.; van den Berg, M.; Tabak, H.F.; Wanders, R.J.A. Peroxisomal β-oxidation of polyunsaturated fatty acids in Saccharomyces cerevisiae: Isocitrate dehydrogenase provides NADPH for reduction of double bonds at even positions. *EMBO J.* **1998**, *17*, 677–687. [CrossRef]
42. Abdelraheim, S.R.; Cartwright, J.L.; Gasmi, L.; McLennan, A.G. The NADH diphosphatase encoded by the *Saccharomyces cerevisiae* NPY1 nudix hydrolase gene is located in peroxisomes. *Arch. Biochem. Biophys.* **2001**, *388*, 18–24. [CrossRef] [PubMed]
43. Prohl, C.; Pelzer, W.; Diekert, K.; Kmita, H.; Bedekovics, T.; Kispal, G.; Lill, R. The yeast mitochondrial carrier Leu5p and its human homologue Graves' disease protein are required for accumulation of coenzyme A in the matrix. *Mol. Cell. Biol.* **2001**, *21*, 1089–1097. [CrossRef] [PubMed]
44. Todisco, S.; Agrimi, G.; Castegna, A.; Palmieri, F. Identification of the mitochondrial NAD transporter in *Saccharomyces cerevisiae*. *J. Biol. Chem.* **2006**, *281*, 1524–1531. [CrossRef] [PubMed]
45. Waterham, H.R.; Ferdinandusse, S.; Wanders, R.J.A. Human disorders of peroxisome metabolism and biogenesis. *Biochim. Biophys. Acta* **2016**, *1863*, 922–933. [CrossRef] [PubMed]
46. Wanders, R.J.A.; Waterham, H.R. Biochemistry of mammalian peroxisomes revisited. *Annu. Rev. Biochem.* **2006**, *75*, 295–332. [CrossRef]
47. Kamijo, K.; Taketani, S.; Yokota, S.; Osumi, T.; Hashimoto, T. The 70-kDa peroxisomal membrane protein is a member of the Mdr (P-glycoprotein)-related ATP-binding protein superfamily. *J. Biol. Chem.* **1990**, *265*, 4534–4540.
48. Mosser, J.; Douar, A.M.; Sarde, C.O.; Kioschis, P.; Feil, R.; Moser, H.; Poustka, A.M.; Mandel, J.L.; Aubourg, P. Putative X-linked adrenoleukodystrophy gene shares unexpected homology with ABC transporters. *Nature* **1993**, *361*, 726–730. [CrossRef]
49. Lombard-Platet, G.; Savary, S.; Sarde, C.O.; Mandel, J.L.; Chimini, G. A close relative of the adrenoleukodystrophy (ALD) gene codes for a peroxisomal protein with a specific expression pattern. *Proc. Natl. Acad. Sci. USA* **1996**, *93*, 1265–1269. [CrossRef]

50. Van Roermund, C.W.T.; Visser, W.F.; Ijlst, L.; van Cruchten, A.; Boek, M.; Kulik, W.; Waterham, H.R.; Wanders, R.J.A. The human peroxisomal ABC half transporter ALDP functions as a homodimer and accepts acyl-CoA esters. *FASEB J.* **2008**, *22*, 4201–4208. [CrossRef]
51. Van Roermund, C.W.T.; Visser, W.F.; Ijlst, L.; Waterham, H.R.; Wanders, R.J.A. Differential substrate specificities of human ABCD1 and ABCD2 in peroxisomal fatty acid b-oxidation. *Biochim. Biophys. Acta* **2011**, *1811*, 148–152. [CrossRef]
52. Van Roermund, C.W.T.; Ijlst, L.; Wagemans, T.; Wanders, R.J.A.; Waterham, H.R. A role for the human peroxisomal half-transporter ABCD3 in the oxidation of dicarboxylic acids. *Biochim. Biophys. Acta* **2013**, *1841*, 563–568. [CrossRef]
53. Ferdinandusse, S.; Jimenez-Sanchez, G.; Koster, J.; Denis, S.; van Roermund, C.W.T.; Silva-Zolezzi, I.; Moser, A.B.; Visser, W.F.; Gulluoglu, M.; Durmaz, O.; et al. A novel bile acid biosynthesis defect due to a deficiency of peroxisomal ABCD3. *Hum. Mol. Genet.* **2015**, *24*, 361–370. [CrossRef] [PubMed]
54. Ferdinandusse, S.; Falkenberg, K.D.; Koster, J.; Mooyer, P.A.; Jones, R.; van Roermund, C.W.T.; Pizzino, A.; Schrader, M.; Wanders, R.J.A.; Vanderver, A.; et al. ACBD5 deficiency causes a defect in peroxisomal very long-chain fatty acid metabolism. *J. Med. Genet.* **2017**, *54*, 330–337. [CrossRef] [PubMed]
55. Imanaka, T. Biogenesis and function of peroxisomes in human disease with a focus on the ABC Transporter. *Biol. Pharm. Bull.* **2019**, *42*, 649–665. [CrossRef] [PubMed]
56. Baker, A.; Carrier, D.J.; Schaedler, T.; Waterham, H.R.; van Roermund, C.W.T.; Theodoulou, F.L. Peroxisomal ABC transporters: Functions and mechanism. *Biochem. Soc. Trans.* **2015**, *43*, 959–965. [CrossRef]
57. Okamoto, T.; Kawaguchi, K.; Watanabe, S.; Agustina, R.; Ikejima, T.; Ikeda, K.; Nakano, M.; Morita, M.; Imanaka, T. Characterization of human ATP-binding cassette protein subfamily D reconstituted into proteoliposomes. *Biochem. Biophys. Res. Commun.* **2018**, *496*, 1122–1127. [CrossRef] [PubMed]
58. Watkins, P.A.; Ellis, J.M. Peroxisomal acyl-CoA synthetases. *Biochim. Biophys. Acta* **2012**, *1822*, 1411–1420. [CrossRef]
59. Grevengoed, T.J.; Klett, E.L.; Coleman, R.A. Acyl-CoA metabolism and partitioning. *Annu. Rev. Nutr.* **2014**, *34*, 1–30. [CrossRef]
60. Steinberg, S.J.; Wang, S.J.; Kim, D.G.; Mihalik, S.J.; Watkins, P.A. Human very-long-chain acyl-CoA synthetase: Cloning, topography, and relevance to branched-chain fatty acid metabolism. *Biochem. Biophys. Res. Commun.* **1999**, *257*, 615–621. [CrossRef]
61. Wiesinger, C.; Kunze, M.; Regelsberger, G.; Forss-Petter, S.; Berger, J. Impaired very long-chain acyl-CoA β-oxidation in human X-linked adrenoleukodystrophy fibroblasts is a direct consequence of ABCD1 transporter dysfunction. *J. Biol. Chem.* **2013**, *288*, 19269–19279. [CrossRef]
62. Hunt, M.C.; Tillander, V.; Alexson, S.E.H. Regulation of peroxisomal lipid metabolism: The role of acyl-CoA and coenzyme A metabolizing enzymes. *Biochimie* **2014**, *98*, 45–55. [CrossRef] [PubMed]
63. Wylin, T.; Baes, M.; Brees, C.; Mannaerts, G.P.; Fransen, M.; Van Veldhoven, P.P. Identification and characterization of human PMP34, a protein closely related to the peroxisomal integral membrane protein PMP47 of Candida boidinii. *Eur. J. Biochem.* **1998**, *258*, 332–338. [CrossRef] [PubMed]
64. Visser, W.F.; van Roermund, C.W.T.; Waterham, H.R.; Wanders, R.J.A. Identification of human PMP34 as a peroxisomal ATP transporter. *Biochem. Biophys. Res. Commun.* **2002**, *299*, 494–497. [CrossRef]
65. Agrimi, G.; Russo, A.; Scarcia, P.; Palmieri, F. The human gene SLC25A17 encodes a peroxisomal transporter of coenzyme A., FAD and NAD. *Biochem. J.* **2012**, *443*, 241–247. [CrossRef] [PubMed]
66. Kim, Y.-I.; Nam, I.-K.; Lee, D.-K.; Bhandari, S.; Charton, L.; Kwak, S.; Lim, J.-Y.; Hong, K.; Kim, S.-J.; Lee, J.N.; et al. Slc25a17 acts as a peroxisomal coenzyme A transporter and regulates multiorgan development in zebrafish. *J. Cell. Physiol.* **2020**, *235*, 151–165. [CrossRef]
67. Van Veldhoven, P.P.; De Schryver, E.; Young, S.G.; Zwijsen, A.; Fransen, M.; Espeel, M.; Baes, M.; Van Ael, E. Slc25a17 gene trapped mice: PMP34 plays a role in the reroxisomal degradation of phytanic and pristanic acid. *Front. Cell Dev. Biol.* **2020**, *8*, 144. [CrossRef]
68. Anderson, J.L.; Carten, J.D.; Farber, S.A. Zebrafish lipid metabolism: From mediating early patterning to the metabolism of dietary fat and cholesterol. *Methods Cell Biol.* **2011**, *101*, 111–141.
69. Jansen, G.A.; Wanders, R.J.A. Alpha-oxidation. *Biochim. Biophys. Acta* **2006**, *1763*, 1403–1412. [CrossRef]
70. Van Veldhoven, P.P. Biochemistry and genetics of inherited disorders of peroxisomal fatty acid metabolism. *J. Lipid Res.* **2010**, *51*, 2863–2895. [CrossRef]

71. Wanders, R.J.A. Phytanic acid metabolism in health and disease. *Biochim. Biophys. Acta* **2011**, *1811*, 498–507. [CrossRef]
72. Gasmi, L.; McLennan, A.G. The mouse Nudt7 gene encodes a peroxisomal nudix hydrolase specific for coenzyme A and its derivatives. *Biochem. J.* **2001**, *357*, 33–38. [CrossRef] [PubMed]
73. Ofman, R.; Speijer, D.; Leen, R.; Wanders, R.J.A. Proteomic analysis of mouse kidney peroxisomes: Identification of RP2p as a peroxisomal nudix hydrolase with acyl-CoA diphosphatase activity. *Biochem. J.* **2006**, *393*, 537–543. [CrossRef] [PubMed]
74. Shumar, S.A.; Kerr, E.W.; Geldenhuys, W.J.; Montgomery, G.E.; Fagone, P.; Thirawatananond, P.; Saavedra, H.; Gabelli, S.B.; Leonardi, R. Nudt19 is a renal CoA diphosphohydrolase with biochemical and regulatory properties that are distinct from the hepatic Nudt7 isoform. *J. Biol. Chem.* **2018**, *293*, 4134–4148. [CrossRef] [PubMed]
75. Fiermonte, G.; Paradies, E.; Todisco, S.; Marobbio, C.M.T.; Palmieri, F. A novel member of solute carrier family 25 (SLC25A42) is a transporter of coenzyme A and adenosine 3′, 5′-diphosphate in human mitochondria. *J. Biol. Chem.* **2009**, *284*, 18152–18159. [CrossRef] [PubMed]
76. Ast, J.; Stiebler, A.C.; Freitag, J.; Bölker, M. Dual targeting of peroxisomal proteins. *Front. Physiol.* **2013**, *4*, 297. [CrossRef] [PubMed]
77. Oeljeklaus, S.; Schummer, A.; Mastalski, T.; Platta, H.W.; Warscheid, B. Regulation of peroxisome dynamics by phosphorylation. *Biochim. Biophys. Acta* **2016**, *1863*, 1027–1037. [CrossRef]
78. Sakai, Y.; Saiganji, A.; Yurimoto, H.; Takabe, K.; Saiki, H.; Kato, N. The absence of Pmp47, a putative yeast peroxisomal transporter, causes a defect in transport and folding of a specific matrix enzyme. *J. Cell Biol.* **1996**, *134*, 37–51. [CrossRef]
79. Kikuchi, M.; Hatano, N.; Yokota, S.; Shimozawa, N.; Imanaka, T.; Taniguchi, H. Proteomic analysis of rat liver peroxisome: Presence of peroxisome-specific isozyme of Lon protease. *J. Biol. Chem.* **2004**, *279*, 421–428. [CrossRef]
80. Pomatto, L.C.D.; Raynes, R.; Davies, K.J.A. The peroxisomal Lon protease LonP2 in aging and disease: Functions and comparisons with mitochondrial Lon protease LonP1. *Biol. Rev. Camb. Philos. Soc.* **2017**, *92*, 739–753. [CrossRef]
81. Fransen, M.; Nordgren, M.; Wang, B.; Apanasets, O. Role of peroxisomes in ROS/RNS-metabolism: Implications for human disease. *BBA Mol. Basis Dis.* **2012**, *1822*, 1363–1373. [CrossRef]
82. Hu, J.; Baker, A.; Bartel, B.; Linka, N.; Mullen, R.T.; Reumann, S.; Zolman, B.K. Plant peroxisomes: Biogenesis and function. *Plant Cell* **2012**, *24*, 2279–2303. [CrossRef] [PubMed]
83. Reumann, S.; Bartel, B. ScienceDirect Plant peroxisomes: Recent discoveries in functional complexity, organelle homeostasis, and morphological dynamics. *Curr. Opin. Plant Biol.* **2016**, *34*, 17–26. [CrossRef]
84. Graham, I.A. Seed storage oil mobilization. *Annu. Rev. Plant Biol.* **2008**, *59*, 115–142. [CrossRef] [PubMed]
85. Theodoulou, F.L.; Eastmond, P.J. Seed storage oil catabolism: A story of give and take. *Curr. Opin. Plant Biol.* **2012**, *15*, 322–328. [CrossRef] [PubMed]
86. Footitt, S.; Slocombe, S.P.; Larner, V.; Kurup, S.; Wu, Y.; Larson, T.; Graham, I.A.; Baker, A.; Holdsworth, M. Control of germination and lipid mobilization by COMATOSE, the Arabidopsis homologue of human ALDP. *EMBO J.* **2002**, *21*, 2912–2922. [CrossRef] [PubMed]
87. Zolman, B.K.; Silva, I.D.; Bartel, B. The Arabidopsis pxa1 mutant is defective in an ATP-binding cassette transporter-like protein required for peroxisomal fatty acid beta-oxidation. *Plant Physiol.* **2001**, *127*, 1266–1278. [CrossRef]
88. Hayashi, M.; Nito, K.; Takei-Hoshi, R.; Yagi, M.; Kondo, M.; Suenaga, A.; Yamaya, T.; Nishimura, M.; Nishimura, M. Ped3p is a peroxisomal ATP-binding cassette transporter that might supply substrates for fatty acid beta-oxidation. *Plant Cell Physiol.* **2002**, *43*, 1–11. [CrossRef]
89. Hooks, M.A.; Turner, J.E.; Murphy, E.C.; Graham, I.A. Acetate non-utilizing mutants of Arabidopsis: Evidence that organic acids influence carbohydrate perception in germinating seedlings. *Mol. Genet. Genom.* **2004**, *271*, 249–256. [CrossRef]
90. De Marcos Lousa, C.; van Roermund, C.W.T.; Postis, V.L.G.; Dietrich, D.; Kerr, I.D.; Wanders, R.J.A.; Baldwin, S.A.; Baker, A.; Theodoulou, F.L. Intrinsic acyl-CoA thioesterase activity of a peroxisomal ATP binding cassette transporter is required for transport and metabolism of fatty acids. *Proc. Natl. Acad. Sci. USA* **2013**, *110*, 1279–1284. [CrossRef]

91. Fulda, M.; Schnurr, J.; Abbadi, A.; Heinz, E.; Browse, J. Peroxisomal Acyl-CoA synthetase activity is essential for seedling development in Arabidopsis thaliana. *Plant Cell* **2004**, *16*, 394–405. [CrossRef]
92. Rinaldi, M.A.; Patel, A.B.; Park, J.; Lee, K.; Strader, L.C.; Bartel, B. The Roles of β-oxidation and cofactor homeostasis in peroxisome distribution and function in *Arabidopsis thaliana*. *Genetics* **2016**, *204*, 1089–1115. [CrossRef]
93. Sapir-Mir, M.; Mett, A.; Belausov, E.; Tal-Meshulam, S.; Frydman, A.; Gidoni, D.; Eyal, Y. Peroxisomal localization of Arabidopsis isopentenyl diphosphate isomerases suggests that part of the plant isoprenoid mevalonic acid pathway is compartmentalized to peroxisomes. *Plant Physiol.* **2008**, *148*, 1219–1228. [CrossRef]
94. Simkin, A.J.; Guirimand, G.; Papon, N.; Courdavault, V.; Thabet, I.; Ginis, O.; Bouzid, S.; Giglioli-Guivarc'h, N.; Clastre, M. Peroxisomal localisation of the final steps of the mevalonic acid pathway in planta. *Planta* **2011**, *234*, 903–914. [CrossRef] [PubMed]
95. Hodges, M.; Jossier, M.; Boex-Fontvieille, E.; Tcherkez, G. Protein phosphorylation and photorespiration. *Plant Biol. J.* **2013**, *15*, 694–706. [CrossRef] [PubMed]
96. Kataya, A.R.A.; Muench, D.G.; Moorhead, G.B. A Framework to Investigate peroxisomal protein phosphorylation in Arabidopsis. *Trends Plant Sci.* **2019**, *24*, 366–381. [CrossRef] [PubMed]
97. Sandalio, L.M.; Gotor, C.; Romero, L.C.; Romero-Puertas, M.C. Multilevel Regulation of peroxisomal proteome by post-translational modifications. *Int. J. Mol. Sci.* **2019**, *20*, 4881. [CrossRef] [PubMed]
98. Fukao, Y.; Hayashi, M.; Hara-Nishimura, I.; Nishimura, M. Novel glyoxysomal protein kinase, GPK1, identified by proteomic analysis of glyoxysomes in etiolated cotyledons of *Arabidopsis thaliana*. *Plant Cell Physiol.* **2003**, *44*, 1002–1012. [CrossRef]
99. Coca, M.; San Segundo, B. AtCPK1 calcium-dependent protein kinase mediates pathogen resistance in Arabidopsis. *Plant J.* **2010**, *2010*, 18. [CrossRef]
100. Agrimi, G.; Russo, A.; Pierri, C.L.; Palmieri, F. The peroxisomal NAD carrier of *Arabidopsis thaliana* transports coenzyme A and its derivatives. *J. Bioenerg. Biomembr.* **2012**, *44*, 333–340. [CrossRef]
101. Pracharoenwattana, I.; Zhou, W.; Smith, S.M. Fatty acid beta-oxidation in germinating Arabidopsis seeds is supported by peroxisomal hydroxypyruvate reductase when malate dehydrogenase is absent. *Plant Mol. Biol.* **2010**, *72*, 101–109. [CrossRef]
102. Pracharoenwattana, I.; Cornah, J.E.; Smith, S.M. Arabidopsis peroxisomal malate dehydrogenase functions in beta-oxidation but not in the glyoxylate cycle. *Plant J.* **2007**, *50*, 381–390. [CrossRef] [PubMed]
103. Leroch, M.; Kirchberger, S.; Haferkamp, I.; Wahl, M.; Neuhaus, H.E.; Tjaden, J. Identification and characterization of a novel plastidic adenine nucleotide uniporter from *Solanum tuberosum*. *J. Biol. Chem.* **2005**, *280*, 17992–18000. [CrossRef] [PubMed]
104. Kirchberger, S.; Tjaden, J.; Neuhaus, H.E. Characterization of the Arabidopsis Brittle1 transport protein and impact of reduced activity on plant metabolism. *Plant J.* **2008**, *56*, 51–63. [CrossRef] [PubMed]
105. Ogawa, T.; Ueda, Y.; Yoshimura, K.; Shigeoka, S. Comprehensive analysis of cytosolic Nudix hydrolases in *Arabidopsis thaliana*. *J. Biol. Chem.* **2005**, *280*, 25277–25283. [CrossRef]
106. Ogawa, T.; Yoshimura, K.; Miyake, H.; Ishikawa, K.; Ito, D.; Tanabe, N.; Shigeoka, S. Molecular characterization of organelle-type Nudix hydrolases in Arabidopsis. *Plant Physiol.* **2008**, *148*, 1412–1424. [CrossRef]
107. Li, J.; Tietz, S.; Cruz, J.A.; Strand, D.D.; Xu, Y.; Chen, J.; Kramer, D.M.; Hu, J. Photometric screens identified Arabidopsis peroxisome proteins that impact photosynthesis under dynamic light conditions. *Plant J.* **2019**, *97*, 460–474. [CrossRef]
108. Tilton, G.B.; Shockey, J.M.; Browse, J. Biochemical and molecular characterization of ACH2, an acyl-CoA thioesterase from *Arabidopsis thaliana*. *J. Biol. Chem.* **2004**, *279*, 7487–7494. [CrossRef]
109. Ito, D.; Yoshimura, K.; Ishikawa, K.; Ogawa, T.; Maruta, T.; Shigeoka, S. A comparative analysis of the molecular characteristics of the Arabidopsis CoA pyrophosphohydrolases AtNUDX11, 15, and 15a. *Biosci. Biotechnol. Biochem.* **2012**, *76*, 139–147. [CrossRef]
110. Webb, M.E.; Smith, A.G. Pantothenate Biosynthesis in Higher Plants. *Adv. Bot. Res.* **2011**, *58*, 203–255.
111. Zallot, R.; Agrimi, G.; Lerma-Ortiz, C.; Teresinski, H.J.; Frelin, O.; Ellens, K.W.; Castegna, A.; Russo, A.; de Crécy-Lagard, V.; Mullen, R.T.; et al. Identification of mitochondrial coenzyme a transporters from maize and Arabidopsis. *Plant Physiol.* **2013**, *162*, 581–588. [CrossRef]


# Manuscript II

## Functional analysis of Arabidopsis peroxisomal channels of the MPV17/PMP22 family

# Functional analysis of Arabidopsis peroxisomal channels of the MPV17/PMP22 family

Anastasija Plett[1,2], Jan Wiese, Philipp Westhoff[2], Andreas PM Weber[1,2] and Nicole Linka[1*]

[1]Institute of Plant Biochemistry, Heinrich Heine University Düsseldorf, Germany

[2]Cluster of Excellence on Plant Sciences, Heinrich Heine University Düsseldorf, Germany

*Corresponding author

**Author contributions**: AP performed localization studies, functional yeast complementation assays, extracted metabolites, generated mutant lines, analyzed data, designed experiments, and wrote the manuscript; JW generated yeast complementation constructs; PW performed amino acid analysis; APMW supervised experiments; NL designed and supervised experiments

## Abstract

Peroxisomes are highly dynamic organelles and essential for central plant metabolism and development, yet the mechanisms by which they connect their metabolic activity with other processes remain unclear. Transport proteins are required for the exchange of metabolites across the peroxisomal membrane, but only a few have been discovered and characterized. Members of the conserved MPV17/PMP22 family function as non-selective pore-forming channels in chloroplasts, mitochondria, and peroxisomes. Here, we investigated the role of *Arabidopsis* PMP22. We confirmed the localization of PMP22 to peroxisomes. Our approach to complement the yeast *sym1Δ* mutant was unsuccessful, indicating that PMP22 cannot functionally restore the mutant. Physiological characterization of a knock-down mutant revealed a higher sensitivity towards JA and altered amino acid content. To overcome the lack of knockout mutants, CRISPR/Cas9 mutants were generated and tested for β-oxidation, but no difference compared to WT was observed. A second member of the MPV17/PMP22 family was localized to peroxisomes and revealed high sequence similarity, hinting toward gene redundancy between both candidates.

## Introduction

One important key characteristic of eukaryotic cells is the presence of subcellular compartments. Metabolic pathways can be split across different organelles, which allows for spatiotemporal control. Peroxisomes are rather small but highly active in metabolism and participate in essential cellular pathways. Compared to their counterparts in the mammalian kingdom, plant peroxisomes are unique in their involvement in photorespiration and the biosynthesis of several secondary metabolites (Deb and Nagotu, 2017). Moreover, fatty acid degradation takes exclusively place in plant peroxisomes. In order to connect peroxisomes to other cellular metabolic pathways, many substances and ions need to enter and leave the peroxisome. The flux of solutes and ions between organelles is restricted and regulated by transport proteins in the membrane. These transporters can be divided into active or passive transporters, channels, and pores. The first identified peroxisomal transporter in *Arabidopsis thaliana* (Arabidopsis) was the ATP-binding cassette (ABC) transporter. It was identified by four different groups and is therefore known as Peroxisomal ABC transporter 1 (PXA1), COMATOSE (CTS), Peroxisome defective 3 (PED3) and Acetate non-utilizing 2 (ACN2) (Zolman et al., 2001; Footitt et al., 2002; Hayashi et al., 2002; Hooks et al., 2004; Footitt et al., 2006). Mutant plants with impaired transport function display a specific phenotype associated with β-oxidation. Therefore, its proposed function is the import of fatty acids. Beyond this, CTS imports several precursors of secondary metabolites such as 12-oxo-phytodienoic acid (OPDA), 2,4-dichlorophenoxybutyric acid, and indole butyric acid (Footitt et al., 2006; Haferkamp and Linka, 2012; Linka and Theodoulou, 2013). The phytohormone jasmonic acid (JA) is a key hormone in plant growth and defense. Its biosynthesis starts with α-linolenic acid in the chloroplast, is further converted to OPDA, exported into the cytosol, and imported into the peroxisomes by the CTS (Ghorbel et al., 2021). OPDA is further metabolized to JA by several rounds of β-oxidation (Wasternack and Song, 2016). Eventually, JA needs to exported form the peroxisomes for long distance transport or conjugation to its bioactive form (Anfang and Shani, 2021).

The next two identified transporters belong to the Mitochondrial Carrier family (MCF). This family is conserved in the eukaryotic kingdom and encodes transport proteins acting as antiporters, uniporters, or proton-coupled symporters. The

Peroxisomal Nucleotide Carriers (PNC1 and PNC2) show a high affinity for adenine nucleotides (ATP, AMP, and ADP). ATP is crucial for β-oxidation, and based on the substrate specificity and phenotype, the function of PNC proteins is mainly connected to fatty acid degradation (Linka et al., 2008). The import of NAD, an important cofactor for β-oxidation, is facilitated by the Peroxisomal NAD carrier (PXN) (Bernhardt et al., 2012). Furthermore, PXN is involved in photorespiration during changing diurnal conditions (Li et al., 2018). Aside from that, no other peroxisomal transporters or channels have been identified and assigned to a certain pathway, although it is known which substrates needs to enter or leave peroxisomes.

In contrast to transporters, channel proteins can be less specific for substrates while mediating fast transport rates. In *Mus musculus* the peroxisomal membrane protein 2 (Pxmp2) has been characterized as a non-selective pore-forming channel. *In vitro* data show that it transports various organic anions, such as glycolate, pyruvate, and 2-oxoglutarate. The estimated diameter of the channel is 1.4 nm, which enables the diffusion of compounds with molecular masses up to 300 Da. Mice with a loss-of-function mutation show a rather mild phenotype, as only elevated levels of uric acid could be detected. Based on sequence similarities, *Pxmp2* can be assigned to the MPV17/PMP22 family (Rokka et al., 2009). The MPV17/PMP22 family is a small eukaryotic family of non-selective pore forming channels. Members of this family are predicted to be membrane proteins with 4 α-helical transmembrane domains (Reinhold et al., 2012). They can localize to peroxisomes, mitochondria, and in case of plants to plastids. In mitochondria, human MPV17 and its yeast homologue SYM1 have been linked to modulation of membrane potential and reactive oxygen species (ROS) regulation (Dallabona et al., 2010; Antonenkov et al., 2015). Loss of function mutations in mammals result in mitochondrial DNA depletion syndrome (MDDS) (Spinazzola et al., 2006). SYM1 in yeast has a calculated pore size of 1.6 nm, allowing diffusion of small substances (Reinhold et al., 2012). It is upregulated under elevated temperatures, and its physiological role has been linked to ethanol metabolism, since the loss-of-function mutant fails to grow on media containing ethanol as the sole carbon source specifically under elevated temperatures (Trott and Morano, 2004). In plants, *PMP22* is highly abundant and ubiquitously expressed (Waese et al., 2017). It has a high sequence similarity to the mouse homologue *Pxmp2*, and the protein localizes to peroxisomes (Tugal et al., 1999; Murphy et al., 2003; Reumann and Singhal, 2014).

Its physiological and biochemical function remains uncharacterized. The aim of this work was to investigate the physiological function of Arabidopsis PMP22. Based on its predicted non-selective pore-forming channel activity we hypothesized that PMP22 mediates metabolite flux across the peroxisomal membrane and contributes to central plant metabolism as of β-oxidation or stress-related metabolism linked to hormones. We applied to approaches: functional yeast complementation of *sym1Δ* and physiological and metabolic characterization of Arabidopsis loos-of-function mutants. Our findings confirm peroxisomal localization of PMP22, while it was not able to rescue the mitochondrial *sym1Δ* under tested conditions. Further, the Arabidopsis mutant exhibits JA hypersensitivity and altered amino acid profiles. Together with gene redundancy indicated PMP22-like, these data suggest that PMP22 family members act as peroxisomal channels in metabolite exchange and stress physiology.

# Results

## PMP22 localizes to the peroxisomes

First described in 1999, PMP22 was identified and localized to the peroxisomes by biochemical analysis (Tugal et al., 1999). We confirmed its peroxisomal localization by subcellular fluorescence studies (Fig. 1). We generated a mCherry fusion at the C-terminus of PMP22 and *Agrobacterium tumefaciens* cells were transformed with the construct. Tobacco leaves were infiltrated with the PMP22-mCherry construct and a CFP fused to the peroxisomal targeting signal (PTS1) construct. Co-localization was analyzed by laser scanning microscopy of tobacco leave protoplasts. Our fluorescent fusion protein showed a clear overlay with the peroxisomal marker (CFP fused to PTS1).

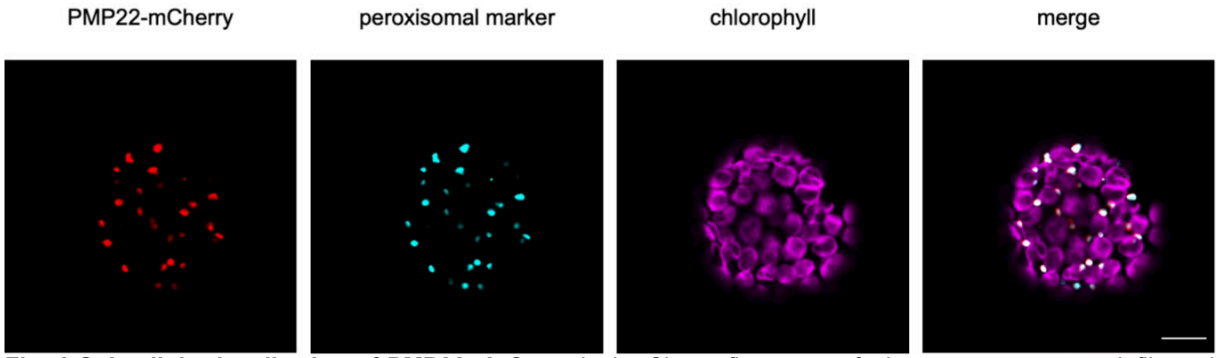


**Fig. 1 Subcellular localization of PMP22. A** C-terminal mCherry fluorescent fusion construct was co-infiltrated with a peroxisomal marker in *N. benthamiana* leaves, and protoplasts were analyzed by confocal microscope 2 days post-infiltration. Images were analyzed using Fiji. Chlorophyll A autofluorescence: magenta, peroxisomal marker: cyan fluorescent protein with C-terminal PTS1, PMP22-mCherry: red. Scale bar: 10 µM.

## PMP22 cannot restore the *sym1Δ* phenotype

The baker's yeast *S. cerevisiae* contains two genes encoding putative channels of the MPV17/PMP22 family. YOR292cp has been localized to the peroxisomal membrane (Antonenkov and Hiltunen, 2012). However, its phenotype or function remains unknown. The second orthologue YLR251W has been characterized as Stress-inducible Yeast MPV17 protein 1 (SYM1p) (Trott and Morano, 2004). The growth of *the sym1Δ* mutant is impaired when cultivated on minimal medium supplemented with non-fermentable carbon sources under heat stress. Transcriptional profiling revealed differences between the wildtype and mutant only under heat stress

conditions (37°C). Moreover, the mutant exhibits reduced succinate dehydrogenase activity and altered mitochondrial membrane structures (Dallabona et al., 2010). Although the substrates of this channel remain unknown, a respiration linked function of this channel has been proposed (Trott and Morano, 2004). Furthermore, the *sym1Δ* mutant was established as a tool to study MPV17/PMP22 function. We used this mutant for functional yeast complementation studies. Since SYM1 localizes to the inner mitochondrial membrane, we used a N-terminal mitochondrial transit peptide (mTP), which has already been used successfully (van Roermund et al., 2016). As expected, the mutant was not able to grow at higher temperatures with ethanol as a carbon source (Fig. 2).

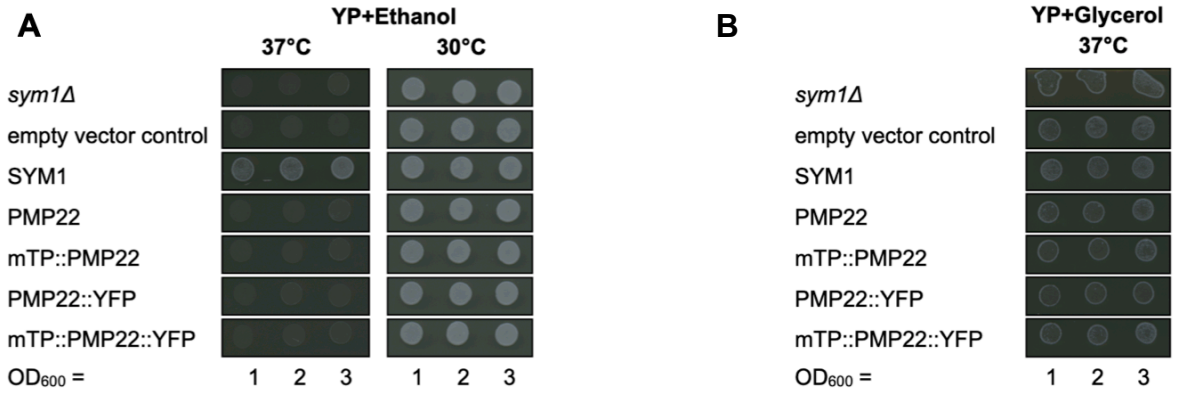


**Fig. 2 Functional yeast complementation of PMP22 in sym1Δ strain.** All yeast cells were plated on YP medium containing ethanol (2%) or glycerol (2%) and incubated at 30 or 37°C. (A) Yeast cells of *sym1Δ, sym1Δ* transformed with the empty vector (empty vector control), wild-type (SYM1), *sym1Δ* transformed with the PMP22 complementation construct (PMP22) or with a N-terminal mitochondrial transit peptide fused to PMP22 (mTP::PMP22), *sym1Δ* transformed with a fluorescent PMP22 localization construct (PMP22::YFP) or with a N-terminal mitochondrial transit peptide fused to the localization construct (mTP::PMP22::YFP) were diluted to an $OD_{600}$ = 1, 2 or 3 and plated on plates with 2% (v/v) ethanol as a nonfermentable carbon source and incubated for 3 days at 30 or 37°C. (B) Same yeast cells were diluted to an $OD_{600}$ = 1, 2 or 3 and plated on plates with 2% (v/v) glycerol as a nonfermentable carbon source and incubated for 3 days at 37°C.

The mutant was not able to grow at higher temperatures with ethanol as a carbon source (Fig. 2A). However, neither mitochondria-targeted nor native PMP22 could restore the mutant's phenotype as no growth could be observed under 37°C and ethanol (Fig. 2A). The control with yeast grown on rich media supplemented with glycerol showed the expected results, as the growth of *sym1Δ* is only compromised on media with ethanol as a nonfermentable carbon source (Fig. 2B). Next, we analyzed the subcellular localization of mitochondrial targeted PMP22 in yeast by fluorescent fusion proteins. Mitochondrial targeted PMP22 was fused to a YFP and was co-

transformed with yeast expressing a COXIV targeting peptide fused to a CFP. Co-localization was analyzed by laser scanning microscopy.

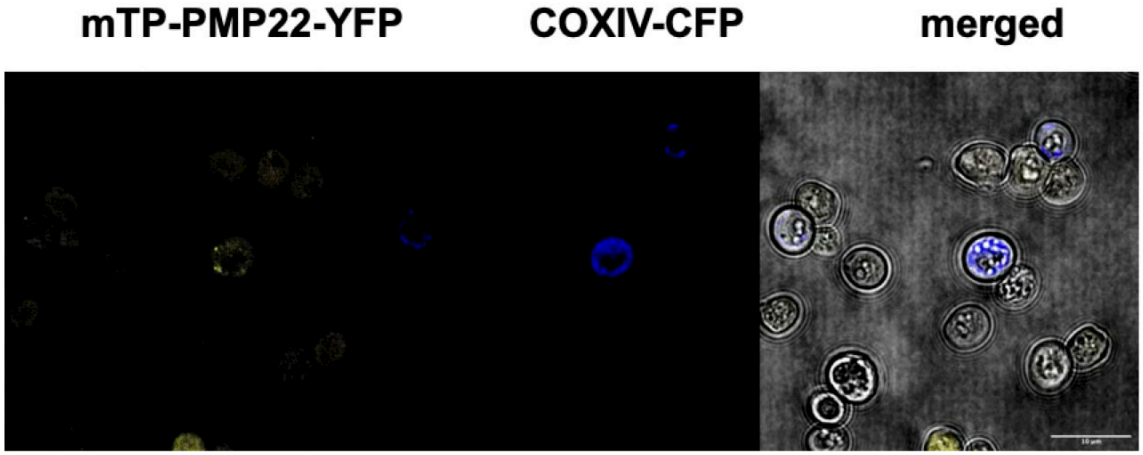


**Fig. 3 Subcellular localization of PMP22 targeted to yeast mitochondria.** N-terminal mTP was fused to PMP22-YFP. Yeast was co-transformed with fluorescent mTP-PMP22-YFP and COXIV mTP fused to a CFP. Images were analyzed using Fiji. Scale bar: 10 µM.

Mitochondrial localization could not be confirmed, as no cells with both mTP-PMP22-YFP and the mitochondrial marker COXIV-CFP were detected (Fig. 3). Based on this result, it remains unclear, whether PMP22 could be successfully targeted to yeast mitochondria and therefore not able to restore the *sym1Δ* phenotype.

### *pmp22* exhibits sensitivity to high JA concentrations

JA biosynthesis requires the import of OPDA into peroxisomes by CTS, but the export of JA from peroxisomes to the cytosol remains unknown. Members of the MPV17/PMP22 function as pore-forming non-selective channels in various organelles, we hypothesized that PMP22 could be involved in the export of JA or otherwise influence JA homeostasis by providing essential cofactors for β-oxidation. In this case we would expect a growth phenotype upon elevated exogenous JA concentrations, leasing to an increased sensitivity. To test this hypothesis, we compared growth of WT and mutant seedling on media supplemented with exogenous JA.

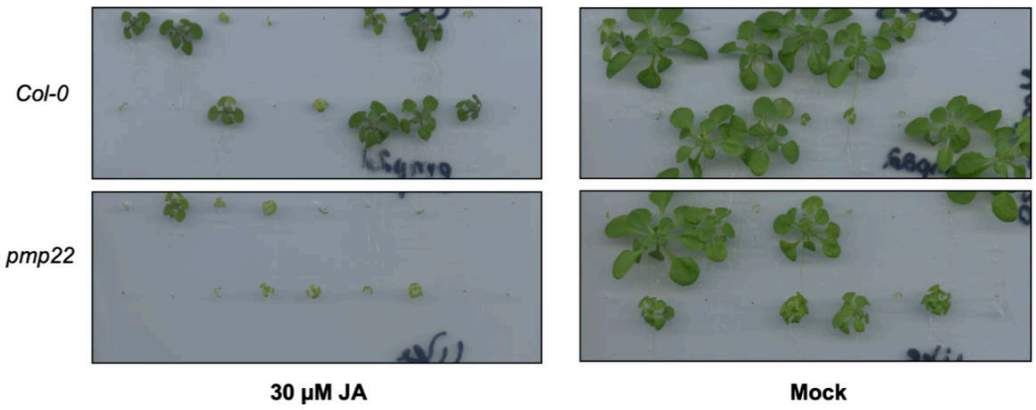


**Fig. 4 Phenotype of *pmp22* under high external JA concentrations.** Seeds of WT (Col-0) and *pmp22* were germinated and directly grown on ½ MS media supplemented with 30 µM JA (left) or ethanol (mock, right). Images were taken after 21 days.

*Arabidopsis* seedlings were germinated and grown on MS agar plates supplemented with 30 µM external JA concentrations (Fig. 4, left) or a mock control (Fig. 4, right). After 21 days, JA treated seedlings showed reduced growth compared to mock- treated plants. Further, *pmp22* showed a more pronounced growth inhibition, indicating a higher sensitivity to external JA concentrations.

JA concentrations increase upon certain environmental stimuli, such as wounding (Castillo et al., 2008). Wounding leads to an increase of cytosolic calcium ($Ca^{2+}$), changes in the membrane surface potential, ligand bulk flow, especially amino acids and eventually to a response by activating defense related genes (Gilroy et al., 2016; Bellandi et al., 2022). We tested the wound-induced response of *pmp22* by measuring amino acid concentrations 1 h post wounding.

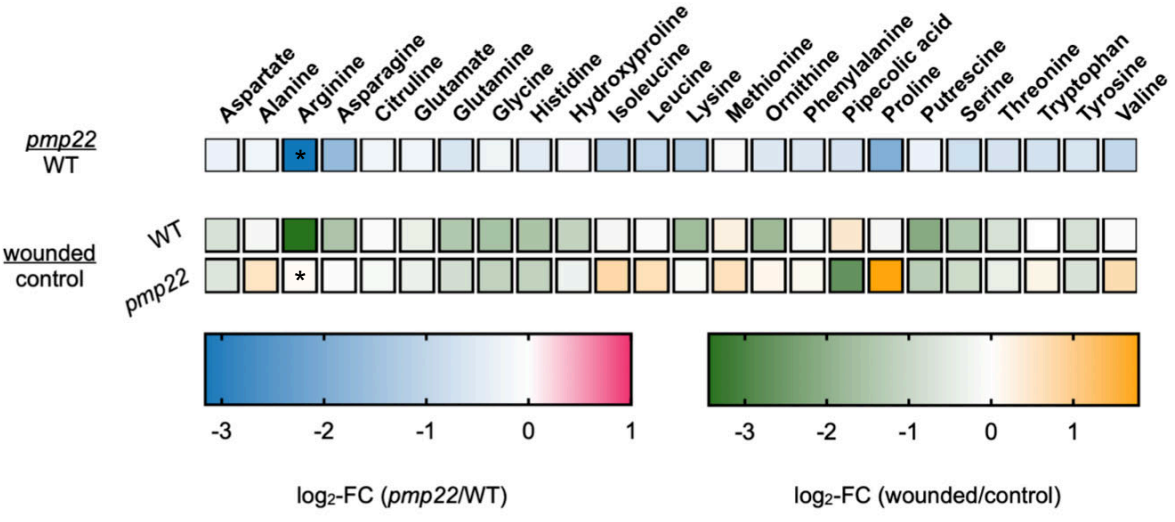

**Fig. 5 Heatmap of relative amino acid abundances in 6-week-old *Arabidopsis* rosettes.** Relative amino acids levels in unwounded plants of *pmp22* and WT (upper panel). Changes in amino acid abundance 1 h post wounding, relative to controls for both genotypes. Colors indicate $log_2$ fold changes. Two-way ANOVA test was used for statistical analysis. $P < 0.05$. N=5 biological replicates

The *pmp22* mutant showed a significant reduction of Arginine under control conditions compared to WT (Fig. 5, top). Overall, the mutant showed a reduction in several amino acids, like Asparagine, Isoleucine, Leucine, Lysine and Proline, but these changes were not significant. Upon wounding, the amino acid profile changed, leading to a reduction of many amino acids in WT (Fig. 5, down). Only Pipecolic acid levels increased in WT, although none of the reduction or increase was significant. Arginine levels in WT were strongly reduced, but not in the *pmp22* mutant. Alanine, Isoleucine, Leucine, Lysine and Proline were slightly upregulated in the mutant, but reduced in WT. These results indicate an altered amino acid content already under control conditions, and later upon stress conditions, suggesting to an involvement of PMP22 in amino acid metabolism.

## Generation of CRISPR/Cas9 mediated knockouts

Since only a single T-DNA insertion line was available, resulting in a knockdown mutant with reduced transcript abundance, we generated additional mutant lines by CRISPR/Cas9. Further independent alleles are necessary to ensure that observed phenotypes can be attributed to the loss of function of PMP22 rather than background mutations or line-specific alleles. The pmp22-1 T-DNA line represents a knock-down allele with residual transcript levels, which could allow partial protein production and only a reduced abundance (Wiese, 2014). Smaller metabolic changes might remain below the detection limit or be interpreted as insignificant, even though they reflect partial loss of function. CRISPR/Cas9 alleles with frameshift mutations or splicing defects could provide stronger evidence for gene function.


| line | mutation |
|---|---|
| *pmp22-1* | T-DNA |
| *pmp22-2* | 1 bp insertion |
| *pmp22-3* | reverse complement between exon 2 and 6 |
| *pmp22-4* | reverse complement between exon 2 and 6 |

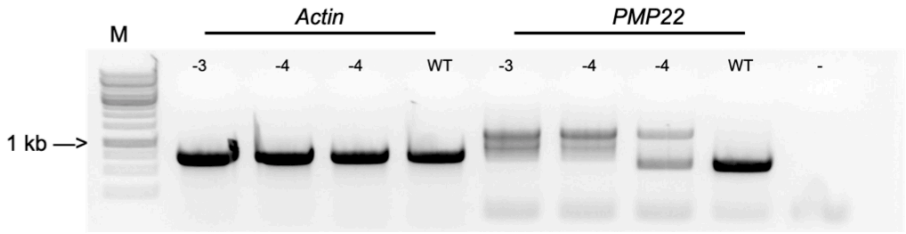


**Fig. 6 Schematic overview of gene structure and genotyping of CRISPR/Cas9 mutants.** Schematic representation of the target gene (top left), with exons shown as green boxes, introns as lines, and positions of gRNAs indicated as orange lines used for CRISPR/Cas9-mediated mutagenesis. Overview of the obtained mutant lines (top right). PCR amplification with gene-specific primers flanking the *PMP22* gene was performed on cDNA. A control PCR was performed targeting the *Actin7* gene.

Three guide RNAs were selected, targeting exon 1, exon 2, and exon 6, in order to create further independent alleles (Fig. 6). We were able to generate three independent lines, which were confirmed by PCR and sequencing of the regions flanking the target site of the guide RNAs. Further, two mutant alleles, *pmp22-3* and *pmp22-4*, revealed splicing defects, as several larger cDNA fragments were amplified compared to the WT control (Fig. 6, lower panel).

### *pmp22* mutants do not display a sucrose-dependent phenotype

β-oxidation is one of the central metabolic functions of plant peroxisomes and requires several cofactors. Since PMP22 localizes to peroxisomes and is highly abundant in the peroxisomal membrane, we hypothesized that it might contribute to β-oxidation by facilitating the transport of small molecules or cofactors required for this pathway. Mutants deficient in β-oxidation display a shorter root phenotype, which can be suppressed by the addition of external sucrose to the media. We tested the impact of sucrose, and therefore the involvement of PMP22 in β-oxidation, by measuring root length on media supplemented with sucrose and on sucrose-free media.

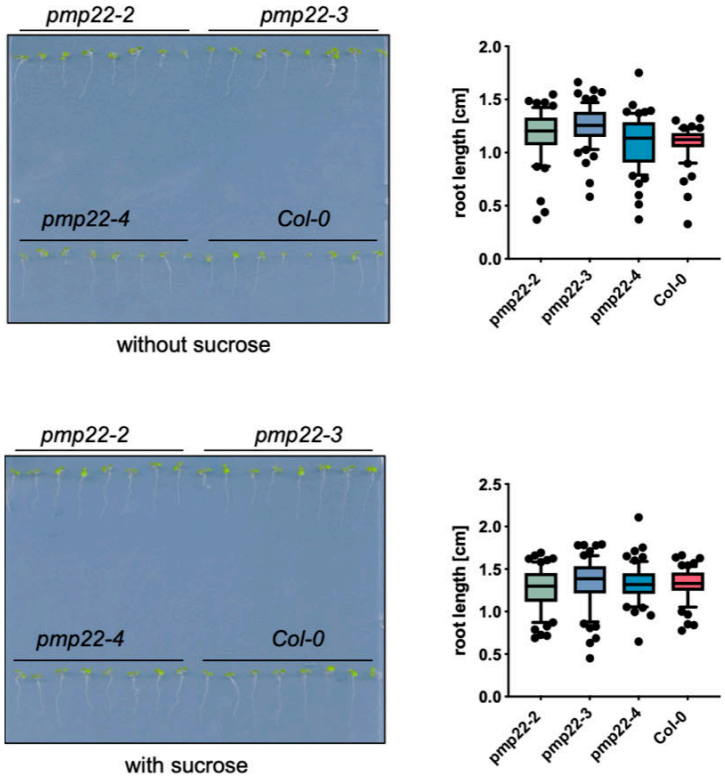


**Fig. 7 Root length of *pmp22* mutants on sucrose-free and sucrose-supplemented ½ MS media.** Seedlings of pmp22-2, pmp22-3, pmp22-4, and Col-0 were germinated and grown for 5 days on ½ MS medium without sucrose (top) and with 2% (w/v) sucrose (bottom). Root length was measured in cm using Fiji software. Biological replicates (N> 50) were plotted. Student's t-test = not significant.

The mutant seedlings showed no significant difference in root length on media without sucrose nor on media supplemented with sucrose (Fig. 7), indicating that the mutant is not sucrose dependent.

## PMP22-like localizes to the peroxisomes

Among the 10 MPV17/PMP22 family in Arabidopsis, a second gene (At4g14305) encoding for PMP22-like is predicted to localize to peroxisomes. A high sequence similarity might result in a functional overlap or redundancy between PMP22 and PMP22-like and could explain the lack of a visible phenotype in *pmp22* single mutants. If both proteins contribute to similar pathways in peroxisomes, loss of one gene may be compensated by the other, therefore masking physiological effects. We confirmed its localization by fluorescent fusion proteins and confocal laser scanning microscopy (Fig. 8 A) and aimed to restore the *sym1Δ* mutant (Fig. 8 C)

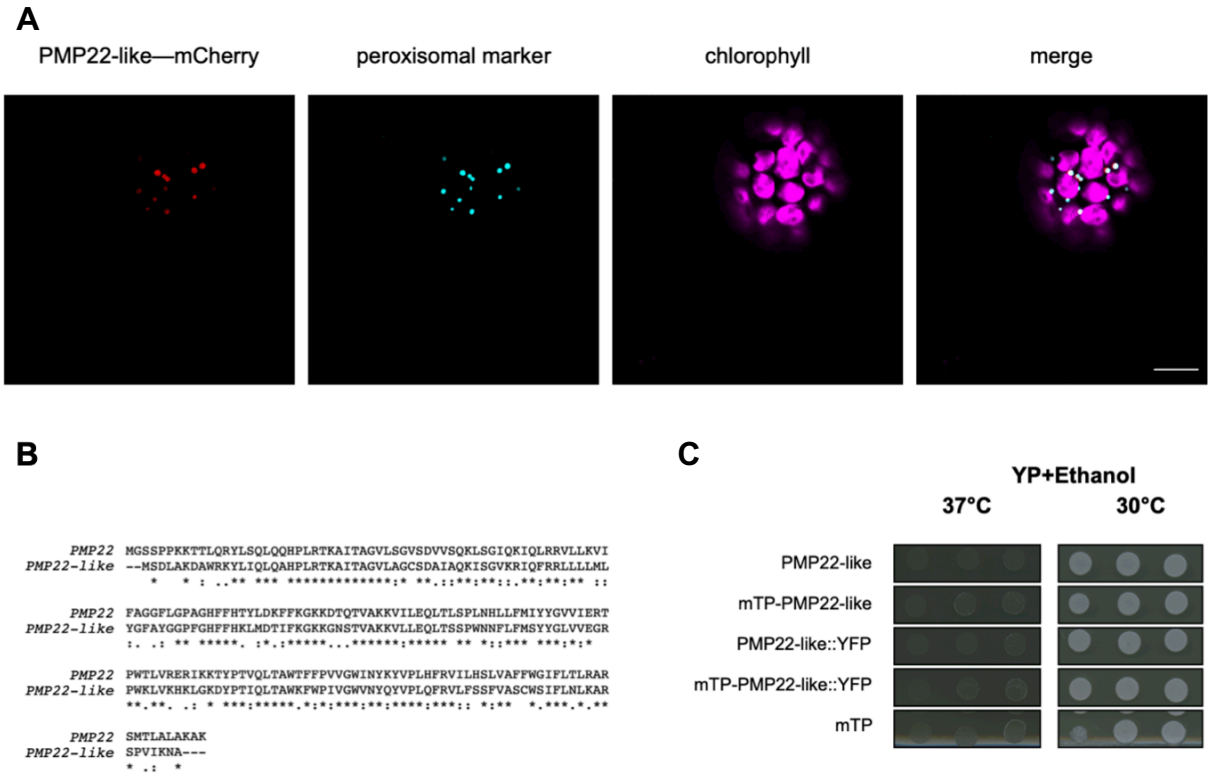


**Fig. 8 Subcellular localization, sequence alignment and functional yeast complementation of PMP22-like.** (A) C-terminal mCherry fluorescent fusion construct was co-infiltrated with a peroxisomal marker in *N. benthamiana* leaves and protoplasts were analyzed by a confocal microscope 2 days post-infiltration. Images were analyzed using Fiji. Chlorophyll A autofluorescence: magenta, peroxisomal marker: cyan fluorescent protein with C-terminal PTS1, PMP22-like-mCherry: red. Scale bar: 10 µM. (B) Amino acid sequence alignment of PMP22 and PMP22-like. (C) Yeast cells of *sym1Δ, sym1Δ* transformed with PMP22-like complementation construct (PMP22-like) or with a N-terminal mitochondrial transit peptide fused to PMP22-like (mTP::PMP22-like), *sym1Δ* transformed with a fluorescent PMP22-like localization construct (PMP22-like::YFP) or with a N-terminal mitochondrial transit peptide fused to the localization construct (mTP::PMP22-like::YFP) were diluted to an $OD_{600}$ = 1, 2 or 3 and plated on plates with 2% ethanol as a nonfermentable carbon source and incubated for 3 days at 30°C or 37°C.

Co-localization studies of a C-terminal mCherry fusion with a peroxisomal marker (CFP fused to PTS1), verified that the closest homologue, PMP22-like, does localize to peroxisomes (Fig. 7A). Amino acid alignment of PMP22 and PMP22-like revealed in 79% sequence similarity (Fig. 8 B). Similar to PMP22, we tested whether PMP22-like could restore the *sym1Δ* mutant by generating complementation constructs. PMP22-like was not able to rescue the mutant when grown on media supplemented with 2% ethanol as the sole carbon source at elevated temperatures (Fig. 7C).

## Discussion

Peroxisomes are highly dynamic organelles, involved in several essential pathways in plant development and metabolism. A single lipid bilayer separates the peroxisomal lumen from the cytoplasm. To connect peroxisomal metabolism to the overall plant metabolism, transport proteins are needed. To date, only a few transporters have been described and characterized. Further studies on isolated peroxisomes revealed channel activity (Reumann et al., 1995). The MPV17/PMP22 family is conserved in the eukaryotic kingdom and acts as non-selective pore-forming channels in mitochondria, peroxisomes and chloroplasts. PMP22 was initially localized to peroxisomes by immunofluorescence and proteomic studies (Murphy et al., 2003; Reumann and Singhal, 2014). We were able to confirm these results by generating fluorescent fusion proteins and co-localizing them with a peroxisomal marker protein using laser scanning microscopy (Fig. 1).

In order to analyze its physiological function, we aimed to complement *sym1Δ* in yeast. This mutant has been characterized as a non-selective pore-forming channel in mitochondria and is connected to ethanol metabolism under elevated temperatures. Further this mutant was functionally restored by the human MPV17 (Trott and Morano, 2004). Since, endogenous SYM1 localizes to mitochondria, we added a mitochondrial targeting peptide at the N-terminus. None of the constructs used was able to rescue the growth defect under 37 °C and ethanol as sole carbon source (Fig. 2, S Fig1, S Fig. 2). This could be explained by mislocalization of PMP22 and instead of the desired mitochondrial localization, or a different function of PMP22.

Two different mTPs were tested: The mitochondrial succinate/fumarate carrier from *Arabidopsis* (At5g01340), which efficiently targeted peroxisomal PXN to yeast mitochondria (van Roermund et al., 2016). We analyzed the localization of the fusion protein with PMP22 and could not confirm a mitochondrial localization (Fig. 3). A second approach used the yeast COXIV target peptide, although the protease cleavage site is missing in the constructs. Still, the chosen sequence should be sufficient for mitochondrial targeting (Hurt et al., 1985). The *sym1Δ* mutant could not be rescued (S Fig.2). Mitochondria have a high membrane potential which is essential for efficient ATP synthesis (Zorova et al., 2018), whereas there is no evidence for a peroxisomal ATP synthase. Gating properties can be based on the membrane

potential, redox conditions, pH or post-translational modifications (Antonenkov et al., 2015). Therefore, PMP22 could still act as a non-selective pore-forming channel, but not in the mitochondrial membrane. The import of carrier proteins into the inner mitochondrial membrane is regulated by the TIM22 (Translocase of mitochondrial inner membrane), as it was shown e.g for the ADP/ATP carrier (AAC)(Sirrenberg et al., 1996). The Import by TIM22 relies on internal targeting signals, whereas import through TIM23 requires a cleavable N-terminal sequence (Sirrenberg et al., 1996; Koehler et al., 1998). Surprisingly, it was shown that SYM1 is imported through TIM23 but in a presequence-independent way, as truncations of the N-terminus still led to mitochondrial targeting by the TIM23 complex (Reinhold et al., 2012). Although we chose two different mTPs, it remains unclear whether this is sufficient for an inner mitochondrial membrane targeting of PMP22, as some internal targeting signals might be missing.

Taking into account that the MPV17/PMP22 family is conserved in the eukaryotic kingdom, linking three organelles, amino acids could be potential substrates, as they are needed in several metabolic pathways such as photorespiration, which links chloroplasts, peroxisomes and mitochondria. Our results indicate that PMP22 might play a role in sensitivity to JA and may be linked to central amino acid metabolism during stress responses (Fig. 4& 5). The precursor OPDA of JA is known to be imported into peroxisomes by CTS (Theodoulou et al., 2005), but the export of JA remains unknown. Indeed, *pmp22* seedlings exhibit a strong growth inhibition compared to WT when grown on high exogenous JA concentrations. This sensitivity might indicate altered endogenous JA concentrations by an impaired export. JA levels increase upon certain stress such as wounding, and are the result of cytosolic $Ca^{2+}$ influx, membrane depolarizations and bulk flow of amino acids (Gilroy et al., 2016; Johns et al., 2021). Therefore, we analyzed amino acid profiles of *pmp22* under stress conditions. The mutant showed a reduction in several amino acids under controlled conditions, with a significant decrease in arginine. Upon wounding, WT plants showed overall reduced content, while several amino acids were slightly upregulated in the mutant. Although almost all of these changes were not statistically significant, the overall trend suggests an altered amino acid content in the mutant. Interestingly, arginine levels are strongly reduced in the mutant. Arginine can act as a source for nitric oxide (NO) via L-arginine dependent NO synthase (Corpas et al., 2020). NO can

interact with different forms of ROS and form reactive nitrogen species (RNS). Enzymes such as catalase and ascorbate peroxidase can be inhibited by NO, leading to an accumulation of ROS during stress responses. The relationship between NO and PMP22 remains unresolved and requires further investigations.

The lack of independent knock-out lines hinders proper studies on the physiological function of PMP22. We therefore generated further lines by CRISPR/Cas9 mediated mutagenesis. We tested those lines for β-oxidation activity by growing seedlings on media supplemented with sucrose and sucrose-free media, but observed no difference in root length compared to WT (Fig. 7). To further test for the involvement in β-oxidation direct measurements of fatty acids are required. *PMP22-like* shares a high similarity in sequence and might be able to rescue the loss of *PMP22* due to gene redundancy (Fig. 8). Double mutant lines could overcome this issue and were generated by CRISP/Cas9, but require further investigations (S Fig.4).

# Materials and Methods

### Plant material and growth conditions

*Arabidopsis thaliana* ecotype Col-0 as WT, *pmp22-1* mutant (SALK_205443) and *pmp22-like* mutant (GABI-380B12) were used in this study. Seeds were surface sterilized by sodium hypochlorite and grown on half-strength Murashige and Skoog medium (½ MS) supplemented with 0.8% (w/v) plant agar. Stratification was carried out for 48 h at 4°C. Seedlings were grown under a 12 h light/ 12 h dark photoperiod with a light intensity of 100 µmol photons $m^{-2}s^{-1}$.

### Generation of *pmp22* knockout mutants by CRISPR/Cas9

CRISPR/Cas9 mediated knockouts were generated in the *Col-0* and *pmp22-like* mutant background. Three guides of *PMP22* were assembled as one transcriptional unit using the polycistronic-tRNA-gRNA (PTG) strategy. All parts were generated by golden gate cloning using the MoClo tool kit. The final level 2 vector contains following features: (1) Basta resistance ($bar^r$), (2) egg- cell specific driven Cas9, (3) assembled guides (4) seed coat specific At2S3-promoter controlled a green fluorescent protein (GFP). Vectors were kindly provided by Claus Peter Witte, University of Hannover, Germany. Final constructs were transformed by Agrobacterium-mediated floral dipping. Transgenic plants were selected by GFP fluorescence and mutant plants were confirmed by PCR and sanger sequencing.

### Generation and transient expression of localization constructs

Coding sequences of *PMP22* and *PMP22-like* were amplified from *Arabidopsis* cDNA and fused to a C-terminal mCherry. A UBIQUITIN10 (UBQ10) promoter from Arabidopsis was used. C-terminal peroxisomal targeting signal 1 (PTS1) was fused to a cyan fluorescent protein (CFP) under the control of the CaMV 35S promoter. *Agrobacterium tumefaciens* strain GV3103 were transformed with the final constructs and positive transformants were confirmed by PCR. An overnight culture with each construct was diluted in infiltration medium (10 mM MES [pH 5.7], 10 mM $MgCl_2$, 100

µM acetosyringone) to an $OD_{600}$ of 0.3. 2-3 leaves of four-week-old *Nicotiana benthamiana* were infiltrated by a syringe. Protoplasts were isolated two days post infection. In brief, leaves were sliced into small pieces, vacuum-infiltrated with a digest solution (20 mM MES [pH 5.7], 400 mM mannitol, 20 mM KCl, 10 mM CaCl2, 1.5% [w/v] cellulase R-10, 0.5% [w/v] macerozyme R-10, 0.1% [w/v] BSA) and incubated for 2 h at 28°C. Protoplasts were washed with W5 solution (154 mM NaCl, 125 mM $CaCl_2$, 5 mM KCl, 2 mM MES [pH 5.7]) and analyzed by confocal laser scanning microscopy. Following excitation/emission wavelength were used: mCherry (561 nm/ 580-625 nm), CFP (450 nm/ 510-550 nm), chlorophyll A (488 nm/ 640-710 nm).

**JA treatment and wounding**

JA was added to ½ MS plates to a final concentration of 30-60 µM. Seeds were surface sterilized, stratified for 48 h at 4°C and grown under a 12 h light/ 12 h dark photoperiod at 100 µmol photons $m^{-2}s^{-1}$ light intensity. Pictures were taken after 21 days and analyzed by Fiji. Leaves of 5-6-weeks old plants were wounded by crushing with forceps and harvested with liquid nitrogen 10- 60 min post wounding.

**Amino acid measurements by mass spectrometry (LC-MS)**

Leaf 8 of a 6-weeks-old plant was collected and frozen in liquid nitrogen 1 h post wounding, with 5 biological replicates. Unwounded leaf 8 served as a negative control. Frozen tissue (20-30 mg) was ground in liquid nitrogen, and 250 µL precooled chloroform/methanol (10:4.28) was added and vortexed. After 1 hour at -20 °C, 560 µL ice-cold water with internal standard (D8-Valine) was added. The samples were vortexed, incubated on ice for 10 min, and centrifuged at 4 °C for 4 min to collect the aqueous phase. The process was repeated, combining the aqueous phases, and sterile water was added to reach 1700 µL. All samples were lyophilized. The dried sample was reconstituted in 500 µL deionized water and filtrated through a 0.2 µm spin filter (VWR). For LC-MS measurements, the sample was diluted 1:10 in the injection solution consisting of 33 % acetonitrile and 66 % ammonium formate (10 mM) at pH 3. An Agilent (Santa Clara, USA) 6490 Triple-Quadrupol mass spectrometer coupled to an Agilent (Santa Clara, USA) 1260 bioinert HPLC system was used to perform the

analysis. The autosampler was set to 8 °C and the column compartment to 45 °C. For chromatographic separation a 150 x 2.1 mm peek coated SEQUANT (MERCK) ZIC-pHILIC with 5 µm pore size in combination with a 20 x 2.1 mm ZIC-pHILIC guard column (MERCK) was used. Eluents were prepared with a 200 mM ammonium formate stock solution that was adjusted to pH 3 with formic acid and further diluted 9:1 in 80:10 water:acetonitrile for mobile phase A or in acetonitrile for mobile phase B leading to a final ionic strength of 20 mM. The gradient starting conditions were 0 % B for 0.5 min followed by an increase to 40 % in 16.5 min. Within 3 min the level of B was further increased to 60 % and held for another 3min. Within 2 min the starting conditions of 0 % B were reached and the equilibration time was set to 10 min. 5 µL of sample were injected with a flow rate of 0.2 ml $min^{-1}$. The mass spectrometer source parameters were set as follows: Gas temperature: 280 °C, Gas flow: 17 l $min^{-1}$, Nebulizer: 25 psi, sheath gas temperature: 400 °C and a sheath gas flow of 12 l $min^{-1}$. The polarity was set to positive with a capillary voltage of 2000 V and a nozzle voltage of 500 V. The detector electron multiplier voltage (EMV) was set to (+) 300 V.

**Yeast strains and media**

*S. cerevisiae* strains BY4741 and *sym1Δ* (YLR251W, Euroscarf, Frankfurt, Germany) were used in this study. Yeast cells were grown in liquid synthetic complete medium (SC) or in rich Yeast-Peptone (YP) medium or on plates at 28°C. 2% (v/v) ethanol, glycerol or glucose were added as carbon sources.

# References

**Anfang M, Shani E** (2021) Transport mechanisms of plant hormones. Curr Opin Plant Biol **63:** 102055

**Antonenkov VD, Hiltunen JK** (2012) Transfer of metabolites across the peroxisomal membrane. Biochim Biophys Acta **1822:** 1374-1386

**Antonenkov VD, Isomursu A, Mennerich D, Vapola MH, Weiher H, Kietzmann T, Hiltunen JK** (2015) The Human Mitochondrial DNA Depletion Syndrome Gene MPV17 Encodes a Non-selective Channel That Modulates Membrane Potential. J Biol Chem **290:** 13840-13861

**Bellandi A, Papp D, Breakspear A, Joyce J, Johnston MG, de Keijzer J, Raven EC, Ohtsu M, Vincent TR, Miller AJ, Sanders D, Hogenhout SA, Morris RJ, Faulkner C** (2022) Diffusion and bulk flow of amino acids mediate calcium waves in plants. Science Advances **8:** eabo6693

**Bernhardt K, Wilkinson S, Weber AP, Linka N** (2012) A peroxisomal carrier delivers NAD(+) and contributes to optimal fatty acid degradation during storage oil mobilization. Plant J **69:** 1-13

**Castillo MC, Sandalio LM, Del Rio LA, Leon J** (2008) Peroxisome proliferation, wound-activated responses and expression of peroxisome-associated genes are cross-regulated but uncoupled in Arabidopsis thaliana. Plant Cell Environ **31:** 492-505

**Corpas FJ, González-Gordo S, Palma JM** (2020) Plant Peroxisomes: A Factory of Reactive Species. Front Plant Sci **11:** 853

**Dallabona C, Marsano RM, Arzuffi P, Ghezzi D, Mancini P, Zeviani M, Ferrero I, Donnini C** (2010) Sym1, the yeast ortholog of the MPV17 human disease protein, is a stress-induced bioenergetic and morphogenetic mitochondrial modulator. Hum Mol Genet **19:** 1098-1107

**Deb R, Nagotu S** (2017) Versatility of peroxisomes: An evolving concept. Tissue Cell **49:** 209-226

**Footitt S, Marquez J, Schmuths H, Baker A, Theodoulou FL, Holdsworth M** (2006) Analysis of the role of COMATOSE and peroxisomal beta-oxidation in the determination of germination potential in Arabidopsis. J Exp Bot **57:** 2805-2814

**Footitt S, Slocombe SP, Larner V, Smita Kurup , Wu Y, Larson T, Graham I, Baker A, Holdsworth M** (2002) Control of germination and lipid mobilization by COMATOSE, the Arabidopsis homologue of human ALDP. The EMBO Journal **21:** 2912-2922

**Ghorbel M, Brini F, Sharma A, Landi M** (2021) Role of jasmonic acid in plants: the molecular point of view. Plant Cell Reports **40:** 1471-1494

**Gilroy S, Bialasek M, Suzuki N, Gorecka M, Devireddy AR, Karpinski S, Mittler R** (2016) ROS, Calcium, and Electric Signals: Key Mediators of Rapid Systemic Signaling in Plants. Plant Physiol **171:** 1606-1615

**Haferkamp I, Linka N** (2012) Functional expression and characterisation of membrane transport proteins. Plant Biology **14:** 675-690

**Hayashi M, Nito K, Takei-Hoshi R, Yagi M, Kondo M, Suenaga A, Yamaya T, Nishimura M** (2002) Ped3p is a Peroxisomal ATP-Binding Cassette Transporter that might Supply Substrates for Fatty Acid β-Oxidation. Plant Cell Physiol **43:** 1-11

**Hooks MA, Turner JE, Murphy EC, Graham IA** (2004) Acetate non-utilizing mutants of Arabidopsis: evidence that organic acids influence carbohydrate perception in germinating seedlings. Mol Genet Genomics **271:** 249-256

**Hurt EC, Pesold-Hurt B, Suda K, Oppliger W, Schatz G** (1985) The first twelve amino acids (less than half of the pre-sequence) of an imported mitochondrial protein can direct mouse cytosolic dihydrofolate reductase into the yeast mitochondrial matrix. The EMBO journal **4:** 2061-2068

**Johns S, Hagihara T, Toyota M, Gilroy S** (2021) The fast and the furious: rapid long-range signaling in plants. Plant Physiol **185:** 694-706

**Koehler CM, Jarosch E, Tokatlidis K, Schmid K, Schweyen RJ, Schatz G** (1998) Import of Mitochondrial Carriers Mediated by Essential Proteins of the Intermembrane Space. Science **279:** 369-373

**Li J, Tietz S, Cruz JA, Strand DD, Xu Y, Chen J, Kramer DM, Hu J** (2018) Photometric screens identified Arabidopsis peroxisome proteins that impact photosynthesis under dynamic light conditions. The Plant Journal **97:** 460-474

**Linka N, Theodoulou FL** (2013) Metabolite transporters of the plant peroxisomal membrane - known and unknown. Subcell Biochem **69:** 169-194

**Linka N, Theodoulou FL, Haslam RP, Linka M, Napier JA, Neuhaus HE, Weber AP** (2008) Peroxisomal ATP import is essential for seedling development in Arabidopsis thaliana. Plant Cell **20:** 3241-3257

**Murphy MA, Phillipson BA, Baker A, Mullen RT** (2003) Characterization of the targeting signal of the Arabidopsis 22-kD integral peroxisomal membrane protein. Plant Physiol **133:** 813-828

**Reinhold R, Kruger V, Meinecke M, Schulz C, Schmidt B, Grunau SD, Guiard B, Wiedemann N, van der Laan M, Wagner R, Rehling P, Dudek J** (2012) The channel-forming Sym1 protein is transported by the TIM23 complex in a presequence-independent manner. Mol Cell Biol **32:** 5009-5021

**Reumann S, Maier E, Benz R, Heldt HW** (1995) The membrane of leaf peroxisomes contains a porin-like channel. J Biol Chem **270:** 17559-17565

**Reumann S, Singhal R** (2014) Isolation of leaf peroxisomes from Arabidopsis for organelle proteome analyses. Methods Mol Biol **1072:** 541-552

**Rokka A, Antonenkov VD, Soininen R, Immonen HL, Pirila PL, Bergmann U, Sormunen RT, Weckstrom M, Benz R, Hiltunen JK** (2009) Pxmp2 is a channel-forming protein in Mammalian peroxisomal membrane. PLoS One **4:** e5090

**Sirrenberg C, Bauer MF, Guiard B, Neupert W, Brunner M** (1996) Import of carrier proteins into the mitochondrial inner membrane mediated by Tim22. Nature **384:** 582-585

**Spinazzola A, Viscomi C, Fernandez-Vizarra E, Carrara F, D'Adamo P, Calvo S, Marsano RM, Donnini C, Weiher H, Strisciuglio P, Parini R, Sarzi E, Chan A, DiMauro S, Rotig A, Gasparini P, Ferrero I, Mootha VK, Tiranti V, Zeviani M** (2006) MPV17 encodes an inner mitochondrial membrane protein and is mutated in infantile hepatic mitochondrial DNA depletion. Nat Genet **38:** 570-575

**Theodoulou FL, Job K, Slocombe SP, Footitt S, Holdsworth M, Baker A, Larson TR, Graham IA** (2005) Jasmonic acid levels are reduced in COMATOSE ATP-binding cassette transporter mutants. Implications for transport of jasmonate precursors into peroxisomes. Plant Physiol **137:** 835-840

**Trott A, Morano KA** (2004) SYM1 is the stress-induced Saccharomyces cerevisiae ortholog of the mammalian kidney disease gene Mpv17 and is required for ethanol metabolism and tolerance during heat shock. Eukaryot Cell **3:** 620-631

**Tugal HB, Pool M, Baker A** (1999) Arabidopsis 22-Kilodalton Peroxisomal Membrane Protein. Nucleotide Sequence Analysis and Biochemical Characterization. Plant Physiology **120:** 309–320

**van Roermund CW, Schroers MG, Wiese J, Facchinelli F, Kurz S, Wilkinson S, Charton L, Wanders RJ, Waterham HR, Weber AP, Link N** (2016) The Peroxisomal NAD Carrier from Arabidopsis Imports NAD in Exchange with AMP. Plant Physiol **171:** 2127-2139

**Waese J, Fan J, Pasha A, Yu H, Fucile G, Shi R, Cumming M, Kelley LA, Sternberg MJ, Krishnakumar V, Ferlanti E, Miller J, Town C, Stuerzlinger W, Provart NJ** (2017) ePlant: Visualizing and Exploring Multiple Levels of Data for Hypothesis Generation in Plant Biology. Plant Cell **29:** 1806-1821

**Wasternack C, Song S** (2016) Jasmonates: biosynthesis, metabolism, and signaling by proteins activating and repressing transciption. Journal of Experimental Botany

**Wiese J** (2014) Propionate metabolism in yeast and plants. Heinrich Heine University

**Zolman BK, Silva ID, Bartel B** (2001) The Arabidopsis pxa1 Mutant Is Defective in an ATP-Binding Cassette Transporter-Like Protein Required for Peroxisomal Fatty Acid β-Oxidation. Plant Physiology **127:** 1266-1278

**Zorova LD, Popkov VA, Plotnikov EY, Silachev DN, Pevzner IB, Jankauskas SS, Babenko VA, Zorov SD, Balakireva AV, Juhaszova M, Sollott SJ, Zorov DB** (2018) Mitochondrial membrane potential. Anal Biochem **552:** 50-59

# Supplemental

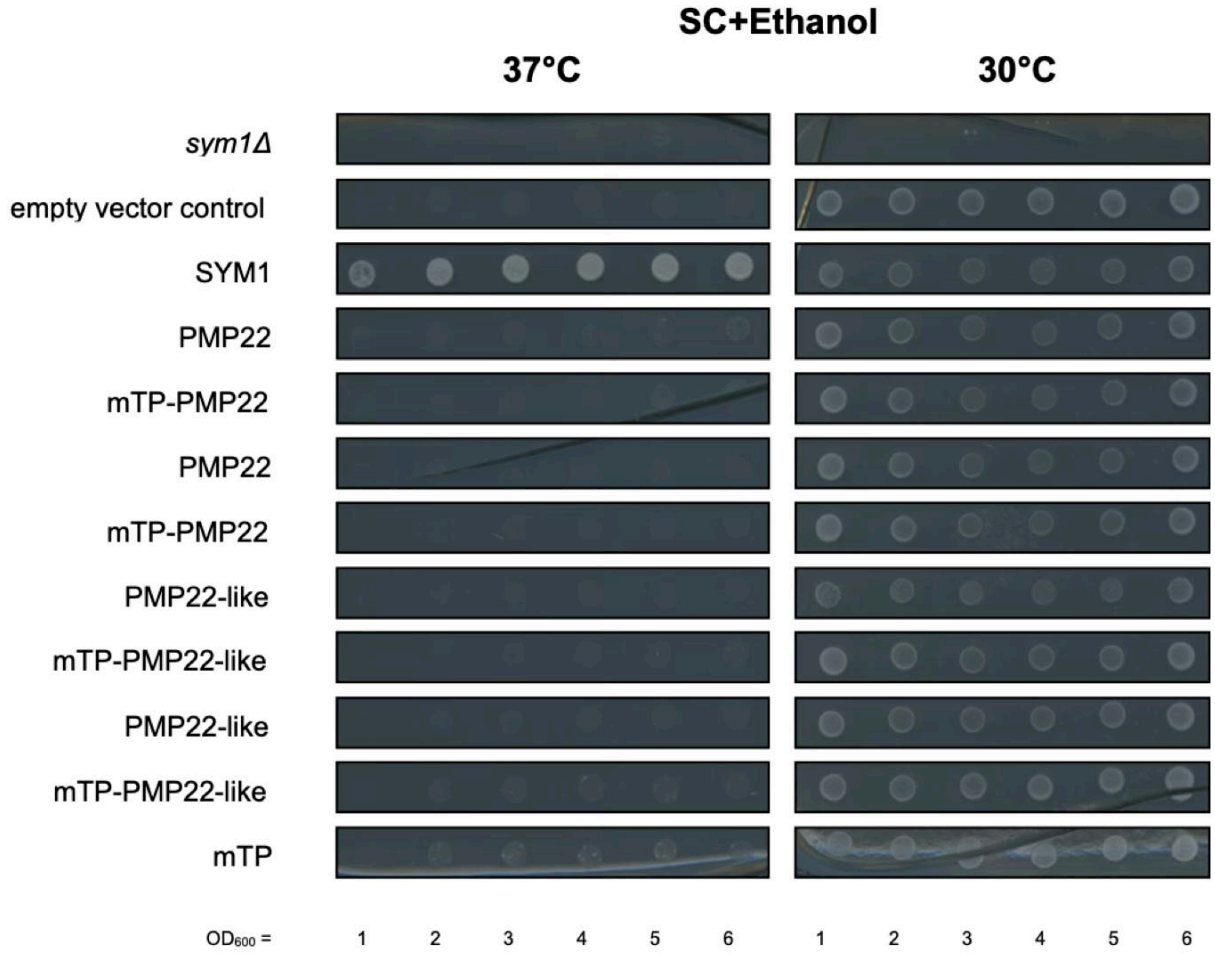


**S Fig. 1 Functional yeast complementation of PMP22 (-like) in *sym1Δ* strain.** All yeast cells were plated on SC medium containing ethanol (2%) and incubated at 30 or 37°C. Yeast cells of *sym1Δ, sym1Δ* transformed with the empty vector (empty vector control) , wild-type (SYM1), *sym1Δ* transformed with PMP22 complementation construct (PMP22) or with a N-terminal mitochondrial transit peptide fused to PMP22 (mTP-PMP22), *sym1Δ* transformed with PMP22-like or with a N-terminal mitochondrial transit peptide fused to the construct (mTP-PMP22-like) were diluted to an $OD_{600}$ = 1, 2, 3, 4, 5 or 6 and plated on plates with 2% ethanol as a nonfermentable carbon source and incubated for 10 days at 30 or 37°C.

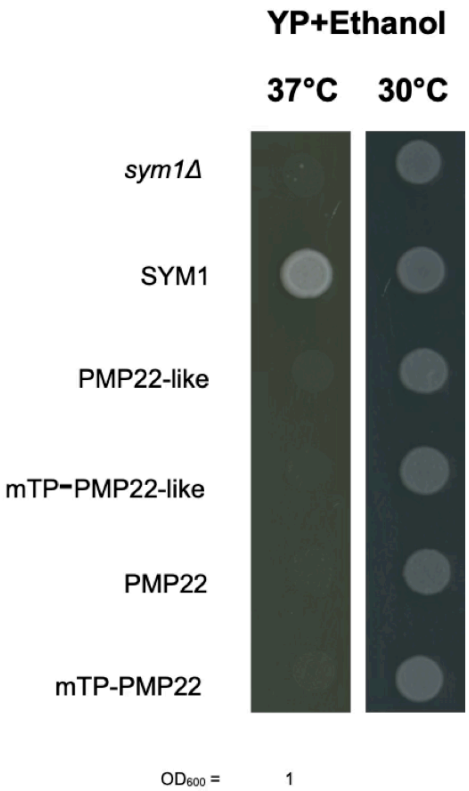


**S Fig. 2 Functional yeast complementation of PMP22 (-like) in *sym1Δ* strain with a different mTP.** All yeast cells were plated on YP medium containing ethanol (2%) and incubated at 30 or 37°C. Yeast cells of *sym1Δ,* wild-type (SYM1), *sym1Δ* transformed with PMP22 complementation construct (PMP22) or with a N-terminal mitochondrial transit peptide fused to PMP22 (mTP-PMP22), *sym1Δ* transformed with PMP22-like or with a N-terminal mitochondrial transit peptide fused to the construct (mTP-PMP22-like) were diluted to an $OD_{600}$ = 1 and plated on plates with 2% ethanol as a nonfermentable carbon source and incubated for 10 days at 30 or 37°C.

**S Fig. 3 Image of WT and *pmp22/pmp22-like* double mutant.** Seedlings were grown for 21 days on soil under 12/12 day/night cycle at 22 °C

# Manuscript III

## Chlamydomonas mutants lacking chloroplast TRIOSE PHOSPHATE TRANSPORTER3 are metabolically compromised and light sensitive

**Status**: published

**Author contributions**: W.H., A.K., A.G., and M.P. conceptualized the study. W.H. generated the CRISPR mutants as well as the complemented strain, localized the TPT2 and TPT3 proteins, and analyzed the photosynthetic performances and starch changes over diel cycle. A.K. performed the experiments of photosynthetic O2 evolution, extraction of samples for LC–MS/MS, and data analysis of LC–MS/MS. **A.P.** and N.L. performed the reconstitution into liposomes and transport activity assays

https://doi.org/10.1093/plcell/koad095 THE PLANT CELL 2023: 35: 2592–2614

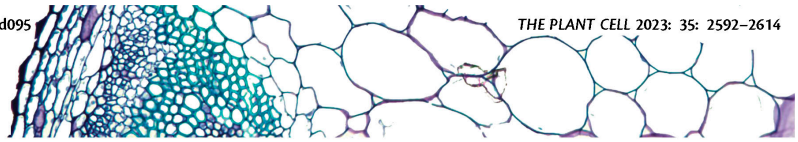

Research Article

# *Chlamydomonas* mutants lacking chloroplast TRIOSE PHOSPHATE TRANSPORTER3 are metabolically compromised and light sensitive

**Weichao Huang (黄伟超) [1,*,†] Anagha Krishnan [2,†] Anastasija Plett [3] Michelle Meagher [4] Nicole Linka [3] Yongsheng Wang [1,5] Bijie Ren [1] Justin Findinier [1] Petra Redekop [1] Neda Fakhimi [1] Rick G. Kim [1] Devin A. Karns [2] Nanette Boyle [4] Matthew C. Posewitz [2] and Arthur R. Grossman [1,*]**

1 Department of Plant Biology, Carnegie Institution for Science, Stanford, CA 94305, USA
2 Department of Chemistry, Colorado School of Mines, Golden, CO 80401, USA
3 Institute of Plant Biochemistry, Heinrich-Heine University Düsseldorf, 40225 Düsseldorf, Germany
4 Department of Chemical and Biological Engineering, Colorado School of Mines, Golden, CO 80401, USA
5 School of Life Sciences, Tsinghua University, 100084 Beijing, China

*Author for correspondence: whuang@carnegiescience.edu (W.H.), agrossman@carnegiescience.edu (A.G.)
†These authors contributed equally.
The author(s) responsible for distribution of materials integral to the findings presented in this article in accordance with the policy described in the Instructions for Authors (https://academic.oup.com/plcell/) are: Weichao Huang (whuang@carnegiescience.edu) and Arthur Grossman (agrossman@carnegiescience.edu).

## Abstract

Modulation of photoassimilate export from the chloroplast is essential for controlling the distribution of fixed carbon in the cell and maintaining optimum photosynthetic rates. In this study, we identified chloroplast TRIOSE PHOSPHATE/PHOSPHATE TRANSLOCATOR 2 (CreTPT2) and CreTPT3 in the green alga *Chlamydomonas* (*Chlamydomonas reinhardtii*), which exhibit similar substrate specificities but whose encoding genes are differentially expressed over the diurnal cycle. We focused mostly on *CreTPT3* because of its high level of expression and the severe phenotype exhibited by *tpt3* relative to *tpt2* mutants. Null mutants for *CreTPT3* had a pleiotropic phenotype that affected growth, photosynthetic activities, metabolite profiles, carbon partitioning, and organelle-specific accumulation of $H_2O_2$. These analyses demonstrated that CreTPT3 is a dominant conduit on the chloroplast envelope for the transport of photoassimilates. In addition, CreTPT3 can serve as a safety valve that moves excess reductant out of the chloroplast and appears to be essential for preventing cells from experiencing oxidative stress and accumulating reactive oxygen species, even under low/moderate light intensities. Finally, our studies indicate subfunctionalization of the TRIOSE PHOSPHATE/PHOSPHATE TRANSLOCATOR (CreTPT) transporters and suggest that there are differences in managing the export of photoassimilates from the chloroplasts of *Chlamydomonas* and vascular plants.

## Introduction

Photosynthetic organisms can absorb excess, potentially damaging levels of light energy during mid-day (when photosynthetic electron transport becomes saturated), and can suffer from extreme damage, especially when experiencing rapid fluctuations in light intensities or when subjected to nutrient-limiting conditions and other environmental stresses that impair the productive utilization of excitation energy (Chaux et al. 2017; Saroussi et al. 2017). To cope with excess excitation energy, plants and algae have evolved mechanisms to dissipate this energy through nonphotochemical quenching (NPQ) (Niyogi and Truong 2013). The excess reductant

Received January 06, 2023. Accepted March 08, 2023. Advance access publication March 27, 2023

## IN A NUTSHELL

**Background:** In photosynthetic eukaryotes, chloroplasts supply energy and fixed/organic carbon to other cellular compartments through numerous transporters in the chloroplast envelope. Modulating metabolite export from the chloroplast can markedly impact the growth and photosynthetic activity of cells. Additionally, the export of metabolites/sugars from chloroplasts can transduce signals to the nucleus and coordinate the expression of chloroplast and nuclear genes in response to environmental changes and the cell's metabolic demands. However, the activities and substrate specificities of several of the transporters, the ways in which they are regulated, and how their functions are integrated are not well defined in microalgae such as *Chlamydomonas*.

**Question:** What metabolite transporters on the chloroplast envelope are critical for the movement of sugars between the chloroplast and cytosol in the green alga *Chlamydomonas*, and how does this export regulate cell growth, metabolism, cellular redox conditions, and the formation of potentially toxic oxygen radicals?

**Findings:** We found that the triose phosphate (triose-P)/phosphate (Pi) translocator 3 (TPT3) is a major conduit for the export of fixed carbon, as simple 3-carbon sugars, from *Chlamydomonas* chloroplasts. Mutants unable to make this transporter are light sensitive and show marked changes in their metabolic profiles relative to unmutated cells; the major shift in cellular metabolism creates a toxic intracellular environment (probably through production of reactive oxygen species) with increasing light absorbance. Additionally, unlike for many vascular plants, *Chlamydomonas* is unable to compensate for the loss of TPT3 through the activities of other sugar transporters.

**Next steps:** This work would further benefit from the use of metabolite flux analyses and characterization of other mutants defective for chloroplast sugar transporters. It offers opportunities for assessing the catalytic features of these transporters and how they are regulated and interact with each other to insure robust metabolism under dynamic environmental conditions.

and energy can also be eliminated by photochemical quenching. While the dominant form of photochemical quenching often involves the use of electrons/reductant to fix inorganic carbon (Ci), which is directed toward growth or stored in the form of starch and lipids (Ge et al. 2014; Krishnan et al. 2015; Huang et al. 2018), redox equivalents can also be trafficked to other outlets where they are not used for anabolic reactions. The main alternative photochemical electron outlets involve the reduction of $O_2$ to $H_2O$ in $H_2O$-to-$H_2O$ cycles that include a (i) Mehler-type reaction that is noncatalytic and functions on the acceptor side of photosystem I (PSI) (Badger et al. 2000), (ii) flavodiiron protein reactions (FLVs, NADPH:flavin oxidoreductase) that catalytically reduce $O_2$ on the acceptor side of PSI without generating reactive oxygen species (ROS) (Helman et al. 2003; Chaux et al. 2017), (iii) the plastid terminal oxidase (PTOX, plastoquinol:oxygen oxidoreductase) reaction that can use electrons from the plastoquinone (PQ) pool to reduce $O_2$ (Houille-Vernes et al. 2011), and (iv) the movement of redox equivalents from the chloroplast to the mitochondrion where they can be used to reduce $O_2$ through various electron transport activities.

Mechanisms also exist in which fixed carbon and reducing equivalents can be shuttled between the chloroplast and cytoplasm. Studies with *Arabidopsis* (*Arabidopsis thaliana*) have revealed that the malate shuttle, which involves multiple malate dehydrogenases (MDH) and malate/oxaloacetate (OAA) translocators (OMTs), functions in the export of reductant from the chloroplast and the management of redox conditions in the chloroplast (Zhao et al. 2018, 2020). In addition to the malate shuttle and triose phosphate (triose-P)/inorganic phosphate (Pi) translocators (TPTs) have been proposed to be involved in moving fixed carbon out of the chloroplast but can also act as a safety valve for eliminating excess reducing power from the chloroplast (Stocking and Larson 1969; Fliege et al. 1978; Flügge et al. 1989; Raghavendra and Padmasree 2003; Johnson and Alric 2013; Lee et al. 2017). The biosynthesis of triose-Ps during photosynthetic $CO_2$ fixation by the Calvin–Benson–Bassham (CBB) cycle is supported by the reducing power/energy (NADPH, ATP) derived from photosynthetic electron transport.

TPTs reside on the inner chloroplast envelope membrane and can transport triose-Ps [glyceraldehyde 3-phosphate (GAP), dihydroxyacetone phosphate (DHAP)] and the 3 carbon acid, 3-phosphoglycerate (3-PGA), in a counter exchange for cytosolic Pi (Fliege et al. 1978; Flügge et al. 1989; Lee et al. 2017). These transporters belong to a family of plastid phosphate translocators (pPTs) that function as antiporter systems involved in exchanging Pi with phosphorylated C3, C5, or C6 compounds (Flügge et al. 2003). Most angiosperms have 2 *TPT* genes in their genome, except for various monocots and 2 dicot families, the Amaranthaceae and the Brassicaceae, which have a single *TPT* gene (Bockwoldt et al. 2019). In plants, cytosolic trioses exported from the chloroplast by TPTs are used for the biosynthesis of sucrose and other metabolites (Riesmeier et al. 1993) and to drive respiratory activity. In addition to TPTs, plants harbor the 3 other pPT subfamilies (Flügge et al. 1989; Fischer et al. 1997; Kammerer et al. 1998; Eicks et al. 2002; Lee et al.

2017). These families comprise glucose 6-phosphate (Glc6P) translocators (GPTs), which import Glc6P into plastids in heterotrophic tissue (Kammerer et al. 1998); xylulose phosphate translocators (XPTs), which play a key role in coordinating the cytosolic and plastid pentose phosphate pathways (Eicks et al. 2002); and phosphoenolpyruvate (PEP) translocators (PPTs), which import PEP into C3 plastids; PEP can be used for the biosynthesis of fatty acids, as substrate for the shikimate pathway (Streatfield et al. 1999; Prabhakar et al. 2010), and for the export of PEP from plastids in C4 plants (Häusler et al. 2000).

Over the last few decades, the physiological functions of TPTs have been examined in some detail. Various plants do not exhibit a strong phenotype if their chloroplast TPT is either eliminated or its abundance is decreased (Riesmeier et al. 1993; Häusler et al. 1998; Schneider et al. 2002; Walters et al. 2004). Lower TPT activity can be compensated for by diverting assimilated carbon into a transitory starch pool that is subjected to accelerated turnover in the light and/or darkness (Riesmeier et al. 1993; Häusler et al. 1998; Walters et al. 2004), leading to the accumulation of starch degradation products that can be exported from the chloroplast and used in other cellular compartments. Interestingly, a loss of TPT function in rice (*Oryza sativa*), a plant that uses sucrose stored in leaves as its major transitory form of fixed carbon, led to severe phenotypic consequences as the plants exhibited diminished photosynthetic rates and decreased levels of both starch and soluble sugars relative to wild-type (WT) plants (Lee et al. 2014).

Microalgae have high photosynthetic conversion efficiencies, can thrive in fresh to hypersaline waters, and can be metabolically versatile. They have attracted considerable interest worldwide because of their ability to synthesize large quantities of lipids (e.g. for biofuels and food products), starch, pigments, and other bioproducts and can serve in the remediation of wastewater (Khan et al. 2018; Bhatt et al. 2022). The transporters used for moving photoassimilates between the chloroplast and other cellular compartments and the mechanisms and regulation of these transporters in microalgae have not been extensively explored. Developing a more informed understanding of central metabolism in microalgae and the movement of metabolites among compartments can enable additional work on the establishment, regulation, and evolution of metabolic networks in algae and the ways in which algae can be tailored for production purposes and for sustained growth under specific environmental conditions.

In this study, we used *Chlamydomonas* (*Chlamydomonas reinhardtii*), a well-established model green algal system that has been extensively used to analyze various aspects of physiology, to dissect the function of chloroplast TPTs. Of the 4 putative *Chlamydomonas* pPTs, we discovered that at least 2 are "genuine" TPTs (CreTPT2 and CreTPT3) based on yeast (*Saccharomyces cerevisiae*) liposome transport assays. CreTPT2 was previously reported to be a PPT based on phylogenetic analysis (Bockwoldt et al. 2019). These 2 TPTs exhibited subfunctionalization, as reflected by the expression levels of their encoding genes and their temporally and environmentally distinct regulatory patterns. Due to the more severe phenotypes exhibited by *tpt3* relative to *tpt2* mutants, we focused our analyses on *Chlamydomonas* TPT3 (CreTPT3). Among the 4 predicted pPTs, *CreTPT3* is highly expressed in the light and strongly induced by various environmental stresses. Through a series of physiological analyses, we demonstrate that CreTPT3 is a major conduit at the chloroplast envelope for the trafficking of fixed carbon, sustaining central carbon metabolism, dissipating excess energy, enabling high rates of photosynthetic electron transport, preventing intracellular hydrogen peroxide ($H_2O_2$) accumulation, and balancing redox conditions at the subcellular level.

## Results

### The triose-P/Pi translocator (DMT/TPT) family

We identified candidate genes encoding TPT in *Chlamydomonas* by performing a BLAST search using *Arabidopsis* TPT (encoded by At5g46110.1) as a query against proteins encoded by the *Chlamydomonas* genome. The TPT family is the largest within the drug/metabolite transporter (DMT) superfamily of eukaryotes and includes triose-P and sugar–phosphate transporters associated with chloroplasts; many of the family members are still not functionally characterized (Jack et al. 2001; Knappe et al. 2003; Weber et al. 2006). We identified 32 genes encoding potential TPTs in version v6.1 of the *Chlamydomonas* genome, with 4 members, CreTPT10 (CreTPT1 in the v5.6 genome), CreTPT2 (CreTPT2 in the v5.6 genome), CreTPT3, and CONSERVED GREEN-LINEAGE 51 (CGL51), named CreTPT25 in the v5.6 genome), predicted to have a chloroplast transit peptide (Supplemental Table S1). These 4 candidates were included in a phylogenetic analysis of plant and algal pPTs that showed that CreTPT3 is a putative TPT, CreTPT2 and CreTPT10 are putative PPTs and CGL51 is a putative GPT or XPT (Bockwoldt et al. 2019).

To examine the potential substrate specificities of the 4 putative pPTs, we aligned their amino acid sequences with those of pPTs from *Arabidopsis* (AtPTs) (Supplemental Fig. S1A). The ability of these transporters to use triose-P/DHAP or 3-PGA as substrate is dependent on 5 highly conserved amino acid residues (H184, K203, Y338, K359, and R360 in AtTPT1) (Lee et al. 2017; Moog et al. 2020). Of the putative pPTs in *Chlamydomonas*, only CreTPT3 and CGL51 contain all 5 of these residues (H170, K189, Y322, K345, and R346 in CreTPT3) (Supplemental Fig. S1A). In AtTPT1, residue F262 (F248 in *Chlamydomonas* in the analogous protein, CreTPT3) is thought to inhibit PEP access to the binding site; this residue is replaced by N in AtPPT1 (PPT) (Lee et al. 2017; Moog et al. 2020). CGL51 has an M at position 248, indicating that unlike CreTPT3, CGL51 might have preference for other substrates. Protein sequence similarity and identity analysis showed that CreTPT3 and

CreTPT2 share the highest and the second highest similarity and identity with AtTPT1 (Supplemental Fig. S1B), with 57% and 49% similarity to AtTPT1, respectively. Furthermore, *CreTPT2* and *CreTPT3* have significantly higher transcript accumulation in the light relative to Cre*TPT10* and *CGL51* (Supplemental Fig. S1, C and D). Given their high similarity and high expression levels, we chose *CreTPT2* and *CreTPT3* for study.

## CreTPT2 and CreTPT3 transport properties

We defined the subcellular localization and substrate preferences of CreTPT2 and CreTPT3. As shown in Fig. 1A, both CreTPT2 and CreTPT3 fused to VENUS localized to the chloroplast envelope. To evaluate the substrate specificity of these transporters, each protein was produced in budding yeast and the resulting recombinant protein was biochemically analyzed using a liposome uptake assay. Accordingly, we cloned codon-optimized Cre*TPT2* and Cre*TPT3* genes in-frame and downstream of a sequence encoding a His-tag and induced the production of each recombinant protein in yeast (Fig. 1B). We isolated total cell membranes and reconstituted them into liposomes (Loddenkötter et al. 1993; Linka et al. 2008). Chloroplast phosphate transporters in vascular plants can catalyze a Pi/Pi homo-exchange in vitro. Both CreTPT2 and CreTPT3 reconstituted in liposomes were able to catalyze this signature Pi homo-exchange; importantly, we detected little Pi uptake in the absence of a counter-exchange substrate (Fig. 1, C and D, left). In contrast, we observed very low Pi uptake rates for liposomes reconstituted with membranes from yeast cells not producing CreTPT2 or CreTPT3 (Supplemental Fig. S2), indicating that the introduced transporters were responsible for the detected Pi import activity in yeast liposomes.

To assess the substrate specificity of the 2 CreTPT transporters, we determined their initial rates of Pi uptake into liposomes preloaded with saturating concentrations (30 mM) of various potential counter-exchange substrates. As the right panels of Fig. 1, C and D show, both CreTPT2 and CreTPT3 exhibited the highest activity when DHAP was used as the substrate for the yeast liposome assay. For both transporters, the relative initial velocity for DHAP/Pi exchange was slightly higher than that of 3-PGA/Pi (the relative 3-PGA/Pi exchange was 75% of DHAP/Pi exchange) while Pi uptake into liposomes preloaded with PEP was much lower (Fig. 1, C and D, right panels). Pi import was negligible when CreTPT2 or CreTPT3 liposomes were preloaded with Glc-6-P, Glc-1-P, Fru-6-P, and Gal-1-P (Fig. 1, C and D, right panels). These results show that CreTPT2 and CreTPT3 have almost the same substrate preferences, with both specifically supporting the transport of triose-P and 3-PGA across the membrane in exchange for Pi.

We characterized the $K_M$ and $K_i$ for CreTPT2 and CreTPT3 to determine the affinity of these transporters to various substrates. CreTPT3 had an apparent Michaelis–Menten constant ($K_M$) of $1.1 \pm 0.2$ mM for Pi (Fig. 1E), which is comparable with the value obtained for its TPT ortholog in vascular plants (Fliege et al. 1978). CreTPT2 had a slightly lower $K_M$ for Pi than CreTPT3 ($0.77 \pm 0.05$ mM) (Fig. 1E). However, while the 3-PGA Ki values were comparable for the 2 transporters, DHAP was more effective in inhibiting CreTPT3-dependent Pi exchange than CreTPT2-dependent Pi exchange (Fig. 1E). These results suggest that CreTPT3 may have a greater specificity for the transport of DHAP than CreTPT2 and that it may be more effective in transporting C3-phosphorylated compounds than CreTPT2. In the case of PEP, we observed no inhibition of Pi/Pi homo-exchange, even at the nonphysiological high concentration of 5 mM. Overall, the results of these in vitro assays indicate that both CreTPT2 and CreTPT3 have a typical plant TPT substrate spectrum (Fliege et al. 1978) and can transport Pi, triose-P (DHAP), and 3-PGA in a counter-exchange mode. However, PEP might not be a physiologically relevant substrate for either CreTPT2 or CreTPT3, as is the case for apoplast TPT homologs in other organisms (Lim et al. 2010; Moog et al. 2020). Furthermore, the values generated in these analyses may not precisely reflect transport kinetics in vivo since the 2 transporters used for these in vitro assays were fused to a His-tag at their *N*-terminus and yeast liposomes would have a different lipid composition than the chloroplast inner envelop membrane, where these transporters are normally localized.

## Isolation of *tpt2* and *tpt3* null mutants of *Chlamydomonas* and their effects on cell growth

To explore the role of CreTPT2 and CreTPT3 in trafficking carbon and potentially reductant across the chloroplast envelope in vivo, we generated knockouts of Cre*TPT2* or Cre*TPT3* by clustered regularly interspaced short palindromic repeat (CRISPR)/CRISPR-associated nuclease 9 (Cas9)-mediated gene editing. We used the CRISPR/Cas9 editing system to disrupt the Cre*TPT2* or Cre*TPT3* locus while at the same time to integrate a hygromycin resistance marker gene (*AphVII*) at the edited site (Figs. 2A and S3 and S4). We obtained 4 independent knockouts for Cre*TPT2* (*t2ko1*, *t2ko2*, *t2ko3*, and *t2ko4*), with the marker gene inserted into exon 8 (Supplemental Fig. S3). Similarly, we isolated 3 independent knockouts for Cre*TPT3*: *t3ko1*, with the marker gene inserted into exon 1, and *t3ko2* and *t3ko3*, with the marker gene inserted into exon 7; we detected no CreTPT3 protein in any of these edited strains (Fig. 2B).

To elucidate the physiological roles of CreTPT2 and CreTPT3, we examined the growth of the parental WT strain and the knockout mutants under either low light (LL, 30 $\mu$mol photons $m^{-2}$ $s^{-1}$), moderate light (ML, 250–300 $\mu$mol photons $m^{-2}$ $s^{-1}$), or high light (HL, 450 $\mu$mol photons $m^{-2}$ $s^{-1}$). The design of the experiments in which the cells were transferred from 1 light condition to another is shown in Supplemental Fig. S5. The 4 *tpt2* mutants (*t2ko1*, *t2ko2*, *t2ko3*, and *t2ko4*) were not affected by growth in LL, but their growth was significantly impaired relative to WT cells under HL on either photoautotrophic (TP) or

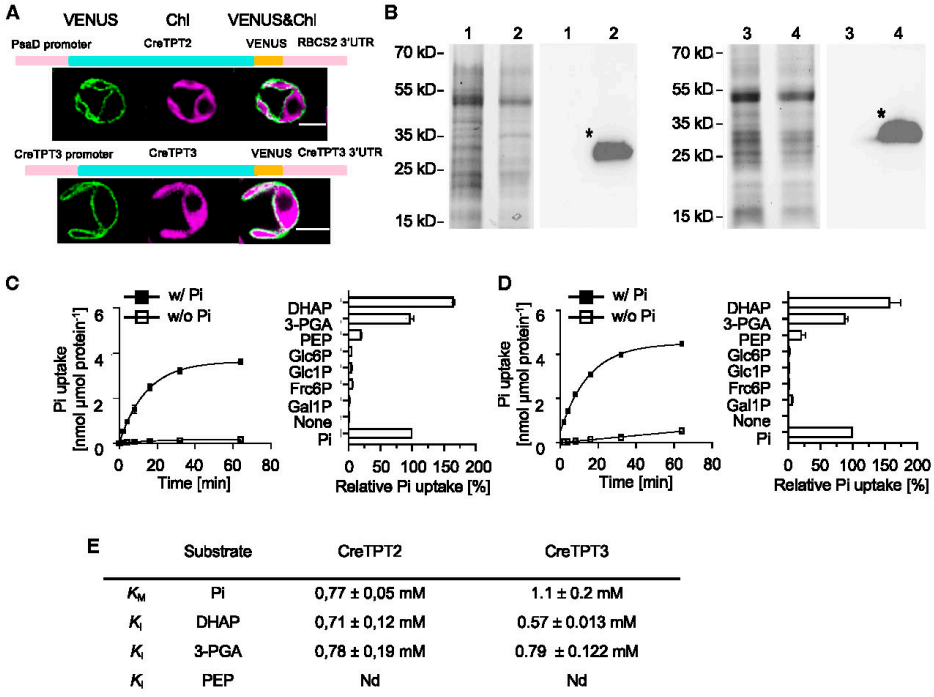


| | Substrate | CreTPT2 | CreTPT3 |
|---|---|---|---|
| $K_M$ | Pi | 0,77 ± 0,05 mM | 1.1 ± 0.2 mM |
| $K_i$ | DHAP | 0,71 ± 0,12 mM | 0.57 ± 0.013 mM |
| $K_i$ | 3-PGA | 0,78 ± 0,19 mM | 0.79 ± 0.122 mM |
| $K_i$ | PEP | Nd | Nd |

**Figure 1.** Subcellular localization of CreTPT2 and 3 and in vitro measurements of transport activities. **A)** Cellular localization of CreTPT2 (upper) and CreTPT3 (lower). A schematic diagram for the construct encoding the CreTPT2/3-VENUS fusion protein is shown above the cell images and described in Materials and methods. VENUS, VENUS fluorescence; Chl, chlorophyll autofluorescence. Scale bars, 5 $\mu$m. **B)** Production of Cre*TPT2* (1, 2) and Cre*TPT3* (3, 4) in yeast. Left in each panel, Coomassie Brilliant Blue-stained SDS-PAGE of proteins from total membranes isolated from yeast cells containing the empty vector (1, 3) or harboring the *His*-Cre*TPT2* (2) or *His*-Cre*TPT3* (4) construct. Right in each panel, corresponding immunoblot detection of recombinant His-CreTPT2 or His-CreTPT3 protein using anti-His antibodies. The calculated molecular masses of the N-terminal His-tagged proteins of CreTPT2 and CreTPT3 were 39 kD and 37 kD, respectively. **C)** Left, kinetics of Pi exchange by His-CreTPT2 in lipid vesicles. Uptake of 0.25 mM Pi into liposomes was measured in the presence (■) or absence (□) of 30 mM Pi loaded into the vesicles. Right, analyses of substrate specificity of His-CreTPT2. **D)** Left, kinetics of Pi exchange by His-CreTPT3 in lipid vesicles. Uptake of 0.25 mM Pi into liposomes was measured in the presence (■) or absence (□) of 30 mM Pi loaded into the vesicles. Right, analyses of substrate specificity of His-CreTPT3. For the left panels of **C** and **D**, the arithmetic mean (±SD) of 3 independent experiments (each with 3 technical replicates) was plotted with respect to the time after initiating the assay. For the right panels of **C** and **D**, liposomes in which His-CreTPT2 and His-CreTPT3, respectively, were incorporated and were preloaded with various substrates (30 mM) and the initial Pi uptake rates (at 0.25 mM external concentration) were determined. Relative velocities were compared with the Pi/Pi homo-exchange, which was set to 100%. The data represent the arithmetic mean (±SD) of 3 independent experiments (each consisting of 3 technical replicates). **E)** Kinetic constants of His-CreTPT2 and His-CreTPT3. The Michaelis–Menten constant ($K_M$) for Pi uptake was determined using various external Pi concentrations (0.05 to 5 mM). The competitive inhibition constant ($K_i$) of the 0.25 mM Pi uptake was measured with increasing competitor concentrations (0.05 to 5 mM). Liposomes were preloaded with 30 mM Pi as the counter-exchange substrate. The data represent the arithmetic mean ± SE of 3 independent experiments. Nd, no competitive inhibitory constant could be measured under the given experimental conditions. DHAP, dihydroxyacetone phosphate; 3-PGA, 3-phosphoglycerate; PEP, phosphoenolpyruvate; Glc6P, glucose 6-P; Glc1P, glucose 1-P; Fru6P, fructose 6-P; Gal1P, galactose 1-P.

heterotrophic (TAP) solid agar medium (Figs. 2C and S3D). In contrast, the Cre*TPT3* mutants (*t3ko1*, *t3ko2*, and *t3ko3*) exhibited severe growth impairment even in LL and completely stopped growing under ML and HL, on either TP or TAP agar medium (Fig. 2, C and D). Due to the striking growth phenotypes caused by the loss of CreTPT3 function, we focused on investigating the physiological functions of TPT3 by analyzing *tpt3* mutants in more detail in this study. The differences in transcript changes between Cre*TPT2* and Cre*TPT3* under various environmental conditions were examined and are described in the Discussion.

We determined growth curves for WT and *tpt3* mutant cells grown in liquid medium (TP) in LL, ML, and HL (Figs. 2E and F); the results were in accordance with those observed for the

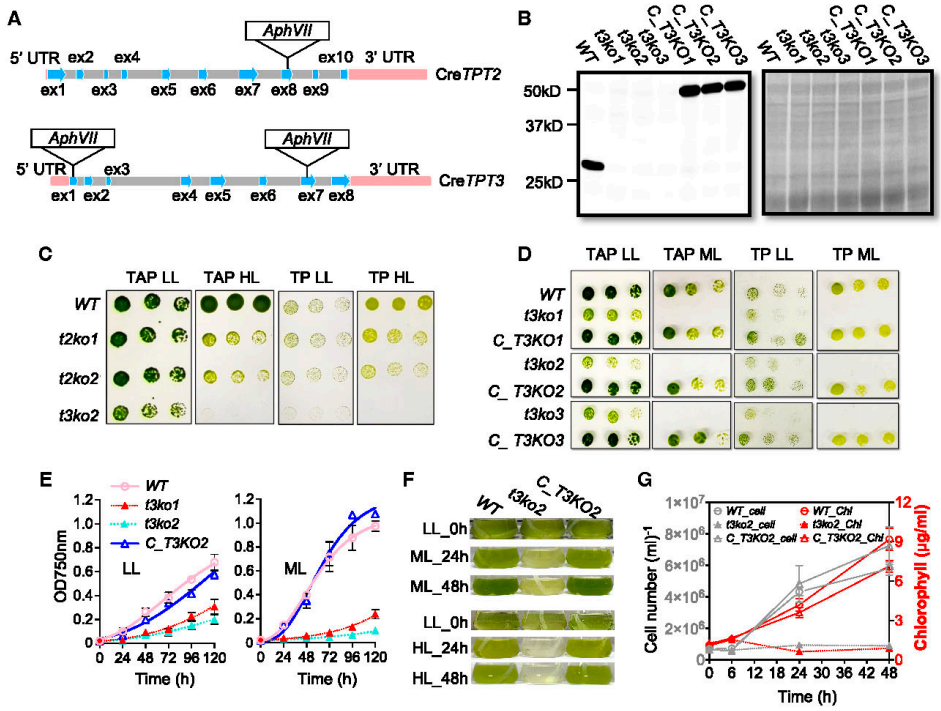


**Figure 2.** Growth characterization of *tpt* mutants and complemented strains. **A)** Molecular map of the Cre*TPT2* (upper) and Cre*TPT3* (lower) genes and the positions of the Cas9 targeted sites. The edited site of Cre*TPT2* is located in exon 8, and edited sites of Cre*TPT3* are located in exons 1 and 7; *t3ko1* has the marker gene inserted in exon 1, and *t3ko2* and *t3ko3* have the marker gene inserted in exon 7. **B)** Immunoblot (left panel) of the stained protein profiles (right panel) for wild type (WT), *t3ko1*, *t3ko2*, *t3ko3*, and the complemented strains (*C_T3KO1*, *C_T3KO2*, and *C_T3KO3*). **C)** Growth of WT, *t2ko1*, *t2ko2*, and *t3ko2* at various dilutions (see below) on agar plates incubated under LL and HL for 4 d. **D)** Growth of WT, *t3ko1*, *t3ko2*, *t3ko3*, and the complemented strains (*C_T3KO1*, *C_T3KO2*, and *C_T3KO3*), at various dilutions (see below) on agar plates incubated under LL or ML for 4 d. **E)** Growth of various strains (indicated) in liquid medium under LL (left panel) or ML (right panel). **F)** Transition of strains from LL to ML (upper) or to HL (lower) for the indicated times. **G)** Cell growth (number) and chlorophyll content of cultures at various times after shifting from LL to ML for up to 48 h. In **C)** and **D)**, cells were spotted on agar plates containing TAP or TP medium and maintained under continuous LL, ML, or HL conditions. The dilution series used was 1.5, 0.75, and 0.375 $\mu$g mL$^{-1}$ chlorophyll equivalent (left to right). For growth in liquid medium, cells were cultured in TP medium to an initial $OD_{750\ nm}$ of 0.02 in air and under continuous LL before initiating the various growth analyses in LL, ML, or HL. Each curve represents the arithmetic mean (±SD) of 3 independent experiments.

solid medium growth assays. Additionally, *tpt3* mutant cells in both LL and ML exhibited an increased cell diameter and formed clusters of cells that appear to be less able to separate following cell division (Supplemental Fig. S6, A and B). To confirm that the growth phenotypes are a consequence of the *tpt3* knockout, we introduced a WT copy of Cre*TPT3* cloned in-frame and upstream of the *VENUS* fluorescent gene into the mutant strains (Fig. 2B, right). As shown in Fig. 2, D to G, ectopic expression of the WT Cre*TPT3* in the *t3ko2* mutant (*C_T3KO2*) rescued the limited growth phenotype of the mutant under all light conditions tested in this study (LL/ML/HL).

We also analyzed the chlorophyll content of photoautotrophically grown cells after transferring them from LL to ML and observed that *t3ko2* has lower chlorophyll content relative to WT cells after 24 h in ML (Figs. 2, F and G, and S7). We quantified cell numbers and total chlorophyll contents following the LL to ML transition. Chlorophyll levels per cell declined in all strains at 24 and 48 h following transfer to ML; however, it was lower by approximately half in *t3ko2* (0.34 $\mu$g/1 × $10^6$ cells) relative to either WT cells or the *C_T3KO2* complemented strain (both ~0.72 $\mu$g/1 × $10^6$ cells) after 24 h of ML (Supplemental Fig. S7), with some additional increase in cell density for WT and *C_T3KO2* after 48 h of ML (which might result in some shading). Finally, mutant cells became strongly bleached when transferred to HL for 24 h (Fig. 2F).

Taken together, these results indicate that the activity of the CreTPT3 transporter is essential for optimal growth over a range of light intensities (LL/ML/HL).

## The *tpt3* mutant exhibits hyperaccumulation of "storage" carbon

To explore the effect of the loss of CreTPT3 activity on carbon partitioning, we quantified the carbon storage (starch and lipids) following a transition of WT and the *t3ko2* mutant from LL to ML. Lugol staining showed extensive starch accumulation in *t3ko2* cells after a 48-h exposure to ML, whereas WT cells were barely stained (Fig. 3B). Furthermore, as shown in Fig. 3A, there was a ~55-fold difference in the level of starch that accumulated in *t3ko2* relative to WT cells (13.29 compared with 0.24 $\mu$g starch/$\mu$g chlorophyll) after 24 h of illumination in ML. The mutant also accumulated >25-fold more lipid than WT and *C_T3KO2* cells (on a chlorophyll basis), as monitored by Nile Red fluorescence,

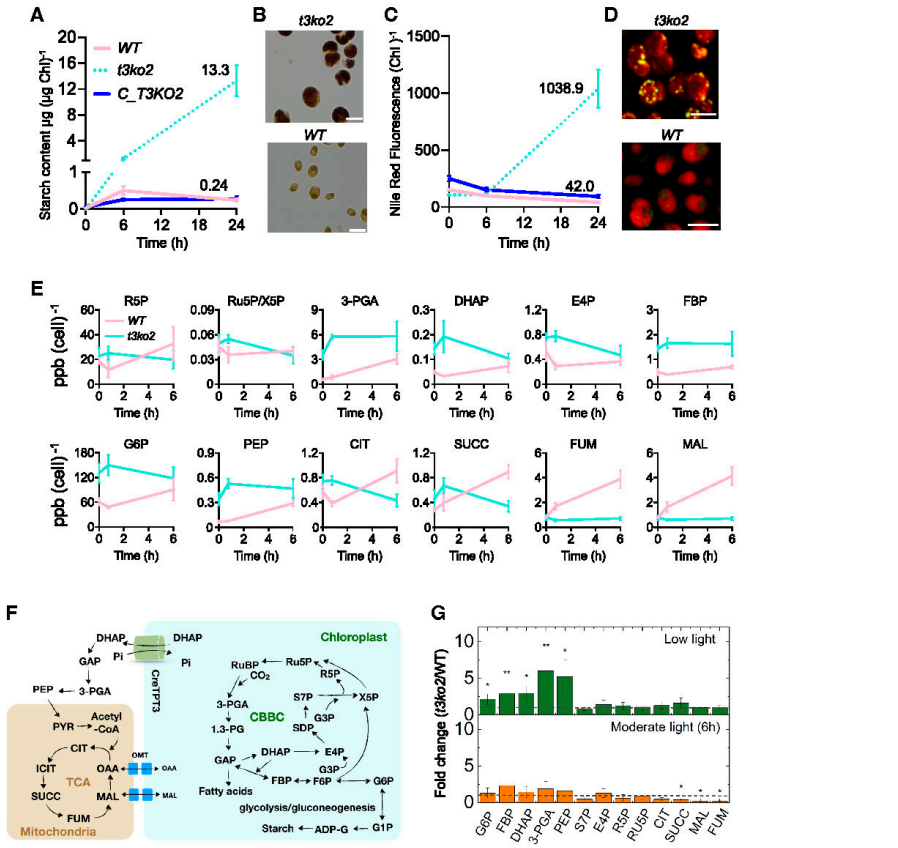


**Figure 3.** Changes in storage carbon and metabolite levels in WT and *t3ko2* after transitioning cells from growth in LL to ML. **A)** Starch content in the indicated strains following 0, 6, or 24 h of ML exposure. **B)** Lugol staining of starch in WT and *t3ko2* after 48 h of ML. **C)** TAG (triacylglycerol) content in the indicated strains following 0, 6, or 24 h of ML exposure. **D)** Nile Red staining of TAG in WT and *t3ko2* following 48 h of ML exposure. **E)** Time course of metabolite accumulation at 0 h (LL), 45 min, or 6 h following ML exposure. Data were normalized to cell numbers. Each data point shows the mean and standard error; the data represent 3 biological replicates for each metabolite. ppb, parts per billion. **F)** Select metabolic pathways in *Chlamydomonas* adapted from Johnson and Alric (2013). **G)** Bar graph representation of fold change for metabolites shown in **E)**, calculated by dividing the mean of pool size in *t3ko2* by that of WT at the respective light levels. A fold change of 1 (no change) is indicated with a dashed line. An asterisk indicates statistically significant difference in pool sizes in *t3ko2* compared with WT [from **E)**] (*$P < 0.05$, **$P < 0.01$, and ***$P < 0.001$) (Supplemental Data Set S1). G6P, glucose-6-P; FBP, fructose bisphosphate; DHAP, dihydroxyacetone phosphate; 3-PGA, 3- phosphoglycerate; PEP, phosphoenolpyruvate; PYR, pyruvate; CIT, citrate; SUCC, succinate; FUM, fumarate; MAL, malate; E4P, erythrose 4-P; R5P, ribose 5-P; RU5P/X5P, ribulose 5-P/xylulose-5-P; OMT, 2-oxoglutarate/malate transporter.

over the same time period (42 for WT and 1,038 for *t3ko2* for Nile Red fluorescence/chlorophyll) (Fig. 3, C and D). Since the chlorophyll content in the mutant on a per cell basis was ~50% relative to that of WT cells after 24 h in ML, the accumulated starch and lipid on a per cell basis represent a ~25-fold increase for starch and ~12-fold increase for lipid in the mutant relative to the WT strain. Additionally, mutant cells were much larger and tended to exhibit more aggregation than WT cells (Supplemental Fig. S6, A and B). These results suggest that the inability to transport triose-P between the chloroplast and the cytosol through CreTPT3 resulted in a repartitioning of photosynthetic assimilates (carbon, reductant, and ATP) toward the biosynthesis of both starch and neutral lipid.

## Cre*TPT3* deletion leads to the accumulation of CBB cycle/glycolytic/gluconeogenic intermediates

To understand the metabolic consequences of the loss of CreTPT3 function on growth under LL and ML, we undertook comparative metabolite analyses of WT and the *t3ko2* mutant using cells grown in LL and after a shift to ML for 45 min or 6 h. As mentioned above, the level of starch increased dramatically in the mutant relative to WT cells (Figs. 3, A and B, and S8A). We then quantified pool sizes of various central carbon metabolites, particularly those of the CBB cycle and glycolysis/gluconeogenesis pathways and intermediates of the tricarboxylic acid (TCA)/glyoxylate cycle (Fig. 3F). Data were normalized by cell number (Fig. 3E) or chlorophyll content (Supplemental Fig. S8B). The fold change in the quantity of each metabolite in the mutant relative to WT under LL or at 45 min or 6 h after the switch to ML is given in Figs. 3G and S8C.

At the time of shifting cells from LL (Fig. 3E, time 0 h) to ML, the *t3ko2* mutant had already accumulated a significantly larger pool (2- to 6-fold) of glycolytic/gluconeogenic intermediates [DHAP, 3-PGA, FBP (all 3 shared with the CBB cycle), G6P, and PEP] compared with WT cells, suggesting that the loss of CreTPT3 function resulted in a back-up of these metabolites within the cell. Our hypothesis is that these metabolites are accumulating in the chloroplast stroma due to the diminished ability of the mutant chloroplast to export fixed carbon, which is supported by the observed accumulation of starch and TAG in the mutant strain (Figs. 3, A to D, and S8A). While the pool sizes of fumarate and malate (metabolites of the TCA/glyoxylate cycle) were similar in both strains under LL, following the transition of the cells to ML, WT cells exhibited a significant increase in the pool sizes of those metabolites while the mutant maintained a lower level, indicating that the loss of CreTPT3 function either directly (by supplying precursors) or indirectly (metabolic rewiring) affects their levels.

Thus, a primary function for CreTPT3 appears to be the export of photosynthetically synthesized reduced carbon, which would drive metabolism in the cytoplasm and other cellular compartments, such as the mitochondrion, while enabling the import of Pi into the chloroplast, which sustains ATP biosynthesis.

## The *tpt3* mutant shows lower photosynthetic activity when grown in ML

To understand the influence of the loss of CreTPT3 activity on PET, we quantified photosynthetic activities following a transition from LL to ML (Supplemental Fig. S5). To this end, we measured photosynthetic $O_2$ evolution rates (OERs) for WT, *t3ko2*, and *C_T3KO2* over a range of light intensities. LL-acclimated cultures of WT, *t3ko2*, and *C_T3KO2* showed comparable OERs at intensities below 200 $\mu$mol photons $m^{-2}$ $s^{-1}$, while at saturating light intensities of ≥600 $\mu$mol photons $m^{-2}$ $s^{-1}$, the OER of *t3ko2* was diminished slightly relative to WT and the complemented strain (Fig. 4A). Upon acclimation of cells to ML for 24 h, the *t3ko2* mutant consistently displayed lower OERs than WT or *C_T3KO2* cells under all actinic light intensities used (Fig. 4A). Additionally, while the *Fv/Fm* in the mutant grown in LL was comparable with that of WT and *C_T3KO2* (Fig. 4B), after exposure of the mutant cells to ML for 6 h, *Fv/Fm* declined to ~50% of the WT and *C_T3KO2* levels; the decline in the mutant continued over a period of 24 h in ML, with a 3-fold decrease in *Fv/Fm* for *t3ko2* compared with that of WT cells (Fig. 4B). These results indicate that damage to photosystem II (PSII) reaction centers occurs following exposure of the mutant to ML.

To examine the redox state of the photosynthetic apparatus, we evaluated the pool of electron acceptors downstream of PSII. We quantified the photochemical efficiency (qL) of all strains at various light intensities after growth in LL or after a shift to ML for 6 or 24 h (Fig. 4C). The photosynthetic parameter qL indicates the redox state of $Q_A$, the primary electron acceptor of the PSII reaction center. Assuming that $Q_A$ and $Q_B$ are in equilibrium, qL reflects the redox status of the PQ pool; a lower qL value indicates a more reduced electron transport chain (Kramer et al. 2004). 1-qL positively correlates with the PQ pool redox state. In LL-acclimated cells, 1-qL was significantly higher in *t3ko2* even at low levels of actinic illumination compared with that of WT cells and the complemented strain. For cells that had been acclimated to ML (6 and 24 h), 1-qL was 70% of the near maximum value for *t3ko2*, even under relatively low actinic light conditions (e.g. 100 $\mu$mol photons $m^{-2}$ $s^{-1}$), indicating a highly reduced PQ pool. In contrast, for WT and the complemented strain at the same light intensity, 1-qL attained only ~20% of the maximum value (Fig. 4C). These results suggest that the PQ pool is much more reduced in LL-acclimated *t3ko2* relative to WT and *C_T3KO2* (Fig. 4C) and that there is a much more pronounced reduction of this pool at all actinic light intensities in ML-grown *t3ko2* mutants. These results suggest a limitation in electron flow downstream of the PQ pool in both LL- and ML-grown *t3ko2*.

Moreover, we analyzed how fast PET became restricted following the transfer of LL-grown *t3ko2*, *C_T3KO2*, and WT cells to HL (400–450 $\mu$mol photons $m^{-2}$ $s^{-1}$) by monitoring changes in the redox state of the PQ pool. We observed that the PQ pool in *t3ko2* begins to be more reduced than that of

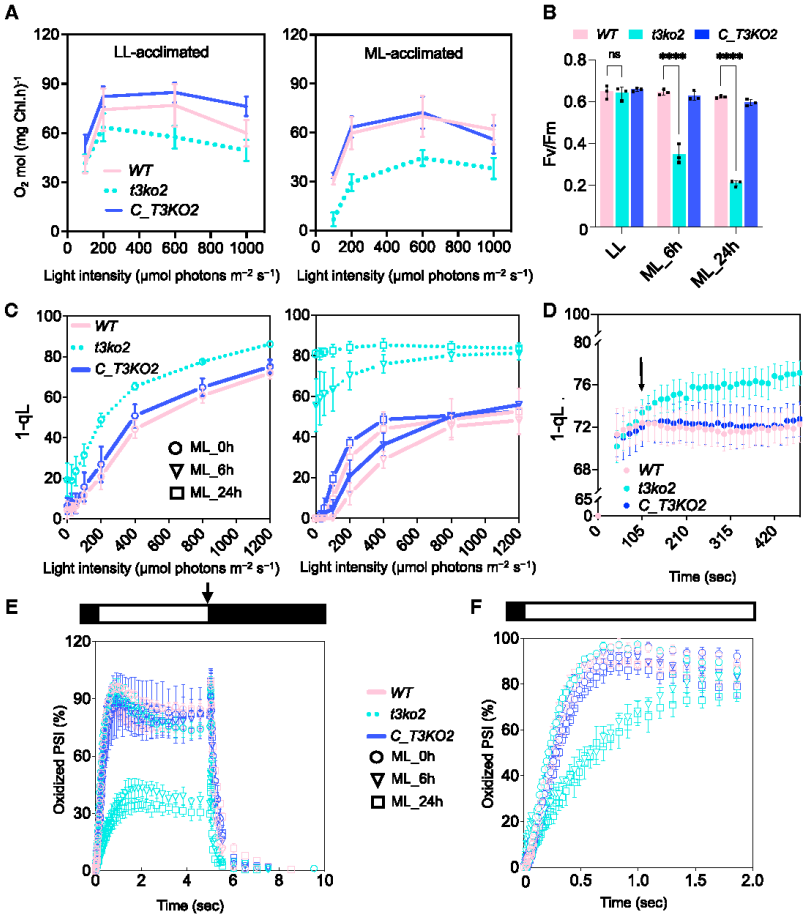


**Figure 4.** Photosynthetic activities following a transition from LL to ML or to HL. **A)** Light intensity curve of $O_2$ evolution of LL- (left) or ML- (right) acclimated cells for the indicated strains. **B)** *Fv/Fm* of WT, *t3ko2*, and the complemented strain (*C_T3KO2*) following 0 (LL), 6, or 24 h in ML. **C)** 1-qL values of LL- (left panel) or ML- (right panel) acclimated cells exposed to increasing actinic light intensities. **D)** Kinetics of 1-qL of LL-acclimated cells after illumination at HL (400 to 450 $\mu$mol photons $m^{-2}$ $s^{-1}$) for the indicated times. **E)** P700 oxidation and reduction kinetics in LL-grown cells and after 6 or 24 h in ML. **F)** Kinetics of P700 oxidation upon dark-to-light transition. P700 measurements were performed in the presence of DCMU and hydroxylamine, as indicated in Materials and methods. Absorbance differences were monitored at 705 nm during continuous illumination with 150 $\mu$mol photons·$m^{-2}$ $s^{-1}$ for 5 s (white box above), followed by a saturating light pulse at 1,500 $\mu$mol photons·$m^{-2}$ $s^{-1}$ (arrow) and a 5-s dark incubation (black box). For panel **E**, the kinetics was normalized by setting maximum oxidation (after light pulse) of WT to 100% and for panel **F**, by setting maximum oxidation (after light pulse) of individual strain to 100%. The data from all panels represent the arithmetic mean (±SD) of 3 independent experiments. For panel **B**, the asterisks represent significant differences determined by ANOVA tests. ****$P < 0.0001$.

WT cells and *C_T3KO2* after 105 s of elevated illumination (Fig. 4D), with an even more pronounced effect upon longer durations in HL. These results suggest that PET can be rapidly limited by diminished triose-P export from the chloroplast; the elimination of CreTPT3 has a strong influence on PET activity.

To determine if PSI was also affected in the mutant cells, we analyzed PSI/P700 oxidation/reduction kinetics following exposure of LL-grown cells to ML in the presence of 20 $\mu$M DCMU (*N*-(3,4-dichlorophenyl)-*N*-dimethylurea) and 1 mM hydroxylamine to block a contribution of electrons from PSII. Levels of photo-oxidizable P700 following exposure to

actinic light for 5 s were similar in all LL-acclimated strains (Fig. 4E). However, the level of photo-oxidized P700 in ML-acclimated cells declined in the mutant to ~40% to 50% of that in WT and *C_T3KO2* cells (Fig. 4E), indicating that PSI is more reduced in the *t3ko2* mutant after ML exposure. As shown in Fig. 4F, the oxidation rate of P700 following a dark-to-light transition was much slower in ML-acclimated *t3ko2* compared with WT. These results suggest that the mutant has a diminished level of available electron acceptors on the acceptor side of PSI (relative to WT and *C_T3KO2*) after growth in ML.

## CreTPT3 inactivation dramatically affects the accumulation and distribution of compartmentalized $H_2O_2$

To investigate the relationship of CreTPT3 activity to oxidative stress, we assayed ROS production in the mutant using the fluorescent probe CM-$H_2$DCFDA, which upon exposure to increasing ROS levels is converted to the green fluorescent molecule dichlorofluorescein (DCF). We visualized DCF fluorescence by confocal microscopy. As shown in Fig. 5, A and B, ROS levels in the *t3ko2* mutant markedly increased (~3-fold) after 48 h in ML, while we detected little difference in ROS levels in WT cells.

For an alternative, dynamic method for evaluating redox changes in the chloroplast, we used the redox-sensitive green fluorescent protein roGFP2, which we targeted to the chloroplast stroma (Fig. 5C, upper panel) or mitochondrion (Fig. 5C, lower panel). roGFP2 monitors ratiometric redox changes of glutathione, which reflects cellular ROS levels (Vevea et al. 2013; Dorion et al. 2021). LL-acclimated WT cells and the *t3ko2* mutant exhibited similar levels of chloroplast roGFP2 oxidation (Fig. 5D). Upon transfer of these cells to ML, the mutant showed an increase in chloroplast oxidative conditions, with a 5.0-fold increase after 1.5 h and a 2-fold increase after 6 h, which was 1.8- and 1.6-fold higher than the values measured in WT cells, respectively (Fig. 5D). Additionally, as triose-P is exported to the cytosol by CreTPT3, triose-P may potentially be further metabolized and donate redox equivalents to the mitochondrial electron transport chain and alter mitochondrial ROS production. Therefore, we also measured mitochondrial redox levels at different light intensities in WT and the *t3ko2* mutant using the roGFP2 sensor targeted to the mitochondrion. Upon a LL-to-ML shift for 1.5 or 6.0 h, neither WT nor *t3ko2* displayed a significant change in fluorescence for mitochondrion-targeted roGFP (Fig. 5E). These results suggest that the mitochondrial redox level is maintained after shifting either LL-acclimated WT or *t3ko2* cells to ML. Overall, the inability to export triose-P through CreTPT3 markedly increased the level of oxidative stress in the chloroplast but not in the mitochondrion.

We also determined if the ROS accumulated in *t3ko2* is $H_2O_2$ and whether this molecule shows differential accumulation in the different subcellular compartments. For this analysis, we employed a hypersensitive sensor of $H_2O_2$,

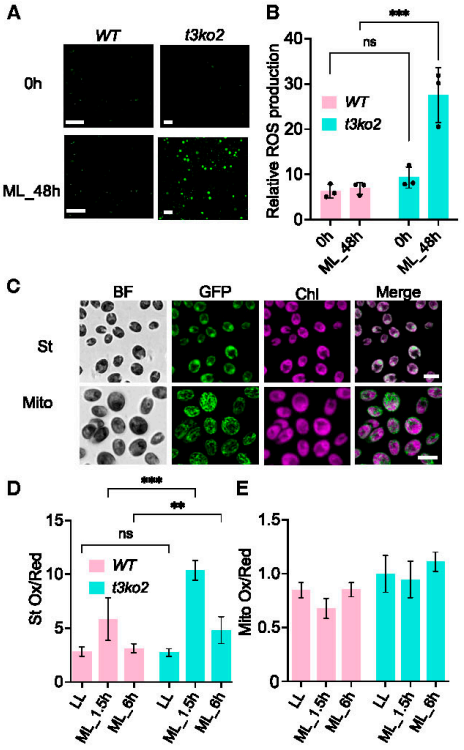


**Figure 5.** Measurement of intracellular ROS in *t3ko2* and WT upon transition from LL to ML. **A)** ROS levels were evaluated by CM-$H_2$DCFDA fluorescence of WT and the *t3ko2* mutant in LL and following exposure to ML for 48 h. Scale bars, 20 $\mu$m. **B)** Quantitation of data in **A)**. Shown are mean values from 3 independent experiments ± SD. **C)** roGFP2 protein targeted to the chloroplast stroma (upper panel) or mitochondrion (lower panel). Scale bars: 10 $\mu$m; BF, bright field; GFP, roGFP2 fluorescence; Chl, chlorophyll autofluorescence. **D to E)** Monitoring redox levels in the stroma **D)** or mitochondrion **E)** after exposure of WT and the *t3ko2* mutant for 1.5 or 6.0 h of ML. Shown are mean values from 3 independent experiments ± SD; 3 to 4 random images were analyzed for each experiment. For panels **B)** and **D)**, the asterisks represent significant differences determined by ANOVA tests. $^{**}P < 0.005$ and $^{***}P < 0.001$.

roGFP2-Tsa2ΔCR, which was previously used for studies in *Chlamydomonas* (Niemeyer et al. 2021). In this analysis, we monitored real-time accumulation of $H_2O_2$ in the stroma, cytosol, mitochondrion, and nucleus (Fig. 6A) following a 20-min exposure of cells to either HL or very low light (Fig. 6, B to E). The stromal $H_2O_2$ level in *t3ko2* increased within 2.5 min of light exposure and reached a 1.4-fold increase after 20 min of illumination with HL compared with the initial level in LL (Fig. 6B). Stromal $H_2O_2$ levels in WT cells showed little change after being shifted to HL; however, their

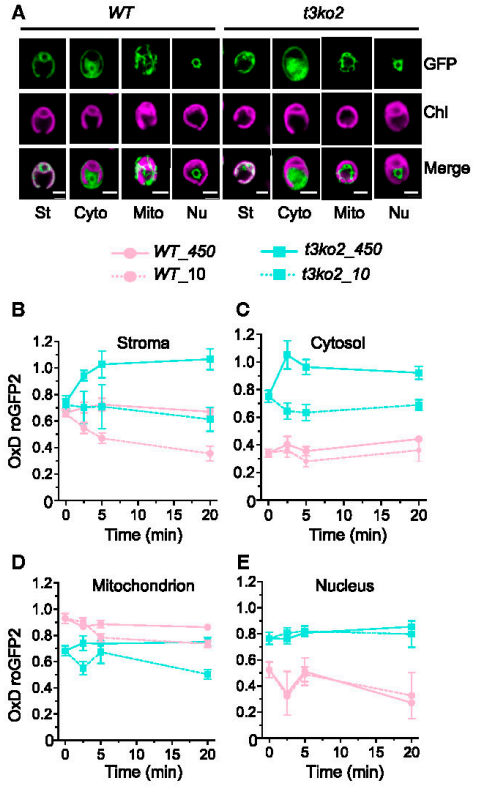


**Figure 6.** Real-time monitoring of $H_2O_2$-compartmentalized distribution in *t3ko2* and WT upon transition from LL to HL. **A)** The hypersensitive $H_2O_2$ sensor (roGFP2-Tsa2ΔCR) protein was targeted to the chloroplast stroma (St), cytosol (Cyto), mitochondrion (Mito), or nucleus (Nu). Shown are GFP fluorescence, chlorophyll autofluorescence (Chl), and the 2 signals merged; scale bars, 5 $\mu$m. **B** to **D)** WT and *t3ko2* transformant cells, accumulating roGFP2-Tsa2ΔCR in the stroma **B)**, cytosol **C)**, mitochondrial matrix **D)**, or nucleus **E)**, were acclimated to LL in TP medium and then were transferred either to HL (450 $\mu$mol photons $m^{-2}$ $s^{-1}$, solid line) or to very LL (10 $\mu$mol photons $m^{-2}$ $s^{-1}$, dotted line) for 20 min. The oxidation state of the sensor was trapped by the addition of NEM, and roGFP2 fluorescence was measured in a plate reader as previously described (Niemeyer et al. 2021). Shown are mean values from 3 independent experiments ± SD.

levels declined when the cells were shifted to 10 $\mu$mol photons $m^{-2}$ $s^{-1}$, or very low light. Notably, after 20 min in HL, the stroma of the *t3ko2* mutant accumulated ~1.6-fold more $H_2O_2$ than that of the WT cells; *t3ko2* mutant cells in very low light accumulated a similar amount of stromal $H_2O_2$ as WT cells after exposure to HL (Fig. 6B). The cytosolic probe also responded rapidly, with a 1.2-fold increase for WT and a 1.4-fold increase for the *t3ko2* mutant (Fig. 6C); note that the initial levels of $H_2O_2$ prior to the transfer of the cells to HL or very low light were much lower in the WT cells than those in the mutant. The *t3ko2* cytosolic $H_2O_2$ level was elevated relative to the level in WT cells by 2.1-fold after 20 min of illumination in HL (Fig. 6C). We did not observe a significant change in $H_2O_2$ levels in the mitochondrion for either the WT or the *t3ko2* mutant after the cells were shifted to the higher light intensity (Fig. 6D). Finally, the *t3ko2* mutant already accumulated much higher levels of $H_2O_2$ in the nucleus in LL compared with that in WT cells, although neither mutant nor WT cells showed significant changes in nuclear $H_2O_2$ levels after HL exposure (Fig. 6E).

## Discussion

### Cre*TPT2* and Cre*TPT3* genes exhibit different expression patterns

In this study, we discovered that *Chlamydomonas* contains at least 2 TPTs that are located at the chloroplast envelope. An earlier report had suggested that CreTPT2 was a plastid PPT (for the transport of PEP) (Bockwoldt et al. 2019), but based on our results, it appears to be functionally more similar to a TPT. In vitro assays showed that CreTPT2 had almost the same substrate specificity as CreTPT3, although it may be less effective in DHAP/Pi exchange (Fig. 1, C to E). To determine the expression patterns of Cre*TPT2* and Cre*TPT3*, we analyzed the abundance of Cre*TPT2* and Cre*TPT3* transcripts using RT-qPCR and by mining published transcriptome deep sequencing (RNA-seq) data sets over the diurnal cycle and during nitrogen, sulfur, or iron limitation (González-Ballester et al. 2010; Urzica et al. 2013; Ngan et al. 2015; Zones et al. 2015) (Supplemental Figs. S1, C and D, and S9). Cre*TPT3* was highly expressed in the light and darkness, with significantly higher transcript accumulation relative to Cre*TPT2* and the other genes (Cre*TPT10* and *CGLS1*) potentially encoding chloroplast-localized pPTs (Supplemental Fig. S1, C and D). Cre*TPT2* and Cre*TPT3* also responded differentially to abiotic stresses. Cre*TPT3* was strongly induced by individual nitrogen, sulfur, and iron limitation and upon exposure to HL, whereas the level of Cre*TPT2* transcripts remained almost unchanged under the same conditions (Supplemental Fig. S9, A to D), suggesting that CreTPT3 plays a more prominent role in exporting triose-P from the chloroplast than CreTPT2, with potentially increasing export from the plastid under HL and nutrient limitation conditions. This hypothesis is supported by the observation that *tpt3* mutants displayed much more severe growth retardation relative to *tpt2* mutants upon exposure to ML or HL (Fig. 2C). There is no evidence showing that the *TPT*s from plants are induced by stress/excess absorbed excitation, and the expression of the *Arabidopsis TPT* gene appears to even decrease following HL exposure (Weise et al. 2019).

Cre*TPT2* and Cre*TPT3* exhibited distinct expression patterns over the diurnal cycle; the expression of Cre*TPT2* increased rapidly after the dark-to-light transition, with peak

accumulation after 1 h in the light, when the transcript level of Cre*TPT3* was at its lowest (Supplemental Fig. S1D). Continued exposure to light led to a decrease in the level of Cre*TPT2* transcripts to near zero, while Cre*TPT3* transcripts increased steadily in the light, reaching a peak in mid-day (Supplemental Fig. S1D). The Cre*TPT2* expression pattern suggests that it might play a role in exporting triose-P at the beginning of the light period, when light intensity and photosynthesis are low and low levels of triose-P would be synthesized in the stroma. As the light intensity increases over the course of the day, higher levels of triose-P are synthesized; its traffic out of the chloroplast for use in other subcellular compartments would likely predominantly involve the activity of CreTPT3. The greater specificity of CreTPT3 than CreTPT2 for transporting DHAP (Fig. 1E) may make it more effective than CreTPT2 in transporting C3-phosphorylated compounds. This possibility is congruent with the finding that there is elevated synthesis/accumulation of *CreTPT3* mRNA during the day when light intensity reaches its peak (Zones et al. 2015) and there would be rapid biosynthesis of C3-phosphorylated compounds. Overall, the subfunctionalization of the 2 *Chlamydomonas* TPTs based on the expression levels, patterns of RNA accumulation over the course of the day and upon nutrient deprivation of their encoding genes, and their substrate specificities may help tune the export of triose-P from the chloroplast with respect to the diurnal cycle and dynamic environmental cues.

## CreTPT3 also potentially serves as a redox valve, transferring reductant to the cytoplasm

It was previously proposed that chloroplast TPTs can catalyze 2 potential reactions in the light (Fig. 7) based on the crystal structure of a red algal (*Galdieria sulphuraria*) TPT (Lee et al. 2017) and in vitro assays using isolated spinach (*Spinacia oleracea*) chloroplasts (Stocking and Larson 1969); both triose-P/Pi and triose-P/3-PGA exchange across the chloroplast inner envelope membrane. The former reaction can route both carbon skeletons and reductants into the cytoplasm while importing Pi back into the chloroplast for ATP regeneration. The latter reaction would import 3-PGA into the chloroplast in exchange for triose-P (DHAP, GAP), which would serve to transfer reductant from the chloroplast to the cytosol while transferring 3-PGA back into the chloroplast where it can be reduced by the CBB cycle and stimulate the regeneration of ribulose 1,5-bisphosphate. Indeed, in vitro, CreTPT3 can actively transport both triose-P and 3-PGA in exchange for Pi (Fig. 1), indicating that this transporter can potentially serve as both a carbon and "reductant shuttle" which would help sustain photosynthetic electron flow.

Studies of photosynthetic activities and growth of WT and *tpt3* mutants (e.g. *t3ko2*) in LL, ML, and HL support the idea that the mutant is highly compromised in its ability to export fixed carbon and potentially also reductant from the chloroplast. In *t3ko2* exposed to LL (after growth in LL), growth was slow (Fig. 2E) and the PQ pool (Fig. 4C) was more reduced than in WT cells, while there was little loss of PSII or PSI activities (Fig. 4, A, B, E, F). These results suggest that there is a reduced rate of $PQH_2$ oxidation. During ML exposure, the mutant stopped growing and experienced severe bleaching when placed in HL (Fig. 2F). The highly reduced PQ pool and PSI reaction center in ML-acclimated *t3ko2* cells (Fig. 4, C and E, respectively) reflect hyperreduction of PET and the generation of "overflow" electrons. The phenotypes of *t3ko2* cells, including an elevated 1-qL (Fig. 4, C and D), slower oxidation rate of PSI in ML-acclimated cells (Fig. 4F), accumulation of storage carbon (Fig. 3, A to D), an increase in intracellular accumulation of triose-P and 3-PGA (Fig. 3E), light-dependent damage to the photosynthetic apparatus (Fig. 4B), and elevated production/accumulation of ROS (Fig. 5, A and B), especially in the chloroplast (Fig. 6B), indicate a block on the acceptor side of PSI, which reflects the function of CreTPT3 and its central role in fixed carbon export from the chloroplast and for fueling central metabolism. Furthermore, the inability to efficiently transport fixed carbon from the chloroplast in ML and HL would result in diminished CBB cycle activity, diminished photosynthetic electron transport, and hyperreduction of the stroma, which would also result in diminished ATP biosynthesis and NADPH production.

The malate-OAA shuttle represents another route that, under high redox stress, might partially compensate for the loss of CreTPT3 by transporting reductant from the chloroplast (schematic in Fig. 7). Intriguingly, malate levels in *t3ko2* were 4-fold lower than in WT cells (Fig. 3, E and G). Moreover, the expression of the genes (Cre*MDH1* and Cre*MDH5*) encoding the plastid-localized MDH was 3-fold to 5-fold lower in the mutant than in WT cells following a transition from LL to ML (Supplemental Fig. S10, D and E), indicating that the malate-OAA shuttle is likely unable to compensate for a loss of CreTPT3. Inactivation of CreTPT3 appears to have a negative effect on the malate-OAA shuttle, potentially because of the compromised physiological state of the *t3ko2* mutant. Furthermore, a previous study of metabolic flux analysis during heterotrophic growth of *Chlamydomonas* showed that the CreTPT shuttle(s) is almost 10-fold more active than the malate-OAA shuttle (Boyle et al. 2017).

## TPT deficiency in *Chlamydomonas* cannot be compensated for by a day/night regime

TPT deficiency in plants can be almost fully compensated for by the starch-mediated night pathways that elicit the breakdown of starch and the export of the breakdown products via the maltose transporter (MEX1) and glucose translocator (GlcT) (Niittylä et al. 2004; Cho et al. 2011). Furthermore, in plants, starch turnover may also be occurring in the light, at the same time as starch is being synthesized (Häusler et al. 1998; Walters et al. 2004). Compared with algae, plant cells appear to display a high plasticity in their capacity to

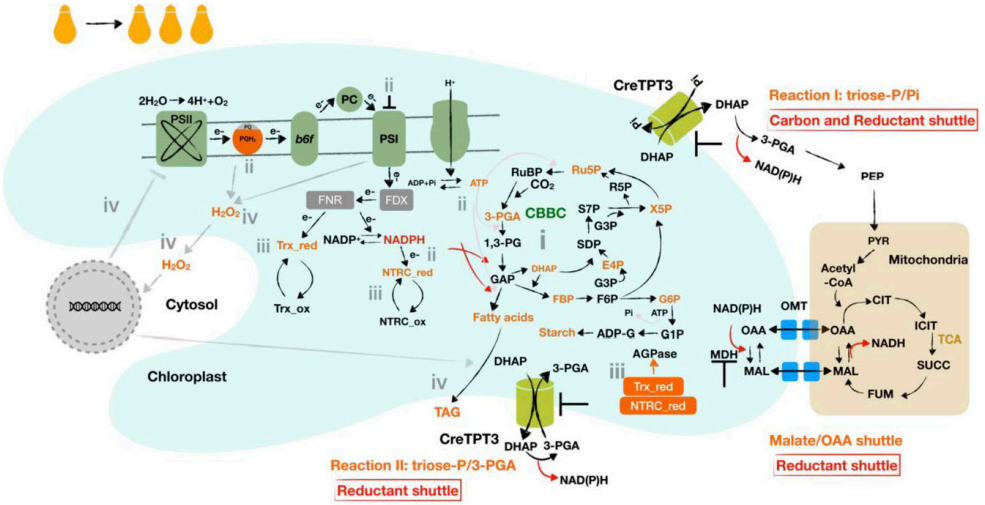


**Figure 7.** Effect of eliminating *Chlamydomonas* TPT3 on the chloroplast metabolic landscape. i, reduced triose-P export leads to the accumulation of the sugar-P in the CBB cycle and glycolysis pathway (e.g. triose-P, hexose-P, and marked in orange), and an elevated ratio of 3-PGA/Pi (which can allosterically activate AGPase activity) begins to stimulate the biosynthesis and accumulation of storage carbon; ii, CBB cycle activity diminishes as a consequence of the hyperaccumulation of the precursors with the fixation of $CO_2$, leading to elevation of reductant (NADPH) and energy (ATP) within the chloroplast; the elevated NADPH:$NADP^+$ and ATP:ADP ratios elicit strong feedback on PET, causing hyperreduction of electron carriers (e.g. overreduced PQ pool and highly reduced PSI) that slows electron flow across the cytochrome $b_6f$ complex; iii, the highly reduced PET system and elevated NADPH can actively reduce FDX/TRX and the NTRC systems, respectively; reduced TRX and/or NTRC can activate AGPase (above the activity elicited by an increase in the 3-PGA/Pi ratio), leading to additional starch accumulation; iv, hyperreduction of PET can also lead to stromal ROS accumulation that can act as a signal that controls the expression of chloroplast and nuclear genes; ROS also cause damage to both PSII and I and lead to neutral lipid accumulation as a consequence of activation of diacylglycerol acyltransferases (DGATs) and phospholipid diacylglycerol acyltransferase (PDAT). Many of these metabolic/acclimatory steps both overlap and are interconnected. Under conditions of extended exposure to ML, the damage in *Chlamydomonas tpt3* mutants can accumulate and lead to cell death; cell death occurs rapidly in HL.

transport fixed carbon between the chloroplast and cytosol. This high degree of plasticity in plants is reflected by the following findings: (i) most dicots contain a larger number of pPTs (from 5 to 16) (Bockwoldt et al. 2019). For example, *Arabidopsis* contains 6 pPTs, consisting of 1 TPT, 2 GPTs, 2 PPTs, and 1 XPT (Bockwoldt et al. 2019), whereas *Chlamydomonas* harbors 4 pPTs, with 2 TPTs, 1 putative PPT (TPT10 in this study), and 1 putative GPT/XPT (CGL51 in this study); (ii) plant TPTs play an important role in the export of carbon from the chloroplast during the day. However, XPT has been shown to transport triose-Ps and partially compensate for the loss of TPTs under both ML and HL conditions (Eicks et al. 2002; Hilgers et al. 2018b). Hence, it appears that the paths for fixed carbon export in plants are cooperative, with contributions of transporters that use various sugars, sugar phosphates, and triose phosphates.

Additionally, the elevated starch content in the *t3ko2* mutant during growth in both LL and ML compared with WT cells suggests that the loss of CreTPT3 function creates a bottleneck in the export of fixed carbon, which in part becomes stored as starch and lipids (Figs. 3, A to D, and S8A). The conversion of triose-P to starch releases Pi within the chloroplast that can at least partially compensate for the shortage of Pi caused by inactivation of CreTPT3 (Börnke and Sonnewald 2011). Thus, photosynthetic carbon assimilation can be maintained until the cellular system is completely compromised. In this study, we found that *Chlamydomonas tpt3* mutants exhibited severe growth retardation and the accumulation of starch and lipid in either continuous light (CL) or when experiencing a day/night regime (Figs. 2, D to G, and 8A). Furthermore, the light-induced electron transport rate (ETR) through PSII in the *t3ko2* mutant maintained on a diurnal cycle was similar to that of WT cells exposed to actinic light intensities of up to 200 $\mu$mol photons $m^{-2}$ $s^{-1}$ but was ~30% lower than that of WT cells at a light intensity of 400 $\mu$mol photons $m^{-2}$ $s^{-1}$ (Fig. 8B). We also observed that diurnally maintained *t3ko2* cells grew slightly better than when the cells were maintained in CL (Fig. 8A), indicating that the loss of CreTPT3 activity might be partially compensated for by starch turnover during the night (or allow for some repair of cellular damage that might accumulate during the day), but to a lesser extent than in plants. We observed night-time starch degradation in *tpt3* cells, although

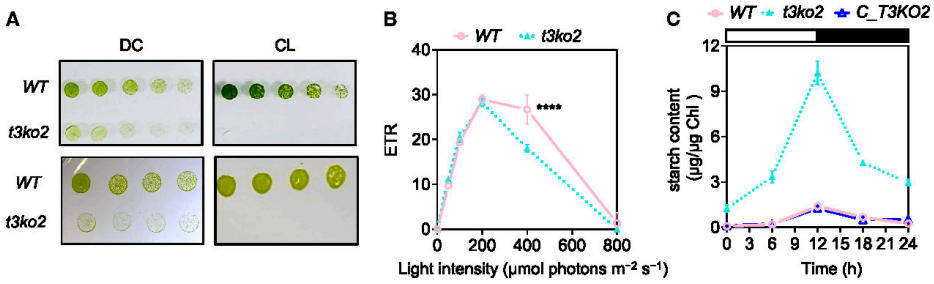


**Figure 8.** Effects of deletion of *CreTPT3* over the diurnal cycle. **A)** Growth of WT and *t3ko2* strains on TP medium agar plates for 4 d under either diurnal cycle (DC) (left panel; 12-h light/12-h dark) or continuous light (CL) (right panel) at an intensity of 60 $\mu$mol photon $m^{-2}$ $s^{-1}$ (upper panel) or HL (lower panel: 450 $\mu$mol photon $m^{-2}$ $s^{-1}$). The dilution series are 3, 1.5, 0.75, and 0.375 $\mu$g $mL^{-1}$ chlorophyll equivalent. **B)** Photosynthetic electron transport rate (ETR) of cells grown under a diurnal rhythm with the light period at an intensity of 60 $\mu$mol photon $m^{-2}$ $s^{-1}$. **C)** Accumulation of starch during growth under a diurnal rhythm at a light intensity of 60 $\mu$mol photon $m^{-2}$ $s^{-1}$.

immediately following the night period a higher level (~5-fold) of undegraded starch remained relative to that of WT cultures (Fig. 8C). These data suggest that starch mobilization may partially compensate for a CreTPT3 deficiency in *Chlamydomonas*.

The mechanism by which starch breakdown products are exported from the chloroplast during the night in *Chlamydomonas* remains largely unknown, although it may involve various transporters including MALTOSE EXCESS 1 (MEX1) (like in plants). *Chlamydomonas* MEX1 can transport starch breakdown products in the form of glucose and/or glucose phosphate, but there is no evidence suggesting that it can export maltose, since a *mex1* mutant did not accumulate maltose or exhibit growth impairment (Findinier et al. 2017). We speculate that the loss of TPT3 function might be partially compensated for by starch turnover in the dark, with degradation products exported via MEX1 or other pPTs whose encoding genes are highly expressed in the dark and downregulated in the light, such as CreTPT10 and CGL51 (Supplemental Fig. S1D). However, even if hexose-P is exported from the chloroplast, it may not be readily converted to triose-P (see below), which would fuel the TCA cycle and respiration and serve to support anabolism.

### *t3ko2* experiences oxidative stress

In plants, the export of sugars and other molecules (e.g. redox equivalents and ROS) can serve as signals that coordinate chloroplast and nuclear gene expression during acclimation to HL (Häusler et al. 2014; Zirngibl et al. 2023). We probed the effect of impaired triose-P export in *t3ko2* on ROS production and accumulation in various subcellular compartments following exposure of cells to ML or HL. In plant cells, $H_2O_2$ is produced as a side product of cellular metabolism including PET, mitochondrial respiration, and substrate level oxidation (Foyer and Noctor 2016; Smirnoff and Arnaud 2019). While ROS stability is generally low, they can accumulate in cells experiencing oxidative stress, with $H_2O_2$ being the most prevalent species that can function as a redox messenger (Li and Kim 2022). Moreover, the trafficking of $H_2O_2$ into or out of different cellular compartments can trigger activation of other retrograde and anterograde signals that may coordinate activities among the compartments, including the nucleus (Shapiguzov et al. 2012; Exposito-Rodriguez et al. 2017; Mittler et al. 2022). Upon exposure to HL, the *t3ko2* mutant accumulated more stromal $H_2O_2$ than WT cells. Cytosolic $H_2O_2$ levels in the mutant exhibited a similar increase, which may reflect the ability of this metabolite to rapidly diffuse from the chloroplast and into the cytoplasm (Fig. 6, B and C). Furthermore, it is unlikely that the mitochondrion contributes to an increase in $H_2O_2$ in *t3ko2* since we observed no (or little) increase in the accumulation of intramitochondrial $H_2O_2$ in the mutant in either LL or ML (Fig. 6D). We also observed an increase in $H_2O_2$ accumulation in the nucleus of *t3ko2* relative to WT cells, although light intensity (HL or LL) did not alter these levels in either WT or the mutant (Fig. 6E); a previous report showed that nuclear $H_2O_2$ level was not significantly affected in WT *Chlamydomonas* cells following exposure to HL (Niemeyer et al. 2021), which may reflect both the level of $H_2O_2$ accumulation and barriers that limit its diffusion. The higher levels of $H_2O_2$ in the nucleus of *t3ko2* cells may trigger retrograde signals that modulate nuclear gene expression, which in turn could ameliorate some of the negative effects of ROS and elicit repair of any damage experienced by the photosynthetic apparatus. A similar response may be elicited in WT cells at higher intensities of actinic light.

Superoxide is predominantly produced by PSI, which can enzymatically be converted into $H_2O_2$ (Foyer 2018). Highly reduced PSI in the *tpt3* mutant can lead to an increase in the production of $H_2O_2$. It was also shown that $H_2O_2$ can be synthesized in thylakoid membranes as a consequence of the oxidation of plastoquinol ($PQH_2$), suggesting a positive correlation between the redox state of the PQ pool and the generation of $H_2O_2$ (Khorobrykh et al. 2015). A similar

finding was noted for both *Nicotiana benthamiana* and *Chlamydomonas* based on the use of hypersensitive $H_2O_2$ sensors (Exposito-Rodriguez et al. 2017; Niemeyer et al. 2021). These 2 organisms were shown to accumulate more stromal $H_2O_2$ in HL, which was dependent on photosynthesis. We observed this positive correlation between PQ pool reduction and the accumulation of $H_2O_2$ in the *t3ko2* mutant; the PQ pool was more reduced in *t3ko2* relative to WT cells after exposing the cells to 105 s of HL (Fig. 4D). In parallel, there was a marked increase in stromal $H_2O_2$ following 2.5 min of HL (Fig. 6B). Therefore, hyperreduction of the PQ pool in the mutant likely results in elevated stromal $H_2O_2$ accumulation, suggesting that CreTPT3 activity and the export of triose-P from the chloroplast are critical for maintaining low-level synthesis/accumulation of $H_2O_2$ and sustaining a high rate of PET in HL; the export of fixed carbon relieves the redox pressure and lessens ROS formation. Additionally, Cre*TPT3* is the most nutrient-deprivation responsive/upregulated of the *pPT* family genes; its expression responds strongly to nitrogen, sulfur, and iron limitations (Supplemental Fig. S9, B to D). These findings are in accord with the hypothesis that the ability to traffic fixed carbon from the chloroplast is important for both distributing carbon to other cellular compartments and relieving oxidative stress in the organelle.

## CreTPT3 is critical for maintaining intracellular partitioning of fixed carbon

Why is the phenotype of the *Chlamydomonas tpt3* mutant so severe? Land plants contain the entire glycolytic pathway in both the chloroplast and cytosol, while the pathway is partitioned between the 2 compartments in *Chlamydomonas*; 90% of the upper activities of the pathways (from F6P→3PG) are associated with the plastid, while over 95% of the activities of the lower part of the pathway (3PG→Pyruvate) occur in the cytosol (Klein 1986; Rochaix et al. 1998). The oxidative pentose phosphate pathway also appears to be in the chloroplast (Klein 1986). The partitioning of glycolysis between the chloroplast and cytosol is supported by the comparative quantification of metabolites, with glucose-1-P, fructose-6-P, and fructose-1,6-P2 being exclusively in the chloroplast and 2-phosphoglycerate only in the cytosol (Klöck and Kreuzberg 1991). It was recently suggested that the flux of metabolites through hexose-P is negligible in the *Chlamydomonas* cytosol (Treves et al. 2022), possibly because of the absence of glycolytic reactions that would facilitate its metabolism. Therefore, even if hexose-P is exported from the chloroplast, it would likely not be rapidly metabolized or maintain rapid cell growth. Overall, the results strongly suggest that triose-P exported from the *Chlamydomonas* chloroplast is likely the major source of fixed carbon transported into the cytoplasm of the cell, facilitating algal growth in the light.

Thus, we hypothesize that the export of triose-P would drive the cytosolic segment of glycolysis and downstream metabolic pathways. This hypothesis is supported by the metabolite analysis: specifically, there is a marked increase of most metabolites associated with the upper-glycolytic/gluconeogenic pathways and a significant decrease of some metabolites of the TCA cycle upon exposure of the mutant cells to either LL or ML (Figs. 3, E to G, and S8, B and C). In contrast, the elimination of the chloroplast-targeted TPT1 protein of *Arabidopsis* showed no significant phenotype, although growth was retarded in the *tpt xpt* double mutants (Hilgers et al. 2018a). Furthermore, based on Pearson's coefficient correlation analyses presented in Supplemental Fig. S11 and Table S4, Cre*TPT3* is coexpressed with many genes involved in respiratory electron transport and with the genes encoding major ATP transporters located at the mitochondrion and chloroplast envelope membranes. In addition, transcript levels of some genes involved in starch degradation, glycolysis, the TCA cycle, and the malate-OAA shuttle shared a high Pearson's correlation coefficient (PCC) with Cre*TPT3*. Together, these data indicate that the export of triose-P from the chloroplast is closely linked to central energy metabolism in *Chlamydomonas*, starting with the production of triose-P in the chloroplast by the CBB cycle or starch degradation (chloroplast-localized reactions of glycolysis), followed by transport to the cytosol that houses the remaining reactions of glycolysis. The products of glycolysis can be trafficked to the mitochondrion where they can be used to drive the TCA cycle, respiratory metabolism, and the generation of ATPs (Supplemental Fig. S11). Hence, triose-P is the major photoassimilate routed from the chloroplast, supplying substrates for downstream metabolic reactions.

Based on our analyses, we propose that various tiers of regulation are responsible for the physiological responses of the *Chlamydomonas t3ko2* mutant, which is illustrated in Fig. 7. When *t3ko2* cells are transferred from LL to ML, the triose-P pool and metabolites derived from that pool accumulate because of the lower capacity of the strain to move triose-P out of the chloroplast where it could be further metabolized. Some compensation may occur through the activity of other transporters, although the expression of Cre*TPT2* is especially low during the day (in the light) and the transport of hexose phosphate may not compensate for the loss of CreTPT3 function because the cytoplasm does not have (or has little of) the activities of glycolysis that would convert hexose-P to DHAP. The compromised ability to export fixed carbon from the chloroplast also suppresses CBB cycle activity and causes hyperreduction of PET and the accumulation of ROS (which would inhibit photosynthetic activity). The highly diminished export of triose-P to the cytoplasm would compromise respiration and downstream biosynthetic reactions. Furthermore, hyperreduction of PET and accumulation of carbon metabolites in the stroma would activate AGPase through allosteric regulation and by the ferredoxin/thioredoxin (FDX/TRX) and NADPH-dependent thioredoxin reductase C (NTRC) redox systems, which would result in starch hyperaccumulation (Ballicora et al. 2000; Lepistö

et al. 2013) (Fig. 7). Increased ROS accumulation in the mutant chloroplast and an elevated PET redox state would also elicit the generation of retrograde signals that mediate changes in nuclear gene expression (Shapiguzov et al. 2012; Suzuki et al. 2012; Wakao and Niyogi 2021), stimulating the biosynthesis of specific activities that may function to ameliorate the effect of the hyperreduced state attained in the chloroplast.

## Materials and methods

### Strains and culture conditions

The WT *Chlamydomonas* (*C. reinhardtii*) strain M10 (CC-4403, isogenic line derived from CC-124) was used as the parental strain for the generation of knockout mutants. Algal cultures were routinely cultivated in growth chambers (LED-41L2, Percival Scientific Inc.) at 25 °C with continuous shaking on an orbital shaker (VWR OS-500 Shaker) at 120 rpm, in Tris-acetate phosphate (TAP) medium (Harris 2009). Cultures were illuminated with continuous cool white LEDs (LED-41L2, Percival Scientific Inc.) at low light (LL, 30 $\mu$mol photons $m^{-2}$ $s^{-1}$). Experiments were mostly performed with cells grown in photoautotrophic Tris phosphate (TP) medium; in some cases, cultures were grown in TAP medium, at 25 °C, and bubbled with air and shaking at 120 rpm in a growth chamber (LED-41L2, Percival Scientific Inc.). For growth assays, cultures were inoculated to a starting cell density of 0.02 at $OD_{750\,nm}$ ($\sim 1 \times 10^5$ cells $mL^{-1}$) in TP bubbled with air under either LL or moderate light (ML, 250 to 300 $\mu$mol photons $m^{-2}$ $s^{-1}$) intensities. For spectrophotometric and chlorophyll fluorescence analyses, the experimental design is described in Supplemental Fig. S5. Growth assays on solid medium were performed with cultures spotted onto medium at different dilutions (as indicated in the text) and exposed to different light intensities; spot tests for photoautotrophic growth were on TP agar plates or on TAP agar plates for mixotrophic growth. Agar plates were incubated for 7 d under either LL or ML (cool white LED) at 25 °C.

### Production of CreTPT2 and CreTPT3 in yeast

The DNA sequence encoding mature CreTPT2 or CreTPT3 was codon optimized for the expression in budding yeast (*S. cerevisiae*) (GeneART, Thermo Fisher Scientific). This coding sequence was inserted in-frame downstream of a sequence encoding a His-tag into the yeast vector pYES-NTa (Thermo Fisher Scientific) using Gibson cloning (NEB). Briefly, pYES-NTa was linearized with BamHI and the Cre*TPT2* and *TPT3* cDNA amplified with the primer pairs listed in Supplemental Table S2. Each cDNA was ligated into the linearized pYES-NTa vector, which was then transformed into the yeast strain INVSc1 (MATa, *his3D1*, *leu2*, *trp1-289*, *ura3-52*/MATa, *his3D1*, *leu2*, *trp1-289*, and *ura3-52*, Thermo Fisher Scientific) using the lithium-acetate/polyethylene glycol (PEG) method (Gietz and Schiestl 2007). Transformed yeast cells were selected on synthetic complete medium containing 2% (*w*/*v*) glucose with the uracil auxotrophic marker. Galactose-inducible production of His-CreTPT2 or CreTPT3 in yeast was performed as described in Linka et al. (2008). The presence of the His-tagged fusion protein was verified by standard SDS-PAGE and immunoblot analysis using an anti-His-antibody conjugated with horseradish peroxidase (Miltenyi Biotech).

### Reconstitution into liposomes and transport assays

For uptake studies, yeast membranes from cells with and without (only empty vector) recombinant His-tagged CreTPT2 or CreTPT3 were enriched and reconstituted into 3% (*w*/*v*) L-alpha-phosphatidylcholine using a freeze–thaw–sonication procedure (Linka et al. 2008). The reconstituted liposomes were preloaded with 30 mM Pi or phosphorylated metabolites to be tested as potential transport substrates. As a negative control for antiporter activity, liposomes were also generated without metabolite preloading. The external counter-exchange substrate was removed via gel filtration on Sephadex G-25 M columns (GE Healthcare). Transport assays were initiated by adding 0.25 mM [alpha-$^{32}$P]-phosphoric acid (6,000 Ci $mmol^{-1}$) to the medium bathing the liposomes and performed as previously described by Linka et al. (2008).

### Transport activity assays

The $K_M$ for Pi was determined by measuring the initial velocity at each of 6 external Pi concentrations between 0.05 and 5 mM. To obtain competitive inhibition constants ($K_I$), the uptake of 0.25 mM Pi into liposomes containing 30 mM Pi was measured over a 4-min period in the presence of increasing external competitor concentrations (0.05 to 5 mM). Three biological replicates were performed for all described experiments. GraphPad Prism software version 9.3.0 was used for nonlinear regression analyses of the kinetic data.

### Vector construction, transformation, and subcellular localization

The pRam118_*VENUS* plasmid, which harbors the *VENUS* gene and the *AphVII* cassette (conferring resistance to hygromycin) (Kaye et al. 2019), was used to individually express Cre*TPT2* (Cre06.g263850_4532) and Cre*TPT3* (Cre01.g045550_4532). The plasmid pRam118_*VENUS* was linearized with HpaI (NEB). Primers g*TPT2*_pRam118_f, g*TPT2*_pRam118_r, and g*TPT3*_pRam118_f, g*TPT3*_pRam118_r (Supplemental Table S1) were used to amplify Cre*TPT2* and Cre*TPT3* genomic DNA fragments containing an overlap with the linearized pRam118_*VENUS* vector. For generating the plasmids pRam118-Cre*TPT2*&*VENUS* and pRam118-Cre*TPT3*&*VENUS*, genomic DNA of Cre*TPT2* or Cre*TPT3* was assembled with pRam118_VENUS plasmid using Gibson assembly (Gibson et al. 2009). The plasmid pRam118-Cre*TPT2*&*VENUS* (2 to 4 $\mu$g), linearized with AseI

(NEB), was transferred into the *Chlamydomonas* M10 strain by electroporation.

A 1,000-bp sequence upstream of Cre*TPT3* and containing the promoter region of the gene was amplified using the primers *TPT3*pro1000_f and *TPT3*pro1000_r (Supplemental Table S2). The 3′ UTR of Cre*TPT3* was amplified using *TPT3*_3UTR_f and *TPT3*_3UTR_r (Supplemental Table S2). The *PSAD* promoter and the *RBCS2* 3′ UTR of pRam118-Cre*TPT3*&*VENUS* were replaced by the amplified fragments of the 1,000-bp upstream region and the 3′ UTR of Cre*TPT3*, respectively. This final vector, designated pRam118_Cre*TPT3*, contains the original Cre*TPT3* promoter (driving the expression of Cre*TPT3*), the genomic DNA sequence of Cre*TPT3*, *VENUS*, and the Cre*TPT3* 3′ UTR plus the AphVII cassette. To localize CreTPT3 and complement the *tpt3* mutant, the mutant was transformed by electroporation with a total amount of 2 to 4 $\mu$g (~500 ng $\mu$L$^{-1}$) of pRam118_Cre*TPT3* that was linearized with AseI.

For each transformation, 2 to 4 $\mu$g of the engineered plasmid was linearized and added to 250 $\mu$L of a cell suspension at ~$3 \times 10^8$ cells mL$^{-1}$. GeneArt MAX Efficiency Transformation Reagent for algae (Invitrogen) was used for introducing the plasmid into algal cells by electroporation according to the instructions provided by the manufacturer. Transformants were selected on solid TAP medium containing 10 $\mu$g mL$^{-1}$ hygromycin (Enzo Life).

Drug-resistant transformants were visualized for VENUS fluorescence as previously described (Kaye et al. 2019). In brief, transgenic strains resistant to hygromycin were screened for VENUS fluorescence using a microplate reader (Infinite M1000; TECAN). Excitation and emission settings were as follows: VENUS, excitation at 515 nm, bandwidth 12 nm, and emission at 550 nm, bandwidth 12 nm; chlorophyll excitation was at 440 nm, bandwidth 9 nm, and emission was at 680 nm, bandwidth 20 nm. A TCS SP8 confocal laser-scanning microscope (Leica) was used to visualize the VENUS fluorescence signal (Kaye et al. 2019).

## CRISPR/Cas9-mediated mutagenesis

The *Chlamydomonas* WT strain M10 (CC-4403, isogenic line derived from CC-124) was used for mutant generation. WT cells were cultured under continuous normal light (NL, 50 $\mu$mol photons m$^{-2}$ s$^{-1}$) for 2 d to a density of 3 to $5 \times 10^6$ cells mL$^{-1}$. The cells were then concentrated to $2 \times 10^8$ cells mL$^{-1}$ in 0.5 × TAP medium supplemented with 80 mM sucrose. Two single-guide RNAs (sgRNAs) were designed by CHOPCHOP (https://chopchop.cbu.uib.no/) and synthesized by Integrated DNA Technologies (IDT). The sequences of the generated sgRNAs are as follows: *TPT2*-sg (5′-AUAAGGG CAAGGACAUGUCAGGG-3) for editing exon 8, *TPT3*-sg1 (5′-CGCUGGGCGTCACUUCCCGGCGG-3′) for editing exon 1, and *TPT3*-sg2 (5′-AAGGCCGCUAUCGCCAACG UGGG-3′) for editing of exon 7. The protocol for disruption of Cre*TPT2* and Cre*TPT3* was adapted from Findinier et al. (2019). Prior to electroporation, Cas9 (IDT) and sgRNAs were incubated together at 37 °C for 30 min. Approximately 500 ng PCR product of the *AphVII* cassette, which confers resistance to hygromycin, was added to the RNP (ribonucleoprotein) mixture. A 250-$\mu$L aliquot was electroporated using a Super Electroporator NEPA21 type II (NEPA GENE). After 16 h of recovery in TAP medium supplemented with 40 mM sucrose, under very low light (10 to 15 $\mu$mol photons m$^{-2}$ s$^{-1}$), cells were plated onto solid TAP medium containing 10 $\mu$g mL$^{-1}$ hygromycin. Sense or antisense-oriented knockins of *AphVII* were determined by amplification using primer pairs with 1 primer annealing to the genomic sequence and the other to the inserted sequence (Supplemental Table S2). The amplified fragments were sequenced to verify the insertion sites (ELIM BIOPHARM, Hayward, USA).

## Complementation of *tpt3* mutants

Mutant strains were transformed with the linearized pRam118_CreTPT3 plasmid. Transformed cells were selected in ML and screened for VENUS fluorescence. Colonies exhibiting VENUS fluorescence and an *AphVII* cassette knocked in at the Cas9 target site were examined for the accumulation of the CreTPT3 protein by immunodetection using anti-CreTPT3 antibodies generated by GenScript USA Inc. (Piscataway, USA). Immunopositive colonies were subjected to growth assays using spot tests under ML on either solid TAP or TP medium.

## P700 activity measurements

Absorbance spectroscopy [JTS-100 spectrophotometer (SpectroLogiX, TN)] was performed to measure P700 activity with dark-adapted liquid cultures [equivalent to 15 $\mu$g mL$^{-1}$ chlorophyll, in 20 mM HEPES-KOH, pH 7.2, and 10% (*w*/*v*) Ficoll] as previously described (Clowez et al. 2021). Actinic light was provided by an orange LED (165 $\mu$mol photons m$^{-2}$ s$^{-1}$) for PSI oxidation, followed by a saturating pulse and dark incubation. Twenty micromolar DCMU and 1 mM hydroxylamine were added to the cell suspension to inhibit linear electron flow (LEF) prior to the measurement. P700 activity was measured by monitoring the absorbance at 705 nm [a 6-nm FWHM (full width at half maximum) interference filter was used to create a narrow excitation beam]; the absorbance at 740 nm was used to correct for unspecific contribution to the 705-nm signal.

## Chlorophyll fluorescence analysis

Chlorophyll fluorescence of cells in a liquid culture was used to evaluate photosynthetic electron transport monitored with a DUAL PAM-100 fluorometer. Cells were acclimated in the dark for 20 min prior to illumination at increasing light intensities (0, 10, 50, 100, 200, 400, 800, 1,000, and 1,200 $\mu$mol photons m$^{-2}$ s$^{-1}$) for 2 min at each intensity or at a constant intensity of 450 $\mu$mol photons m$^{-2}$ s$^{-1}$ for 10 min to evaluate 1-qL. A volume of 8 $\mu$L of 0.5 M $NaHCO_3$ (2 mM) was added to the 2-mL reaction mix as an electron acceptor for the CBBC.

### ROS measurements and roGFP2 imaging analysis

All strains were grown photoautotrophically in LL for 16 to 24 h. After dilution in fresh medium, the cultures were transferred to ML and stained with CM-$H_2$DCFDA (Thermo Fisher Scientific) as described in Kong et al. (2018) for detecting ROS. Briefly, after various treatments (e.g. 48 h in ML), 1 × $10^7$ *Chlamydomonas* cells were pelleted (1,459 × *g*, 3 min, at room temperature) and washed once with 1× phosphate-buffered saline (PBS). The cells were then resuspended in 1× PBS containing 8 $\mu$M CM-$H_2$DCFDA and incubated at room temperature in the dark for 30 min. Following this incubation, the cells were washed 3 times with 1× PBS buffer. The fluorescent signals were either visualized using a TCS SP8 confocal laser-scanning microscope (Leica) or quantified with a microplate reader (Infinite M1000; TECAN). Excitation and emission settings for the microscope were as follows: 488 nm/510 to 530 nm HyD SMD hybrid detector for ROS and 488 nm/650 to 700 nm HyD SMD hybrid detector for chlorophyll autofluorescence. Excitation and emission settings for the plate reader were as follows: ROS excitation 488/5 nm and emission 530/12 nm and chlorophyll excitation 514/5 nm and emission 690/5 nm.

Constructs encoding chloroplast or mitochondrion targeting sequences (Crozet et al. 2018) fused to codon-optimized roGFP2 (Vevea et al. 2013) were transformed into WT and mutant strains. Transgenic colonies were screened for green roGFP2 fluorescence using a microplate reader (Infinite M1000; TECAN); excitation was at 488 nm, bandwidth 9 nm, and emission at 525 nm, bandwidth 10 nm. Cells with strong green fluorescence were cultured as depicted in Supplemental Fig. S5. Signals from the transformed strains were visualized using a TCS SP8 confocal laser-scanning microscope (Leica). roGFP2 signals were collected and analyzed as previously described (Vevea et al. 2013). Using the sequential setup of the SP8, roGFP2 signals were collected at the emission wavelength of 510 to 550 nm immediately following excitation at 405 and 488 nm (Vevea et al. 2013). The degree of roGFP2 oxidation was analyzed as the ratio of the emission signals after excitation at 405 and 488 nm (Vevea et al. 2013).

Plasmids encoding the $H_2O_2$ roGFP2-Tsa2ΔCR sensors (Niemeyer et al. 2021) were obtained from the Chlamydomonas Resource Center (https://www.chlamycollection.org/) (Supplemental Table S3). Cells in which roGFP2-Tsa2ΔCR was targeted to the stroma, cytosol, mitochondrion matrix, or nucleus were initially grown in LL in TAP medium to the exponential growth phase. Cells were then grown in TP medium in LL for 2 h and shifted either to HL or very low light (10 $\mu$mol photons $m^{-2}$ $s^{-1}$). Prior to collecting algal samples, *N*-ethylmaleimide (NEM) (in 100 mM MES–Tris buffer, pH 7.0) was added to a centrifuge tube to trap the oxidation state of the sensor. The final concentration of NEM was 10 mM after adding to the algal culture. After centrifugation (1,459 × *g*, 3 min, room temperature), cells were resuspended in 100 mM MES–Tris buffer (pH 7.0) to reach a chlorophyll concentration of 30 $\mu$g $mL^{-1}$; roGFP2 fluorescence was measured in a plate reader (Infinite M1000; TECAN). For calibration and data calculation, fully oxidized sensors in control samples were prepared by adding $H_2O_2$ to a final concentration of 5 mM, and fully reduced sensors were prepared by adding DTT to a final concentration of 100 mM. Signals were detected using excitation wavelengths of 410 and 488 nm and an emission wavelength of 514 nm. The degree of sensor oxidation (OxD) was calculated using the previous equation as described in Niemeyer et al. (2021).

### Photosynthesis–irradiance curve

Photosynthesis–irradiance curves were measured using a custom Pt-Ag/AgCl polarographic electrode system (ALGI) with a water jacketed (for temperature control), 1-mL glass reaction chamber. YSI 5331A electrodes (Yellow Springs Instruments) were polarized to −0.8 V. The cultures used for the assays were concentrated to 2.5 to 5 $\mu$g $mL^{-1}$ chlorophyll equivalent, supplemented with 15 $\mu$L of 0.5-M sodium bicarbonate in water, and then purged with 1% $CO_2$/99% He (*v*/*v*). Using a gas-tight syringe, the sample was transferred into the reaction chamber that was also purged with 1% $CO_2$/99% He (*v*/*v*). The rate of change in $O_2$ levels was measured sequentially at the light intensities 100, 200, 600, and 1,000 $\mu$mol photons $m^{-2}$ $s^{-1}$ (photosynthetic active radiation, PAR); each intensity was maintained for 3 to 5 min followed by a 3-min intervening dark period, and then, the light level was raised to the next higher intensity (stepped change) until the full range of intensities was tested. At 1,000 $\mu$mol photons $m^{-2}$ $s^{-1}$, the light was held for 10 min followed by an 8-min dark period. Before the measurement of each experimental series, the electrodes were calibrated with air (~21% $O_2$) and 1% $CO_2$/99% He mixture (0% $O_2$). The initial slope of the response was used to determine the $O_2$ evolution rate.

### Starch and TAG quantification

Cells were grown under the LL to mid-exponential phase, diluted to 0.5 $\mu$g $mL^{-1}$ Chl equivalent with fresh TAP medium, and transferred to and then grown in ML for 24 h or more, as indicated. Starch was measured according to Klein and Betz (1978), with slight modifications. In brief, cells were collected by centrifugation and pigments were extracted in methanol. Dried cell pellets were resuspended in water and heated at 100 °C to break the cells and release the starch. After cooling, amyloglucosidase and α-amylase (2.25 U $mL^{-1}$) were used to hydrolyze starch and the products of hydrolysis were quantified using a Glucose Colorimetric Detection Kit (Thermo Fisher Scientific). Triacylglycerol (TAG) levels were estimated by a fluorometric assay using the dye Nile Red (Thermo Fisher Scientific) (Yu et al. 2009). A Nile Red solution (500 $\mu$g $mL^{-1}$ in acetone) was added to 1 mL of cell suspensions to a final concentration of 0.5 $\mu$g $mL^{-1}$. Samples were then incubated at room temperature for 30 min, and the

Nile Red fluorescence emission was quantified at 575 nm following excitation at 530 nm using a microplate reader (Infinite M1000; TECAN).

## Metabolic analysis

Cells grown in LL were shifted to ML for 45 min or 6 h, as indicated. A volume of 45 mL of culture was rapidly quenched in cold saline solution [0.9% (0.15 M) NaCl] (−2 to −3 °C), extracted using cold methanol, and then analyzed by LC–MS/MS. Quenching and analysis of metabolites were performed, with modifications, according to Sake et al. (2020). The quenching solution, filtered saline (9 g $L^{-1}$ NaCl), was prechilled to 4 °C in a refrigerator. Thirty mL of the quenching solution was transferred to a 50-mL conical tube kept in an ice bath mixed with salt to maintain the temperature between −3 and −1 °C. Then, 15 mL of the culture was rapidly plunged into the 30 mL of quenching solution and the samples were centrifuged at 1459 × *g* for 10 min at 4 °C. Cell pellets were washed with fresh prechilled saline solution and centrifuged again at 4,000 rpm for 10 min in a 2-mL centrifuge tube. For each replicate, 45 mL of the culture was sampled and the 3 cell pellets per culture were pooled. Washed pellets were frozen at −80 °C until extraction. Metabolite extraction and further analysis were modified from Young et al. (2011). To each cell pellet, 500-$\mu$L methanol was added along with the internal standards ribitol and PIPES to a final concentration of 2 $\mu$M each. Samples were then vortexed for 30 s, frozen in liquid nitrogen as described in Winder et al. (2008), and allowed to thaw at 0 °C.

This vortex freeze–thaw cycle was repeated twice more before the samples were centrifuged at 10,000 × *g* at 1 °C for 5 min. The supernatant was collected, and the remaining pellets were extracted twice more with 500 $\mu$L of a 50:50 (*v*/*v*) mixture of methanol and water, with 3 vortex–freeze–thaw cycles done for each extraction. Supernatants from each extraction procedure were pooled and dried on a Thermo Fisher SpeedVac Concentrator. Dried extracts were then resuspended in 500-$\mu$L water and cleaned to remove any residual large cell debris by filtration, first through a 0.22-$\mu$m pore size Spin-X centrifugal tube filter, followed by 10 K molecular mass cutoff filters, followed finally by 3 K molecular mass cutoff filters. After each filtration step, filters were rinsed with 50-$\mu$L water, which was added to the total sample volume for subsequent steps. Filtered extracts were dried again and resuspended in 200-$\mu$L water for LC–MS/MS analysis.

Metabolite extracts were analyzed using LC–MS/MS, as adapted from Young et al. (2011). A Phenomenex 150 mm × 2 mm Synergi Hydro-RP column was used on an Agilent 1200 Series HPLC system coupled to an AB Sciex 5500 QTRAP system. LC was performed with a liquid injection volume of 20 $\mu$L and a gradient elution with 10 mM tributylamine and 15 mM acetic acid (aqueous phase) in acetonitrile (organic phase) (reagent B) at a constant flow rate of 0.3 mL $min^{-1}$ and a constant temperature of 40 °C. The gradient profile of the organic phase was as follows (all % *v*/*v*): 0% B (0 min), 8% B (10 min), 16% B (15 min), 30% B (16.5 min), 30% B (19 min), 90% B (21.5 min), 90% B (28 min), 0% B (28.5 min), and 0% B (35 min). MS analysis was performed in negative mode using a multiple reaction monitoring (MRM) acquisition method. Data acquisition was performed with ABSciex Analyst 1.7 software. Absolute quantification of intracellular metabolites was performed using the quantitation mode on the Analyst software. All chemicals used for metabolite extraction and LC–MS/MS analysis were Optima grade reagents.

## Protein extraction and immunoblot analysis

Affinity-purified polyclonal antibodies against CreTPT3 were custom-made by GenScript. The antigen sequence used for antibody generation was KSWSFGRPVTKQEF.

*Chlamydomonas* cells were grown in liquid cultures to 2 to 5 × $10^6$ cells $mL^{-1}$ and collected by centrifugation (1,459 × *g*, 5 min, at room temperature). Cells were resuspended in resuspension buffer [5 mM HEPES-KOH, pH 7.5, 10 mM EDTA pH 7.5, 1× protease inhibitor "complete EDTA-free" (Roche)]. For cell disruption, bead-beating was performed using a mini beadbeater (BioSpec) in 2 cycles of 30 s $min^{-1}$, with a 1-min period of cooling on ice between cycles. Disrupted cells were centrifuged at 4 °C, 30 min, 14,000 × *g* in a microfuge. The supernatant was removed, and the pellet was resuspended in sample buffer [resuspension buffer containing 100 mM $Na_2CO_3$, 100 mM DTT, 2% (*w*/*v*) SDS, and 12% (*w*/*v*) sucrose].

SDS-PAGE was performed using a 12% polyacrylamide gel (Bio-Rad), with electrophoresis for 90 min at 120 V. The proteins within the gel were transferred onto a PVDF membrane (Bio-Rad) using Trans-Blot Turbo (Bio-Rad). The dilution for the primary antibody is 1:500. Goat Anti-Rabbit IgG (Bio-Rad, 1706515) was used for the secondary antibody. The detection was performed using Clarity Max Western ECL Substrate (Bio-Rad).

## RT-qPCR

RT-qPCR was performed as described previously (Kaye et al. 2019). Briefly, total RNA was isolated using an RNeasy Plant Mini Kit (Qiagen) and treated with DNase I (Qiagen). First-strand cDNA was generated by reverse transcription of 0.5 $\mu$g total RNA using an iScript cDNA Synthesis Kit (Bio-Rad). qPCR using a Roche LightCycler 480 was performed with a SensiMix No-ROX SYBR Green I Kit as described by the manufacturer (Bioline). Primers used in this research for analyzing the expression levels of Cre*TPT10/TPT2/TPT3/CGLS1* are listed in Supplemental Table S1. mRNA levels were calculated using the DeltaC (T) method (Silver et al. 2006). The *CBLP* gene was used as an internal control.

## Analysis of transcript levels in response to different conditions

To analyze the transcript level of Cre*TPT* genes under different conditions, we obtained RNA-seq data published

previously in which cells experienced a diurnal cycle and nitrogen, sulfur, or $Fe^{2+}$ limitation (González-Ballester et al. 2010; Ngan et al. 2015; Zones et al. 2015; Urzica et al. 2013; Strenkert et al. 2019). The $\log_2$ fold change of each gene was calculated based on the ratio of transcript abundance at different time points over transcript level at time point 0 h. The fold change was visualized as a heatmap, and the color bar is the scale of $\log_2$ (fold change).

### Correlation analysis based on Cre*TPT3* transcript abundance under different conditions

The Z-score of each gene was calculated as follows: the mean transcript level of each gene across all conditions was subtracted from the transcript level of each gene in each sample. This difference was divided by the SD of the transcript level of each gene under all conditions to obtain Z-scores. The entire Z-score matrix for every gene under all conditions was used to calculate the Pearson's correlation matrix by using the Python Dataframe.corr() function. The genes highly correlated with Cre*TPT3* were selected if their correlation value was higher than 0.75. PCC values of Cre*TPT3* highly correlated genes were plotted based on their KEGG pathway.

### In vivo polymeric carbohydrate staining

Lugol's iodine [aqueous solution of 1.8% (*w*/*v*) iodine and 3% (*w*/*v*) potassium iodide] was used to stain in vivo polymeric carbohydrates. Briefly, 0.5 mL of the cell culture was pelleted, resuspended in 10 $\mu$L of Lugol's iodine, and visualized under a bright-field microscope. Lugol's iodine selectively binds to alpha-1,4 glucans and stains it blue-black.

### Accession numbers

Genes analyzed in this article have the following accession numbers in Phytozome v13 (https://phytozome-next.jgi.doe.gov/): Cre*TPT2* (Cre06.g263850_4532), Cre*TPT3* (Cre01.g045550_4532), Cre*TPT10* (Cre08.g379350_4532), *CGL51* (Cre16.g663800_4532), Cre*MDH1* (Cre03.g194850_4532), and Cre*MDH5* (Cre09.g410700_4532).

## Acknowledgments

W.H. thanks Dr. Masayuki Onishi for the advice on the generation of CRISPR mutants and Adrien Burlacot for the help with PQ pool measurements.

## Author contributions

W.H., A.K., A.G., and M.P. conceptualized the study. W.H. generated the CRISPR mutants as well as the complemented strain, localized the TPT2 and TPT3 proteins, and analyzed the photosynthetic performances and starch changes over diel cycle. A.K. performed the experiments of photosynthetic $O_2$ evolution, extraction of samples for LC–MS/MS, and data analysis of LC–MS/MS. A.P. and N.L. performed the reconstitution into liposomes and transport activity assays. M.M. and N.B. performed LC–MS/MS and analyses of metabolite data. W.H. and Y.W. analyzed the redox status in the cell. B.R. performed data mining for transcriptome and the Nile Red staining. J.F. and N.F. analyzed starch changes upon transition from LL to ML. W.H., P.R., and A.G. analyzed PSI and PSII activities. J.F. and B.R. constructed roGFP2-associated vectors. W.H. and A.G. wrote the manuscript. A.G., M.P., A.K., N.L., N.B., A.P., M.M., and all the other authors helped in writing and revising the manuscript.

## Supplemental data

The following materials are available in the online version of this article.

**Supplemental Figure S1**. Features of putative plastid phosphate transporter (pPT) in *A. thaliana* and *C. reinhardtii*.

**Supplemental Figure S2**. Background activity of Pi uptake with the endogenous yeast transporters reconstituted in into liposomes.

**Supplemental Figure S3**. Mutations generated in the Cre*TPT2* gene by CRISPR/Cas9-mediated insertion.

**Supplemental Figure S4**. Types of mutations generated in the Cre*TPT3* gene by CRISPR/Cas9-mediated insertion with sgRNA1 in exon 1 and sgRNA2 in exon 7.

**Supplemental Figure S5**. Experimental setup.

**Supplemental Figure S6**. Comparison of cell morphology between *WT* and *t3ko2*.

**Supplemental Figure S7**. Quantification of chlorophyll contents in the indicated strains after exposure to ML for 24 and 48 h.

**Supplemental Figure S8**. Starch and metabolites in WT and *t3ko2*.

**Supplemental Figure S9**. Transcript changes of Cre*TPT2* and Cre*TPT3* under various conditions.

**Supplemental Figure S10**. Transcript changes of p*PT*s and plastid *MDH*s in the indicated strains after exposure to ML.

**Supplemental Figure S11**. List of genes with strong correlation relative to Cre*TPT3*.

**Supplemental Table S1**. Members of the triose phosphate transporter family in *C. reinhardtii* and their predicted subcellular localization based on TargetP2.0.

**Supplemental Table S2**. Primers used in this study.

**Supplemental Table S3**. Plasmids of $H_2O_2$ *roGFP2-Tsa2ΔCR* sensors (Niemeyer et al. 2021).

**Supplemental Table S4**. List of genes with strong PCC to *CreTPT3*.

**Supplemental Data Set S1**. Statistical test performed and used across figures to detect significant differences.

## Funding

This project has been supported by DOE award DE-SC0019417 to A.G. W.H. was supported solely by a grant from the US Department of Energy, Office of Science, Basic Energy Systems (DE-SC0019417). A.K. and M.P. were supported solely by a grant from the US Department of

Energy, Office of Science, Basic Energy Systems (DE-SC0019341 to M.P.). N.B. and M.M. were supported by the US Department of Energy, Office of Science, Office of Biological and Environmental Research (B.R.), (DE-SC0018301 to N.B.). N.L. and A.P. were supported by German Research Foundations (DFG Grant LI1781/2-2). B.R. was supported by the National Science Foundation (Award Number 1645164). R.K. and J.F. were supported by the Department of Plant Biology of the Carnegie Institution for Science. P.R. was supported by the Human Frontier Science Program (HFSP) RGP0046/2018 (to A.G.).

*Conflict of interest statement.* The authors declare no conflict of interest regarding this study.

## Data availability

All data are available in the main text or the supplementary materials.

## References

**Badger MR, von Caemmerer S, Ruuska S, Nakano H**. Electron flow to oxygen in higher plants and algae: rates and control of direct photoreduction (Mehler reaction) and rubisco oxygenase. Philos Trans R Soc Lond B Biol Sci. 2000:**355**(1402):1433–1446. https://doi.org/10.1098/rstb.2000.0704

**Ballicora MA, Frueauf JB, Fu Y, Schürmann P, Preiss J**. Activation of the potato tuber ADP-glucose pyrophosphorylase by thioredoxin. J Biol Chem. 2000:**275**(2):1315–1320. https://doi.org/10.1074/jbc.275.2.1315

**Bhatt P, Bhandari G, Turco RF, Aminikhoei Z, Bhatt K, Simsek H**. Algae in wastewater treatment, mechanism, and application of biomass for production of value-added product. Environ Pollut. 2022:**309**:119688. https://doi.org/10.1016/j.envpol.2022.119688

**Bockwoldt M, Heiland I, Fischer K**. The evolution of the plastid phosphate translocator family. Planta. 2019:**250**(1):245–261. https://doi.org/10.1007/s00425-019-03161-y

**Börnke F, Sonnewald S**. Biosynthesis and metabolism of starch and sugars. In: Plant metabolism and biotechnology. Chichester, UK: John Wiley & Sons, Ltd; 2011. p. 1–25.

**Boyle NR, Sengupta N, Morgan JA**. Metabolic flux analysis of heterotrophic growth in *Chlamydomonas reinhardtii*. PLoS One. 2017:**12**(5):e0177292. https://doi.org/10.1371/journal.pone.0177292

**Chaux F, Burlacot A, Mekhalfi M, Auroy P, Blangy S, Richaud P, Peltier G**. Flavodiiron proteins promote fast and transient $O_2$ photoreduction in *Chlamydomonas*. Plant Physiol. 2017:**174**(3):1825–1836. https://doi.org/10.1104/pp.17.00421

**Cho M-H, Lim H, Shin DH, Jeon J-S, Bhoo SH, Park Y-I, Hahn T-R**. Role of the plastidic glucose translocator in the export of starch degradation products from the chloroplasts in *Arabidopsis thaliana*. New Phytol. 2011:**190**(1):101–112. https://doi.org/10.1111/j.1469-8137.2010.03580.x

**Clowez S, Renicke C, Pringle JR, Grossman AR**. Impact of menthol on growth and photosynthetic function of *Breviolum minutum* (Dinoflagellata, Dinophyceae, Symbiodiniaceae) and interactions with its *Aiptasia* host. J Phycol. 2021:**57**(1):245–257. https://doi.org/10.1111/jpy.13081

**Crozet P, Navarro FJ, Willmund F, Mehrshahi P, Bakowski K, Lauersen KJ, Pérez-Pérez M-E, Auroy P, Rovira AG, Sauret-Gueto S, et al.** Birth of a photosynthetic chassis: a MoClo toolkit enabling synthetic biology in the microalga *Chlamydomonas reinhardtii*. ACS Synth Biol. 2018:**7**(9):2074–2086. https://doi.org/10.1021/acssynbio.8b00251

**Dorion S, Ouellet JC, Rivoal J**. Glutathione metabolism in plants under stress: beyond reactive oxygen species detoxification. Metabolites. 2021:**11**(9):641. https://doi.org/10.3390/metabo11090641

**Eicks M, Maurino V, Knappe S, Flügge U-I, Fischer K**. The plastidic pentose phosphate translocator represents a link between the cytosolic and the plastidic pentose phosphate pathways in plants. Plant Physiol. 2002:**128**(2):512–522. https://doi.org/10.1104/pp.010576

**Exposito-Rodriguez M, Laissue PP, Yvon-Durocher G, Smirnoff N, Mullineaux PM**. Photosynthesis-dependent $H_2O_2$ transfer from chloroplasts to nuclei provides a high-light signalling mechanism. Nat Commun. 2017:**8**(1):49. https://doi.org/10.1038/s41467-017-00074-w

**Findinier J, et al.** The Chlamydomonas mex1 mutant shows impaired starch mobilization without maltose accumulation. J Exp Bot. 2017:**68**:5177–5189.

**Findinier J, Delevoye C, Cohen MM**. The dynamin-like protein Fzl promotes thylakoid fusion and resistance to light stress in *Chlamydomonas reinhardtii*. PLoS Genet. 2019:**15**(3):e1008047. https://doi.org/10.1371/journal.pgen.1008047

**Fischer K, Kammerer B, Gutensohn M, Arbinger B, Weber A, Hausler RE, Flugge U-I**. A new class of plastidic phosphate translocators: a putative link between primary and secondary metabolism by the phosphoenolpyruvate/phosphate antiporter. Plant Cell. 1997:**9**(3):453. https://doi.org/10.1105/tpc.9.3.453

**Fliege R, Flügge U-I, Werdan K, Heldt HW**. Specific transport of inorganic phosphate, 3-phosphoglycerate and triosephosphates across the inner membrane of the envelope in spinach chloroplasts. Biochim Biophys Acta Bioenerg. 1978:**502**(2):232–247. https://doi.org/10.1016/0005-2728(78)90045-2

**Flügge UI, Fischer K, Gross A, Sebald W, Lottspeich F, Eckerskorn C**. The triose phosphate-3-phosphoglycerate-phosphate translocator from spinach chloroplasts: nucleotide sequence of a full-length cDNA clone and import of the in vitro synthesized precursor protein into chloroplasts. EMBO J. 1989:**8**(1):39–46. https://doi.org/10.1002/j.1460-2075.1989.tb03346.x

**Flügge UI, Häusler RE, Ludewig F, Fischer K**. Functional genomics of phosphate antiport systems of plastids. Physiol Plant. 2003:**118**(4):475–482. https://doi.org/10.1034/j.1399-3054.2003.00137.x

**Foyer CH**. Reactive oxygen species, oxidative signaling and the regulation of photosynthesis. Environ Exp Bot. 2018:**154**:134–142. https://doi.org/10.1016/j.envexpbot.2018.05.003

**Foyer CH, Noctor G**. Stress-triggered redox signalling: what's in pROSpect? Plant Cell Environ. 2016:**39**(5):951–964. https://doi.org/10.1111/pce.12621

**Ge F, Huang W, Chen Z, Zhang C, Xiong Q, Bowler C, Yang J, Xu J, Hu H**. Methylcrotonyl-CoA carboxylase regulates triacylglycerol accumulation in the model diatom *Phaeodactylum tricornutum*. Plant Cell. 2014:**26**(4):1681–1697. https://doi.org/10.1105/tpc.114.124982

**Gibson DG, Young L, Chuang R-Y, Venter JC, Hutchison CA, 3rd, Smith HO**. x. Nat Methods. 2009:**6**:343–345.

**Gietz RD, Schiestl RH**. High-efficiency yeast transformation using the LiAc/SS carrier DNA/PEG method. Nat Protoc. 2007:**2**:31–34.

**González-Ballester D, Casero D, Cokus S, Pellegrini M, Merchant SS, Grossman AR**. RNA-seq analysis of sulfur-deprived *Chlamydomonas* cells reveals aspects of acclimation critical for cell survival. Plant Cell. 2010:**22**(6):2058–2084. https://doi.org/10.1105/tpc.109.071167

**Harris EH**. Chlamydomonas sourcebook: introduction to Chlamydomonas and its laboratory use. 2nd ed. San Diego (CA): Academic Press; 2009.

**Häusler RE, Baur B, Scharte J, Teichmann T, Eicks M, Fischer KL, Flügge UI, Schubert S, Weber A, Fischer K**. Plastidic metabolite transporters and their physiological functions in the inducible crassulacean acid metabolism plant *Mesembryanthemum crystallinum*. Plant J. 2000:**24**(3):285–296. https://doi.org/10.1046/j.1365-313x.2000.00876.x

**Häusler RE, Heinrichs L, Schmitz J, Flügge U-I**. How sugars might coordinate chloroplast and nuclear gene expression during acclimation

to high light intensities. Mol Plant. 2014:**7**(7):1121–1137. https://doi.org/10.1093/mp/ssu064

**Häusler RE, Schlieben NH, Schulz B, Flügge UI**. Compensation of decreased triose phosphate/phosphate translocator activity by accelerated starch turnover and glucose transport in transgenic tobacco. Planta. 1998:**204**(3):366–376. https://doi.org/10.1007/s004250050268

**Helman Y, Tchernov D, Reinhold L, Shibata M, Ogawa T, Schwarz R, Ohad I, Kaplan A**. Genes encoding A-type flavoproteins are essential for photoreduction of $O_2$ in cyanobacteria. Curr Biol. 2003:**13**(3):230–235. https://doi.org/10.1016/S0960-9822(03)00046-0

**Hilgers EJA, Schöttler MA, Mettler-Altmann T, Krueger S, Dörmann P, Eicks M, Flügge U-I, Häusler RE**. The combined loss of triose phosphate and xylulose 5-phosphate/phosphate translocators leads to severe growth retardation and impaired photosynthesis in *Arabidopsis thaliana* tpt/xpt double mutants. Front Plant Sci. 2018a:**9**:1331. https://doi.org/10.3389/fpls.2018.01331

**Hilgers EJA, Staehr P, Flügge U-I, Häusler RE**. The xylulose 5-phosphate/phosphate translocator supports triose phosphate, but not phosphoenolpyruvate transport across the inner envelope membrane of plastids in *Arabidopsis thaliana* mutant plants. Front Plant Sci. 2018b:**9**:1461. https://doi.org/10.3389/fpls.2018.01461

**Houille-Vernes L, Rappaport F, Wollman F-A, Alric J, Johnson X**. Plastid terminal oxidase 2 (PTOX2) is the major oxidase involved in chlororespiration in *Chlamydomonas*. Proc Natl Acad Sci U S A. 2011:**108**(51):20820–20825. https://doi.org/10.1073/pnas.1110518109

**Huang W, Haferkamp I, Lepetit B, Molchanova M, Hou S, Jeblick W, Río Bártulos C, Kroth PG**. Reduced vacuolar β-1,3-glucan synthesis affects carbohydrate metabolism as well as plastid homeostasis and structure in *Phaeodactylum tricornutum*. Proc Natl Acad Sci U S A. 2018:**115**(18):4791–4796. https://doi.org/10.1073/pnas.1719274115

**Jack DL, Yang NM, Saier MH, Jr**. The drug/metabolite transporter superfamily. Eur J Biochem. 2001:**268**(13):3620–3639. https://doi.org/10.1046/j.1432-1327.2001.02265.x

**Johnson X, Alric J**. Central carbon metabolism and electron transport in *Chlamydomonas reinhardtii*: metabolic constraints for carbon partitioning between oil and starch. Eukaryot Cell. 2013:**12**(6):776–793. https://doi.org/10.1128/EC.00318-12

**Kammerer B, Fischer K, Hilpert B, Schubert S, Gutensohn M, Weber A, Flügge UI**. Molecular characterization of a carbon transporter in plastids from heterotrophic tissues: the glucose 6-phosphate/phosphate antiporter. Plant Cell. 1998:**10**(1):105–117. https://doi.org/10.1105/tpc.10.1.105

**Kaye Y, Huang W, Clowez S, Saroussi S, Idoine A, Sanz-Luque E, Grossman AR**. The mitochondrial alternative oxidase from *Chlamydomonas reinhardtii* enables survival in high light. J Biol Chem. 2019:**294**(4):1380–1395. https://doi.org/10.1074/jbc.RA118.004667

**Khan MI, Shin JH, Kim JD**. The promising future of microalgae: current status, challenges, and optimization of a sustainable and renewable industry for biofuels, feed, and other products. Microb Cell Fact. 2018:**17**(1):36. https://doi.org/10.1186/s12934-018-0879-x

**Khorobrykh SA, Karonen M, Tyystjärvi E**. Experimental evidence suggesting that $H_2O_2$ is produced within the thylakoid membrane in a reaction between plastoquinol and singlet oxygen. FEBS Lett. 2015:**589**(6):779–786. https://doi.org/10.1016/j.febslet.2015.02.011

**Klein U**. Compartmentation of glycolysis and of the oxidative pentose-phosphate pathway in *Chlamydomonas reinhardii*. Planta. 1986:**167**(1):81–86. https://doi.org/10.1007/BF00446372

**Klein U, Betz A**. Fermentative metabolism of hydrogen-evolving *Chlamydomonas moewusii*. Plant Physiol. 1978:**61**(6):953–956. https://doi.org/10.1104/pp.61.6.953

**Klöck G, Kreuzberg K**. Compartmented metabolite pools in protoplasts from the green alga *Chlamydomonas reinhardtii*: changes after transition from aerobiosis to anaerobiosis in the dark. Biochim Biophys Acta. 1991:**1073**(2):410–415. https://doi.org/10.1016/0304-4165(91)90150-F

**Knappe S, Flügge U-I, Fischer K**. Analysis of the plastidic *phosphate translocator* gene family in Arabidopsis and identification of new *phosphate translocator*-homologous transporters, classified by their putative substrate-binding site. Plant Physiol. 2003:**131**(3):1178–1190. https://doi.org/10.1104/pp.016519

**Kong F, Burlacot A, Liang Y, Légeret B, Alseekh S, Brotman Y, Fernie AR, Krieger-Liszkay A, Beisson F, Peltier G, et al.** Interorganelle communication: peroxisomal MALATE DEHYDROGENASE2 connects lipid catabolism to photosynthesis through redox coupling in Chlamydomonas. Plant Cell. 2018:**30**(8):1824–1847. https://doi.org/10.1105/tpc.18.00361

**Kramer DM, Johnson G, Kiirats O, Edwards GE**. New fluorescence parameters for the determination of QA redox state and excitation energy fluxes. Photosynth Res. 2004:**79**(2):209–218. https://doi.org/10.1023/B:PRES.0000015391.99477.0d

**Krishnan A, Kumaraswamy GK, Vinyard DJ, Gu H, Ananyev G, Posewitz MC, Dismukes GC**. Metabolic and photosynthetic consequences of blocking starch biosynthesis in the green alga *Chlamydomonas reinhardtii sta6* mutant. Plant J. 2015:**81**(6):947–960. https://doi.org/10.1111/tpj.12783

**Lee S-K, Eom J-S, Voll LM, Prasch CM, Park Y-I, Hahn T-R, Ha S-H, An G, Jeon J-S**. Analysis of a triose phosphate/phosphate translocator-deficient mutant reveals a limited capacity for starch synthesis in rice leaves. Mol Plant. 2014:**7**(11):1705–1708. https://doi.org/10.1093/mp/ssu082

**Lee Y, Nishizawa T, Takemoto M, Kumazaki K, Yamashita K, Hirata K, Minoda A, Nagatoishi S, Tsumoto K, Ishitani R, et al.** Structure of the triose-phosphate/phosphate translocator reveals the basis of substrate specificity. Nat Plants. 2017:**3**(10):825–832. https://doi.org/10.1038/s41477-017-0022-8

**Lepistö A, Pakula E, Toivola J, Krieger-Liszkay A, Vignols F, Rintamäki E**. Deletion of chloroplast NADPH-dependent thioredoxin reductase results in inability to regulate starch synthesis and causes stunted growth under short-day photoperiods. J Exp Bot. 2013:**64**(12):3843–3854. https://doi.org/10.1093/jxb/ert216

**Li M, Kim C**. Chloroplast ROS and stress signaling. Plant Commun. 2022:**3**(1):100264. https://doi.org/10.1016/j.xplc.2021.100264

**Lim L, Linka M, Mullin KA, Weber APM, McFadden GI**. The carbon and energy sources of the non-photosynthetic plastid in the malaria parasite. FEBS Lett. 2010:**584**(3):549–554. https://doi.org/10.1016/j.febslet.2009.11.097

**Linka M, Jamai A, Weber APM**. Functional characterization of the plastidic phosphate translocator gene family from the thermoacidophilic red alga *Galdieria sulphuraria* reveals specific adaptations of primary carbon partitioning in green plants and red algae. Plant Physiol. 2008:**148**(3):1487–1496. https://doi.org/10.1104/pp.108.129478

**Loddenkötter B, Kammerer B, Fischer K, Flügge UI**. Expression of the functional mature chloroplast triose phosphate translocator in yeast internal membranes and purification of the histidine-tagged protein by a single metal-affinity chromatography step. Proc Natl Acad Sci U S A. 1993:**90**(6):2155–2159. https://doi.org/10.1073/pnas.90.6.2155

**Mittler R, Zandalinas SI, Fichman Y, Van Breusegem F**. Reactive oxygen species signalling in plant stress responses. Nat Rev Mol Cell Biol. 2022:**23**(10):663–679. https://doi.org/10.1038/s41580-022-00499-2

**Moog D, Nozawa A, Tozawa Y, Kamikawa R**. Substrate specificity of plastid phosphate transporters in a non-photosynthetic diatom and its implication in evolution of red alga-derived complex plastids. Sci Rep. 2020:**10**(1):1167. https://doi.org/10.1038/s41598-020-58082-8

**Ngan CY, Wong C-H, Choi C, Yoshinaga Y, Louie K, Jia J, Chen C, Bowen B, Cheng H, Leonelli L, et al.** Lineage-specific chromatin signatures reveal a regulator of lipid metabolism in microalgae. Nat Plants. 2015:**1**(8):15107. https://doi.org/10.1038/nplants.2015.107

**Niemeyer J, Scheuring D, Oestreicher J, Morgan B, Schroda M.** Real-time monitoring of subcellular $H_2O_2$ distribution in *Chlamydomonas reinhardtii*. Plant Cell. 2021:**33**(9):2935–2949. https://doi.org/10.1093/plcell/koab176

**Niittylä T, Messerli G, Trevisan M, Chen J, Smith AM, Zeeman SC.** A previously unknown maltose transporter essential for starch degradation in leaves. Science. 2004:**303**(5654):87–89. https://doi.org/10.1126/science.1091811

**Niyogi KK, Truong TB.** Evolution of flexible non-photochemical quenching mechanisms that regulate light harvesting in oxygenic photosynthesis. Curr Opin Plant Biol. 2013:**16**(3):307–314. https://doi.org/10.1016/j.pbi.2013.03.011

**Prabhakar V, et al.** Phosphoenolpyruvate provision to plastids is essential for gametophyte and sporophyte development in *Arabidopsis thaliana*. Plant Cell. 2010:**22**(8):2594–2617. https://doi.org/10.1105/tpc.109.073171

**Raghavendra AS, Padmasree K.** Beneficial interactions of mitochondrial metabolism with photosynthetic carbon assimilation. Trends Plant Sci. 2003:**8**(11):546–553. https://doi.org/10.1016/j.tplants.2003.09.015

**Riesmeier JW, Flügge UI, Schulz B, Heineke D, Heldt HW, Willmitzer L, Frommer WB.** Antisense repression of the chloroplast triose phosphate translocator affects carbon partitioning in transgenic potato plants. Proc Natl Acad Sci U S A. 1993:**90**(13):6160–6164. https://doi.org/10.1073/pnas.90.13.6160

**Rochaix J-D, Goldschmidt-Clermont M, Merchant S.** The molecular biology of chloroplasts and mitochondria in Chlamydomonas. **Rochaix J-D, Goldschmidt-Clermont M, Merchant S**, editors. Dordrecht: Plenum Publishing Corporation; 1998.

**Sake CL, Newman DM, Boyle NR.** Evaluation of quenching methods for metabolite recovery in photoautotrophic *Synechococcus sp.* PCC 7002. Biotechnol Prog. 2020:**36**(5):e3015. https://doi.org/10.1002/btpr.3015

**Saroussi S, Sanz-Luque E, Kim RG, Grossman AR.** Nutrient scavenging and energy management: acclimation responses in nitrogen and sulfur deprived Chlamydomonas. Curr Opin Plant Biol. 2017:**39**:114–122. https://doi.org/10.1016/j.pbi.2017.06.002

**Schneider A, Häusler RE, Kolukisaoglu Ü, Kunze R, Van der Graaff E, Schwacke R, Catoni E, Desimone M, Flügge UI.** An *Arabidopsis thaliana* knock-out mutant of the chloroplast triose phosphate/phosphate translocator is severely compromised only when starch synthesis, but not starch mobilisation is abolished. Plant J. 2002:**32**(5):685–699. https://doi.org/10.1046/j.1365-313X.2002.01460.x

**Shapiguzov A, Vainonen JP, Wrzaczek M, Kangasjärvi J.** ROS-talk—how the apoplast, the chloroplast, and the nucleus get the message through. Front Plant Sci. 2012:**3**:292. https://doi.org/10.3389/fpls.2012.00292

**Silver N, Best S, Jiang J, Thein SL.** Selection of housekeeping genes for gene expression studies in human reticulocytes using real-time PCR. BMC Mol Biol. 2006:**7**(1):33. https://doi.org/10.1186/1471-2199-7-33

**Smirnoff N, Arnaud D.** Hydrogen peroxide metabolism and functions in plants. New Phytol. 2019:**221**(3):1197–1214. https://doi.org/10.1111/nph.15488

**Stocking CR, Larson S.** A chloroplast cytoplasmic shuttle and the reduction of extraplastid NAD. Biochem Biophys Res Commun. 1969:**37**(2):278–282. https://doi.org/10.1016/0006-291X(69)90731-1

**Streatfield SJ, Weber A, Kinsman EA, Hausler RE, Li J, Post-Beittenmiller D, Kaiser WM, Pyke KA, Flugge U-I, Chory J.** The phosphoenolpyruvate/phosphate translocator is required for phenolic metabolism, palisade cell development, and plastid-dependent nuclear gene expression. Plant Cell. 1999:**11**(9):1609–1621. https://doi.org/10.1105/tpc.11.9.1609

**Strenkert D, Schmollinger S, Gallaher SD, Salomé PA, Purvine SO, Nicora CD, Mettler-Altmann T, Soubeyrand E, Weber APM, Lipton MS, et al.** Multiomics resolution of molecular events during a day in the life of Chlamydomonas. Proc Natl Acad Sci USA. 2019:**116**:2374–2383.

**Suzuki N, Koussevitzky S, Mittler R, Miller G.** ROS and redox signalling in the response of plants to abiotic stress. Plant Cell Environ. 2012:**35**(2):259–270. https://doi.org/10.1111/j.1365-3040.2011.02336.x

**Treves H, Küken A, Arrivault S, Ishihara H, Hoppe I, Erban A, Höhne M, Moraes TA, Kopka J, Szymanski J, et al.** Carbon flux through photosynthesis and central carbon metabolism show distinct patterns between algae, C3 and C4 plants. Nat Plants. 2022:**8**(1):78–91. https://doi.org/10.1038/s41477-021-01042-5

**Urzica EI, Vieler A, Hong-Hermesdorf A, Page MD, Casero D, Gallaher SD, Kropat J, Pellegrini M, Benning C, Merchant SS.** Remodeling of membrane lipids in iron-starved Chlamydomonas. J Biol Chem. 2013:**288**(42):30246–30258. https://doi.org/10.1074/jbc.M113.490425

**Vevea JD, Alessi Wolken DM, Swayne TC, White AB, Pon LA.** Ratiometric biosensors that measure mitochondrial redox state and ATP in living yeast cells. J Vis Exp. 2013:(77):50633. https://doi.org/10.3791/50633

**Wakao S, Niyogi KK.** *Chlamydomonas* as a model for reactive oxygen species signaling and thiol redox regulation in the green lineage. Plant Physiol. 2021:**187**(2):687–698. https://doi.org/10.1093/plphys/kiab355

**Walters RG, Ibrahim DG, Horton P, Kruger NJ.** A mutant of Arabidopsis lacking the triose-phosphate/phosphate translocator reveals metabolic regulation of starch breakdown in the light. Plant Physiol. 2004:**135**(2):891–906. https://doi.org/10.1104/pp.104.040469

**Weber APM, Linka M, Bhattacharya D.** Single, ancient origin of a plastid metabolite translocator family in Plantae from an endomembrane-derived ancestor. Eukaryot Cell. 2006:**5**(3):609–612. https://doi.org/10.1128/EC.5.3.609-612.2006

**Weise SE, Liu T, Childs KL, Preiser AL, Katulski HM, Perrin-Porzondek C, Sharkey TD.** Transcriptional regulation of the glucose-6-phosphate/phosphate translocator 2 is related to carbon exchange across the chloroplast envelope. Front Plant Sci. 2019:**10**:827. https://doi.org/10.3389/fpls.2019.00827

**Winder CL, Dunn WB, Schuler S, Broadhurst D, Jarvis R, Stephens GM, Goodacre R.** Global metabolic profiling of Escherichia coli cultures: an evaluation of methods for quenching and extraction of intracellular metabolites. Anal Chem. 2008:**80**:2939–2948.

**Young JD, Shastri AA, Stephanopoulos G, Morgan JA.** Mapping photoautotrophic metabolism with isotopically nonstationary $^{(13)}C$ flux analysis. Metab Eng. 2011:**13**(6):656–665. https://doi.org/10.1016/j.ymben.2011.08.002

**Yu ET, Zendejas FJ, Lane PD, Gaucher S, Simmons BA, Lane TW.** Triacylglycerol accumulation and profiling in the model diatoms *Thalassiosira pseudonana* and *Phaeodactylum tricornutum* (Baccilariophyceae) during starvation. J Appl Phycol. 2009:**21**(6):669–681. https://doi.org/10.1007/s10811-008-9400-y

**Zhao Y, Luo L, Xu J, Xin P, Guo H, Wu J, Bai L, Wang G, Chu J, Zuo J, et al.** Malate transported from chloroplast to mitochondrion triggers production of ROS and PCD in *Arabidopsis thaliana*. Cell Res. 2018:**28**(4):448–461. https://doi.org/10.1038/s41422-018-0024-8

**Zhao Y, Yu H, Zhou J-M, Smith SM, Li J.** Malate circulation: linking chloroplast metabolism to mitochondrial ROS. Trends Plant Sci. 2020:**25**(5):446–454. https://doi.org/10.1016/j.tplants.2020.01.010

**Zirngibl M-E, Araguirang GE, Kitashova A, Jahnke K, Rolka T, Kühn C, Nägele T, Richter AS.** Triose phosphate export from chloroplasts and cellular sugar content regulate anthocyanin biosynthesis during high light acclimation. Plant Commun. 2023:**4**(1):100423. https://doi.org/10.1016/j.xplc.2022.100423

**Zones JM, Blaby IK, Merchant SS, Umen JG.** High-resolution profiling of a synchronized diurnal transcriptome from *Chlamydomonas reinhardtii* reveals continuous cell and metabolic differentiation. Plant Cell. 2015:**27**(10):2743–2769. https://doi.org/10.1105/tpc.15.00498

# Manuscript IV

## Analysis of Photorespiratory Intermediates Under Transient Conditions by Mass Spectrometry

**Status**: published

**Author contributions**: AP, PW, and NL contributed equally with writing

# Chapter 15

## Analysis of Photorespiratory Intermediates Under Transient Conditions by Mass Spectrometry

**Anastasija Plett, Philipp Westhoff, and Nicole Linka**


### Abstract

Photorespiration is an essential process of phototropic organisms caused by the limited ability of rubisco to distinguish between $CO_2$ and $O_2$. To understand the metabolic flux through the photorespiratory pathway, we combined a mass spectrometry-based approach with a shift experiment from elevated $CO_2$ (3000 ppm) to ambient $CO_2$ (390 ppm). Here, we describe a protocol for quantifying photorespiratory intermediates, starting from plant cultivation through extraction and evaluation.


**Key words** Photorespiration, Mass Spectrometry, Gas chromatography

## 1 Introduction

The dual function of rubisco as a carboxylase as well as oxygenase leads to the production of 3-phosphoglycerate (3-PGA) as well as 2-phosphoglycolate (2-PG). While 3-PGA is further processed in the Calvin Benson Bassham cycle, 2-PG must be detoxified by the photorespiratory cycle. Changing (high-to-ambient) $CO_2$ transitions can induce photorespiration [1–3]. Therefore, those conditions can help to characterize plant mutants that are involved in photorespiration but lack a pronounced visible phenotype.

Gas chromatography coupled with mass spectrometry (GC-MS) is a reliable method for measuring most intermediates in the photorespiratory cycle. This analytical system is robust and versatile, and relatively easy to maintain compared to liquid chromatography systems. In addition, electron impact (EI) ionization results in target-specific molecular fragmentation patterns that allow or unambiguous identification of compounds, even with

Anastasija Plett and Philipp Westhoff contributed equally with all other contributors.

Berkley J. Walker (ed.), *Photorespiration: Methods and Protocols*, Methods in Molecular Biology, vol. 2792,
https://doi.org/10.1007/978-1-0716-3802-6_15,

"simple" MS systems such as single quadrupoles. In this chapter, we outline an experimental pipeline for GC-MS-based metabolic profiling focused on photorespiratory intermediates.

## 2 Materials

### 2.1 Reagents and Solutions

1. Sodium hypochlorite (12% active chlorine).
2. Concentrated HCL (*see* **Note 1**).
3. Ultrapure water ($H_2O$).
4. Solid plant cultivation medium: 2.2 g/L MS salts, 10 mL/L 0.5 M MES/KOH pH 5.7, 8 g/L plant Agar.
5. Liquid nitrogen (*see* **Note 2**).
6. Extraction solution **A**: methanol/chloroform (10: 4.28), MS grade (*see* **Note 3**).
7. Extraction solution **B**: ultrapure water containing 4.46 μM ribitol (CAS-Nr: 488-81-3) & N,N-dimethylphenylalanine (CAS-Nr: 17469-89-5) as internal standards (ISTD; *see* **Note 4**).
8. Methoxylamine hydrochloride (CAS-Nr: 593-56-6).
9. N-Methyl-N-(trimethylsilyl)trifluoroacetamide (MSTFA; CAS-Nr: 24589-78-4).
10. Hexane (for GC ≥98% purity).
11. Ethanol (absolute ≥99.8% purity).
12. Pyridine (for HPLC).

### 2.2 Equipment

1. Reaction tubes: 1.5 mL, 2 mL, safe-lock (*see* **Note 5**).
2. Petri dishes (round, 92 × 16 mm).
3. Surgical tape (breathable).
4. Plant growth chamber.
5. Aluminum foil.
6. Mortar and pestle.
7. Precision balance (±0.1 mg).
8. Vortex.
9. Centrifuge precooled to 4 °C.
10. Freeze dryer.
11. Vacuum centrifuge.
12. Thermomixer.
13. Crimp vial 1.5 mL.
14. Magnetical crimp cap with PTFE seal.
15. Deactivated glass insert (250 μL) with polymer foot.

16. GC-MS-System). The described procedure can be performed with any common GC-MS system (*see* **Note 6**).
17. GC Column: low bleed 5%-phenyl-methylpolysiloxane phase capillary column length: 30 m, inner diameter: 0.25 mm, film thickness 0.25 μm.

## 3 Methods

### 3.1 Plant Cultivation

1. Aliquot seeds into 2 mL reaction tubes and sterilize by surface sterilization with chlorine gas: place the seed rack with open tubes in a desiccator under the fume hood. Place the beaker with 100 mL sodium hypochlorite next to the seed rack. Add 3 mL concentrated HCL into the beaker and close the lid of the desiccator. Sterilize for 1.5–2 h.
2. Streak sterilized seeds onto ½ MS agar plates and seal with surgical tape.
3. Stratify seeds at 4 °C for 2 days.
4. Transfer plates to a plant growth chamber with elevated $CO_2$ concentrations (3000 ppm).
5. After 11 days, shift the seedlings to a plant growth chamber with ambient $CO_2$ concentrations (390 ppm) and incubate for another 3 days.

### 3.2 Harvest and Aliquoting of Plant Material

To prepare for harvesting, remove the surgical tape of all petri dishes at once to save time during harvest. Pre-fold aluminum foil into bags to harvest and store the material. Precool spatulas in liquid nitrogen.

1. Take the plant plates one by one out of the chamber and pour the liquid nitrogen directly (and as fast as possible) onto the petri dish and wait a few seconds until everything is frozen, including the plant cultivation medium. Scratch down the shoot tissue with a precooled spatula into the precooled aluminum bag and place the closed bag into liquid nitrogen (*see* **Note 7**).
2. Place the frozen material in a mortar and crush with pestle under liquid nitrogen. Transfer the fine powder into 2 mL safe-lock reaction tubes.
3. Weigh 20–25 mg of the fine powder and place it in a new 2 mL safe-lock reaction tube for analysis. Note the exact weight (*see* **Note 8**).

### 3.3 Extraction

The extraction was performed according to Arrivault et al. [4] with minor modifications. The harvested material should be kept frozen (in liquid nitrogen) to avoid sample degradation. Before extraction,

precool all equipment (spatulas, reaction tubes) in liquid nitrogen, the extraction solution at −20 °C, and the $H_2O$ on ice.

1. Place the 2 mL reaction tubes containing the sample upright in liquid nitrogen (*see* **Note 9**).
2. Add 350 µL of extraction solution **A** to every sample.
3. Take the samples out and vortex thoroughly.
4. Incubate at −20 °C for 1 h with occasional shaking (*see* **Note 10**).
5. Add 560 µL extraction solution **B.**
6. Vortex and incubate on ice for 10 min.
7. Spin down at 4 °C for 4 min at 20.000 × *g*.
8. Collect the (upper) aqueous phase in a new 2 mL reaction tube and store it on ice.
9. Add 560 µL $H_2O$ to the previous tube and vortex.
10. Spin down at 4 °C for 4 min at 20.000 × *g*.
11. Collect the upper phase and combine it with the previous aqueous phase (**step 8**).
12. Fill the vial up to 1700 µL with $H_2O$ (*see* **Note 11**).
13. Dry the sample by lyophilization overnight.
14. Reconstitute the sample in 500 µL ice-cold $H_2O$.
15. Transfer an aliquot of 10–50 µL into a glass inlet and add the same amount of methanol. The actual volumes needed might be partially system and experiment dependent and should be evaluated using a pooled sample (QC) (*see* **Note 12**). A proper sample amount allows to detect low abundant compounds such as glycolate but does not overload the column or the MS detector with high abundant signals such as glycine.
16. Dry the sample by vacuum centrifugation (approx. 4 h at 1.5 mbar or overnight)
17. The dried samples can be stored short-term at −20 °C and long-term (up to 6 months) at −80 °C.

### 3.4 Measurement and Evaluation

For the steps prior to injection, we recommend using a multifunctional dual-head autosampler for automated online derivatization (*see* **Note 6**). Such systems allow a time-optimized procedure, which is ideal for high-throughput measurements due to the nested sample processing together with an automatic liner exchange system. The liner should be changed every 15–20 samples, and after each change, blank samples (empty inlet derivatization) should be measured to evaluate background. In addition, a quality control (QC) sample should be measured at the beginning and end of each batch to verify system performance (*see* **Note 12**). To evaluate matrix background or matrix effects, we recommend running a chemical reference standard once per batch, with all compounds

of interest as a concentration-defined pooled sample (standard mix). We strongly advise randomizing sample batches, especially if samples are processed manually, to avoid possible systematic bias.

1. Place the samples for 30 min in a vacuum centrifuge to remove any residual condensation water (*see* **Note 13**).
2. Freshly prepare 20 mg/mL methoxyamine hydrochloride in pure pyridine (*see* **Note 14**).
3. Add 10 µL methoxyamine hydrochloride to the dried sample and incubate while shaking at 37 °C for 90 min.
4. Add 90 µL MSTFA and incubate while shaking at 37 °C for 30 min.
5. Let the sample rest for 2 h at room temperature (*see* **Note 15**).
6. Inject 1 µL of derivatized sample with a GC-column flow of 1 mL/min helium. Between injections, let the autosampler needle perform wash injections with ethanol first and then hexane into a waste vial to clean the needle and to avoid needle damage (*see* **Notes 16** and **17**).
7. After injection, hold oven temperature constant at 70 °C for 2 min, ramp at 12.5 °C/min to 320 °C, and then hold constant for 5 min, resulting in a total run time of 27 min.
8. Set the MS parameters as follows: Ionize metabolites with an electron impact source at 70 eV Set mass range from 60 *m/z* to m/z 600 at 20 scans per sec.

### 3.5 Data Analysis

1. Evaluate measurements by screening chromatograms for background, ISTD intensity, and peak shape. With the setup described here, chromatograms can be reviewed with MassHunter Qualitative (Agilent Technologies, *see* **Note 18**, Fig. 1).

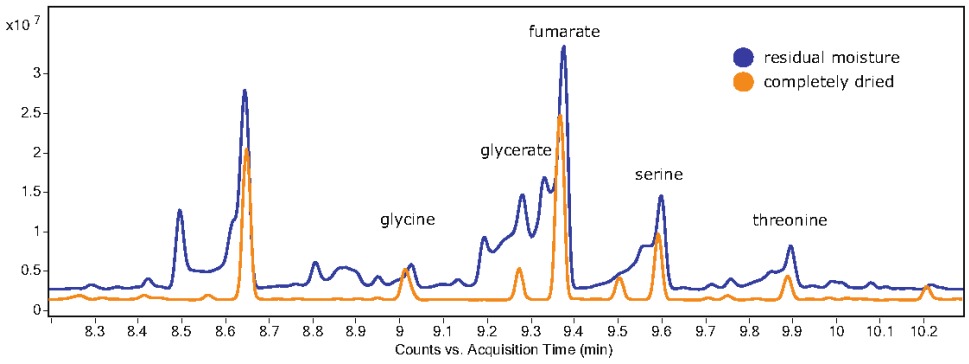


**Fig. 1** Chromatogram of completely dried and partially moisture samples. Completely dried samples (orange) result in distinct peaks, which can be easily annotated. Residual moisture (blue) leads to a higher background, improper peak shapes, and double peaks, eventually leading to ambiguous interpretations

2. Identify metabolites by spectra comparison with the NIST14 Mass Spectral Library and the authentic standard.
3. To set up a data integration method in MassHunter Quantitative (Agilent Technologies), assign a quantifier ion (Q1) and a qualifier ion (Q2) for each metabolite. For the intermediates of the photorespiratory pathway, we recommend to use the following *m/z* pairs: glycolate Q1(177)/Q2 (161); glyoxylate Q1 (160)/Q2 (89); glycine Q1(174)/Q2 (248); serine Q1(204)/Q2 (218); and glycerate Q1(189)/Q2 (292) (*see* **Note 19**).
4. After integration, normalize the areas under the curve to the ISTD signal and to the fresh weight of the sample (*see* **Note 20**).

## 4 Notes

1. Handle under fume hood, this compound is corrosive.
2. Liquid nitrogen can freeze skin tissue, causing cold burns and or permanent eye damage. Wear gloves and safety glasses.
3. Handle under fume hood, this compound is toxic.
4. Internal standards should be carefully selected based on the target analyte and biological sample. They should reflect the physico-chemical behavior of the target metabolites during extraction and measurement but must not be present in the biological sample itself.
5. Do not autoclave, use new.
6. In this protocol, we use the multifunctional dual-head autosampler MPS for scheduled and high throughput sample preparations. However, all steps can also be performed manually in a similar manner.
7. Frozen material can be stored at −80 °C.
8. Homogenized material can be stored at −80 °C.
9. This can be easily done with a permeable reaction tube rack. The liquid nitrogen should not be in direct contact with the powder.
10. When the samples are taken out of the freezer for shaking, place them on ice.
11. The organic content in the polar phase should be less than 15% of the total volume to prevent sample loss during lyophilization. Adjust the amount of water added to the sample accordingly if the extraction volume changes.
12. We highly recommend to create a pooled sample for quality control measurements. To do this, several aliquots from

different samples reflecting all sample groups should be pooled and aliquoted in the same manner as the samples. Two quality control samples are required per GC-MS batch.

13. Derivatization reaction is very sensitive to water. Incomplete derivatization results in bad peak shapes and reduced sensitivity.
14. Weigh 20 mg dry methoxyamine hydrochloride into a 1.5 mL glass vial, add 1 mL of pure (water free) pyridine, and support complete solubilization by heating to 30 °C and shaking for 10 min.
15. The derivatization process continues even at room temperature. To ensure consistency, we recommend scheduled sample processing with an automated derivatization system. This allows each sample to be incubated for exactly the same amount of time. However, this method is impractical for manual sample handling. In such cases, we recommend working with batches of 8–10 samples and extending the resting time at room temperature to 6–8 h before measurement. This will ensure that the derivatization state is approximately the same for all samples, even if the last sample is incubated at room temperature longer than the first measured sample. However, it should be noted that incubation times may vary depending on sample composition and should be tested and optimized accordingly.
16. Here, we use a cold injection system (CIS) with an initial temperature of 50 °C. After injection, the system heats up to 250 °C with a ramp rate of 12 °C/sec. A cold injection system is recommended to standardize the injection process and lead to reproducible retention times. However, a conventional split/splitless injector can also be used. Here, we recommend an injection temperature of 230–250 °C.
17. We use baffled deactivated CIS low-volume liners for cold split injections to create good mixing of sample. For common split/splitless injectors, we recommend deactivated split liners with glass wool.
18. Agilent systems produce "*.D-files*" which are hard to read using open-source software. For that, we recommend generating ".mzXML" or ".CDF" files (e.g. with proteo wizard [5] or metalign [6]).
19. Due to the fixed electron voltage of 70 eV in common GC-MS, the fragmentation pattern is very reproducible. The ratio of Q1/Q2 can therefore be used to identify underlying masses that might interfere with accurate analysis.
20. MS response for different targets may be different for the same concentration. Therefore, the resulting relative concentrations should not be compared between different metabolites.

## References


1. Timm S et al (2012) High-to-low CO 2 acclimation reveals plasticity of the photorespiratory pathway and indicates regulatory links to cellular metabolism of Arabidopsis. PLoS One 7:e42809
2. Eisenhut M et al (2017) Photorespiration is crucial for dynamic response of photosynthetic metabolism and stomatal movement to altered CO2 availability. Mol Plant 10:47 61
3. Roell M-S et al (2021) A synthetic C4 shuttle via the β -hydroxyaspartate cycle in C3 plants:1 9. https://doi.org/10.1073/pnas.2022307118
4. Arrivault S et al (2009) Use of reverse-phase liquid chromatography, linked to tandem mass spectrometry, to profile the Calvin cycle and other metabolic intermediates in Arabidopsis rosettes at different carbon dioxide concentrations. Plant J 59:826 839
5. Chambers MC et al (2012) A cross-platform toolkit for mass spectrometry and proteomics. Nat Biotechnol 30:918 920
6. Lommen A, Kools HJ (2012) MetAlign 3.0: performance enhancement by efficient use of advances in computer hardware. Metabolomics 8:719 726

# Published Articles

## A synthetic C4 shuttle via the β-hydroxyaspartate cycle in C3 plants

SEE CORRECTION FOR THIS ARTICLE

# A synthetic C4 shuttle via the β-hydroxyaspartate cycle in C3 plants

Marc-Sven Roell[a], Lennart Schada von Borzyskowski[b,1], Philipp Westhoff[a,c], Anastasija Plett[a,c], Nicole Paczia[b], Peter Claus[b], Urte Schlueter[a], Tobias J. Erb[b,d], and Andreas P.M. Weber[a,c,2]

[a]Institute of Plant Biochemistry, Heinrich Heine University, 40225 Düsseldorf, Germany; [b]Department of Biochemistry and Synthetic Metabolism, Max Planck Institute for Terrestrial Microbiology, 35043 Marburg, Germany; [c]Cluster of Excellence on Plant Science, Heinrich Heine University, 40225 Düsseldorf, Germany; and [d]LOEWE Center for Synthetic Microbiology, Philipps-University Marburg, 35043 Marburg, Germany

Edited by Donald R. Ort, University of Illinois at Urbana–Champaign, Urbana, IL, and approved April 7, 2021 (received for review November 2, 2020)

**Plants depend on the enzyme ribulose-1,5-bisphosphate carboxylase/oxygenase (Rubisco) for $CO_2$ fixation. However, especially in C3 plants, photosynthetic yield is reduced by formation of 2-phosphoglycolate, a toxic oxygenation product of Rubisco, which needs to be recycled in a high-flux–demanding metabolic process called photorespiration. Canonical photorespiration dissipates energy and causes carbon and nitrogen losses. Reducing photorespiration through carbon-concentrating mechanisms, such as C4 photosynthesis, or bypassing photorespiration through metabolic engineering is expected to improve plant growth and yield. The β-hydroxyaspartate cycle (BHAC) is a recently described microbial pathway that converts glyoxylate, a metabolite of plant photorespiration, into oxaloacetate in a highly efficient carbon-, nitrogen-, and energy-conserving manner. Here, we engineered a functional BHAC in plant peroxisomes to create a photorespiratory bypass that is independent of 3-phosphoglycerate regeneration or decarboxylation of photorespiratory precursors. While efficient oxaloacetate conversion in *Arabidopsis thaliana* still masks the full potential of the BHAC, nitrogen conservation and accumulation of signature C4 metabolites demonstrate the proof of principle, opening the door to engineering a photorespiration-dependent synthetic carbon–concentrating mechanism in C3 plants.**

photosynthesis | photorespiration | synthetic biology | crop improvement | C4

Future agriculture must reconcile sustainability with increased productivity to supply global food demands that will have doubled by 2050 (1, 2). To fulfill this goal, agricultural yields will have to increase annually by 2.4%. However, yields currently plateau at a 1% annual increase in major food crops [i.e., maize, rice, and wheat (3, 4)]. In high-yielding crop varieties, both plant architecture and the harvest index—the fraction of total energy in plant biomass contained in the harvestable organs—approach their theoretical limits (5).

Synthetic biology–based approaches are focusing on improving the carbon conversion efficiency of plants that currently only reaches 20% of its theoretical potential (5, 6). Synthetic biology applies engineering principles to biological systems and multiple synthetic biological solutions to improve the carbon conversion efficiency of plants were recently proposed (6, 7). These include pathways for improved $CO_2$ fixation (Rubisco based and Rubisco independent), such as the crotonyl-coenzyme A (CoA)/ethylmalonyl-CoA/hydroxybutyryl-CoA cycle (8, 9), photorespiratory bypasses, including the Tartonyl-CoA (TaCo) pathway and a modified 3-hydroxypropionate bicycle (10), as well as synthetic carbon–concentrating mechanisms. Altogether, these proposed solutions showcase the potential of plant synthetic biology to increase productivity and sustainability of future agriculture beyond the realms of natural evolution (7, 11, 12).

Natural carbon-concentrating mechanisms boost carbon fixation by concentrating $CO_2$ at the site of Rubisco and have independently evolved in cyanobacteria [carboxysomes (13)], green algae [pyrenoids (14)], and plants [C4 photosynthesis, single-cell C4 photosynthesis, and crassulacean acid metabolism (7)]. In C4 photosynthesis, primary $CO_2$ fixation is spatially separated from Rubisco. First, $CO_2$ is captured into a C4 acid via phosphoenolpyruvate carboxylase (PEPC) in mesophyll cells, and this C4 acid is then decarboxylated in bundle sheath cells, where Rubisco is located. The increase in the local $CO_2$ concentration reduces the oxygenation reaction of Rubisco as well as the subsequent process of photorespiration (15). Consequently, implementation of C4 photosynthesis into C3 plants has received much attention to increase yield in crop plants that experience photorespiration (16, 17).

Another target to improve plant growth is photorespiration itself. During natural photorespiration, the Rubisco oxygenation product 2-phosphoglycolate is recycled back into 3-phosphoglycerate. However, natural photorespiration comes with the loss of up to 30% of previously fixed carbon (18), release of nitrogen, and the dissipation of energy (19), which has led to the engineering of photorespiratory bypasses to mitigate the deleterious effects of photorespiration. In particular, glycolate, formed by dephosphorylation of 2-phosphoglycolate, has been considered an ideal starting

### Significance

Photorespiration is essential for photosynthesis in an oxygen-containing atmosphere. By mass flow, photorespiration is exceeded only by photosynthetic carbon assimilation. Photorespiration, initiated by the oxygenation reaction of Rubisco, is a major constraint on the photosynthetic efficiency of C3 plants and consequently on crop yield. Mitigating the negative effects of photorespiration holds potential for yield increases and contributes to achieving food and energy security for a growing population. This work presents a synthetic bypass to natural photorespiration (i.e., the conversion of photorespiratory glycolate into a C4 compound via a recently discovered microbial glycolate assimilation pathway, the β-hydroxyaspartate cycle [BHAC]). Simultaneous expression of four enzymes of microbial origin in the land plant model *Arabidopsis thaliana* enables efficient glycolate conversion into BHAC products.

Author contributions: M.-S.R., L.S.v.B., P.W., A.P., T.J.E., and A.P.M.W. designed research; M.-S.R., L.S.v.B., P.W., A.P., N.P., P.C., and U.S. performed research; M.-S.R., L.S.v.B., P.W., A.P., U.S., T.J.E., and A.P.M.W. analyzed data; and M.-S.R., L.S.v.B., P.W., A.P., T.J.E., and A.P.M.W. wrote the manuscript.

Competing interest statement: The Heinrich Heine University and the Max-Planck-Gesellschaft zur Förderung der Wissenschaften are the patent applicants for European patent application no. EP 19190404.4, which includes a method for the production of plants with altered photorespiration and improved CO2 fixation due to the BHAC.

This article is a PNAS Direct Submission.



[1]Present address: Institute of Biology Leiden, Leiden University, Leiden, 2333 BE, The Netherlands.

[2]To whom correspondence may be addressed. Email: andreas.weber@hhu.de.

This article contains supporting information online at https://www.pnas.org/lookup/suppl/doi:10.1073/pnas.2022307118/-/DCSupplemental.

Published May 17, 2021.

metabolite for several photorespiratory bypasses (7, 20). Photorespiratory bypasses that recycle glycolate into 3-phosphoglycerate by the cyanobacterial "glycerate pathway" or oxidize glycolate in the chloroplast have already shown growth benefits in greenhouse-grown *Arabidopsis thaliana* (21, 22) and tobacco and rice in field experiments (23, 24). However, all of these bypasses still release $CO_2$, which limits their efficiency compared to natural photorespiration.

Recently, the β-hydroxyaspartate cycle (BHAC) was described as primary pathway of glycolate assimilation in marine proteobacteria (25). In this pathway, glycolate is first oxidized into glyoxylate, which is further converted into oxaloacetate (OAA) in four enzymatic steps, the core of the BHAC (Fig. 1). Notably, the BHAC enables the direct formation of a C4 compound from glycolate, without the loss of carbon and nitrogen, which renders the BHAC more efficient than natural photorespiration and all other photorespiration bypasses engineered in vivo so far.

Here, we demonstrate the implementation of the BHAC in *A. thaliana* (*Arabidopsis*) peroxisomes. We validate activity of the BHAC in planta by demonstrating β-hydroxyaspartate (BHA) formation under photorespiratory conditions. Furthermore, we show improved nitrogen conservation through the BHAC, which results in reduced free ammonia levels compared to natural photorespiration. We also determine the metabolic fate of BHAC-derived OAA and outline a strategy to use BHAC-derived OAA to establish a synthetic C4 cycle in C3 plants. Altogether, our proof-of-principle study demonstrates an approach to turn a photorespiratory bypass into a carbon concentrating mechanism by synergistically coupling photorespiration and C4 metabolism. By engineering two of the main targets in primary plant metabolism, this study creates opportunities for improved agricultural productivity in the future.

## Results

**BHAC Implementation in Plant Peroxisomes.** Photorespiratory glycolate is converted to glyoxylate in peroxisomes. Since glyoxylate is the starting substrate of the BHAC, we implemented the BHAC in the peroxisomal matrix. The four BHAC enzymes, aspartate:glyoxylate aminotransferase (AGAT, Enzyme Commission [EC]: 2.6.1.35), β-hydroxyaspartate aldolase (BHAA, EC: 4.1.3.41), β-hydroxyaspartate dehydratase (BHAD, EC: 4.3.1.20), and iminosuccinate reductase (ISR), were targeted to plant peroxisomes by fusion of a peroxisomal target signal (PTS). AGAT, BHAD, and ISR were C terminally fused with PTS1 (26). BHAA was fused N terminally with the PTS2 from *Arabidopsis* citrate synthase 3 [At2g42790 (26)]. Peroxisomal localization of the four BHAC enzymes was confirmed by fluorescence colocalization with a peroxisomal marker in *Nicotiana benthamiana* protoplasts and extrapolated for BHAC implementation in *Arabidopsis* (Fig. 2*A*).

We selected four *Arabidopsis* photosynthetic promoters [Rubisco small subunit 1B, 2B, 3B (27), and chlorophyll A/B–binding protein 1 (28)] to restrict BHAC enzyme expression to photosynthetic tissue (*SI Appendix*, Fig. S1). Furthermore, we hypothesized that reduced conversion of glyoxylate to glycine would enhance metabolic flux through the BHAC. Besides *Arabidopsis* wild-type *Col-0* (WT), we therefore selected the photorespiratory *ggt1-1* mutant as background for BHAC implementation. The *ggt1-1* mutant is deficient in the peroxisomal glutamate glyoxylate aminotransferase 1 (29) and shows a strong photorespiratory phenotype, which allowed us to screen for the function of the BHAC via a convenient visual readout.

In total, 14 and 11 primary transformants that harbor the complete transfer DNA insertion were identified in the WT and *ggt1-1* background, respectively. Out of these two independent lines, each were established in the WT (*Col::BHAC #1* and *#2*) and *ggt1-1* background, respectively (*ggt1-1::BHAC #1* and *#2*, *SI Appendix*, Fig. S1), based on immunoblot analysis to verify expression of all four BHAC enzymes in the transgenic lines (*SI Appendix*, Fig. S1). We quantified activity of each BHAC enzyme in mature rosette leaf extracts of 4-wk-old air-grown plants by enzyme activity assays (Fig. 2*B*). AGAT was highest in both WT and *ggt1-1* backgrounds compared to BHAA and BHAD activity (Fig. 2*B*). Iminosuccinate is a labile product formed by BHAD (25). To demonstrate functional expression of ISR, we therefore quantified the rate of $^{15}N$ incorporation into L-aspartate, which confirmed ISR activity in BHAC plants (Fig. 2*B*). In summary, these experiments confirmed the successful expression of all enzymes in planta.

**Peroxisomal BHAC Functions as Photorespiratory Bypass.** Next, we verified that the peroxisomal BHAC functions as photorespiratory bypass by steady-state metabolomics on green tissue of 14-d-old seedlings either grown in $CO_2$-enriched air (3,000 ppm $CO_2$, high carbon, HC), ambient air (400 ppm $CO_2$, ambient carbon, AC), or shifted from $CO_2$-enriched to ambient air 3 d before sampling (Shift, Fig. 3). Our metabolomics analysis included the BHAC

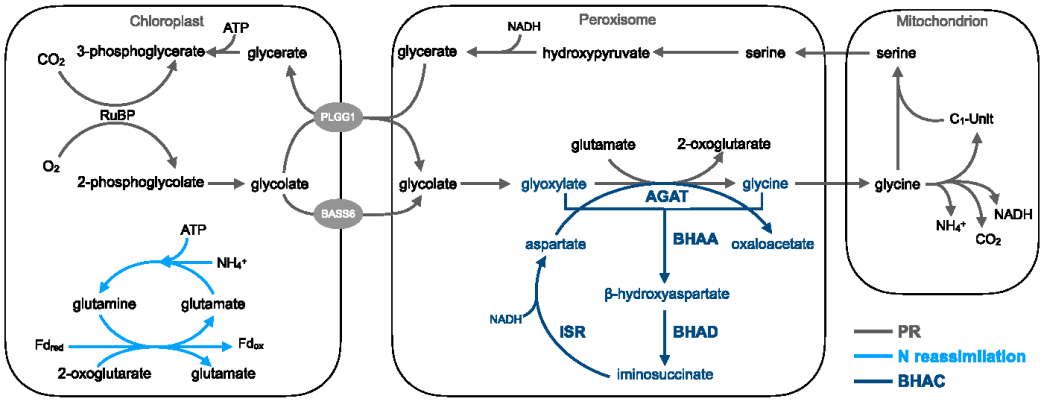


**Fig. 1.** The BHAC as photorespiratory bypass in plant peroxisomes. A schematic representation of plant photorespiration (PR) and photorespiratory nitrogen (N) reassimilation (light blue) and the BHAC (dark blue) AGAT, BHAA, BHAD, ISR, GGT1, ribulose-1,5-bisphosphate (RuBP), plastidial glycolate/glycerate transporter 1 (PLGG1), and bile acid sodium symporter 6 (BASS6).

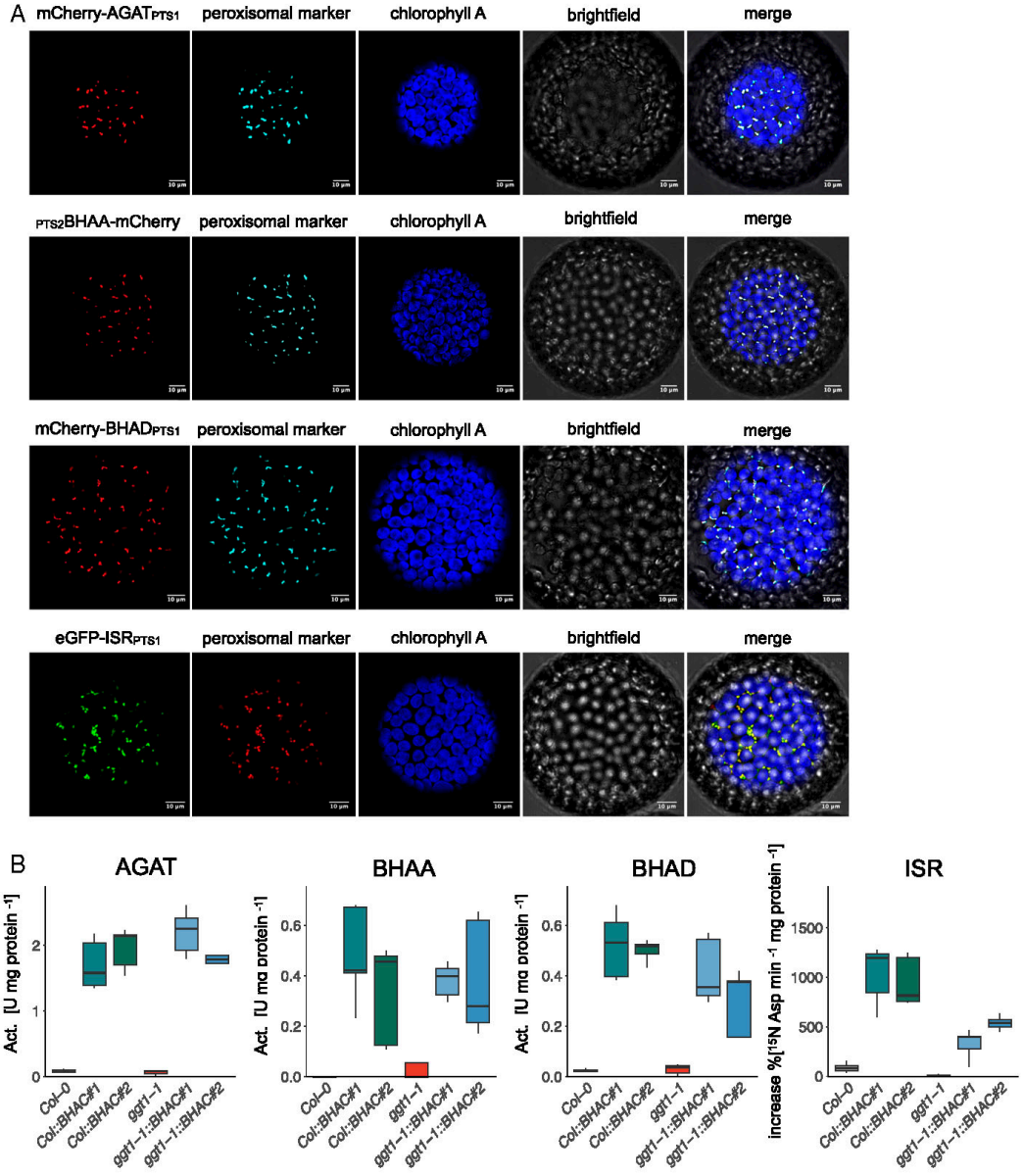


**Fig. 2.** Peroxisomal targeting and enzyme activity of the BHAC. (*A*) Fluorescent fusion constructs for each BHAC enzyme were coinfiltrated with a peroxisomal marker in *N. benthamiana* leaves, and protoplasts were analyzed by confocal microscopy 2 d postinfection. Both the peroxisomal targeting sequence (subscripted) and the fluorescent fusion protein are indicated based on the protein N- or C-terminal position. AGAT, BHAA, BHAD, and ISR. Blue: chlorophyll A autofluorescence, Peroxisomal marker: cyan fluorescent protein or mCherry (only for ISR) with C-terminal PTS1 (Scale bar,10 μm). (*B*) BHAC enzyme activity in *Arabidopsis* mature rosette leave extracts of 4-wk-old air-grown plants. For the ISR assay, the percentual $^{15}N$ label enrichment into aspartate was quantified over time. $n = 3$.

intermediates BHA and glycine; malate, produced by reduction of BHAC-derived OAA by peroxisomal NAD–dependent MDH (30), as well as aspartate, which can be regarded both as BHAC intermediate and product of OAA transamination (Fig. 3).

BHA is a unique metabolite of the BHAC and not naturally present in *Arabidopsis* (Fig. 3 *A* and *B*). We analyzed analytical standards of BHA diastereomers via gas chromatography–time-of-flight mass spectrometry (GC/MS Q-TOF) to annotate BHA according to the electron impact mass spectral fragmentation pattern (*SI Appendix*, Fig. S2). As expected, BHA-specific fragments were neither detected in WT nor in *ggt1-1* controls under all conditions tested. In contrast, BHA could be detected in plants carrying the BHAC (*SI Appendix*, Fig. S3). However, relative quantification revealed that BHA was only detectable when plants were grown in ambient air or shifted from $CO_2$-enriched to ambient air but not in $CO_2$-enriched air (Fig. 3 *A* and *B*). This confirmed function of the BHAC in planta and suggested that BHA formation is exclusively linked to photorespiratory conditions.

Glycine levels decreased twofold in both *Col::BHAC* lines, which is consistent with glycine conversion into BHA by BHAA under photorespiratory conditions in ambient air (Fig. 3*C*). In the *ggt1-1* mutant total glycine levels were 10-fold lower compared to WT (29) and remained unaltered in *ggt1-1::BHAC* plants (Fig. 3*C*) despite partial restoration of peroxisomal glyoxylate to glycine conversion through a promiscuous aminotransferase activity of AGAT in the *ggt1-1* mutant (Fig. 3*C*). In line with BHAC activity, aspartate and malate levels were elevated sixfold and twofold, respectively, in ambient air–grown BHAC plants of both background genotypes compared to WT (Fig. 3*C*). Together, the formation and accumulation of BHAC-specific metabolites exclusively in photorespiratory conditions demonstrated that the peroxisomal BHAC indeed functions as photorespiratory bypass.

**The BHAC Reshapes Carbon and Nitrogen Metabolism.** To better understand the metabolic implications of the BHAC, we generated metabolite profiles for all four BHAC lines (BHAC plants) and their background genotypes at different $CO_2$ concentrations (HC, AC, and Shift; *SI Appendix*, Fig. S4). Growth condition–dependent principal component analysis revealed that the metabolic profiles of BHAC plants are clearly distinct from their background genotypes (Fig. 4*A*) and that all BHAC plants cluster together, independent of their genetic background under photorespiratory conditions (AC or Shift; Fig. 4*A*). Notably, we did not observe such clustering of genotypes under HC (Fig. 4*A*), which is consistent with the observation that the BHAC is only active under photorespiration.

We further focused on the metabolite profile of BHAC plants in comparison to the WT and *ggt1-1* mutant backgrounds grown under photorespiratory conditions in ambient air (Fig. 4*B*). In plant photorespiration mitochondrial glycine decarboxylase is the major hub of carbon and nitrogen losses (19, 31). Nitrogen conservation by the BHAC is assumed to prevent mitochondrial ammonia release and avoid chloroplastic nitrogen reassimilation by glutamine synthase. Consequently, cellular free ammonia levels were reduced on average by 20% in ambient air–grown BHAC plants compared to WT under photorespiratory conditions (Fig. 4*C*). Furthermore, ambient air–grown BHAC plants accumulated soluble amino acids that are either involved in the urea cycle (glutamate and ornithine) or depend on OAA-derived carbon skeletons (lysine and methionine; Fig. 4*B*).

Besides peroxisomal reduction to malate, three further routes of OAA assimilation are theoretically possible that are all coupled to the direct export of OAA from the peroxisome (32). Cytosolic phosphoenolpyruvate carboxykinase 1 (PCK1) could decarboxylate OAA to phosphoenolpyruvate [PEP (33)]. PEP is then used either for gluconeogenesis or converted into pyruvate by pyruvate kinase [PK (34)]. The accumulation of pyruvate strongly indicated that the cytosolic PK route is active in BHAC plants and that PEP is not channeled into gluconeogenesis, which was supported by reduced glucose and fructose levels in the same plants (Fig. 4*B*). In addition to cytosolic decarboxylation, OAA could also be transported into mitochondria, where it could fuel the mitochondrial tricarboxylic acid (TCA) cycle. Accumulation of citrate in ambient air–grown BHAC plants suggested that this route was also active, eventually in combination with an increased flux of pyruvate into the TCA cycle (Fig. 4*B*).

To further validate that reshaping of the metabolome in BHAC plants is caused by an active BHAC and not AGAT alone, we complemented the *ggt1-1* mutant with AGAT under control of the chlorophyll A/B–binding protein 1 promoter, which was also used for AGAT expression in *ggt1-1:BHAC* plants (*SI Appendix*, Fig. S5). Steady-state metabolomics on plants grown under photorespiratory conditions in ambient air revealed that AGAT expression was not sufficient to cause the distinct metabolome signature of BHAC plants. Instead, AGAT expression only restored canonical photorespiration, probably by utilizing aspartate as amino donor for the peroxisomal transamination reaction (*SI Appendix*, Fig. S5).

In summary, these experiments showed that the BHAC is active under photorespiratory conditions and reshapes the metabolome in plants by altering nitrogen metabolism (amino acid accumulation and free ammonia reduction) and OAA utilization in the cytosol and/or mitochondrial TCA cycle.

**The BHAC Reduces Plant Growth by Impaired Photosynthesis in the WT Background.** Despite carbon and nitrogen conservation by the BHAC, *Col::BHAC* plants are reduced in growth compared to WT controls in ambient air (Fig. 5*A* and *SI Appendix*, Fig. S6). Rosettes of 4-wk-old air-grown *Col::BHAC* plants are decreased by 70% in area and 50% in diameter (*SI Appendix*, Fig. S7). However, BHAC implementation in the *ggt1-1* mutant partially suppressed the photorespiratory phenotype of the mutant (Fig. 5*A*) and growth was comparable to *Col::BHAC* plants (*SI Appendix*, Fig. S7). In $CO_2$-enriched air, growth of BHAC plants was not altered compared to the background genotype (Fig. 5*A* and *SI Appendix*, Fig. S7).

In order to test the hypothesis that reduced plant growth is caused by suppressed photorespiratory 3-phosphoglycerate regeneration in BHAC plants, we analyzed steady-state levels of phosphorylated intermediates in green tissue of 14-d-old air-grown plants (Fig. 5*B* and *SI Appendix*, Fig. S8). Whereas 2-phosphoglycolate levels were not significantly altered between all genotypes, the 3-phosphoglycerate levels were reduced in BHAC plants compared to WT and notably very similar to the *ggt1-1* mutant, impaired in photorespiratory 3-phosphoglycerate regeneration (Fig. 5*B*). In addition, in BHAC plants, 3-phosphoglycerate levels were similar to the *ggt1-1* mutant, impaired in photorespiratory 3-phosphoglycerate regeneration (Fig. 5*B*). Furthermore, sedoheptulose-7-phosphate, an intermediate of the Calvin-Benson-Bassham cycle (CBBC), showed reduced levels in BHAC plants, whereas ribose/ribulose-5-phosphate levels were not altered (Fig. 5*B*). We directly assessed the photosynthetic capacity of BHAC plants and generated A/$C_i$ curves, the rate of $CO_2$ assimilation (A) in relation to intercellular $CO_2$ concentration ($C_i$) under saturating light (1,000 $\mu mol \cdot s^{-1} \cdot m_2^{-2}$), by leaf gas exchange measurements of 6-wk-old ambient air–grown plants (*SI Appendix*, Fig. S9). Based on the A/$C_i$ curve, we determined the $CO_2$ compensation point (CCP), a net quotient of zero for photosynthetic $CO_2$ assimilation and respiratory $CO_2$ release (35). *Col::BHAC* plants displayed an increased CCP compared to WT (Table 1). The *ggt1-1* mutant itself has a higher CCP, and the BHAC did not significantly alter the CCP in this photorespiratory mutant (Table 1). In addition, the maximal assimilation rate at saturated $CO_2$ ($A_{max}$) and the initial slope as in vivo measure of the carboxylation efficiency were inferred from the A/$C_i$ curves (36). Compared to WT, both $A_{max}$ and initial slope were reduced

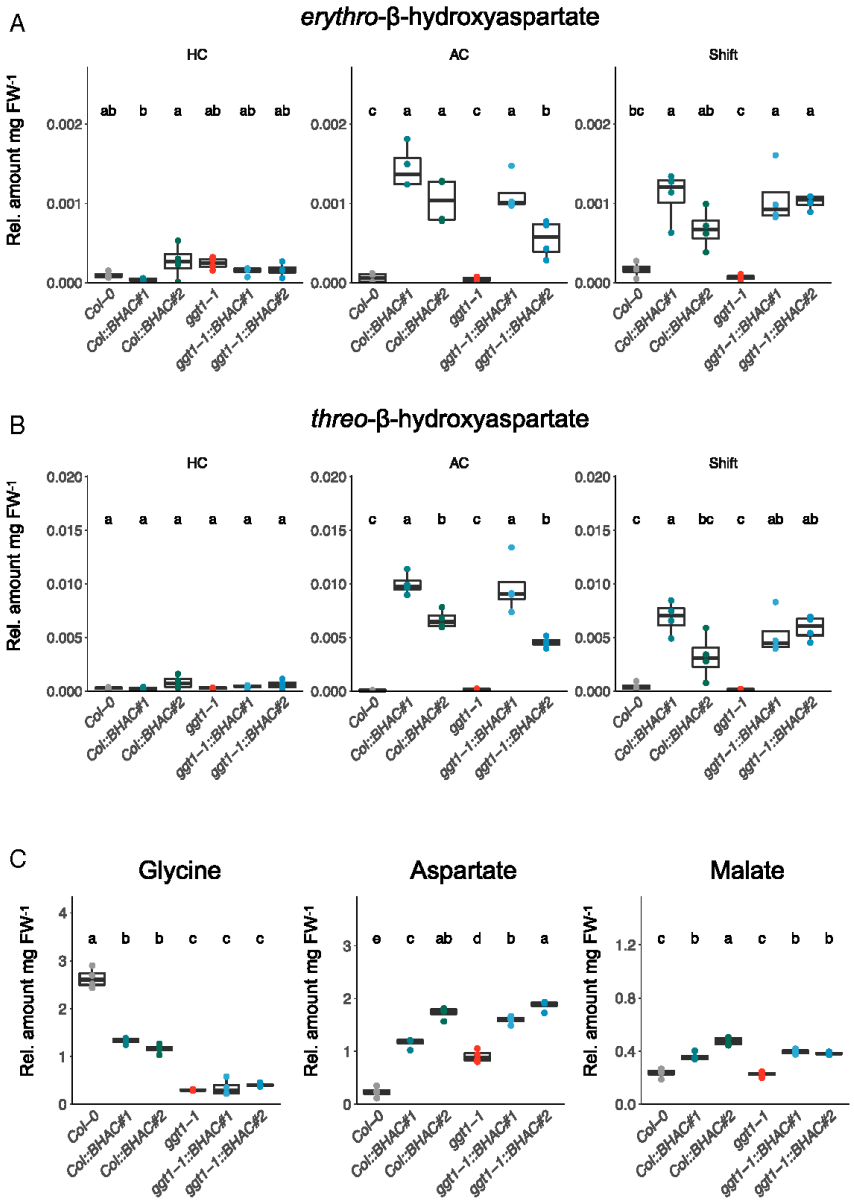


**Fig. 3.** The BHAC functions as photorespiratory bypass. (*A* and *B*) Relative metabolite levels per mg fresh weight (FW) of in vivo *erythro*-β-hydroxyaspartate (*A*) and *threo*-β-hydroxyaspartate (*B*) formation in BHAC plants. Green tissue of 14-d-old seedlings was harvested in the middle of the light phase. The plants were grown either in $CO_2$-enriched air (3,000 ppm $CO_2$, HC), ambient air (400 ppm $CO_2$, AC), or shifted from HC to AC 3 d prior to harvest (Shift). (*C*) Relative metabolite levels per mg FW of glycine, aspartate, and malate in BHAC plants grown in ambient air. Each box–whisker plot represents the 25th and 75th percentiles and whiskers the 10th and 90th percentile. The median is indicated as a crossbar. One-way ANOVA with a post hoc Tukey honest significant difference test was used for statistical analysis. The different letters indicate significant differences between genotypes at $P < 0.05$. $n = 4$.

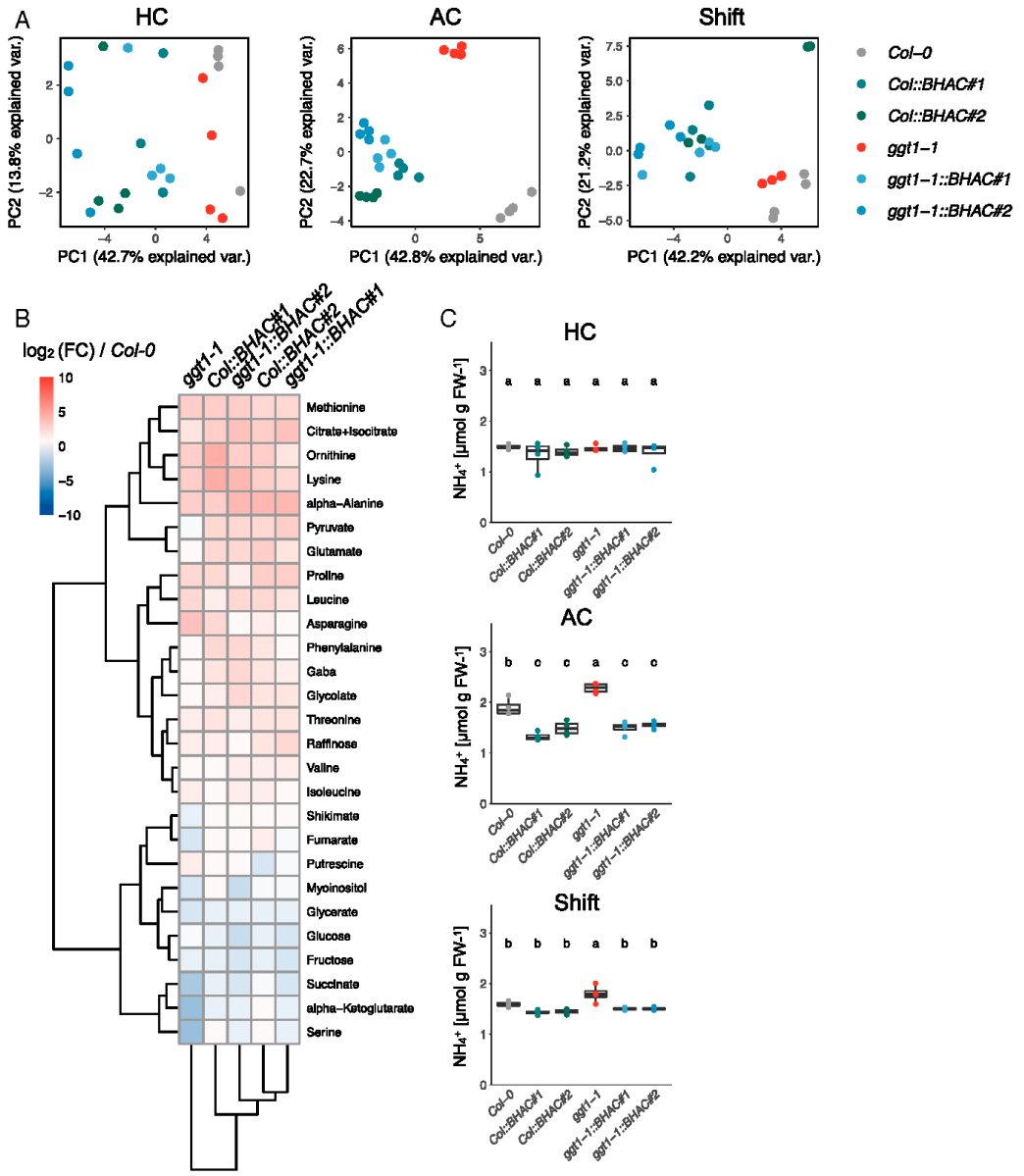


**Fig. 4.** The BHAC reshapes the plant metabolome. Metabolite profiles were generated using green tissue of 14-d-old seedlings grown either at 3,000 (HC), 400 (AC), or shifted from 3,000 to 400 ppm $CO_2$ 3 d (Shift) prior to harvest at the middle of the light phase. (*A*) Principal component analysis of the metabolome profiles. (*B*) Metabolome profiles of AC grown plants. The log2 fold change (FC) was calculated compared to wild-type *Col-0* and clustered based on Pearson correlation. (*C*) Quantification of free ammonium in BHAC plants. Each box-whisker plot represents the 25th and 75th percentiles and whiskers the 10th and 90th percentile. The median is indicated as a crossbar. One-way ANOVA with a post hoc Tukey honest significant difference test was used for statistical analysis. The different letters indicate significant differences between genotypes at $P < 0.05$. $n = 4$ biological replicates measured in technical triplicates.

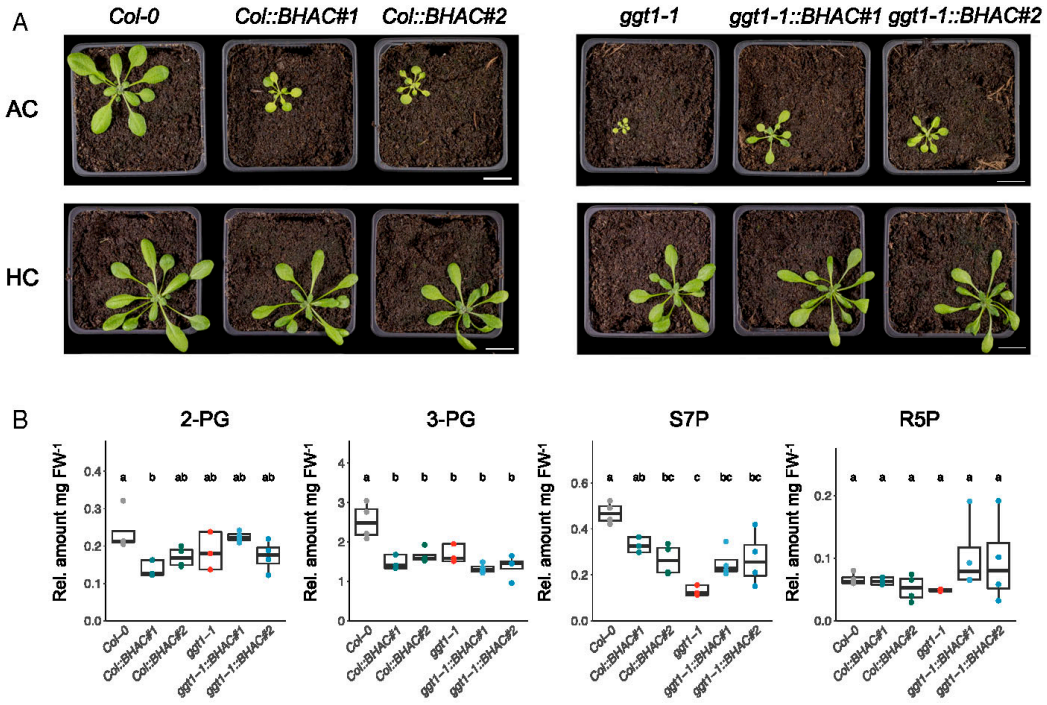


**Fig. 5.** The BHAC reduces plant growth in air by impaired photosynthesis. (*A*) Representative images of BHAC plants in ambient air (400 ppm $CO_2$, AC) or $CO_2$-enriched air (3,000 ppm $CO_2$, HC). The images were taken 28 d after transfer to light (Scale bar, 2 cm). (*B*) Relative levels of phosphorylated metabolites per mg fresh weight (FW) of 2-phosphoglycolate (2-PG), 3-phosphoglycerate (3-PG), seduheptulose-7-phosphate (S7P), and ribulose/ribose-5-phosphate (R5P) in BHAC plants grown in ambient air. Each box–whisker plot represents the 25th and 75th percentiles and whiskers the 10th and 90th percentile. The median is indicated as a crossbar. One-way ANOVA with a post hoc Tukey honest significant difference test was used for statistical analysis. The different letters indicate significant differences between genotypes at $P < 0.05$. $n \geq 3$.

by 25% in *Col::BHAC* plants, while they behaved comparably in *ggt1-1::BHAC* plants (Table 1). Remarkably, neither dark respiration, assessed by light response curve measurements at constant $CO_2$ (400 μbar) nor the CCP under low-oxygen conditions (4% $O_2$) were altered across all genotypes, except a slightly elevated CCP in *ggt1-1::BHAC#2* plants (Table 1 and *SI Appendix*, Fig. S9). Western blot analysis of the Rubisco large subunit and the Rieske–Fe protein demonstrated that the reduced initial slope and $A_{max}$ in BHAC plants was not caused by altered protein content of these enzymes (*SI Appendix*, Fig. S10).

## Discussion

An estimated loss of 30% photosynthetically fixed carbon define photorespiration as a limiting factor of plant growth. However, photorespiratory bypasses can address this issue and improve plant yield (6, 12). The recently described BHAC, naturally found in marine proteobacteria, allows the direct conversion of glyoxylate into OAA, providing options to assimilate photorespiratory glyoxylate without the loss of carbon and nitrogen (25). Here, we report on engineering a functional BHAC in *Arabidopsis* peroxisomes to demonstrate a photorespiratory bypass independent

**Table 1. Physiological parameters of BHAC plants**

| | CCP (μmol · mol$^{-1}$) | $A_{max}$ (μmol $CO_2$ m$^{-2}$ · s$^{-1}$) | A/$C_i$ slope (mol · m$^{-2}$ · s$^{-1}$) | $R_{dark}$ (μmol $CO_2$ m$^{-2}$ · s$^{-1}$) | CCP $^{4\%}$ $^{O}{}_2$ (μmol · mol$^{-1}$) |
|---|---|---|---|---|---|
| *Col-0* | 61.17 ± 2.5$^{b}$ | 16.52 ± 2.2$^{a}$ | 0.045 ± 0.005$^{a}$ | −1.07 ± 0.2$^{a}$ | 15.8 ± 3.3$^{b}$ |
| *Col::BHAC#1* | 71.20 ± 3.3$^{ab}$ | 12.36 ± 1.5$^{b}$ | 0.035 ± 0.003$^{ab}$ | −0.82 ± 0.1$^{a}$ | 17.3 ± 0.7$^{ab}$ |
| *Col::BHAC#2* | 73.53 ± 3.7$^{a}$ | 10.82 ± 2.2$^{b}$ | 0.031 ± 0.007$^{bc}$ | −0.81 ± 0.1$^{a}$ | 19.7 ± 1.7$^{ab}$ |
| *ggt1-1* | 80.20 ± 4.2$^{a}$ | 13.52 ± 1.0$^{ab}$ | 0.021 ± 0.004$^{c}$ | −0.94 ± 0.2$^{a}$ | 19.7 ± 0.6$^{ab}$ |
| *ggt1-1::BHAC#1* | 77.98 ± 3.6$^{a}$ | 11.8 ± 1.1$^{b}$ | 0.030 ± 0.002$^{bc}$ | −0.78 ± 0.2$^{a}$ | 19.8 ± 2.2$^{ab}$ |
| *ggt1-1::BHAC#2* | 77.58 ± 9.8$^{a}$ | 10.35 ± 1.4$^{b}$ | 0.026 ± 0.005$^{bc}$ | −1.02 ± 0.3$^{a}$ | 22.8 ± 2.4$^{a}$ |

The CCP, $A_{max}$, and the slope were determined from the A/$C_i$ curves (*SI Appendix*, Fig. S8). Dark respiration ($R_{dark}$) was determined from the light response curves, and the $O_2$ dependency of the CCP was determined at low oxygen concentrations (4%). One-way ANOVA with a post hoc Tukey honest significant difference test was used for statistical analysis. The different superscript letters indicate significant differences between genotypes at $P < 0.05$. $n \geq 3$. Shown are mean ± SD.

of 3-phosphoglycerate regeneration or decarboxylation of a photorespiratory precursor.

Redirecting the metabolic flux toward a synthetic pathway was demonstrated by combining transcriptional suppression of the plastidial glycolate/glycerate transporter 1 with chloroplastic glycolate decarboxylation in field-grown tobacco plants (23). Similarly, implementing the BHAC in the *ggt1-1* mutant to push pathway flux improved plant growth compared to the mutant background. In plant peroxisomes, the BHAC bypasses the mitochondrial glycine decarboxylase complex that would otherwise release ammonia during photorespiration (Fig. 1). Ammonia reassimilation by passive transport to the chloroplast and refixation by the glutamine synthetase 2/ferredoxin–dependent glutamine:oxoglutarate aminotransferase complex (GS2/Fd-GOGAT) is an integral part of photorespiration (19, 37). Based on the metabolite profiles, we hypothesize three metabolic adaptations that compensate the impaired nitrogen shuttle in BHAC plants. A general response upon impaired GS2/Fd-GOGAT–dependent nitrogen assimilation is the use of cytosolic glutamine synthetases and glutamate dehydrogenases (38). Furthermore, excess nitrogen is stored in the urea cycle (39) and the ornithine–citrulline shuttle that might underpin mitochondrial chloroplastic nitrogen exchange (40). Finally, BHAC-derived OAA can be directly converted into aspartate by aspartate aminotransferase (41). Produced aspartate is used for chloroplastic de-novo biosynthesis of amino acids dependent on C4-carbon skeletons, in particular lysine, threonine, and methionine, that accumulate in BHAC plants [Fig. 4 (42, 43)]. This implies that the BHAC functions as a nitrogen-conserving pathway and allows rerouting of photorespiratory glycolate into amino acids.

In contrast to previous photorespiratory bypasses (21–24), the BHAC also alters the carbon stoichiometry of photorespiration. C3 plants depend on the regeneration of 3-PGA by photorespiration, which is exemplified by the strong phenotype of several photorespiratory mutants (29, 44–46). In BHAC plants, glycolate is directly converted into OAA, and the reduced carboxylation efficiency (initial slope) and $A_{max}$ are caused by lowered metabolic flux in the 3-phosphoglycerate–regenerating branch of photorespiration in the WT background and comparable to the photorespiratory *ggt1-1* mutant (Fig. 5*B* and Table 1).

Whereas previously described photorespiratory bypasses release four $CO_2$ molecules per two molecules of glycolate (22, 23), the BHAC is carbon neutral and maximally releases one $CO_2$ molecule in case OAA is decarboxylated into PEP (25). We note that the introduction of the BHAC into plant peroxisomes did not improve the CCP compared to WT (Table 1). This suggests that either streamlining OAA assimilation or reintegration of the produced C3-intermediate PEP and/or $CO_2$ into the CBBC will be the key to achieve the full potential of the BHAC. At current stage, however, pleiotropic effects of diffuse OAA metabolism by several routes (amino acid biosynthesis, TCA cycle, and PEP/pyruvate metabolism) and reduced 3-phosphoglycerate regeneration that lowers the photosynthetic efficiency likely mask the full potential of the BHAC (Fig. 4). Integrating the BHAC into kinetic- and genome-scale metabolic models will help to identify further engineering targets (20, 47–49). Finally, the construction of a synthetic C4 cycle based on BHAC-derived OAA, either in a single cell or spatially separated cycle between mesophyll- and bundle-sheath cells would allow to enhance carbon assimilation in plants (17, 50) (*SI Appendix*, Fig. S11). We note that using photorespiration as source of the synthetic C4 cycle would circumvent the need to establish PEPC-dependent $CO_2$ fixation in C3 plants, make an ATP-dependent regeneration of PEP dispensable, and ultimately conserve energy.

In summary, this work on engineering a functional BHAC into *Arabidopsis* is a starting point to turn a photorespiratory bypass into a synthetic C4 cycle, constituting a promising approach toward creating higher crop yields in the future.

## Materials and Methods

**Chemicals.** D-*erythro*-BHA ([2R,3S]-β-hydroxyaspartate) was custom synthesized and determined to be >95% pure by NMR analysis (NewChem). DL-*threo*-BHA was purchased as racemic mixture (Sigma Aldrich).

**Plasmid Construction.** BHAC genes were codon optimized for expression in *A. thaliana* by gene synthesis (ThermoFisher Scientific) and matured for golden-gate cloning. All plasmids were generated with the MoClo tool kit, including vector backbones and genetic parts (51). Plasmids were sequenced by Sanger sequencing (Microsynth). Plasmids and primers used in this study are listed in *SI Appendix*, Tables S1 and S2, respectively.

**BHAC Enzyme Activity Assays.** BHAC enzyme activity was measured in total leaf protein extracts from 4-wk-old air-grown *Arabidopsis* plants. Purified recombinant BHAC enzymes were produced as described in ref. 25. The reaction mixture to assay AGAT activity contained 100 mM potassium phosphate buffer (pH = 7.5), 0.1 mM PLP, 0.2 mM NADH, 5 mM glyoxylate, 20 mM aspartate, 25 µL of leaf extract, and 8.75 µg NAD-dependent malate dehydrogenase (Sigma Aldrich). The reaction mixture to assay BHAA activity contained 100 mM potassium phosphate buffer (pH = 7.5), 0.1 mM PLP, 0.2 mM NADH, 0.5 mM $MgCl_2$, 5 mM glyoxylate, 10 mM glycine, 25 µL of leaf extract, and 7 µg purified BHAD and 7 µg purified ISR enzyme. The reaction mixture to assay BHAD activity contained 100 mM potassium phosphate buffer (pH = 7.5), 0.1 mM PLP, 0.2 mM NADH, 2 mM *erythro*-BHA, 25 µL of leaf extract, and 7 µg purified ISR enzyme. The reaction mixture to assay ISR activity contained 100 mM potassium phosphate buffer (pH = 7.5), 0.1 mM PLP, 0.2 mM NADH, 5 mM glyoxylate, and 10 mM $^{15}$N-glycine, 50 µL of leaf extract, and 7 µg purified BHAA and BHAD enzyme. The formation of $^{15}$N-aspartate by ISR activity was confirmed by liquid chromatography with tandem mass spectrometry (LC-MS/MS). A detailed description of the LC-MS/MS method is provided in the *SI Appendix*, Text.

**Plant Material and Cultivation Conditions.** The *A. thaliana* ecotype *Col-0* and the *ggt1-1* mutant (29), deficient in the peroxisomal glutamate:glyoxylate aminotransferase 1 (GGT1) were used as reference backgrounds. Seeds were surface sterilized using the vapor-phase sterilization method (52). Seeds were grown on half-strength Murashige and Skoog medium (pH = 5.7) supplemented with 0.8% (wt/vol) agar. Seeds were cold stratified for 2 d at 4 °C. After germination, seedlings were grown for 14 d at 100 µmol $m^{-2} \cdot s^{-1}$ light intensity at atmospheric $CO_2$ concentration (400 ppm) or in $CO_2$-enriched air (3,000 ppm) in 12-h light/12-h dark photoperiod prior transfer to soil.

**Metabolite Profiling.** For metabolite profiling, green tissue of 14-d-old seedlings was harvested by immediate quenching with liquid nitrogen at the middle of the light phase. A total of 50 mg leaf material was extracted as previously described (53) and analyzed by GC/MS Q-TOF (Agilent). For ion chromatography–mass spectrometry (IC/MS, Thermo Fisher Scientific), tissue was extracted as previously described (54). For relative quantification, metabolite peak areas were normalized to the internal extraction standard and the material fresh weight. A detailed description of the GC/MS Q-TOF and IC/MS methods and the respective data analysis is provided in the *SI Appendix*, Text.

**Gas Exchange Measurements.** Mature rosette leaves of 6-wk-old air-grown plants were used for gas exchange measurements. Measurements were performed using a LICOR6800 (Licor Bioscience) with a flow set to 300 µmol $s^{-1}$, saturating light intensity of 1,000 µmol $m^{-2} \cdot s^{-1}$, leaf temperature of 25 °C, and a vapor pressure deficit below 1.5 kPa. $A/C_i$ curves were measured via stepwise changes in external $CO_2$ supply ranging from 0 to 1,600 µbar. From the $A/C_i$ curves the $CO_2$ compensation point was determined as x-intercept (36). The initial slope of the $A/C_i$ curve was calculated in the linear range between 0 and 200 µbar external $CO_2$, and the maximal assimilation rate ($A_{max}$) above 1,000 µbar $CO_2$ was determined. Dark respiration was determined by light response measurements at constant external $CO_2$ of 400 µbar, and light intensities were stepwise reduced from 1,600 to 0 µmol $m^{-2} \cdot s^{-1}$. The $O_2$ dependency of the $CO_2$ compensation point was determined by stepwise reducing the external $CO_2$ from 400 to 10 µbar under an applied $N_2$-pressured air mixture at a ratio of 4:1, providing an estimated $O_2$ concentrations of 4%. The gas mixture was realized with the help two variable air flowmeters. The leaves were always allowed to adjust to the $O_2$ conditions for ~15 min.

**Data Availability.** Data analysis was performed in R. For analysis of gas exchange measurements, the "plantecophys" package was used (55). The data are summarized in Datasets S1–S10. All other study data are included in the article and/or supporting information.

**ACKNOWLEDGMENTS.** We thank Raja Stracke, Elisabeth Klemp, Maria Graf, and Katrin Weber for excellent technical assistance and Nina Cortina for her contribution in developing the ISR MS method. Work in the laboratory of A.P.M.W was funded by the German Research Foundation (DFG) under Germany's Excellence Strategy (CEPLAS [Cluster of Excellence on Plant Science]), the iGRAD Plant Graduate School (IGK 2466), and European Union H2020 Project 862087-GAIN4CROPS. The CEPLAS metabolism and metabolomics laboratory is funded by the DFG under Germany's Excellence Strategy (EXC-2048/1–Project 390686111). Work in the laboratory of T.J.E. was funded by the Max Planck Society and the DFG (SFB987 "Microbial diversity in environmental signal response").

1. D. Tilman, C. Balzer, J. Hill, B. L. Befort, Global food demand and the sustainable intensification of agriculture. *Proc. Natl. Acad. Sci. U.S.A.* **108**, 20260–20264 (2011).
2. C. A. Jones, R. D. Sands, Impact of agricultural productivity gains on greenhouse gas emissions: A global analysis. *Am. J. Agric. Econ.* **95**, 1309–1316 (2013).
3. D. K. Ray, N. D. Mueller, P. C. West, J. A. Foley, Yield trends are insufficient to double global crop production by 2050. *PLoS One* **8**, e66428 (2013).
4. P. Pradhan, G. Fischer, H. van Velthuizen, D. E. Reusser, J. P. Kropp, Closing yield gaps: How sustainable can we be? *PLoS One* **10**, e0129487 (2015).
5. S. P. Long, A. Marshall-Colon, X.-G. Zhu, Meeting the global food demand of the future by engineering crop photosynthesis and yield potential. *Cell* **161**, 56–66 (2015).
6. E. T. Wurtzel *et al.*, Revolutionizing agriculture with synthetic biology. *Nat. Plants* **5**, 1207–1210 (2019).
7. A. P. M. Weber, A. Bar-Even, Update: Improving the efficiency of photosynthetic carbon reactions. *Plant Physiol.* **179**, 803–812 (2019).
8. T. Schwander, L. Schada von Borzyskowski, S. Burgener, N. S. Cortina, T. J. Erb, A synthetic pathway for the fixation of carbon dioxide in vitro. *Science* **354**, 900–904 (2016).
9. T. E. Miller *et al.*, Light-powered $CO_2$ fixation in a chloroplast mimic with natural and synthetic parts. *Science* **368**, 649–654 (2020).
10. M. Scheffen *et al*, A new-to-nature carboxylation module to improve natural and synthetic $CO_2$ fixation. *Nat. Catal.* **4**, 105–115 (2021).
11. A. Bar-Even, E. Noor, N. E. Lewis, R. Milo, Design and analysis of synthetic carbon fixation pathways. *Proc. Natl. Acad. Sci. U.S.A.* **107**, 8889–8894 (2010).
12. M.-S. Roell, M. D. Zurbriggen, The impact of synthetic biology for future agriculture and nutrition. *Curr. Opin. Biotechnol.* **61**, 102–109 (2020).
13. C. A. Kerfeld, C. Aussignargues, J. Zarzycki, F. Cai, M. Sutter, Bacterial microcompartments. *Nat. Rev. Microbiol.* **16**, 277–290 (2018).
14. J. H. Hennacy, M. C. Jonikas, Prospects for engineering biophysical $CO_2$ concentrating mechanisms into land plants to enhance yields. *Annu. Rev. Plant Biol.* **71**, 461–485 (2020).
15. U. Schlüter, A. P. M. Weber, Regulation and evolution of C4 photosynthesis. *Annu. Rev. Plant Biol.* **71**, 183–215 (2020).
16. M. L. Schuler, O. Mantegazza, A. P. M. Weber, Engineering C4 photosynthesis into C3 chassis in the synthetic biology age. *Plant J.* **87**, 51–65 (2016).
17. M. Ermakova, F. R. Danila, R. T. Furbank, S. von Caemmerer, On the road to $C_4$ rice: Advances and perspectives. *Plant J.* **101**, 940–950 (2020).
18. B. J. Walker, A. VanLoocke, C. J. Bernacchi, D. R. Ort, The costs of photorespiration to food production now and in the future. *Annu. Rev. Plant Biol.* **67**, 107–129 (2016).
19. M. Eisenhut, M.-S. Roell, A. P. M. Weber, Mechanistic understanding of photorespiration paves the way to a new green revolution. *New Phytol.* **223**, 1762–1769 (2019).
20. D. L. Trudeau *et al.*, Design and in vitro realization of carbon-conserving photorespiration. *Proc. Natl. Acad. Sci. U.S.A.* **115**, E11455–E11464 (2018).
21. R. Kebeish *et al.*, Chloroplastic photorespiratory bypass increases photosynthesis and biomass production in *Arabidopsis thaliana*. *Nat. Biotechnol.* **25**, 593–599 (2007).
22. A. Maier *et al.*, Transgenic introduction of a glycolate oxidative cycle into *A. thaliana* chloroplasts leads to growth improvement. *Front. Plant Sci.* **3**, 38 (2012).
23. P. F. South, A. P. Cavanagh, H. W. Liu, D. R. Ort, Synthetic glycolate metabolism pathways stimulate crop growth and productivity in the field. *Science* **363**, eaat9077 (2019).
24. B.-R. Shen *et al.*, Engineering a new chloroplastic photorespiratory bypass to increase photosynthetic efficiency and productivity in rice. *Mol. Plant* **12**, 199–214 (2019).
25. L. Schada von Borzyskowski *et al.*, Marine Proteobacteria metabolize glycolate via the β-hydroxyaspartate cycle. *Nature* **575**, 500–504 (2019).
26. T. Lingner *et al.*, Identification of novel plant peroxisomal targeting signals by a combination of machine learning methods and in vivo subcellular targeting analyses. *Plant Cell* **23**, 1556–1572 (2011).
27. A. Dedonder, R. Rethy, H. Fredericq, M. Van Montagu, E. Krebbers, Arabidopsis *rbcS* genes are differentially regulated by light. *Plant Physiol.* **101**, 801–808 (1993).
28. A. Mitra, J. Han, Z. J. Zhang, A. Mitra, The intergenic region of *Arabidopsis thaliana cab1* and *cab2* divergent genes functions as a bidirectional promoter. *Planta* **229**, 1015–1022 (2009).
29. Y. Dellero, M. Lamothe-Sibold, M. Jossier, M. Hodges, *Arabidopsis thaliana ggt1* photorespiratory mutants maintain leaf carbon/nitrogen balance by reducing RuBisCO content and plant growth. *Plant J.* **83**, 1005–1018 (2015).
30. A. B. Cousins, I. Pracharoenwattana, W. Zhou, S. M. Smith, M. R. Badger, Peroxisomal malate dehydrogenase is not essential for photorespiration in Arabidopsis but its absence causes an increase in the stoichiometry of photorespiratory $CO_2$ release. *Plant Physiol.* **148**, 786–795 (2008).
31. A. R. Fernie, H. Bauwe, Wasteful, essential, evolutionary stepping stone? The multiple personalities of the photorespiratory pathway. *Plant J.* **102**, 666–677 (2020).
32. L. Charton, A. Plett, N. Linka, Plant peroxisomal solute transporter proteins. *J. Integr. Plant Biol.* **61**, 817–835 (2019).
33. P. J. Eastmond *et al.*, Arabidopsis uses two gluconeogenic gateways for organic acids to fuel seedling establishment. *Nat. Commun.* **6**, 6659 (2015).
34. S. Wulfert, S. Schilasky, S. Krueger, Transcriptional and biochemical characterization of cytosolic pyruvate kinases in *Arabidopsis thaliana*. *Plants* **9**, 353 (2020).
35. U. Schluter *et al.*, Photosynthesis in C3-C4 intermediate Moricandia species. *J. Exp. Bot.* **68**, 191–206 (2017).
36. T. D. Sharkey, C. J. Bernacchi, G. D. Farquhar, E. L. Singsaas, Fitting photosynthetic carbon dioxide response curves for $C_3$ leaves. *Plant Cell Environ.* **30**, 1035–1040 (2007).
37. A. J. Bloom, Photorespiration and nitrate assimilation: A major intersection between plant carbon and nitrogen. *Photosynth. Res.* **123**, 117–128 (2015).
38. C. M. Pérez-Delgado, M. García-Calderón, A. J. Márquez, M. Betti, Reassimilation of photorespiratory ammonium in *Lotus japonicus* plants deficient in plastidic glutamine synthetase. *PLoS One* **10**, e0130438 (2015).
39. C. Blume, J. Ost, M. Mühlenbruch, C. Peterhänsel, M. Laxa, Low $CO_2$ induces urea cycle intermediate accumulation in *Arabidopsis thaliana*. *PLoS One* **14**, e0210342 (2019).
40. M. Linka, A. P. M. Weber, Shuffling ammonia between mitochondria and plastids during photorespiration. *Trends Plant Sci.* **10**, 461–465 (2005).
41. C. J. Schultz, G. M. Coruzzi, The aspartate aminotransferase gene family of Arabidopsis encodes isoenzymes localized to three distinct subcellular compartments. *Plant J.* **7**, 61–75 (1995).
42. M. Kirma, W. L. Araújo, A. R. Fernie, G. Galili, The multifaceted role of aspartate-family amino acids in plant metabolism. *J. Exp. Bot.* **63**, 4995–5001 (2012).
43. S. Ravanel *et al.*, Methionine metabolism in plants: Chloroplasts are autonomous for de novo methionine synthesis and can import S-adenosylmethionine from the cytosol. *J. Biol. Chem.* **279**, 22548–22557 (2004).
44. R. Boldt *et al.*, D-GLYCERATE 3-KINASE, the last unknown enzyme in the photorespiratory cycle in Arabidopsis, belongs to a novel kinase family. *Plant Cell* **17**, 2413–2420 (2005).
45. L. M. Voll *et al.*, The photorespiratory Arabidopsis *shm1* mutant is deficient in SHM1. *Plant Physiol.* **140**, 59–66 (2006).
46. M. Eisenhut *et al.*, Arabidopsis A BOUT DE SOUFFLE is a putative mitochondrial transporter involved in photorespiratory metabolism and is required for meristem growth at ambient $CO_2$ levels. *Plant J.* **73**, 836–849 (2013).
47. L. J. Sweetlove, R. G. Ratcliffe, Flux-balance modeling of plant metabolism. *Front. Plant Sci.* **2**, 38 (2011).
48. A. Kuken, Z. Nikoloski, Computational approaches to design and test plant synthetic metabolic pathways. *Plant Physiol.* **179**, 894–906 (2019).
49. A. Matuszyńska, N. P. Saadat, O. Ebenhöh, Balancing energy supply during photosynthesis - a theoretical perspective. *Physiol. Plant.* **166**, 392–402 (2019).
50. I. Jurić, J. M. Hibberd, M. Blatt, N. J. Burroughs, Computational modelling predicts substantial carbon assimilation gains for $C_3$ plants with a single-celled $C_4$ biochemical pump. *PLoS Comput. Biol.* **15**, e1007373 (2019).
51. C. Engler *et al.*, A golden gate modular cloning toolbox for plants. *ACS Synth. Biol.* **3**, 839–843 (2014).
52. S. J. Clough, A. F. Bent, Floral dip: A simplified method for agrobacterium-mediated transformation of *Arabidopsis thaliana*. *Plant J.* **16**, 735–743 (1998).
53. O. Fiehn *et al.*, Metabolite profiling for plant functional genomics. *Nat. Biotechnol.* **18**, 1157–1161 (2000).
54. S. Arrivault *et al.*, Use of reverse-phase liquid chromatography, linked to tandem mass spectrometry, to profile the Calvin cycle and other metabolic intermediates in Arabidopsis rosettes at different carbon dioxide concentrations. *Plant J.* **59**, 826–839 (2009).
55. R. A. Duursma, Plantecophys–An R package for analysing and modelling leaf gas exchange data. *PLoS One* **10**, e0143346 (2015).

# Plant peroxisomal solute transporter proteins



JIPB Journal of Integrative Plant Biology

## Plant peroxisomal solute transporter proteins[OO]

Lennart Charton[†], Anastasija Plett[†] and Nicole Linka[*]

Institute for Plant Biochemistry and Cluster of Excellence on Plant Sciences (CEPLAS), Heinrich Heine University, Universitätsstrasse 1, 40225 Düsseldorf, Germany
[†]These authors contributed equally to this work.
doi: 10.1111/jipb.12790

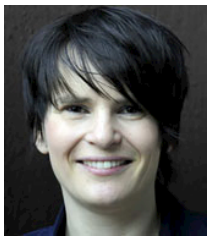

**Nicole Linka**
*Correspondence:
Nicole.Linka@hhu.de

**Abstract** Plant peroxisomes are unique subcellular organelles which play an indispensable role in several key metabolic pathways, including fatty acid β-oxidation, photorespiration, and degradation of reactive oxygen species. The compartmentalization of metabolic pathways into peroxisomes is a strategy for organizing the metabolic network and improving pathway efficiency. An important prerequisite, however, is the exchange of metabolites between peroxisomes and other cell compartments. Since the first studies in the 1970s scientists contributed to understanding how solutes enter or leave this organelle. This review gives an overview about our current knowledge of the solute permeability of peroxisomal membranes described in plants, yeast, mammals and other eukaryotes. In general, peroxisomes contain in their bilayer membrane specific transporters for hydrophobic fatty acids (ABC transporter) and large cofactor molecules (carrier for ATP, NAD and CoA). Smaller solutes with molecular masses below 300–400 Da, like the organic acids malate, oxaloacetate, and 2-oxoglutarate, are shuttled via non-selective channels across the peroxisomal membrane. In comparison to yeast, human, mammals and other eukaryotes, the function of these known peroxisomal transporters and channels in plants are discussed in this review.

**Edited by:** Jianping Hu, Michigan State University, USA
**Received** Oct. 15, 2018; **Accepted** Feb. 11, 2019; **Online on** Feb. 14, 2019
OO: OnlineOpen

Invited Expert Review

OnlineOpen

## INTRODUCTION

Peroxisomes are surrounded by a single membrane which functions as a permeability barrier to solutes by forming a confined compartment for peroxisomal metabolism. To connect peroxisomes to the metabolic network of the cell, the peroxisomal bilayer membrane embeds different transport proteins allowing the passage of a variety of solutes (Rottensteiner and Theodoulou 2006; Antonenkov and Hiltunen 2012; Linka and Theodoulou 2013). Since peroxisomes are highly metabolically active, a massive transfer of metabolites across the peroxisomal membrane has to take place (Antonenkov and Hiltunen 2012; Linka and Esser 2012; Linka and Theodoulou 2013). Recent progress defines the permeability of the peroxisomal membrane to solutes into two types of transport proteins: non-selective pore-forming channels facilitate the passage of small solutes down the electrochemical gradient, like the β-barrel porins found in the outer membrane of gram-negative bacteria, mitochondria and plastids (Antonenkov and Hiltunen 2012); specific transporters mediate the passive flux of larger molecules in a uniport or antiport mechanism, typical for the inner mitochondrial and envelope membrane (Linka and Esser 2012; Linka and Theodoulou 2013). Thus, the peroxisomal

bilayer membrane is comparable to the plasma membrane and endoplasmic reticulum (ER) membrane, since permeability is conducted by both, channel and carrier proteins. The combination of non-selective pore-forming channels to transfer small molecules as well as specific carrier proteins for 'bulky' solutes is a highly efficient way to cope with a massive flux of a variety of metabolites across the peroxisomal border. While solute transport through a pore-forming channel occurs at a much faster rate, carriers bind their solutes tightly and are thus highly specific to their transport substrate.

Peroxisomal pore-forming channels are present in the membrane of plants, mammals, and yeast peroxisomes as well as in glycosomal membranes of *Trypanosoma brucei* (Reumann et al. 1995; Reumann et al. 1996; Reumann et al. 1998; Antonenkov et al. 2009; Rokka et al. 2009; Gualdrón-López et al. 2012; Mindthoff et al. 2015). These channel proteins are general pores consisting of transmembrane α-helices, and thus, distinct to the β-barrel porins. The peroxisomal channels allow the rapid and unrestricted diffusion of small hydrophilic molecules with molecular masses up to 300–400 Da, but prevent diffusion of larger molecules across the peroxisomal membrane (Antonenkov and Hiltunen 2012). The transport is driven by the concentration gradient of the transported solute. Recently, two putative channel proteins have been identified for peroxisomes: the peroxisomal membrane protein of 22 kDa (PMP22) and peroxin 11 (PEX11) (Figure 1) (Rokka et al. 2009; Mindthoff et al. 2015).

To date, specific solute transporters belonging to the mitochondrial transporter family (MCF) and the ATP-binding cassette (ABC) transporter family have been found in the peroxisomal membranes of mammals, plants and yeast (Figure 1) (Linka and Esser 2012; Linka and Theodoulou 2013). These two families of proteins each consist of transmembrane α-helical domains and catalyze a passive or active transport, respectively. Three peroxisomal members of the MCF are passive carriers mediating the facilitated diffusion of solutes down their electrochemical gradient (Palmieri et al. 2001; van Roermund et al. 2001; Visser et al. 2002; Arai et al. 2008; Linka et al. 2008; Agrimi et al. 2011; Agrimi et al. 2012; Bernhardt et al. 2012). In contrast, the peroxisomal ABC transporter is an active transporter pumping its substrate across the membrane against their electrochemical gradient, which is coupled to the hydrolysis of ATP as energy source (Morita and Imanaka 2012; Baker et al. 2015; Theodoulou and Kerr 2015). In summary, both peroxisomal carrier types perform the traffic of large molecules (up to $< 400$ Da), including acyl-CoA esters and some cofactors like ATP, $NAD^+$, CoA.

## PEROXISOMAL ABC TRANSPORTERS

The peroxisomal ABC transporters belong to the D subfamily of the ATP-binding cassette (ABC) transporter family (Morita and Imanaka 2012; Baker et al. 2015; Theodoulou and Kerr 2015). Like all eukaryotic ABC transporters, they have a core structure consisting of two conserved domains: a transmembrane domain (TMD) with multiple α-helices and a nucleotide-binding domain (NBD) with Walker A and Walker B motifs. The TMDs bind and translocate substrates, whereas the NBDs form a 'sandwich dimer' capable of binding and hydrolyzing ATP. The hydrolysis of ATP provides the energy for the translocation of the substrate against an electrochemical gradient across the membrane (Higgins 1992; Rees et al. 2009). The peroxisomal ABCD proteins from human, mammals and fungi function as dimers of two TMD-NBD 'half transporters' (Morita and Imanaka 2012; Baker et al. 2015; Theodoulou and Kerr 2015). In contrast, plant peroxisomes possess a full-sized transporter encoded by a single gene. This plant ABCD protein contains two homologous but distinct halves that are attached as heterodimers with the topology TMD1-NBD1–TMD2-NBD2 (Dietrich et al. 2009). The fusion of two half transporters into one 'pseudo-heterodimeric' protein was a single event in the evolution of the green plant lineage which occurred before the divergence of bryophytes (Morita and Imanaka 2012; Baker et al. 2015; Theodoulou and Kerr 2015). The role of the peroxisomal ABCD proteins has been intensively studied in yeast, human and plants. Cross-species complementation studies revealed a conserved function for members of the ABCD family, mediating the uptake of β-oxidation substrates into peroxisomes (Table 1).

Yeast contains two peroxisomal half-ABC transporters ScPxa1p and ScPxa2p (Hettema et al. 1996; Shani and Valle 1996; Verleur et al. 1997). Single knockout mutants are impaired in growth on oleate-containing medium, indicating that they are unable to utilize oleate (C18:1) as a sole carbon source (Hettema et al. 1996; Verleur et al. 1997). The double yeast mutant *pxa1*Δ/*pxa2*Δ did not display an enhanced phenotype compared to the single mutants, suggesting that the

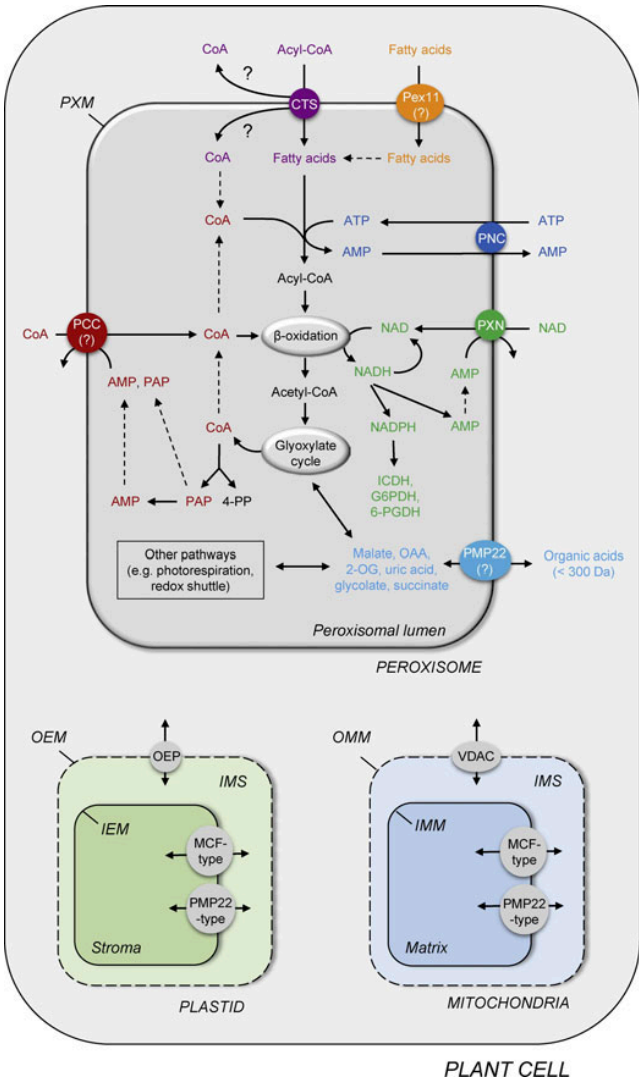


**Figure 1. Scheme of a plant cell presenting the known peroxisomal transporter and channel proteins connecting peroxisomal metabolism with that of the cell**

Based on the proposed transport mechanism, the peroxisomal ABC transporter CTS import acyl-CoA esters into the peroxisomes. During this import process, the substrates is hydrolyzed to fatty acids and CoA and released into the peroxisomal matrix. Such a transport mode requires the intra-peroxisomal ATP-dependent re-esterification to CoA for fatty acid activation. The peroxisomal ATP carrier PNC import cytosolic ATP in exchange with AMP, which is produced during fatty acid activation. ATP is also required for other ATP-dependent reaction inside peroxisomes, including auxin biosynthesis, protein phosphorylation and mevalonate pathway. NAD-dependent reactions inside peroxisomes, like fatty acid oxidation, depend on the import of NAD from the cytosol catalyzed by the peroxisomal NAD carrier PXN. The exchange partner for the NAD uptake is generated by peroxisomal NADH hydrolysis. NAD can be phosphorylated to NADPH, which is the cofactor for NADP-dependent ICDH and the OPPP enzymes G6PDH and

**Table 1. Plant peroxisomal transport proteins described in this review, their predicted transport substrates and transport mode**

| Transporter | Transport substrates | Transport mode |
|---|---|---|
| PNC | $ATP_{in}/ADP_{out}$<br>$ATP_{in}/AMP_{out}$ | Passive transport down the chemical gradient in an antiport mechanism |
| PXN | $NAD_{in}/AMP_{out}$ | Passive transport down the chemical gradient in an antiport mechanism |
| PCC | $CoA_{in}/AMP_{out}$<br>$CoA_{in}/PAP_{out}$ | Passive transport down the chemical gradient in an antiport mechanism |
| PMP22 | Organic acids like Malate, OAA, 2-OG, glycolate succinate | Passive transport down the chemical gradient in an uniport mechanism |
| PEX11 | long-chain and medium-chain fatty acids | Passive transport down the chemical gradient in an uniport mechanism |
| CTS | Acetyl-CoA | ATP-dependent active transport in an uniport mechanism |

two half-size transporters heterodimerize to form a fully functional transporter. This was confirmed by protein–protein interaction studies (Shani and Valle 1996; Chuang et al. 2014). The growth defect was restricted to only very-long chain fatty acids (VLCFA; >C22:0), indicating that ScPxa1p/ScPxa2p is involved in the import of fatty acids with 18 or more carbons as CoA esters into the peroxisome for their further degradation by β-oxidation (Hettema et al. 1996; Verleur et al. 1997). In yeast an alternative uptake route exists for medium-chain free fatty acids, which is independent of the peroxisomal ABC transporter (van Roermund et al. 2003). These β-oxidation substrates can enter the peroxisome in the non-esterified form via the proposed ScPex11 channel protein (Mindthoff et al. 2015). Inside the peroxisomal matrix, they are activated by the peroxisomal acyl-CoA synthetase ScFaa2p (fatty acid activation protein 2) (Hettema et al. 1996), prior to β-oxidation, a process which requires ATP imported by the peroxisomal ATP carrier ScAnt1p (adenine nucleotide transporter1) (Palmieri et al. 2001; van Roermund et al. 2001).

Humans have three ABCD family members residing in the peroxisomal membrane (ABCD1-3) (Kamijo et al. 1990; Mosser et al. 1993; Lombard-Platet et al. 1996). They are half transporters and function *in vivo* as active homodimers. The human ABCD proteins have distinct but partially overlapping substrate specificities to

6-PGDH. In addition, peroxisomes require a peroxisomal CoA carrier (PCC) mediating the uptake of CoA, which has not been identified for plant peroxisomes. If the CoA is cleaved off at the cytosolic side of the peroxisomal membrane during the transport of acyl-CoA, the peroxisomal CoA carrier imports cytosolic CoA into peroxisomes required for fatty acid activation. Peroxisomal CoA is also used to remove acetyl-CoA from the fatty acyl chain in the last step of β-oxidation, whereas the glyoxylate cycle produces free CoA. To regulate CoA homeostasis, CoA can be hydrolyzed to PAP or 4-PP, which are suitable counter-exchange substrates for the CoA import. The further hydrolysis of PAP yields AMP, another putative export substrate for the peroxisomal CoA carrier. Other intermediates of the peroxisomal metabolism, such as organic acids, might be shuttled via the peroxisomal channel protein called PMP22 across the peroxisomal membrane. Pex11 as a second channel might be involved in the uptake of free fatty acids into the peroxisomes, as a redundant system to the peroxisomal ABC transporter. Other compartments of a plant cell, like plastids and mitochondria, possess a large variety of transporter and channel proteins for shuttling metabolites across their bilayer membranes, including the outer envelope proteins OEPs, plastidial MCF-type carriers, plastidial PMP22-type channels, voltage-dependent anion channels (VDACs), mitochondrial MCF carriers, and mitochondrial PMP22-type channels. Abbreviations: PAP, 3',5'-ADP; 4-PP, 4-Phosphopantetheine; OAA, oxaloacetate; 2-OG, 2-oxoglutarate; ICDH, isocitrate dehydrogenase; G6PDH, glucose-6-phopshate dehydrogenase; 6-PGDH, 6-phosphogluconate dehydrogenase; OEM, outer envelope membrane; IEM, inner envelope membrane; OMM, outer mitochondrial membrane; IMM, inner mitochondrial membrane; IMS, intermembrane space.

different acyl-CoA esters. HsABCD1 shares functional redundancy with HsABCD2 (van Roermund et al. 2008, 2011). A defect in the human ABCD1 protein (or ALDP) causes X-linked adrenoleukodystrophy (X-ALD) (Mosser et al. 1993). This most common peroxisomal disorder is characterized by an impaired peroxisomal β-oxidation and consequently accumulation of VLCFA in tissues, especially the brain and the adrenal glands (Wiesinger et al. 2013). Although human ABCD proteins have functional redundancy, the basal expression levels of HsABCD2 and HsABCD3 are not sufficient to compensate the lack of HsABCD1 in X-ALD patients. Human ABCD2 (or ALDR) prefers shorter VLCFA and polyunsaturated fatty acids as transport substrates (van Roermund et al. 2011), whereas human ABCD3 (or PMP70) has the broadest substrate specificity (van Roermund et al. 2014). It is involved in the transport of saturated fatty acids, unsaturated fatty acids, branched-chain fatty acids, dicarboxylic fatty acids, and C27 bile acid intermediates (Ferdinandusse et al. 2015).

The *Arabidopsis* ABCD1 is the most studied and best understood plant peroxisomal ABC transporter. It has been independently identified by four different groups, and hence is also known as CTS (Comatose [Footitt et al. 2002]), PXA1 (peroxisomal ABC transporter 1 [Zolman et al. 2001]), PED3 (peroxisome defective 3 [Hayashi et al. 2002]) and ACN2 (acetate non-utilizing 2) (Hooks et al. 2004). In this review, we use the name CTS. *Arabidopsis* plants defective in CTS exhibit different phenotypes with respect to β-oxidation. Besides fatty acid degradation β-oxidation is involved in a wide range of metabolic and signaling processes in plants, including the synthesis of signaling molecules and secondary products. Hence, *Arabidopsis* CTS has been implicated not only to import fatty acyl-CoAs into the peroxisome, but also various other β-oxidation substrates, such as the jasmonic acid (JA) precursor 12-oxo-phytodienoic acid (OPDA) (Theodoulou et al. 2005; Dave et al. 2011), the synthetic auxin precursor 2,4-dichlorophenoxybutyric acid (2,4-DB) (Hayashi et al. 2002) and indole butyric acid (IBA) (Zolman et al. 2001), precursors of ubiquinone synthesis (Block et al. 2014) and cinnamic acid (Bussell et al. 2014), which is required for the synthesis of benzoic acid.

An unusual transport mechanism has been proposed for the human and *Arabidopsis* ABCDs shuttling their substrates across the peroxisomal membrane (Figure 1). Acyl-CoA esters and not 'free' (non-esterified) fatty acids are bound to the human ABCD1-3 and CTS transporter, demonstrated by the stimulated ATPase activity in the presence of fatty acyl-CoA derivatives (Nyathi et al. 2010). Once the acyl-CoA substrate is bound by ABCD or CTS, the CoA moiety is cleaved off during transfer across the lipid bilayer. The CoA cleavage during the transport cycle of CTS was confirmed using isotopic labelling of yeast cells with $^{18}O$ (van Roermund et al. 2012). Furthermore, it was experimentally shown that the human ABCD1-3 and CTS itself possess an intrinsic acyl-CoA thioesterase activity (De Marcos-Lousa et al. 2013; Geillon et al. 2017; Okamoto et al. 2018), although no motif homologous to either α/β-hydrolases or hot-dog fold thioesterases were detected (De Marcos-Lousa et al. 2013). Such a transport mechanism subsequently requires a re-activation within the peroxisome by a peroxisomal acyl-CoA synthetase (ACS), which interacts with the transporter (De Marcos-Lousa et al. 2013). It was shown that functional complementation of the *pxa1*Δ/*pxa2*Δ yeast mutant by CTS depends on the presence of ScFaa2p or the equivalent *Arabidopsis* long-chain acyl CoA synthetases 6 and/or 7 (LACS6/7) inside yeast peroxisomes (De Marcos-Lousa et al. 2013). Coupling the translocation process to the peroxisomal ATP-dependent re-activation with CoA might be a potential regulation point for the entry of fatty acids and other substrates into the β-oxidation pathway. The cleavage and re-esterification of the acyl-CoA consumes two molecules of ATP and thus seems to be energetically wasteful. Still, it solves the biophysical challenge of shuttling an amphipathic molecule across the peroxisomal membrane and enables separate permeation pathways for the hydrophilic (CoA) and hydrophobic (fatty acid) moieties of β-oxidation substrates. In addition, the human ABCD and plant CTS transporter are able to accept disparate CoA derivatives as transport molecules via the intrinsic thioesterase domain, which recognizes the CoA moiety as an important determinant. We do not know yet, on which side of the peroxisomal membrane the CoA cleavage by the HsABCD1-3 or CTS transporter occurs. If CoA is released in the cytosol, the question how it enters peroxisomes remains to be answered.

## PEROXISOMAL MEMBERS OF THE MITOCHONDRIAL CARRIER FAMILY

The mitochondrial carrier family (MCF) represents the largest group of eukaryotic transport proteins with 35

members in *Saccharomyces cerevisiae* (Palmieri et al. 2000, 2006) and more than 50 putative candidates in human (Palmieri 2014). The *Arabidopsis* genome encodes for 58 MCF members evenly distributed across the five chromosomes (Haferkamp 2007; Palmieri et al. 2011; Haferkamp and Schmitz-Esser 2012). All MCF carriers contain three tandemly repeated homologous domains, each consisting of two hydrophobic membrane spanning α-helices linked by a conserved sequence motif (Palmieri et al. 2011; Haferkamp and Schmitz-Esser 2012; Taylor 2017). They are highly variable in terms of size and charge of the transported molecule and the underlying transport mode. The predominant mechanism follows a 1:1 exchange of solutes (antiport), but unidirectional substrate transport (uniport) and proton compensated anion symport have been shown to be mediated by certain MCF carriers (Palmieri et al. 2011; Haferkamp and Schmitz-Esser 2012; Palmieri 2014; Taylor 2017). According to their substrate specificity, they can be divided into four subfamilies. The first group includes the nucleotide and nucleotide derivate transporters. Carriers for the transport of di- and tri-carboxylates and keto-acids belong to the second subfamily. The third group comprises carriers catalyzing the transport of amino acids and their derivatives. Other carriers are grouped together with uncoupling proteins in the fourth and last subfamily (Palmieri et al. 2011; Haferkamp and Schmitz-Esser 2012; Palmieri 2014; Taylor 2017). Despite their name several MCF carriers have been localized to other cellular compartments, such as plasma membrane, ER membrane, plastids and peroxisomes. Up to now, three peroxisomal MCF carriers have been characterized in human, mammals, fungi and plants mediating the transport of ATP, NAD and CoA (Figure 1, Table 1) (Palmieri et al. 2001; van Roermund et al. 2001; Arai et al. 2008; Linka et al. 2008; Agrimi et al. 2011; Agrimi et al. 2012; Bernhardt et al. 2012). These essential cofactors are synthetized outside the peroxisomes, and therefore, have to be imported into the peroxisomal lumen (Figure 1). In all cases a specific carrier is required, because ATP, NAD and CoA cannot be transported through a peroxisomal pore-forming channel due to their size.

**The peroxisomal ATP carrier**

The first peroxisomal MCF carrier found was the ATP carrier from *S. cerevisiae*, called ScAnt1p (Adenine nucleotide transporter 1) (Palmieri et al. 2001; van Roermund et al. 2001). Based on sequence similarity to ScAnt1p, two *Arabidopsis* MCF members have been identified called AtPNC1 and AtPNC2 (Peroxisomal adenine Nucleotide Carrier) (Arai et al. 2008; Linka et al. 2008). Their transport function has been investigated by *in vitro* uptake experiments using liposomes reconstituted with recombinantly expressed proteins (Table 1). The yeast and plant carrier accept the adenine nucleotides ATP, ADP and AMP as transport substrates and catalyze a strict counter exchange of ATP against AMP or ADP (Palmieri et al. 2001; Linka et al. 2008). The import of cytosolic ATP into peroxisomes is essential for the ATP-dependent activation of fatty acids for their degradation by peroxisomal β-oxidation (Figure 1) (Palmieri et al. 2001; van Roermund et al. 2001; Arai et al. 2008; Linka et al. 2008). In yeast and plants, the fatty acid β-oxidation exclusively takes place inside peroxisomes (Goepfert and Poirier 2007; Graham 2008; van Roermund et al. 2012). Consequently, yeast cells deficient in ScAnt1p were unable to metabolize medium-chain fatty acids, such as lauric acid (C16:0) as carbon and energy source due to the lack of intra-peroxisomal ATP (Palmieri et al. 2001; van Roermund et al. 2001). *Arabidopsis* PNC1 and PNC2 were shown to be able to complement the β-oxidation phenotype of the *ant1*Δ yeast mutant, indicating that the plant carrier, like the yeast ortholog, are able to supply β-oxidation with ATP (Linka et al. 2008). A similar phenotype was observed for PNC1 and PNC2 *Arabidopsis* mutant plants. While the phenotype of single *pnc Arabidopsis* lines was not distinguishable from the wild type, plants in which both AtPNC proteins are suppressed were impaired in peroxisomal β-oxidation, leading to a block in storage oil mobilization (Linka et al. 2008). Since storage of carbohydrates (starch) and proteins is minor in *Arabidopsis* seeds (Goepfert and Poirier 2007; Graham 2008), *pnc1/pnc2 Arabidopsis* seedlings depend on exogenous sucrose to allow seedling establishment (Linka et al. 2008). This strongly emphasizes that AtPNC1 and AtPNC2 are the sole site of peroxisomal ATP supply. The fatty acid activation step by peroxisomal acyl-CoA synthetases produces AMP and $PP_i$ in yeast and *Arbaidopsis* (Hettema et al. 1996; Fulda et al. 2004). While AMP is the direct counter-exchange substrate for the peroxisomal ATP carrier-mediated ATP import, the destiny of $PP_i$ remains unknown. So far, a peroxisomal pyrophosphatase, catalyzing the hydrolysis of $PP_i$ to 2 molecules of $P_i$ has not been found in peroxisomes.

This raises the question how $PP_i$ and/or $P_i$ are shuttled out of the peroxisomes (Linka and Theodoulou 2013). Due to their polar nature, both solutes are unlikely to freely diffuse across the peroxisomal membrane. Experiments using isolated bovine kidney peroxisomes observed transport activity for $P_i$ and to a lesser extent $PP_i$ (Visser et al. 2005). Whether specific transporters or unspecific channels mediate this solute transport was not addressed in this study.

Beyond fatty acid β-oxidation peroxisomal ATP is required for other enzymatic reactions inside peroxisomal lumen. In plants, for example, β-oxidation is involved in phytohormone biosynthesis (Wasternack and Strnad 2017; Wasternack and Feussner 2018). Jasmonates constitute a family of bioactive oxylipids that regulate a variety of defense responses and developmental processes. Its biosynthesis starts with the production of OPDA and dinor-OPDA in the chloroplasts and continues in peroxisomes by an alternative β-oxidation cycle (Wasternack and Strnad 2017; Wasternack and Feussner 2018). The peroxisomal import of OPDA is at least partially mediated by the peroxisomal ABC transporter CTS in *Arabidopsis* (Theodoulou et al. 2005). Inside the peroxisomal matrix it is then reduced to OPC-8 and activated by peroxisomal AtOPC-8:CoA ligase (Kienow et al. 2008). *Arabidopsis* null mutants lacking this enzyme are compromised in JA biosynthesis, leading to reduced JA levels (50–60%) and hyperaccumulation of OPC8:0 in wound-induced leaves (Koo et al. 2006). Finally, the last steps comprise several cycles of β-oxidation, by which an even number of carbons is removed from the carboxyl side chains of OPC-8, giving rise to JA in *Arabidopsis*. We also observed in the *pnc1/2 Arabidopsis* silencing mutant significantly reduced JA levels, indicating a role for PNC proteins in JA biosynthesis in plants (personal communication).

In addition to JA, plant peroxisomes are involved in the synthesis of indolce-3-acetic acid (IAA), short auxin (Korasick et al. 2013). This phytohormone plays a fundamental role in plant growth and development. It can be stored in inactive forms, conjugated to amino acids or sugars (Korasick et al. 2013). One of several auxin precursors in plants is IBA. Auxin derived from IBA is important during seedling development, when it influences lateral rooting (De Rybel et al. 2012), cotyledon and root hair expansion, and apical hook formation (Strader et al. 2010; Strader et al. 2011). The synthesis of auxin from IBA occurs in plant peroxisomes by the action of an alternative peroxisomal β-oxidation pathway. Like OPDA and fatty acids, IBA has to be esterified with CoA, an ATP-consuming reaction in plants. However, in contrast to fatty acid β-oxidation, an alternative peroxisomal acyl-CoA synthetase is required, since *Arabidopsis* double knockout mutants of the two *Arabidopsis* fatty acid acyl-CoA synthetases LACS6/7 are sensitive to IBA (Cassin-Ross and Hu 2014a). However, even if catalyzed by another enzyme, ATP is still mandatory for the CoA esterification since *pnc1/pnc2 Arabidopsis* mutant plants are less sensitive to IBA as well as to the synthetic auxin precursor 2,4-DB (Arai et al. 2008; Linka et al. 2008).

Interestingly, there is no obvious phenotype of *Arabidopsis* plants lacking PNC1 and PNC2 after the seedling becomes photoautotrophic (personal communications). Since ATP as the energy currency plays such an important role in the cellular metabolism, it is likely that other peroxisomal pathways in addition to β-oxidation need ATP. This includes the mevalonate pathway (MVA) in plants that is involved in the formation of isopentenyl diphosphate (IPP) and dimethylallyl pyrophosphate (DMAPP), the building blocks of isoprenoids (Simkin et al. 2011; Rodríguez-Concepción and Boronat 2015). In *Arabidopsis*, two ATP-dependent enzymes of the mevalonate pathway (MVA) are located to peroxisomes: phosphomevalonate kinase (PMK) and mevalonate diphosphate decarboxylase (MVD) (Sapir-Mir et al. 2008; Simkin et al. 2011). AtPMK catalyzes the phosphorylation of mevalonate phosphate to mevalonate diphosphate, consuming ATP and releasing ADP. Mevalonate diphosphate is subsequently decarboxylated by AtMVD to IPP, coupled to the hydrolysis of ATP to ADP and $P_i$ (Simkin et al. 2011). IPP derived from the MVA pathway is required in plants for the formation of triterpenes, sesquiterpenes, phytosterols, ubiquinone, vitamin D and primary metabolites important for cell integrity (Rodríguez-Concepción and Boronat 2015). In parallel to the MVA, IPP can be produced by the plastidic 2-C-methyl-D-erythritol-4-phosphate (MEP) pathway in plants, which is used as a precursor for the synthesis of monoterpenes, carotenoids, apocarotenoids and the side chain of chlorophylls, tocopherols and prenylquinones (Rodríguez-Concepción and Boronat 2015). Interaction between MVA and MEP pathways has been documented, explaining the less prominent phenotype of single mutants in either of the two

pathways (Hemmerlin et al. 2012). However, the plant-specific carrier and channel involved in peroxisomal and plastidic transport steps have not been identified, yet (Linka and Theodoulou 2013). Since *Arabidopsis* PNCs are the sole source of peroxisomal ATP, *pnc1/2* mutant plants should be affected in MVA-synthesized isoprenoid molecules, like sterols and volatiles as it was shown for *mvd* mutant plants (Henry et al. 2015). However, a severe phenotype for *Arabidopsis pnc1/2* mutants might not be visible under normal conditions due to the presence of the functional MEP pathway.

Reversible post-translational modification by phosphorylation is an essential fast responding regulatory mechanism that controls many cellular processes (Cohen 2000; Friso and van Wijk 2015). For this, protein kinases transfer the γ-phosphate group from ATP to the hydroxyl group of serine, threonine or tyrosine residues, whereas protein phosphatases hydrolyze the phosphoester bond to dephosphorylate proteins. In plants, several soluble peroxisomal proteins involved in β-oxidation, glyoxylate cycle and photorespiration have been shown to be phosphorylated under certain conditions (Hodges et al. 2013; Kataya et al. 2015). But the physiological effects are still unknown. While many kinases have been identified and characterized, the knowledge about peroxisomal kinases is still limited. The first identified peroxisomal kinase was glyoxysomal protein kinase 1 (GPK1) in *Arabidopsis* (Fukao et al. 2003). AtGPK1 is a serine/threonine protein kinase, most likely anchored to the peroxisomal membrane with its kinase domain facing the peroxisomal lumen. The targets of AtGPK1 have not been identified, but regulation of proteins involved in fatty acid degradation may be required to prevent an overproduction of sucrose and hence protect against waste of energy in early post-germinative seedlings. In addition, *Arabidopsis* calcium-dependent protein kinase 1 (CDPK1) has been localized to peroxisomes and oil bodies and has been reported to be involved in salt and drought stress response as well as pathogen resistance (Coca and San Segundo 2010). It is suggested to play a role in lipid metabolism in plants since *Arabidopsis* mutants are partially resistant to the synthetic auxin precursor 2,4-DB and OPDA (Cassin-Ross and Hu 2014b). Further research is required to determine the signal transduction pathway of AtCDPK1. Although the *Arabidopsis pnc1/2* silencing plants develop normally through the plant life cycle, it might be interesting to investigate, to what extent the peroxisomal phospho-proteome was altered in these plant mutant lines.

NAD and its phosphorylated analog (NADP) have become well established as key energy transducers (Pollak et al. 2007; Houtkooper et al. 2010). The *Arabidopsis* genome harbors about 800 predicted oxidoreductases, which are likely to use NAD or NADP as cofactors. They play a fundamental role in reduction/oxidation (redox) metabolism through their contribution to the redox status of compounds, such as glutathione, thioredoxins and ascorbate (Noctor and Foyer 2016). In plant peroxisomes NADP-depending reactions are catalyzed by enzymes of the oxidative pentose phosphate pathway, such as glucose-6-phosphate dehydrogenase and 6-phosphogluconate dehydrogenase, but also the peroxisomal isocitrate dehydrogenase depends on NADP (Meyer et al. 2011; Hölscher et al. 2014, 2016). All three enzymes are key components of the defense machinery against oxidative stress in plants. The only pathway for *de novo* synthesis of NADP and NADPH is the ATP-dependent phosphorylation of NAD and NADH, respectively. This reaction is catalyzed in *Arabidopsis* by members of the NAD(H) kinase family ATNADK1, AtNADK2 and AtNADK3. While AtNADK1 and AtNADK2 localize to the cytosol and plastids, respectively, AtNADK3 was shown to reside in peroxisomes (Turner et al. 2004, 2005; Chai et al. 2006; Waller et al. 2010). In contrast to AtNADK1 and AtNADK2, AtNADK3 phosphorylates NADH, but has a lower affinity to NAD (Turner et al. 2005). This might prevent the intraperoxisomal phosphorylation of NAD, which is required for oxidative reactions like β-oxidation. NADPH produced by *Arabidopsis* NADK3 is not only used for the detoxification of the concomitantly generated $H_2O_2$ in the peroxisomal matrix. It is also required in plants to reduce unsaturated fatty acids (Behrends et al. 1988; Gurvitz et al. 1997; Hua et al. 2012) and the JA precursor OPDA for their conversion via β-oxidation (Schaller et al. 2000; Stintzi and Browse 2000). The depletion of peroxisomal NADP(H) in case of the *Arabidopsis nadk3* knockout led to impaired biotic and abiotic stress responses either directly linked to pathogen resistance or as part of the peroxisomal antioxidant machinery (Chai et al. 2006; Waller et al. 2010).

All of the above described peroxisomal reactions depend on the import of cytosolic ATP, since plant peroxisomes are unable to synthesize ATP by

substrate-level phosphorylation. As AtPNC1 and AtPNC2 are up to now the only known peroxisomal ATP import route in *Arabidopsis*, *pnc1/2* silencing plants should be deficient in more processes than just fatty acid β-oxidation. Thus, the generation of *Arabidopsis* null mutants for both PNC1 and PNC2, if vital, are required to explore the impact of ATP deficiency for other ATP-dependent processes in plant peroxisomes.

**The peroxisomal NAD carrier**

Peroxisomes require a specific carrier that mediates the import of NAD into the peroxisomal matrix to supply numerous peroxisomal redox reactions inside peroxisomes (Figure 1) (Noctor et al. 2006; Gakière et al. 2018). In plants, peroxisomal pathways, such as β-oxidation, photorespiration and ROS detoxification, are essential for peroxisome function and strictly require NAD as cofactor (Hu et al. 2012). To maintain the flux through these metabolic pathways, regeneration of reducing equivalents needs to be assured (Linka and Esser 2012; Linka and Theodoulou 2013). It is widely accepted that the peroxisomal malate/oxaloacetate shuttle is essential for the indirect exchange of the oxidized and reduced forms of NAD in plant peroxisomes (Pracharoenwattana et al. 2007, 2010). The peroxisomal malate dehydrogenase, which is part of this shuttle, produces either NAD or NADH by catalyzing the reversible reduction of oxaloacetate to malate. These dicarboxylates are exported to the cytosol for the re-conversion by cytosolic malate dehydrogenase and re-imported into peroxisomes via peroxisomal pore-forming channels (Antonenkov and Hiltunen 2012).

Since the *de novo* biosynthesis of NAD as well as salvage pathways are located in the cytosol in plants, NAD has to be imported into the peroxisomal lumen (Noctor et al. 2006; Hashida et al. 2009). A peroxisomal NAD carrier has been discovered in *Arabidopsis* (Agrimi et al. 2012; Bernhardt et al. 2012). This *Arabidopsis* carrier, called PXN, catalyzes the transport of NAD, NADH, AMP, ADP and CoA in a strict exchange mode *in vitro* using a liposome uptake system (Table 1) (Agrimi et al. 2012; Bernhardt et al. 2012). In contrast to previously characterized plastidial and mitochondrial NAD antiporters, AtPXN accepts NADH and CoA as substrates. Concentration-dependent CoA uptake experiments demonstrated that AtPXN had a lower affinity to CoA, catalyzing only marginal CoA uptake into liposomes even at high CoA concentrations (van Roermund et al. 2016). Since the cellular CoA levels are rather low in plants, a physiological role of AtPXN in supplying peroxisomes with CoA is unlikely. To elucidate whether AtPXN mediates the exchange of NAD/AMP or NAD/NADH in a living system, selected *S. cerevisiae* mutants were used (van Roermund et al. 2016). A yeast strain lacking the peroxisomal malate dehydrogenase 3 (ScMdh3p) led to yeast cells that were unable to metabolize fatty acids via peroxisomal β-oxidation, because NAD is completely reduced to NADH and cannot be re-oxidized (van Roermund et al. 1995). Under this condition the peroxisomal NADH pyrophosphatase 1 (Npy1p) from *S. cerevisiae* hydrolyzes NADH to AMP, preventing the accumulation of NADH in the peroxisomal matrix (AbdelRaheim et al. 2001). Thus, in this mutant background mainly AMP would be available for AtPXN as internal substrate for the uptake of NAD into yeast peroxisomes. Furthermore, the gene encoding for ScNpy1p was deleted in the *mdh3*Δ yeast background (van Roermund et al. 2016). It was expected that the elevated NADH pool in the peroxisomes of this double mutant supports the NAD import against peroxisomal NADH, mediated by the overexpressed AtPXN. However, AtPXN was able to enhance the fatty acid degradation activity in the *mdh3*Δ yeast mutant, but not in the *mdh3/npy1*Δ yeast double mutant, indicating that the function of ScNpy1p is crucial for phenotype suppression (van Roermund et al. 2016). It is assumed that AtPXN catalyzes the influx of NAD into yeast peroxisomes versus AMP *in vivo*. As a consequence, how is net influx of NAD into peroxisomes guaranteed via such an antiport mechanism? To balance the loss of peroxisomal AMP, cytosolic AMP is re-imported into peroxisomes by an unknown peroxisomal carrier. An adenylate uniporter could refill the peroxisomal adenine nucleotide pool. In contrast, AMP as counter-exchange substrate for the NAD import is provided by the hydrolysis of NADH mediated by the peroxisomal nudix hydrolase NUDT19 in *Arabidopsis* (Ogawa et al. 2005, 2008; Reumann et al. 2009). The recombinant protein exhibits NADH hydrolysis activity, and thus is a promising candidate catalyzing this enzymatic step.

To investigate whether *Arabidopsis* PXN provides peroxisomal reactions with NAD in plants, a loss-of-function would affect the action of NAD-dependent pathways, such as β-oxidation, photorespiration and ROS detoxification. Indeed, the mobilization rate of

seed-stored fatty acids via β-oxidation is impaired in *Arabidopsis pxn* knockout plants (Bernhardt et al. 2012). However, the degradation of fatty acid is not completely blocked, allowing a normal seedling establishment. The *Arabidopsis* T-DNA insertion lines for AtPXN displayed an obvious affect during plant development under standard growth conditions (personal communications), indicating that other peroxisomal NAD-dependent reactions are not restricted in plants. A photometric screen discovered a possible contribution of AtPXN to photorespiration under fluctuating and high light conditions (Li et al. 2018). This weak *Arabidopsis pxn* phenotype suggests alternative routes for the NAD uptake in plant peroxisomes (Bernhardt et al. 2012). Most likely a redundant carrier takes over the function of AtPXN in importing NAD into the plant peroxisomal matrix.

**The peroxisomal CoA carrier**

CoA is an essential acyl group carrier and carbonyl-activating group and it is utilized in the biosynthesis and catabolism of both primary and secondary metabolites; in plants, for example, for the citric acid cycle (mitochondria), fatty acid biosynthesis (plastids) and degradation (peroxisomes) (Coxon et al. 2005). The CoA biosynthesis is mainly localized to the cytosol in eukaryotes and starts with the condensation of pantoate to β-alanine to form pantothenate (vitamin B5) catalyzed by pantothenate synthase. Subsequent enzymatic steps lead to the production of dephospho-CoA that is finally phosphorylated by dephospho-CoA kinase to produce CoA (Rubio et al. 2006; Tilton et al. 2006; Rubio et al. 2008). To supply CoA dependent metabolic reactions in different organelles (cell compartments), the transfer of CoA across biological membranes is essential (Linka and Esser 2012; Linka and Theodoulou 2013). Members of the MCF have been shown to mediate this shuttle for an efficient subcellular distribution of this cofactor within the eukaryotic cell (Figure 1).

Leu5p and SLC25A42 represent mitochondrial CoA carriers in yeast and human, respectively (Prohl et al. 2001; Fiermonte et al. 2009). Based on sequence similarity, both mitochondrial CoA carriers from *Arabidopsis* AtCoAC1 and AtCoAC2 and their maize homologs have been identified (Zallot et al. 2013). All four proteins were able to functionally complement a ScLeu5 deficient yeast strain (Zallot et al. 2013). Yeast cells lacking LEU5 display retarded growth on rich media containing a non-fermentable carbon source, such as glycerol, and the CoA levels in intact *leu5*Δ mitochondria were strongly reduced (Prohl et al. 2001). Transport measurements in liposomes reconstituted with *E. coli* expressed human CoA carrier SLC25A42 demonstrated that this carrier transports, besides CoA, dephospho-CoA, adenosine 3',5'-diphosphate (PAP), and the adenine nucleotides by counter-exchange (Fiermonte et al. 2009).

In plants though, a peroxisomal CoA carrier (PCC) is still unknown (Figure 1). The peroxisomal NAD carrier PXN from *Arabidopsis* showed transport activities for CoA *in vitro* (Agrimi et al. 2012), but such a CoA import function is unlikely to occur under physiological conditions (van Roermund et al. 2016). The only peroxisomal CoA carrier, characterized so far, is the human MCF member SLC25A17, which is also known as ANT1 or PMP34 (Agrimi et al. 2011). *In vitro* uptake assays revealed that the recombinant SLC25A17 protein – as its mitochondrial counterpart – also exhibits a broad substrate specificity (Agrimi et al. 2012). Notably, the human SLC25A17 is able to catalyze the flux of intermediates of the CoA biosynthesis and salvage pathway. In *Arabidopsis*, proteomic data imply that dephospho-CoA kinase is localized to peroxisomes, plastids and the cytosol (Reumann et al. 2009), thus giving the possibility that dephospho-CoA is transported in addition or instead of CoA. Transport function for PAP by the human SLC25A17 carrier gives rise to a potential CoA salvage pathway within peroxisomes in general. The yeast peroxisomal Pcd1p is a nudix hydrolase with specificity to CoA producing PAP and 4'-phosphopantetheine (4-PP) (Cartwright et al. 2000). NUDT7a and Y87G2A.14, the Pcd1p homologs in mouse and *C. elegans*, respectively, also show CoA hydrolase activity (Gasmi and McLennan 2001; AbdelRaheim and McLennan 2002; Reilly et al. 2008). While in *Arabidopsis* CoA hydrolysis activity of AtNUDT19 is almost undetectable (Ogawa et al. 2005, 2008), NUDT15 might be a better candidate catalyzing this reaction in *Arabidopsis* (Ito et al. 2012). AtNUDT15 has a splice variant NUDT15a with an early stop codon unveiling a putative peroxisomal targeting signal. Both variants have an N-terminal mitochondrial target peptide. Masking this domain results in a peroxisomal localization (Ito et al. 2012). The product of the CoA hydrolysis (PAP and 4-PP) might be used as counter-exchange substrates for the CoA

import. 4-PP as a CoA precursor can then enter CoA biosynthesis pathway in the cytosol. Putative transport function of 4-PP by the peroxisomal CoA carrier in plants needs to be tested *in vitro*. As an alternative fate for PAP inside peroxisomes, it could be converted to AMP by an unknown peroxisomal hydrolase. The resulted AMP might function as exchange partner for CoA or NAD import (Table 1).

As a reminder, for the peroxisomal ABC transporter in *Arabidopsis* CTS it was demonstrated that during the transport process of acyl-CoA esters the CoA moiety is cleaved off. If the CoA molecule is released into the peroxisomal matrix, the need for a peroxisomal CoA importer would obliviate. In this scenario, the role of a peroxisomal CoA carrier in plants could be to regulate the peroxisomal CoA homeostasis by exporting CoA from the peroxisomes. For instance, in plants each glyoxylate cycle releases free CoA into the peroxisomal lumen. Still, due to the presence of the human peroxisomal CoA carrier it is most likely that in plants the CoA carrier is also a member of the MCF.

## PEROXISOMAL PORE-FORMING CHANNELS

Several reports provided evidence on pore-forming channels in membranes of peroxisomes from human, mammals, plant, yeast and *Trypanosoma brucei*, indicating that the existence of these channel proteins is highly conserved within the eukaryote lineage (Reumann et al. 1995, 1996, 1998; Antonenkov et al. 2009; Rokka et al. 2009; Gualdrón-López et al. 2012; Mindthoff et al. 2015). The detected channel activities in the peroxisomal membrane were studied using the lipid bilayer technique (Andreoli 1974; Ehrlich 1992). Integral proteins were detergent-solubilized from peroxisomal membranes and incorporated into the planar lipid bilayer (also called 'black membrane') which is formed over an aperture located in a septum separating two chambers. Each chamber is filled with buffered ionic solution, for example, with potassium chloride (KCl) solution as electrolyte (Andreoli 1974; Ehrlich 1992). This experimental set-up allows to record the facilitated diffusion of ions or various organic anions through the channel-forming pore. For a detailed overview of the lipid bilayer measurements describing peroxisomal channel activities we refer the reader to a review by Antonenkov and Hiltunen (2012).

Electrophysiological studies revealed that the peroxisomal channels mediate the transfer of solutes with a broad substrate specificity through the peroxisomal bilayer membrane. In different plant species, such as spinach and castor bean, only one peroxisomal channel protein with comparable characteristics has been investigated (Reumann et al. 1995, 1996, 1997, 1998), whereas in other eukaryotes, such as mouse and yeast, more than one type of channel-forming proteins with distinct properties has been detected (Antonenkov et al. 2005; Antonenkov et al. 2009; Grunau et al. 2009; Gualdrón-López et al. 2012). In general, the activities of the peroxisomal channels from different eukaryotes are comparable to each other, but they differ in their properties from known β-barrel channels, *e.g.* porins of the Gram-negative bacteria, voltage-dependent anion channel of the outer mitochondrial membrane (VDAC) and the outer envelope proteins of plastids (OEPs) (Zeth and Thein 2010). Candidates responsible of these peroxisomal pore-forming activities have been recently identified, such as PMP22 and PEX11, which are described in the next chapter.

### The peroxisomal membrane protein of 22 kDa (PMP22)

The peroxisomal membrane protein of 22 kDa (PMP22) is one of the most abundant integral peroxisomal membrane proteins found in eukaryotes. It belongs to a small family of putative uncharacterized transport proteins, called MPV17/PMP22 family (Saier et al. 2009). This class of channels consists of two subgroups. One subgroup includes members that are found in mitochondria, named after the inner mitochondrial membrane in human (MPV17) (Spinazzola et al. 2006), whereas the other subdivision contains peroxisomal members, like PMP22. Proteins of the MPV17/PMP22 family are multi-spanning membrane proteins with four putative $\alpha$-helical transmembrane domains. They contain a conserved protein motif at the C-terminus (PF04117) and are predicted to form homotrimers. Several reports demonstrated that both the mitochondrial and peroxisomal members of this family are non-selective channels with similar basic properties (Rokka et al. 2009; Reinhold et al. 2012; Antonenkov et al. 2015). Since the MPV17/PMP22 members do not share sequence or structural similarities with known porin

proteins or other channels, they represent a novel channel-type. Best-known mitochondrial members of this family are the mitochondrial inner membrane protein MPV17 in human (Spinazzola et al. 2006) and the stress-inducible yeast MPV17 homolog Sym1 (Trott and Morano 2004; Dallabona et al. 2010). The PMP22 members described so far are the peroxisomal membrane protein 2 in mouse (Pxmp2; Rokka et al. 2009; Vapola et al. 2014) and the peroxisomal membrane protein 22 kDa in *Arabidopsis* (PMP22) (Tugal et al. 1999; Murphy et al. 2003).

The channel activities of the human MPV17 and yeast Sym1p were investigated by lipid bilayer experiments using recombinant proteins (Reinhold et al. 2012; Antonenkov et al. 2015). Both channels form a membrane pore with a similar diameter (1.6–1.8 nm). The size of the pore is large enough to facilitate the transmembrane diffusion of nearly all mitochondrial solutes, including inorganic ions, different metabolites, and even ATP molecules. These non-selective channels were constitutively open at low and moderate voltages, but they are in the closed conformation at high voltages (±100 mV) (Reinhold et al. 2012; Antonenkov et al. 2015). In case of the peroxisomal members of this MVP17/PMP22 channel family, the channel function of the mouse Pxmp2 protein has been verified (Rokka et al. 2009; Vapola et al. 2014). The recombinant protein also forms a relatively wide, water-filled pore with an estimated size diameter of 1.4 nm in an artificial lipid bilayer, allowing the passive diffusion of various organic acids with molecular masses up to 300 Da, such as glycolate, pyruvate, and 2-ketoglutarate (Table 1) (Rokka et al. 2009; Vapola et al. 2014). The basic characteristics of the channel activities of the recombinant Pxmp2 protein are comparable to those measured for the peroxisomal membrane preparations purified from mouse liver (Rokka et al. 2009; Vapola et al. 2014).

In *Arabidopsis* the peroxisomal member of this channel family, called PMP22, was identified as one of the first plant peroxisomal membrane proteins by subcellular fractionation (Tugal et al. 1999). Later immunofluorescence imaging (Murphy et al. 2003) and experimental proteomics (Eubel et al. 2008; Reumann et al. 2009) confirmed this finding. However, whether the *Arabidopsis* PMP22 functions as pore-forming channel, like the mouse Pxmp2 and contribute to the permeability of plant peroxisomes is so far unknown (Figure 1). Both proteins are members of the same transport protein family and share 30% identity on protein sequence level (Saier et al. 2009).

### The Peroxin 11 (PEX11)

Peroxin 11 (PEX11) is an integral membrane protein of the peroxisomal bilayer membrane with at least two predicted α-helical transmembrane domains and both termini exposed to the cytosol (Thoms and Erdmann 2005). PEX11 is considered a key player in peroxisomal proliferation, regulating peroxisome size and number in all eukaryotic organisms. The PEX11 protein family consists of three members in human and mammals (Pex11α, Pex11β, and Pex11γ), five members in *Arabidopsis* (PEXa, PEXb, PEXc, PEXd, and PEXe), and three members in yeast (Pex11, Pex25, and Pex27) (Abe and Fujiki 1998; Rottensteiner et al. 2003; Tanaka et al. 2003; Lingard and Trelease 2006). Unexpectedly, the yeast Pex11p also represents a non-selective channel responsible for transfer of solutes across peroxisomal membrane.

A small part of the PEX11 proteins (~100 aa) shares 40% sequence similarity to the transient receptor potential cation-selective channel (Mindthoff et al. 2015). Due to its relationship to the TRP channel family, the yeast PEX11 protein was recombinantly expressed and reconstituted into lipid bilayer to assess channel properties (Mindthoff et al. 2015). The electrophysiological experiments clearly demonstrated that ScPex11p exhibits channel-forming activities. A pore-diameter of around 0.6 nm was calculated, implying that molecules with up to 400 Da can pass the non-selective channel (Mindthoff et al. 2015). Comparative multi-channel analysis of Pex11-deficient yeast peroxisomes revealed pore-forming activities with different characteristics to those of the recombinant ScPex11p, indicating that the yeast peroxisomes possess more than one pore-forming channel (Mindthoff et al. 2015).

Ectopic overexpression of proteins of the PEX11 family from yeast, plants, mammals or humans induces peroxisome proliferation, leading to the formation of elongated peroxisomes (Abe and Fujiki 1998; Li and Gould 2002; Lingard and Trelease 2006; Nito et al. 2007; Orth et al. 2007; Koch et al. 2010). The deletion of PEX11 in yeast, however, results in fewer but giant peroxisomes in yeast (Erdmann and Blobel 1995). *Arabidopsis* has five paralogs of PEX11, which were subdivided into group 1 (AtPEX11a and AtPEX11b) and group 2 (AtPEX11c, ATPEX11d, and ATPEX11e). In *Arabidopsis* mutant plants

in which single PEX11 genes were silenced the peroxisome number and size were reduced (Orth et al. 2007), whereas double and triple *Arabidopsis* knockdown mutants *pex11a*/*pex11b* and *pex11c*/*pex11d*/*pex11e* contain large peroxisomes in the cells of roots and leaves (Nito et al. 2007). Peroxisome proliferation is a multistep process including elongation, constriction and fission (Schrader et al. 2016). Based on the altered peroxisome morphology, it has been implicated that PEX11 proteins directly participate in the first two steps. It enables membrane elongation by stabilizing peroxisomal membrane tubules and thus initiates the formation of constriction sites by recruiting the mitochondrial fission machinery to peroxisomes (Schrader et al. 2016).

Beside the peroxisome proliferation phenotype, yeast cells lacking Pex11p are unable to metabolize long- and medium-chain fatty acids, such as oleic acid (C18:1) and lauric acid (C12:0), as sole carbon and energy source (Table 1) (van Roermund et al. 2000). While the overexpression of ScPex11p led to enhanced β-oxidation activities in intact yeast cells (Mindthoff et al. 2015). This leads to the question how the peroxisomal fatty acid degradation is linked to the supposed role of PEX11. Changes in PEX11 as an essential regulator of peroxisome proliferation might indirectly lead to dysfunctional peroxisomes with an impaired metabolism. Alternatively, PEX11 as a solute channel mediating the import of medium- and long-chain fatty acids into peroxisomes, supplies peroxisomal β-oxidation with its substrates. The peroxisomal ABC transporter is essential for the import of very long-chain fatty acids, but the absence of a pore-forming protein might alter concentration and composition of solutes inside the peroxisomal lumen. This in turn could negatively influence the process of peroxisome proliferation. Enlarged peroxisomes have been reported for several *Arabidopsis* β-oxidation mutants, such as *kat2* (β-Ketothiolase; Germain et al. 2001), *mfp2* (Multifunctional protein; Rylott et al. 2006), and *pxn* (peroxisomal NAD carrier; Mano et al. 2011), assuming that a defective fatty acid degradation indirectly disturbs peroxisome proliferation.

Since other PEX11 orthologs from plants, mammals and humans are able to restore the inability of the *pex11*Δ yeast mutant to grow on oleic acid and rescue the peroxisome morphology phenotype, it remains to be solved how PEX11 proteins can fulfill two distinct functions in the eukaryotic cell – as a solute channel and as a factor required for peroxisome proliferation (Figure 1).

## CONCLUSION

Peroxisomes have to exchange intermediates with other cell compartments to fulfill their role in cellular metabolism. For this functional interplay they rely on the peroxisomal transporters and channels described in this review. For a high-flux of solutes between two organelles, the membranes of both compartments need also to be in close proximity. Otherwise the slow diffusion of solutes to their cellular destination would rate-limit the metabolic flux through this pathway. Recently, protein complexes have been discovered that physically connect peroxisomes to mitochondria, for example, via membrane contact sites (MCSs) (Schrader et al. 2015). These membrane regions of tethered organelles are beneficial for rapid solute channeling due to an enrichment of specific transporters and channels and the generation of concentration gradients of solutes at these sites. Further insights into the peroxisomal solute transport processes in respect to specificity and regulation, would be a great step towards using peroxisomes as synthetic organelles for heterologous pathway compartmentalization (Kessel-Vigelius et al. 2013).

An alternative mechanism for peroxisomes to exchange solutes is the transfer of vesicles from the ER or mitochondria, which both play an important role in peroxisome biogenesis. Peroxisomes derive *de novo* from vesicles from the ER and mitochondria and replicate by growth and division (Sugiura et al. 2017). Therefore, such a vesicular transport might provide peroxisomes with membrane proteins and enzymes, but also with lipids and other metabolites and cofactors.

## ACKNOWLEDGEMENTS

The authors would like to thank members of the Weber Lab for helpful discussions and support. Special thanks to Dominik Brilhaus for reading the manuscript. This work was supported by the DFG grants LI1781/1-3 and LI1781/2-2.

## REFERENCES


AbdelRaheim SR, Cartwright JL, Gasmi L, McLennan AG (2001) The NADH diphosphatase encoded by the *Saccharomyces cerevisiae NPY1* nudix hydrolase gene is located in peroxisomes. **Arch Biochem Biophys** 388: 18–24

AbdelRaheim SR, McLennan AG (2002) The *Caenorhabditis elegans* Y87G2A.14 Nudix hydrolase is a peroxisomal coenzyme A diphosphatase. **BMC Biochem** 3: 5

Abe I, Fujiki Y (1998) cDNA cloning and characterization of a constitutively expressed isoform of the human peroxin Pex11p. **Biochem Biophys Res Commun** 252: 529–533

Agrimi G, Russo A, Scarcia P, Palmieri F (2011) The human gene SLC25A17 encodes a peroxisomal transporter of coenzyme A, FAD and NAD. **Biochem J** 443: 241–247

Agrimi G, Russo A, Pierri CL, Palmieri F (2012) The peroxisomal NAD carrier of *Arabidopsis thaliana* transports coenzyme A and its derivatives. **J Bioenerg Biomembr** 44: 333–340

Andreoli TE (1974) Planar lipid bilayer membranes. **Meth Enzymol** 32: 513–539

Antonenkov VD, Rokka A, Sormunen RT, Benz R, Hiltunen JK (2005) Solute traffic across mammalian peroxisomal membrane - single channel conductance monitoring reveals pore-forming activities in peroxisomes. **Cell Mol Life Sci** 62: 2886–2895

Antonenkov VD, Mindthoff S, Grunau S, Erdmann R, Hiltunen JK (2009) An involvement of yeast peroxisomal channels in transmembrane transfer of glyoxylate cycle intermediates. **Int J Biochem Cell Biol** 41: 2546–2554

Antonenkov VD, Hiltunen JK (2012) Transfer of metabolites across the peroxisomal membrane. **Biochim Biophys Acta** 1822: 1374–1386

Antonenkov VD, Isomursu A, Mennerich D, Vapola MH, Weiher H, Kietzmann T, Hiltunen JK (2015) The human mitochondrial DNA depletion syndrome gene *MPV17* encodes a non-selective channel that modulates membrane potential. **J Biol Chem** 290: 13840–13861

Arai Y, Hayashi M, Nishimura M, Nishimura M (2008) Proteomic identification and characterization of a novel peroxisomal adenine nucleotide transporter supplying ATP for fatty acid β-oxidation in soybean and *Arabidopsis*. **Plant Cell** 20: 3227–3240

Baker A, Carrier DJ, Schaedler T, Waterham HR, van Roermund CWT, Theodoulou FL (2015) Peroxisomal ABC transporters: Functions and mechanism. **Biochem Soc Trans** 43: 959–965

Behrends W, Thieringer R, Engeland K, Kunau WH, Kindl H (1988) The glyoxysomal β-oxidation system in cucumber seedlings: Identification of enzymes required for the degradation of unsaturated fatty acids. **Arch Biochem Biophys** 263: 170–177

Bernhardt K, Wilkinson S, Weber APM, Linka N (2012) A peroxisomal carrier delivers NAD and contributes to optimal fatty acid degradation during storage oil mobilization. **Plant J** 69: 1–13

Block A, Widhalm JR, Fatihi A, Cahoon RE, Wamboldt Y, Elowsky C, Mackenzie SA, Cahoon EB, Chapple C, Dudareva N, Basset GJ (2014) The origin and biosynthesis of the benzenoid moiety of ubiquinone (Coenzyme Q) in *Arabidopsis*. **Plant Cell** 26: 1938–1948

Bussell JD, Reichelt M, Wiszniewski AAG, Gershenzon J, Smith SM (2014) Peroxisomal ATP-binding cassette transporter COMATOSE and the multifunctional protein ABNORMAL INFLORESCENCE MERISTEM are required for the production of benzoylated metabolites in *Arabidopsis* seeds. **Plant Physiol** 164: 48–54

Cartwright JL, Gasmi L, Spiller DG, McLennan AG (2000) The *Saccharomyces cerevisiae PCD1* gene encodes a peroxisomal nudix hydrolase active toward coenzyme A and its derivatives. **J Biol Chem** 275: 32925–32930

Cassin-Ross G, Hu J (2014a) Systematic phenotypic screen of *Arabidopsis* peroxisomal mutants identifies proteins involved in β-oxidation. **Plant Physiol** 166: 1546–1559

Cassin-Ross G, Hu J (2014b) A simple assay to identify peroxisomal proteins involved in 12-oxo-phytodienoic acid metabolism. **Plant Signal Behav** 9: e29464

Chai MF, Wei PC, Chen QJ, An R, Chen J, Yang S, Wang XC (2006) NADK3, a novel cytoplasmic source of NADPH, is required under conditions of oxidative stress and modulates abscisic acid responses in *Arabidopsis*. **Plant J** 47: 665–674

Chuang CY, Chen LY, Fu RH, Chen SM, Ho MH, Huang JM, Hsu CC, Wang CC, Chen MS, Tsai RT (2014) Involvement of the carboxyl-terminal region of the yeast peroxisomal half ABC transporter Pxa2p in its interaction with Pxa1p and in transporter function. **PLoS ONE** 9: e104892

Coca M, San Segundo B (2010) AtCPK1 calcium-dependent protein kinase mediates pathogen resistance in *Arabidopsis*. **Plant J** 63: 526–540

Cohen P (2000) The regulation of protein function by multisite phosphorylation: A 25 year update. **Trends Biochem Sci** 25: 596–601

Coxon KM, Chakauya E, Ottenhof HH, Whitney HM, Blundell TL, Abell C, Smith AG (2005) Pantothenate biosynthesis in higher plants. **Biochem Soc Trans** 33: 743–746

Dallabona C, Marsano RM, Arzuffi P, Ghezzi D, Mancini P, Zeviani M, Ferrero I, Donnini C (2010) Sym1, the yeast ortholog of the MPV17 human disease protein, is a stress-induced bioenergetic and morphogenetic mitochondrial modulator. **Human Mol Gen** 19: 1098–1107

Dave A, Hernandez ML, He Z, Andriotis VM, Vaistij FE, Larson TR, Graham IA (2011) 12-oxo-phytodienoic acid accumulation during seed development represses seed germination in *Arabidopsis*. **Plant Cell** 23: 583–599

De Marcos Lousa C, van Roermund CWT, Postis VLG, Dietrich D, Kerr ID, Wanders RJA, Baldwin SA, Baker A, Theodoulou FL (2013) Intrinsic acyl-CoA thioesterase activity of a peroxisomal ATP binding cassette transporter is required for transport and metabolism of fatty acids. **Proc Natl Acad Sci USA** 110: 1279–1284

De Rybel B, Audenaert D, Xuan W, Overvoorde P, Strader LC, Kepinski S, Hoye R, Brisbois R, Parizot B, Vanneste S, Liu X,

Gilday A, Graham IA, Nguyen L, Jansen L, Nijo MF, Inze D, Bartel B, Beeckman T (2012) A role for the root cap in root branching revealed by the non-auxin probe naxillin. **Nat Chem Biol** 8: 798–805

Dietrich D, Schmuths H, De Marcos Lousa C, Baldwin JM, Baldwin SA, Baker A, Theodoulou FL, Holdsworth MJ (2009) Mutations in the *Arabidopsis* peroxisomal ABC transporter COMATOSE allow differentiation between multiple functions in planta: Insights from an allelic series. **Mol Biol Cell** 20: 530–543

Ehrlich BE (1992) Planar lipid bilayers on patch pipettes: Bilayer formation and ion channel incorporation. **Meth Enzymol** 207: 463–470

Erdmann R, Blobel G (1995) Giant peroxisomes in oleic acid-induced *Saccharomyces cerevisiae* lacking the peroxisomal membrane protein Pmp27p. **J Cell Biol** 128: 509–523

Eubel H, Meyer EH, Taylor NL, Bussell JD, O'Toole N, Heazlewood JL, Castleden I, Small ID, Smith SM, Millar AH (2008) Novel proteins, putative membrane transporters, and an integrated metabolic network are revealed by quantitative proteomic analysis of *Arabidopsis* cell culture peroxisomes. **Plant Physiol** 148: 1809–1829

Ferdinandusse S, Jimenez-Sanchez G, Koster J, Denis S, van Roermund CWT, Silva-Zolezzi I, Moser AB, Visser WF, Gulluoglu M, Durmaz O, Demirkel M, Waterham HR, Gökcay G, Wanders RJA, Valle D (2015) A novel bile acid biosynthesis defect due to a deficiency of peroxisomal ABCD3. **Human Mol Genet** 24: 361–370

Fiermonte G, Paradies E, Todisco S, Marobbio CMT, Palmieri F (2009) A novel member of solute carrier family 25 (SLC25A42) is a transporter of coenzyme A and adenosine 3',5'-diphosphate in human mitochondria. **J Biol Chem** 284: 18152–18159

Footitt S, Slocombe SP, Larner V, Kurup S, Wu Y, Larson T, Graham IA, Baker A, Holdsworth M (2002) Control of germination and lipid mobilization by COMATOSE, the *Arabidopsis* homologue of human ALDP. **EMBO J** 21: 2912–2922

Friso G, van Wijk KJ (2015) Update: Post-translational protein modifications in plant metabolism. **Plant Physiol** 169: 1469–1487

Fukao Y, Hayashi M, Hara-Nishimura I, Nishimura M (2003) Novel glyoxysomal protein kinase, GPK1, identified by proteomic analysis of glyoxysomes in etiolated cotyledons of *Arabidopsis thaliana*. **Plant Cell Physiol** 44: 1002–1012

Fulda M, Schnurr J, Abbadi A, Heinz E, Browse J (2004) Peroxisomal Acyl-CoA synthetase activity is essential for seedling development in *Arabidopsis thaliana*. **Plant Cell** 16: 394–405

Gakière B, Fernie AR, Pétriacq P (2018) More to NAD than meets the eye: A regulator of metabolic pools and gene expression in *Arabidopsis*. **Free Radic Biol Med** 122: 86–95

Gasmi L, McLennan AG (2001) The mouse *Nudt7* gene encodes a peroxisomal nudix hydrolase specific for coenzyme A and its derivatives. **Biochem J** 357: 33–38

Geillon F, Gondcaille C, Raas Q, Dias AMM, Pecqueur D, Truntzer C, Lucchi G, Ducoroy P, Falson P, Savary S, Trompier D (2017) Peroxisomal ATP-binding cassette transporters form mainly tetramers. **J Biol Chem** 292: 6965–6977

Goepfert S, Poirier Y (2007) β-oxidation in fatty acid degradation and beyond. **Curr Opin Plant Biol** 10: 245–251

Germain V, Rylott EL, Larson TR, Sherson SM, Bechtold N, Carde JP, Bryce JH, Graham IA, Smith SM (2001) Requirement for 3-ketoacyl-CoA thiolase-2 in peroxisome development, fatty acid β-oxidation and breakdown of triacylglycerol in lipid bodies of *Arabidopsis* seedlings. **Plant J** 28: 1–12

Graham IA (2008) Seed storage oil mobilization. **Annu Rev Plant Biol** 59: 115–142

Grunau S, Mindthoff S, Rottensteiner H, Sormunen RT, Hiltunen JK, Erdmann R, Antonenkov VD (2009) Channel-forming activities of peroxisomal membrane proteins from the yeast *Saccharomyces cerevisiae*. **FEBS J** 276: 1698–1708

Gualdrón-López M, Vapola MH, Miinalainen IJ, Hiltunen JK, Michels PAM, Antonenkov VD (2012) Channel-forming activities in the glycosomal fraction from the bloodstream form of *Trypanosoma brucei*. **PLoS ONE** 7: e34530

Gurvitz A, Rottensteiner H, Kilpeläinen SH, Hartig A, Hiltunen JK, Binder M, Dawes IW, Hamilton B (1997) The *Saccharomyces cerevisiae* peroxisomal 2,4-dienoyl-CoA reductase is encoded by the oleate-inducible gene *SPS19*. **J Biol Chem** 272: 22140–22147

Haferkamp I, Schmitz-Esser S (2012) The plant mitochondrial carrier family: Functional and evolutionary aspects. **Front Plant Sci** 3: 2

Haferkamp I (2007) The diverse members of the mitochondrial carrier family in plants. **FEBS Lett** 581: 2375–2379

Hashida SN, Takahashi H, Uchimiya H (2009) The role of NAD biosynthesis in plant development and stress responses. **Ann Bot** 103: 819–824

Hayashi M, Nito K, Takei-Hoshi R, Yagi M, Kondo M, Suenaga A, Yamaya T, Nishimura M, Nishimura M (2002) Ped3p is a peroxisomal ATP-binding cassette transporter that might supply substrates for fatty acid β-oxidation. **Plant Cell Physiol** 43: 1–11

Henry LK, Gutensohn M, Thomas ST, Noel JP, Doudareva N (2015) Orthologs of the archaeal isopentenyl phosphate kinase regulate terpenoid production in plants. **Proc Natl Acad Sci USA** 112: 10050–10055

Hemmerlin A, Harwood JL, Bach TJ (2012) A raison d'être for two distinct pathways in the early steps of plant isoprenoid biosynthesis? **Prog Lipid Res** 51: 95–148

Hettema EH, van Roermund CWT, Distel B, van den Berg M, Vilela C, Rodrigues-Pousada C, Wanders RJA, Tabak HF (1996) The ABC transporter proteins Pat1 and Pat2 are required for import of long-chain fatty acids into peroxisomes of *Saccharomyces cerevisiae*. **EMBO J** 15: 3813–3822

Higgins CF (1992) ABC transporters: From microorganisms to man. **Annu Rev Cell Biol** 8: 67–113

Hodges M, Jossier M, Boex-Fontvieille E, Tcherkez G (2013) Protein phosphorylation and photorespiration. **Plant Biol J** 15: 694–706

Hooks MA, Turner JE, Murphy EC, Graham IA (2004) Acetate non-utilizing mutants of *Arabidopsis*: Evidence that organic acids influence carbohydrate perception in germinating seedlings. **Mol Genet Genomics** 271: 249–256

Hölscher C, Meyer T, Schaewen von A (2014) Dual-targeting of *Arabidopsis* 6-Phosphogluconolactonase 3 (PGL3) to chloroplasts and peroxisomes involves interaction with Trx m2 in the cytosol. **Mol Plant** 7: 252–255

Hölscher C, Lutterbey M-C, Lansing H, Meyer T, Fischer K, Schaewen von A (2016) Defects in peroxisomal 6-phosphogluconate dehydrogenase isoform PGD2 prevent gametophytic interaction in *Arabidopsis thaliana*. **Plant Physiol** 171: 192–205

Houtkooper RH, Canto C, Wanders RJ, Auwerx J (2010) The secret life of NAD+: an old metabolite controlling new metabolic signaling pathways. **Endocr Rev** 31: 194–223

Hu J, Baker A, Bartel B, Linka N, Mullen RT, Reumann S, Zolman BK (2012) Plant peroxisomes: Biogenesis and function. **Plant Cell** 24: 2279–2303

Hua T, Wu D, Ding W, Wang J, Shaw N, Liu ZJ (2012) Studies of human 2,4-dienoyl-CoA reductase shed new light on peroxisomal β-oxidation of unsaturated fatty acids. **J Biol Chem** 287: 28956–28965

Ito D, Yoshimura K, Ishikawa K, Ogawa T, Maruta T, Shigeoka S (2012) A comparative analysis of the molecular characteristics of the *Arabidopsis* CoA pyrophosphohydrolases AtNUDX11, 15, and 15a. **Biosci Biotechnol Biochem** 76: 139–147

Kamijo K, Taketani S, Yokota S, Osumi T, Hashimoto T (1990) The 70-kDa peroxisomal membrane protein is a member of the Mdr (P-glycoprotein)-related ATP-binding protein superfamily. **J Biol Chem** 265: 4534–4540

Kataya ARA, Schei E, Lillo C (2015) Towards understanding peroxisomal phosphoregulation in *Arabidopsis thaliana*. **Planta** 243:699–701

Kessel-Vigelius S, Wiese J, Schroers M, Wrobel T, Han F, Linka N (2013) An engineered plant peroxisomes and its application in biotechnology. **Plant Sci** 210: 232–240

Kienow L, Schneider K, Bartsch M, Stuible HP, Weng H, Miersch O, Wasternack C, Kombrink E (2008) Jasmonates meet fatty acids: Functional analysis of a new acyl-coenzyme A synthetase family from *Arabidopsis thaliana*. **J Exp Bot** 59: 403–419

Koch J, Pranjic K, Huber A, Ellinger A, Hartig A, Kragler F, Brocard C (2010) PEX11 family members are membrane elongation factors that coordinate peroxisome proliferation and maintenance. **J Cell Sci** 123: 3389–3400

Koo AJ, Chung HS, Kobayashi Y, Howe GA (2006) Identification of a peroxisomal acyl-activating enzyme involved in the biosynthesis of jasmonic acid in *Arabidopsis*. **J Biol Chem** 281: 33511–33520

Korasick DA, Enders TA, Strader LC (2013) Auxin biosynthesis and storage forms. **J Exp Bot** 64: 2541–2555

Li J, Tietz S, Cruz JA, Strand DD, Xu Y, Chen J, Kramer DM, Hu J (2018) Photometric screens identified *Arabidopsis* peroxisome proteins that impact photosynthesis under dynamic light conditions. **Plant J** 97: 460–474

Lingard MJ, Trelease RN (2006) Five *Arabidopsis* peroxin 11 homologs individually promote peroxisome elongation, duplication or aggregation. **J Cell Sci** 119: 1961–1972

Linka N, Theodoulou FL, Haslam RP, Linka M, Napier JA, Neuhaus HE, Weber APM (2008) Peroxisomal ATP import is essential for seedling development in *Arabidopsis thaliana*. **Plant Cell** 20: 3241–3257

Linka N, Esser C (2012) Transport proteins regulate the flux of metabolites and cofactors across the membrane of plant peroxisomes. **Front Plant Sci** 3: 3

Linka N, Theodoulou FL (2013) Metabolite transporters of the plant peroxisomal membrane: Known and unknown. **Subcell Biochem** 69: 169–194

Lombard-Platet G, Savary S, Sarde CO, Mandel JL, Chimini G (1996) A close relative of the adrenoleukodystrophy (ALD) gene codes for a peroxisomal protein with a specific expression pattern. **Proc Natl Acad Sci USA** 93: 1265–1269

Mano S, Nakamori C, Fukao Y, Araki M, Matsuda A, Kondo M, Nishimura M (2011) The defect of peroxisomal membrane protein 38 causes enlargement of peroxisomes. **Plant Cell Physiol** 52: 2157–2172

Meyer T, Hölscher C, Schwöppe C, Schaewen von A (2011) Alternative targeting of *Arabidopsis* plastidic glucose-6-phosphate dehydrogenase G6PD1 involves cysteine-dependent interaction with G6PD4 in the cytosol. **Plant J** 66: 745–758

Mindthoff S, Grunau S, Steinfort LL, Girzalsky W, Hiltunen JK, Erdmann R, Antonenkov VD (2015) Peroxisomal Pex11 is a pore-forming protein homologous to TRPM channels. **Biochim Biophys Acta** 1863: 271–283

Morita M, Imanaka T (2012) Peroxisomal ABC transporters: Structure, function and role in disease. **Biochim Biophys Acta** 1822: 1387–1396

Mosser J, Douar AM, Sarde CO, Kioschis P, Feil R, Moser H, Poustka AM, Mandel JL, Aubourg P (1993) Putative X-linked adrenoleukodystrophy gene shares unexpected homology with ABC transporters. **Nature** 361: 726–730

Murphy MA, Phillipsen BA, Baker A, Mullen RT (2003) Characterization of the targeting signal of the *Arabidopsis* 22-kD integral peroxisomal membrane protein. **Plant Physiol** 133: 813–828

Nito K, Kamigaki A, Kondo M, Hayashi M, Nishimura M (2007) Functional classification of *Arabidopsis* peroxisome biogenesis factors proposed from analyses of knockout mutant. **Plant Cell Physiol** 48: 763–774

Noctor G, Queval G, Gakiere B (2006) NAD(P) synthesis and pyridine nucleotide cycling in plants and their potential importance in stress conditions. **J Exp Bot** 57: 1603–1620

Noctor G, Foyer CH (2016) Intracellular redox compartmentation and ROS-related communication in regulation and signaling. **Plant Physiol** 171: 1581–1592

Nyathi Y, De Marcos Lousa C, van Roermund CWT, Wanders RJA, Johnson B, Baldwin SA, Theodoulou FL, Baker A (2010) The *Arabidopsis* peroxisomal ABC transporter, comatose, complements the *Saccharomyces cerevisiae pxa1/pxa2*Δ mutant for metabolism of long-chain fatty acids and exhibits fatty acyl-CoA-stimulated ATPase activity. **J Biol Chem** 285: 29892–29902

Ogawa T, Ueda Y, Yoshimura K, Shigeoka S (2005) Comprehensive analysis of cytosolic Nudix hydrolases in *Arabidopsis thaliana*. **J Biol Chem** 280: 25277–25283

Ogawa T, Yoshimura K, Miyake H, Ishikawa K, Ito D, Tanabe N, Shigeoka S (2008) Molecular characterization of organelle-type Nudix hydrolases in *Arabidopsis*. **Plant Physiol** 148: 1412–1424

Okamoto T, Kawaguchi K, Watanabe S, Agustina R, Ikejima T, Ikeda K, Nakano M, Morita M, Imanaka T (2018) Characterization of human ATP-binding cassette protein subfamily D reconstituted into proteoliposomes. **Biochem Biophys Res Commun** 496: 1122–1127

Orth T, Reumann S, Zhang X, Fan J, Wenzel D, Quan S, Hu J (2007) The PEROXIN11 protein family controls peroxisome proliferation in *Arabidopsis*. **Plant Cell** 19: 333–350

Palmieri L, Lasorsa FM, Vozza A, Agrimi G, Fiermonte G, Runswick MJ, Walker JE, Palmieri F (2000) Identification and functions of new transporters in yeast mitochondria. **Biochim Biophys Acta** 1459: 363–369

Palmieri L, Rottensteiner H, Girzalsky W, Scarcia P, Palmieri F, Erdmann R (2001) Identification and functional reconstitution of the yeast peroxisomal adenine nucleotide transporter. **EMBO J** 20: 5049–5059

Palmieri F, Agrimi G, Blanco E, Castegna A, Di Noia MA, Iacobazzi V, Lasorsa FM, Marobbio CMT, Palmieri L, Scarcia P, Todisco S, Vozza A, Walker J (2006) Identification of mitochondrial carriers in *Saccharomyces cerevisiae* by transport assay of reconstituted recombinant proteins. **Biochim Biophys Acta** 1757: 1249–1262

Palmieri F, Pierri CL, De Grassi A, Nunes-Nesi A, Fernie AR (2011) Evolution, structure and function of mitochondrial carriers: A review with new insights. **Plant J** 66: 161–181

Palmieri F (2014) Mitochondrial transporters of the SLC25 family and associated diseases: A review. **J Inherit Metab Dis** 37: 565–575

Pollak N, Dölle C, Ziegler M (2007) The power to reduce: Pyridine nucleotides–small molecules with a multitude of functions. **Biochem J** 402: 205–218

Pracharoenwattana I, Cornah JE, Smith SM (2007) *Arabidopsis* peroxisomal malate dehydrogenase functions in β-oxidation but not in the glyoxylate cycle. **Plant J** 50: 381–390

Pracharoenwattana I, Zhou W, Smith SM (2010) Fatty acid β-oxidation in germinating *Arabidopsis* seeds is supported by peroxisomal hydroxypyruvate reductase when malate dehydrogenase is absent. **Plant Mol Biol** 72: 101–109

Prohl C, Pelzer W, Diekert K, Kmita H, Bedekovics T, Kispal G, Lill R (2001) The yeast mitochondrial carrier Leu5p and its human homologue Graves' disease protein are required for accumulation of coenzyme A in the matrix. **Mol Cell Biol** 21: 1089–1097

Rees DC, Johnson E, Lewinson O (2009) ABC transporters: The power to change. **Nat Rev Mol Cell Biol** 10: 218–227

Reilly SJ, Tillander V, Ofman R, Alexson SE, Hunt MC (2008) The nudix hydrolase 7 is an Acyl-CoA diphosphatase involved in regulating peroxisomal coenzyme A homeostasis. **J Biochem** 144: 655–663

Reinhold R, Krüger V, Meinecke M, Schulz C, Schmidt B, Grunau SD, Guiard B, Wiedemann N, van der Laan M, Wagner R, Rehling P, Dudek J (2012) The channel-forming Sym1 protein is transported by the TIM23 complex in a presequence-independent manner. **Mol Cell Biol** 32: 5009–5021

Reumann S, Maier E, Benz R, Heldt HW (1995) The membrane of leaf peroxisomes contains a porin-like channel. **J Biol Chem** 270: 17559–17565

Reumann S, Maier E, Benz R, Heldt HW (1996) A specific porin is involved in the malate shuttle of leaf peroxisomes. **Biochem Soc Trans** 24: 754–757

Reumann S, Bettermann M, Benz R, Heldt HW (1997) Evidence for the presence of a porin in the membrane of glyoxysomes of castor bean. **Plant Physiol** 115: 891–899

Reumann S, Maier E, Heldt HW, Benz R (1998) Permeability properties of the porin of spinach leaf peroxisomes. **Eur J Biochem** 251: 359–366

Reumann S, Quan S, Aung K, Yang P, Manandhar-Shrestha K, Holbrook D, Linka N, Switzenberg R, Wilkerson CG, Weber APM, Olsen LJ, Hu J (2009) In-depth proteome analysis of *Arabidopsis* leaf peroxisomes combined with *in vivo* subcellular targeting verification indicates novel metabolic and regulatory functions of peroxisomes. **Plant Physiol** 150: 125–143

Rodríguez-Concepción M, Boronat A (2015) Breaking new ground in the regulation of the early steps of plant isoprenoid biosynthesis. **Curr Opin Plant Biol** 25: 17–22

Rokka A, Antonenkov VD, Soininen R, Immonen HL, Pirilä PL, Bergmann U, Sormunen RT, Weckström M, Benz R, Hiltunen JK (2009) Pxmp2 is a channel-forming protein in mammalian peroxisomal membrane. **PLoS ONE** 4: e5090

Rottensteiner H, Stein K, Sonnenhol E, Erdmann R (2003) Conserved function of pex11p and the novel pex25p and pex27p in peroxisome biogenesis. **Mol Biol Cell** 14: 4316–4328

Rottensteiner H, Theodoulou FL (2006) The ins and outs of peroxisomes: Co-ordination of membrane transport and peroxisomal metabolism. **Biochim Biophys Acta** 1763: 1527–1540

Rubio S, Larson TR, Gonzalez-Guzman M, Alejandro S, Graham IA, Serrano R, Rodriguez PL (2006) An *Arabidopsis* mutant impaired in coenzyme A biosynthesis is sugar dependent for seedling establishment. **Plant Physiol** 140: 830–843

Rubio S, Whitehead L, Larson TR, Graham IA, Rodriguez PL (2008) The coenzyme a biosynthetic enzyme phosphopantetheine adenylyltransferase plays a crucial role in plant growth, salt/osmotic stress resistance, and seed lipid storage. **Plant Physiol** 148: 546–556

Rylott EL, Eastmond PJ, Gilday AD, Slocombe SP, Larson TR, Baker A, Graham IA (2006) The *Arabidopsis thaliana*

multifunctional protein gene (*MFP2*) of peroxisomal beta-oxidation is essential for seedling establishment. **Plant J** 45: 930–941

Saier MH, Yen MR, Noto K, Tamang DG, Elkan C (2009) The transporter classification database: Recent advances. **Nucleic Acids Res** 37: D274–D278

Sapir-Mir M, Mett A, Belausov E, Tal-Meshulam S, Frydman A, Gidoni D, Eyal Y (2008) Peroxisomal localization of *Arabidopsis* isopentenyl diphosphate isomerases suggests that part of the plant isoprenoid mevalonic acid pathway is compartmentalized to peroxisomes. **Plant Physiol** 148: 1219–1228

Schaller F, Biesgen C, Müssig C, Altmann T, Weiler EW (2000) 12-Oxophytodienoate reductase 3 (OPR3) is the isoenzyme involved in jasmonate biosynthesis. **Planta** 210: 979–984

Schrader M, Godinho LF, Costello JL, Islinger M (2015) The different facets of organelle interplay: An overview of organalle interactions. **Front Cell Dev Biol** 3: 56

Schrader M, Costello JL, Godinho LF, Azadi AS, Islinger M (2016) Proliferation and fission of peroxisomes - An update. **Biochim Biophys Acta** 1863: 971–983

Shani N, Valle D (1996) A *Saccharomyces cerevisiae* homolog of the human adrenoleukodystrophy transporter is a heterodimer of two half ATP-binding cassette transporters. **Proc Natl Acad Sci USA** 93: 11901–11906

Simkin AJ, Guirimand G, Papon N, Courdavault V, Thabet I, Ginis O, Bouzid S, Giglioli-Guivarc'h N, Clastre M (2011) Peroxisomal localisation of the final steps of the mevalonic acid pathway in planta. **Planta** 234: 903–914

Spinazzola A, Viscomi C, Fernandez-Vizarra E, Carrara F, D'Adamo P, Calvo S, Marsano RM, Donnini C, Weiher H, Strisciuglio P, Parini R, Sarzi E, Chan A, Di Mauro S, Rötig A, Gasparini P, Ferrero I, Mootha VK, Tiranti V, Zeviani M (2006) MPV17 encodes an inner mitochondrial membrane protein and is mutated in infantile hepatic mitochondrial DNA depletion. **Nat Genet** 38: 570–575

Sugiura A, Mattie S, Prudent J, McBride HM (2017) Newly born peroxisomes are a hybrid of mitochondrial and ER-derived pre-peroxisomes. **Nature** 542: 251–254

Stintzi A, Browse J (2000) The *Arabidopsis* male-sterile mutant, *opr3*, lacks the 12-oxophytodienoic acid reductase required for jasmonate synthesis. **Proc Natl Acad Sci USA** 97: 10625–10630

Strader LC, Culler AH, Cohen JD, Bartel B (2010) Conversion of endogenous indole-3-butyric acid to indole-3-acetic acid drives cell expansion in *Arabidopsis* seedlings. **Plant Physiol** 153: 1577–1586

Strader LC, Wheeler DL, Christensen SE, Berens JC, Cohen JD, Rampey RA, Bartel B (2011) Multiple facets of *Arabidopsis* seedling development require indole-3-butyric acid-derived auxin. **Plant Cell** 23: 984–999

Tanaka A, Okumoto K, Fujiki Y (2003) cDNA cloning and characterization of the third isoform of human peroxin Pex11p. **Biochem Biophys Res Commun** 300: 819–823

Taylor EB (2017) Functional properties of the mitochondrial carrier system. **Trends Cell Biol** 27: 633–644

Theodoulou FL, Job K, Slocombe SP, Footitt S, Holdsworth M, Baker A, Larson TR, Graham IA (2005) Jasmonic acid levels are reduced in COMATOSE ATP-binding cassette transporter mutants. Implications for transport of jasmonate precursors into peroxisomes. **Plant Physiol** 137: 835–840

Theodoulou FL, Kerr ID (2015) ABC transporter research: Going strong 40 years on. **Biochem Soc Trans** 43: 1033–1040

Thoms S, Erdmann R (2005) Dynamin-related proteins and Pex11 proteins in peroxisome division and proliferation. **FEBS J** 272: 5169–5181

Tilton GB, Wedemeyer WJ, Browse J, Ohlrogge JB (2006) Plant coenzyme A biosynthesis: Characterization of two pantothenate kinases from *Arabidopsis*. **Plant Mol Biol** 61: 629–642

Trott A, Morano KA (2004) SYM1 is the stress-induced *Saccharomyces cerevisiae* ortholog of the mammalian kidney disease gene *Mpv17* and is required for ethanol metabolism and tolerance during heat shock. **Eukaryot Cell** 3: 620–631

Tugal HB, Pool M, Baker A (1999) *Arabidopsis* 22-kilodalton peroxisomal membrane protein. Nucleotide sequence analysis and biochemical characterization. **Plant Physiol** 120: 309–320

Turner WL, Waller JC, Vanderbeld B, Snedden WA (2004) Cloning and characterization of two NAD kinases from *Arabidopsis*. Identification of a calmodulin binding isoform. **Plant Physiol** 135: 1243–1255

Turner WL, Waller JC, Snedden WA (2005) Identification, molecular cloning and functional characterization of a novel NADH kinase from *Arabidopsis thaliana* (thale cress). **Biochem J** 385: 217–223

van Roermund CWT, Elgersma Y, Singh N, Wanders RJA, Tabak HF (1995) The membrane of peroxisomes in *Saccharomyces cerevisiae* is impermeable to NAD(H) and acetyl-CoA under *in vivo* conditions. **EMBO J** 14: 3480–3486

van Roermund CWT, Tabak HF, van den Berg M, Wanders RJA, Hettema EH (2000) Pex11p plays a primary role in medium-chain fatty acid oxidation, a process that affects peroxisome number and size in *Saccharomyces cerevisiae*. **J Cell Biol** 150: 489–498

van Roermund CWT, Drissen R, van den Berg M, Ijlst L, Hettema EH, Tabak HF, Waterham HR, Wanders RJA (2001) Identification of a peroxisomal ATP carrier required for medium-chain fatty acid β-oxidation and normal peroxisome proliferation in *Saccharomyces cerevisiae*. **Mol Cell Biol** 21: 4321–4329

van Roermund CWT, Waterham HR, Ijlst L, Wanders RJA (2003) Fatty acid metabolism in *Saccharomyces cerevisiae*. **Cell Mol Life Sci** 60: 1838–1851

van Roermund CWT, Visser WF, Ijlst L, van Cruchten A, Boek M, Kulik W, Waterham HR, Wanders RJA (2008) The human peroxisomal ABC half transporter ALDP functions as a homodimer and accepts acyl-CoA esters. **FASEB J** 22: 4201–4208

van Roermund CWT, Visser WF, Ijlst L, Waterham HR, Wanders RJA (2011) Differential substrate specificities of human ABCD1 and ABCD2 in peroxisomal fatty acid β-oxidation. **Biochim Biophys Acta** 1811: 148–152

van Roermund CWT, Ijlst L, Majczak W, Waterham HR, Folkerts H, Wanders RJA, Hellingwerf KJ (2012) Peroxisomal fatty acid uptake mechanism in *Saccharomyces cerevisiae*. **J Biol Chem** 287: 20144–20153

van Roermund CWT, Ijlst L, Wagemans T, Wanders RJA, Waterham HR (2014) A role for the human peroxisomal half-transporter ABCD3 in the oxidation of dicarboxylic acids. **Biochim Biophys Acta** 1841: 563–568

van Roermund CWT, Schroers MG, Wiese J, Facchinelli F, Kurz S, Wilkinson S, Charton L, Wanders RJA, Waterham HR, Weber APM, Linka N (2016) The peroxisomal NAD carrier from *Arabidopsis* imports NAD in exchange with AMP. **Plant Physiol** 171: 2127–2139

Vapola MH, Rokka A, Sormunen RT, Alhonen L, Schmitz W, Conzelmann E, Wärri A, Grunau S, Antonenkov VD, Hiltunen JK (2014) Peroxisomal membrane channel Pxmp2 in the mammary fat pad is essential for stromal lipid homeostasis and for development of mammary gland epithelium in mice. **Dev Biol** 391: 66–80

Verleur N, Hettema EH, van Roermund CWT, Tabak HF, Wanders RJA (1997) Transport of activated fatty acids by the peroxisomal ATP-binding-cassette transporter Pxa2 in a semi-intact yeast cell system. **Eur J Biochem** 249: 657–661

Visser WF, van Roermund CWT, Waterham HR, Wanders RJA (2002) Identification of human PMP34 as a peroxisomal ATP transporter. **Biochem Biophys Res Commun** 299: 494–497

Visser WF, van Roermund CWT, Ijlst L, Hellingwerf KJ, Wanders RJA, Waterham HR (2005) Demonstration and characterization of phosphate transport in mammalian peroxisomes. **Biochem J** 389: 717–722

Waller JC, Dhanoa PK, Schumann U, Mullen RT, Snedden WA (2010) Subcellular and tissue localization of NAD kinases from *Arabidopsis*: Compartmentalization of *de novo* NADP biosynthesis. **Planta** 231: 305–317

Wasternack C, Strnad M (2017) Jasmonates are signals in the biosynthesis of secondary metabolites - Pathways, transcription factors and applied aspects: A brief review. **N Biotechnol** 48: 1–11

Wasternack C, Feussner I (2018) The oxylipin pathways: Biochemistry and function. **Annu Rev Plant Biol** 69: 363–386

Wiesinger C, Kunze M, Regelsberger G, Forss-Petter S, Berger J (2013) Impaired very long-chain acyl-CoA β-oxidation in human X-linked adrenoleukodystrophy fibroblasts is a direct consequence of ABCD1 transporter dysfunction. **J Biol Chem** 288: 19269–19279

Zallot R, Agrimi G, Lerma-Ortiz C, Teresinski HJ, Frelin O, Ellens KW, Castegna A, Russo A, de Crécy-Lagard V, Mullen RT, Palmieri F, Hanson AD (2013) Identification of mitochondrial coenzyme a transporters from maize and *Arabidopsis*. **Plant Physiol** 162: 581–588

Zeth K, Thein M (2010) Porins in prokaryotes and eukaryotes: Common themes and variations. **Biochem J** 431: 13–22

Zolman BK, Silva ID, Bartel B (2001) The *Arabidopsis pxa1* mutant is defective in an ATP-binding cassette transporter-like protein required for peroxisomal fatty acid β-oxidation. **Plant Physiol** 127: 1266–1278

# Acknowledgements

First and foremost, I would like to thank **apl. Prof. Dr. Nicole Linka** for her outstanding supervision. I am deeply grateful for the opportunity to work on this project, for all the knowledge that she passed on and her time whenever I needed it. Thank you for your constant support and kindness over the years.

Further, I would like to thank my thesis advisor **Prof. Dr. Andreas P.M. Weber**, who constantly contributed valuable discussions and constructive feedback.

I want to thank Prof. **Dr. Stanislav Kopriva** for fruitful discussions during all TAC meetings.

Special thanks to **Dr. Philipp Westhoff** for his never-ending enthusiasm for metabolites, hours of discussions and for introduction me to the world of metabolites. Further I would like to express my gratitude to **Katrin Weber**, **Elisabeth Klemp** and **Maria Graf** for their technical assistance during the project.

Many, many thanks to **Dr. Franziska Kuhnert**, **Dr. Franziska Fichtner**, **Dr. Marc-Sven Röll, Thomas Wrobel**, **Dr. Lennart Charton**, and **Dr. Björn Hielscher** for their continuous support, for all the funny lunch and coffee breaks and for sharing some drinks after work.

I want to thank **Samantha Flachbart** for every method that you taught me since day 1 in the Weberlab. Thanks to **Anja Nöcker** for help with the bureaucratic part of the university.

Thanks to the whole **Weberlab** for creating a nice working atmosphere.

Also, thanks to the **CEPLAS office** and **coordination** for always providing a solution.

Finally, I would like to thank my family and friends outside of work for support and genuine interest in my project.